

Deep Eutectic Solvents Derived From Inorganic Salts

Thesis submitted for the degree of
Doctor of Philosophy
at the University of Leicester

By

Stefan John Davis MChem

Department of Chemistry

University of Leicester

December 2015



**University of
Leicester**

Abstract

Deep Eutectic Solvents Derived From Inorganic Salts

STEFAN JOHN DAVIS

UNIVERSITY OF LEICESTER

2015

Mixtures of metal salts with complexing agents, such as urea, form liquids, which are known as deep eutectic solvents (DESS). This has previously been applied to metal salts such as ZnCl_2 , AlCl_3 and $\text{CrCl}_3 \cdot 6\text{H}_2\text{O}$. The aim of this thesis was to see if this model could be expanded to include alkali metal salts. Some of the hydrogen bond donors (HBDs) investigated were found to form liquid mixtures with a limited number of alkali metal salts, which showed melting temperatures below $25\text{ }^\circ\text{C}$. Utilising glycerol as a HBD exhibited the highest mutual solubility with the alkali metal salts of interest, therefore this study focussed on sodium salt:glycerol mixtures. Four sodium salts were chosen: NaBr , NaOAc , $\text{NaOAc} \cdot 3\text{H}_2\text{O}$ or $\text{Na}_2\text{B}_4\text{O}_7 \cdot 10\text{H}_2\text{O}$, which provided a range of fluidities and contained hydrates and anhydrous salts.

The ionic conductivity and viscosity of these salts with glycerol were studied, and it was found that unlike previous studies of choline chloride with glycerol where the salt decreases the viscosity of glycerol, all of the sodium salts increased the viscosity of glycerol. This suggests that sodium salts have a structure making, kosmotropic effect, rather than structure breaking, chaotropic effect, on glycerol. This phenomenon is probably due to the high charge density of Na^+ , which coordinates to the glycerol.

The ion transport properties and molecular dynamics of sodium salt:glycerol mixtures have been investigated at the microscopic level using nuclear magnetic resonance and electrochemical techniques. Self-diffusion coefficients of the components of the systems of interest were found to be 10^{-11} - $10^{-13}\text{ m}^2\text{ s}^{-1}$ range. T_1 relaxation times were investigated and all systems showed a transition from a diffusion-limited, slow molecular tumbling regime to a fast molecular, high mobility, tumbling regime. Poor solubility was experienced with a range of transition metal salt probes, which was attributed to complex ion speciation. It was concluded that the sodium salt:glycerol systems studied are not ideal for electrochemical applications.

The ability of the salts to form viscous gels made them ideal plasticisers for starch. Starch DES mixtures were tested as a binder for medium density fibreboard (MDF). The properties of MDF samples were tested as a function of processing conditions and composition. Pilot scale production of plasticised starch MDF composites was successful, demonstrating the current industrial infrastructure can be utilised for large-scale production at a similar cost to MDF bound with urea formaldehyde resins.

Publications

Papers

1. A. P. Abbott, T. Z. Abolibda, S. J. Davis, F. Emmerling, D. Lourdin, E. Leroy and W. R. Wise, *RSC Adv.*, 2014, **4**, 40421

Oral Presentations

1. S. J. Davis and A. P. Abbott, Deep Eutectic Solvents Derived From Inorganic Salts, *Department Of Chemistry Postgraduate Research Day*, 14th April 2015, University of Leicester, Leicester

Poster Presentations

1. S. J. Davis, A. A. Al-Barzinjy and A. P. Abbott, Deep Eutectic Solvents with Metal Containing Cations, *EUCHEM Conference*, July 5th-11th, Tallinn, Estonia

Statement

The accompanying thesis submitted for the degree of Ph. D. entitled "Deep Eutectic Solvents Derived From Inorganic Salts" is based upon work conducted by the author in the Department of Chemistry at the University of Leicester during the period between October 2012 and September 2015.

All the work recorded in this thesis is original unless otherwise acknowledged in the text or by references. None of the work has been submitted for another degree in this or any other university.

Signed:

Date:

Acknowledgements

Firstly, I have to thank Prof. Andrew Abbott, for all of his support, encouragements and all of the opportunities he has provided during the past three years. I am truly grateful for his funding, and I am proud to say I have worked with his group. I have learnt so much over the last few years, and it has been an unforgettable experience.

I am thankful to all the members of the materials group, but most notably: Dr Robert Harris, Dr Alex Goddard, Dr Andrew Ballantyne and Dr Chris Zaleski and Dr. Luka Wright for their guidance and friendship. I would like to thank my fellow students, particularly: Shannon Stodd, Marian Perera and Salih Cihangir for providing a friendly environment whilst writing this thesis. I would not have been able to do much of the research discussed in this thesis without the help of the technical and support staff of the Chemistry Department, with particular thanks to Mr. Praful Chauhan. Acknowledgements need to go to all of the staff at the BioComposites Centre for providing the equipment and the manpower required to facilitate the scale up aspect of this project.

My never-ending appreciation and gratitude go to my: mother, stepfather and brothers. Thank you for your unconditional love, support and generally just putting up with me.

Last and by no means least, I must thank Dr William Wise for the opportunities to work with external partners, and for convincing me to undertake this PhD in the first place.

“If God needs money, why doesn't he just write another Bible? The first one sold pretty well.”

- *H. J. Simpson*

Abbreviations

E_a	Activation energy	T_g	Glass transition temperature
E_D	Activation energy of diffusivity	δ	Gradient pulse duration
E_k	Activation energy of ionic conductivity	g	Grams
E_η	Activation energy of viscous flow	g cm^{-3}	Grams per cubic centimetre
I	Angular momentum	g h^{-1}	Grams per hour
A	Area	γ_H	Gyromagnetic ratio
k_B	Boltzmann constant	φ	Heat flow
C	Capacitance	α	Hydrogen-bonding acidity
cm	Centimetre	β	Hydrogen-bonding basicity
$\text{cm}^3 \text{ mol}^{-1}$	Centimetre cubed per mole	Z	Impedance
cm^2	Centimetre squared	cm^{-1}	Inverse centimetre
cP	Centipoise	h^{-1}	Inverse hour
Q	Charge	K^{-1}	Inverse kelvin
V_{comp}	Component volume	min^{-1}	Inverse minute
c	Concentration	P^{-1}	Inverse poise
dc/dx	Concentration gradient	1/T	Inverse temperature
i	Current	z	Ion charge
$\text{dm}^3 \text{ mol}^{-1}$	Decimetres per mole	κ	Ionic conductivity
°	Degree	K	Kelvin
°C	Degree Celsius	keV	Kiloelectron volt
°C min^{-1}	Degree Celsius per minute	Kg	Kilogram
ρ	Density	kg m^{-3}	Kilograms per cubic metre
D	Diffusion coefficient	kJ mol^{-1}	Kilojoules per mole
\$	Dollar	kN	Kilonewton
$\text{\$ kg}^{-1}$	Dollar per kilogram	l	Length
C_{DL}	Double layer capacitance	L	Litre
K	Equilibrium constant	T_1	Longitudinal relaxation constant
€	Euro	g	Magnetic field strength
F	Faraday constant	MPa	Megapascal
φ	Fluidity	m	Metre
J	Flux	m^3	Metre cubed
V_{free}	Free volume	$\text{m}^3 \text{ year}^{-1}$	Metre cubed per year
ω	Frequency	m^2	Metre squared
e	Fundamental charge of an electron	$\text{m}^2 \text{ s}^{-1}$	Metre squared per second
ΔG	Gibbs free energy		

μA	Microampere	$\delta u/\delta y$	Shear rate
μl	Microlitre	τ	Shear stress
μm	Micrometre	$\text{S cm}^2 \text{ mol}^{-1}$	Siemen centimetre squared per mole
$\mu\text{S cm}^{-1}$	Microsiemens per centimetre	$\text{S g cm}^{-1} \text{ mol}^{-1}$	Siemen centimetre squared per mole
mm min^{-1}	Millimetre per minute	$\text{S g cm}^{-1} \text{ mol}^{-1} \text{ P}$	Siemen centimetre squared per mole poise
mA	Milliampere	S	Signal intensity
mA cm^{-2}	Milliamperes per centimetre squared	r	Species radius
mbar	Millibar	\sqrt{c}	Square root of concentration
mg	Milligram	$\text{dm}^{3/2}$	Square root of
mm	Millimetre	$\text{mol}^{-1/2}$	decimetres per mole
mM	Millimoles	$\text{mole}^{1/2} \text{ dm}^{-3/2}$	Square root of moles per decimetre cubed
mS	Millisiemens	γ	Surface tension
mS cm^{-1}	Millisiemens per centimetre	T	Temprature
mV s^{-1}	Millivolt per second	ϵ	Tensile strain
V_{free}^*	Minimum free volume	σ	Tensile strength
Λ	Molar conductivity	T	Tesla
R	Molar gas constant	$T \text{ m}^{-1}$	Tesla per metre
V_{m}	Molar volume	t	Time
M	Molarity	$E_{\text{T}}(30)$	Transition energy
x	Mole fraction	T_2	Translational relaxation constant
mole dm^{-3}	Moles per decimetre cubed	η	Viscosity
E_{g}/E_0	NMR signal decay	V	Volt
M_{n}	Number average molar mass	$\Delta\eta$	Walden product
Δ	Observation time	W	Watts
ppm	Part per million	w/w	Weight by weight
i_{p}	Peak current	E	Young's modulus
cm^{-3}	Per cubic centimeter	<i>et al.</i>	And others
$\%$	Percent	aq	Aqueous solution
π	Pi	ATR	Attenuated total reflection
π^*	Polarisability	BC	Before Christ
E	Potential	DES	Deep eutectic solvent
k	Rate constant	DP	Degrees of polymerization
Q	Reaction quotient	DSC	Differential scanning calorimetry
M_{r}	Relative molecular weight	EXAFS	Extended X-ray atomic fine structure
η_{r}	Relative viscosity	FAB-MS	Fast atom bombardment mass sepectrometry
R	Resistance	FT	Fourier transform
ν	Scan rate		

HSAB	Hard, soft acids and bases	(DMPIImTF SA)	1,2-dimethyl-3-propylimidazolium bis(trifluoromethylsulfonyl)amide
HF	Hartree-Fock		
H-bond	Hydrogen bond		
IR	Infrared	[BEIM] ⁺	1-butyl-3-ethylimidazolium
IB	Internal bond strength		
IL	Ionic liquid	[BMIM] ⁺	1-butyl-3-methylimidazolium
MDF	Medium density fibreboard	[DMIM] ⁺	1-deca-3-methylimidazolium
MF	Melamine formaldehyde		
M Pt	Melting point	[EMIM] ⁺	1-ethyl-3-methylimidazolium
MOE	Modulus of elasticity	[OAc] ⁻	Acetate
MOR	Modulus of rupture	NR ₃	Amine
NMR	Nuclear magnetic resonance	[HTFSI]	bis(trifluoromethanesulfonyl)imide
OSB	Orientated strand board	[(CF ₃ SO ₂) ₂ N] ⁻	bis(trifluoromethanesulfonyl)imide
PB	Particle board		
PF	Phenol formaldehyde	[NTf ₂] ⁻	bis(trifluoromethanesulfonyl)imide
PIL	Protic ionic liquid		
PS	Plasticised starch	[AlBr ₄] ⁻	Bromoaluminate
PVA/PVOH	Polyvinyl alcohol	[HA]	Brønsted acid
PFG	Pulsed field gradient	[AlCl ₄] ⁻	Chloroaluminate
PGSE	Pulsed gradient spin echo	ChCl	Choline chloride
PGSTE	Pulsed gradient stimulated echo	DIMCARB	dimethylammonium dimethyl carbamate
QAS	Quaternary ammonium salt	DMF	Dimethylformamide
RA	Relative area	DMDHEU	Dimethyloldihydroxyethyleneurea
RPM	Revolutions per minute	DMSO	Dimethylsulfoxide
TGA	Thermogravimetric analysis	[EtNH ₃] ⁺	Ethylammonium
TPS	Thermoplastic starch	GA	Glutaraldehyde
TS	Thickness swelling	R'X	Haloalkane
3D	Three dimensional	[PF ₆] ⁻	Hexafluorophosphate
TEF	Total emitted formaldehyde	HBD	Hydrogen bond donor
UTS	Ultimate tensile strength	[HSO ₄] ⁻	Hydrosulfate
UHV	Ultrahigh vacuum	OH	Hydroxyl
UF	Urea formaldehyde	MX _y	Lewis acid
VDW	Van der Waals	MUF	Melamine urea formaldehyde
VFT	Vogel-Tammann-Fulcher model	[MA]	Metal salt
VOC	Volatile organic compound	MeNH ₂	Methylamine
WHO	World health organisation	NMA	N-methylol acrylamide
		[NO ₃] ⁻	Nitrate
		[N _{abcd}] ⁺	Quaternary ammonium
		[SO ₄] ²⁻	Sulphate
		[BF ₄] ⁻	Tetrafluoroborate

$[(C_8H_{17})(C_4H_9)_3N]^+$	Tributyloctyl ammonium
$[CF_3SO_3]^-$	Triflate
$[CF_3CO_2]^-$	Trifluoroacetate
$[(CH_3)_3S]^+$	Trimethyl sulfonium

Table of contents

Abstract	II
Publications	III
Statement	IV
Acknowledgements	V
Abbreviations	VII
Table of contents	XI
1. Introduction to Ionic Liquids and Deep Eutectic Solvents	1
1.1. Introduction.....	2
1.2. History of Ionic Liquids.....	2
1.3. Components of Ionic Liquids	3
1.4. Synthesis	4
1.5. Physical Properties.....	7
1.5.1. Melting Point	7
1.5.2. Decomposition Temperature.....	8
1.5.3. Vapour Pressure.....	8
1.5.4. Density	9
1.5.5. Viscosity	9
1.5.6. Solubility in Ionic Liquids	10
1.5.7. Ionic Conductivity	11
1.6. Applications	12
1.7. Deep Eutectic Solvents	14
1.7.1. Synthesis and Phase Behaviour of DESs.....	14
1.7.2. Applications of DESs.....	18
1.7.3. Use of Organic Salts in DESs	20
1.8. Aims.....	20
1.9. References.....	21
2. Experimental	29
2.1. Introduction.....	31
2.2. Chemicals and Materials.....	31
2.2.1. Chemicals.....	31
2.2.2. Materials	32
2.3. Preparation of Ionic Solutions	32

2.3.1.	Synthesis of solutions	32
2.3.2.	Inorganic ionic solutions.....	32
2.3.3.	Deep Eutectic Solvents	33
2.3.4.	Copper Solutions in Ionic Solvents	33
2.4.	Physical Properties.....	33
2.4.1.	Viscosity	33
2.4.2.	Conductivity.....	34
2.4.3.	Density	34
2.4.4.	Surface Tension	34
2.4.5.	Infrared Spectroscopy	34
2.4.6.	Nuclear Magnetic Resonance Spectroscopy.....	35
2.5.	Thermal properties.....	36
2.5.1.	Differential Scanning Calorimetry.....	36
2.5.2.	Thermogravimetric Analysis	36
2.6.	Electrochemical Measurements	36
2.6.1.	Voltammetry	37
2.6.2.	Bulk Deposition	37
2.6.3.	Electropolishing of Stainless Steel	38
2.7.	Surface Analysis	38
2.7.1.	Scanning Electron Microscopy and Energy-Dispersive X-Ray Spectroscopy	38
2.7.2.	3D Microscopy	39
2.7.3.	Microscopy	39
2.8.	Preparation of Thermoplastic Starch	39
2.9.	Preparation of Resinated Wood Fibre.....	39
2.9.1.	Large Scale Preparation of Plasticiser	39
2.9.2.	In-house Resination Process	40
2.9.3.	Aspirator Resination Process	40
2.10.	Preparation of Fibreboards.....	42
2.10.1.	9 x 9 x 1.5 cm Fibreboards	42
2.10.2.	1 m x 1 m Fibreboards.....	42
2.11.	Fibreboard Analysis.....	43
2.11.1.	Density	43
2.11.2.	Tensile Stress Testing.....	43

2.11.3.	Differential Scanning Calorimetry	44
2.12.	References.....	44
3.	Physical Properties of Novel Ionic Solvents.....	45
3.1.	Introduction.....	46
3.1.1.	Glycerol	46
3.1.2.	Use of Glycerol in Deep Eutectic Solvents	48
3.1.3.	Aims.....	49
3.2.	Component Selection.....	50
3.3.	Thermophysical Properties of Novel Ionic Solvents	52
3.3.1.	Phase Behaviour	53
3.3.2.	Density	57
3.3.3.	Surface Tension and Free Volume.....	58
3.3.4.	Viscosity	62
3.3.5.	Fluid Behaviour	72
3.3.6.	Ionic Conductivity	74
3.3.7.	Molar Conductivity.....	79
3.4.	Application of Walden's Rule	83
3.5.	Future Developments.....	88
3.6.	Conclusions.....	90
3.7.	References.....	91
4.	Diffusion Studies and Electrochemical Properties of DES Derived from Inorganic Salts	97
4.1.	Introduction.....	98
4.1.1.	NMR Techniques.....	99
4.1.2.	Aims.....	103
4.2.	Dynamics and Diffusion Investigations Using PFG NMR.....	104
4.2.1.	Self-Diffusion Studies.....	105
4.2.2.	NMR T ₁ Relaxation studies	112
4.2.3.	Conclusions.....	117
4.3.	Diffusion Studies of Solutes in Sodium Salt:Glycerol Mixtures by Electrochemical Methods	118
4.3.1.	Introduction.....	118
4.3.2.	Aims.....	123

4.3.3.	Electrochemical Windows of Sodium Salt:Glycerol mixtures	124
4.3.4.	Redox Behaviour of Copper in Sodium Salt:Glycerol Mixtures..	126
4.3.5.	Future Work	135
4.3.6.	Conclusions	136
4.4.	References	137
5.	Application of Novel Ionic Solvents as Modifiers for Bio-composite Materials	143
5.1.	Introduction	144
5.1.1.	Engineered Wood	144
5.1.2.	Synthetic Adhesives	146
5.1.3.	Thermoplastic Starch Adhesives	153
5.1.4.	Aims	157
5.2.	Preparation of Plasticised Starches	158
5.2.1.	Choice of Ionic Solvent	158
5.2.2.	Thermal Properties of Plasticised Starch	160
5.2.3.	Mechanical Properties of Plasticised Starch	161
5.3.	Plasticised Starch as a Binder for Fibreboards	168
5.3.1.	Effect of Ionic Solvent on Structure	169
5.3.2.	Effect of Ionic Solvent on mechanical properties	171
5.3.3.	Effect of Ionic solvent on Thermal properties	192
5.3.4.	Pilot Scale production Medium Density Fibreboard	195
5.4.	Future Developments	196
5.5.	Conclusions	198
5.6.	References	199
6.	Conclusions and Future Work	206
6.1.	Conclusions	207
6.2.	Future Work	211
7.	Appendices	213
7.1.	Appendix A	214
7.2.	Appendix B	230
7.3.	Appendix C	235

1. Introduction to Ionic Liquids and Deep Eutectic Solvents

1.1. Introduction	2
1.2. History of Ionic Liquids	2
1.3. Components of Ionic Liquids	3
1.4. Synthesis.....	4
1.5. Physical Properties	7
1.5.1. Melting Point.....	7
1.5.2. Decomposition Temperature	8
1.5.3. Vapour Pressure	8
1.5.4. Density.....	9
1.5.5. Viscosity.....	9
1.5.6. Solubility in Ionic Liquids.....	10
1.5.7. Ionic Conductivity.....	11
1.6. Applications.....	12
1.7. Deep Eutectic Solvents.....	14
1.7.1. Synthesis and Phase Behaviour of DESs	14
1.7.2. Applications of DESs	18
1.7.3. Use of Organic Salts in DESs.....	20
1.8. References	21

1.1. Introduction

Solvents are fundamental to most areas of chemistry including: synthetic, analytical, pharmaceutical, food and flavour chemistry, and the materials and coating industries.¹ Utilising a solvent as a reaction medium allows control of reaction conditions including: pressure, pH, temperature, concentration and kinetics.¹ For most solution-phase processes the solvent is typically present in ten times higher concentration than the solute.¹ Water is the most common solvent as it is cheap, readily available, easily purified and able to dissolve a wide range of solutes.² However, some substances are not soluble or can react with water, and some reactions are not possible in water due to solvent effects.² Any water that is used in a process must always be returned to the watercourse, which can require extensive decontamination procedures that add cost to any process.²

Non-aqueous solvents have been investigated over the last 60 years that combat many of the issues associated with water as a solvent, but many of the molecular solvents used are problematic to human health and the environment, which has initiated efforts to design benign media for chemical processes.³ Over the last decade, research into the use of alternative solvents including: supercritical fluids, renewable solvents and tuneable solvent systems has grown significantly.¹ Researchers have investigated the idea of *solvent free* chemistry, where reaction systems utilise a system component as the mobile phase, but this approach to chemistry provides its own unique issues.⁴

Ionic liquids (ILs) are a particular solvent class that has gained significant interest over the last 20 years.⁵ ILs are salts with relatively low and sometimes ambient melting temperatures.⁶ ILs have a range of properties that are preferential for their use as reaction media.^{5,7} ILs have nominal vapour pressure, which allows distillation of volatile reaction products, and the thermal stability allows utilisation over a wide temperature range.⁸ Typically, at least one of the ionic components is organic, which in the majority of cases it is the cation.⁹ Careful choice of the ionic components allows the physical properties ILs to be fine-tuned for a specific purpose.^{3,9,10}

1.2. History of Ionic Liquids

Although ILs are a fast growing research area, they were first documented in 1914 with the first example being [EtNH₃][NO₃], which has a melting point of 12 °C.¹¹ The next significant studies in ILs were in the early 1960s with the advent of

chloroaluminates: mixtures of alkali halides and aluminium chloride, which were prepared as alternatives to LiCl/KCl thermal batteries.¹¹ Mixtures of NaCl/AlCl₃ have been reported to have a melting point of 107 °C, compared the LiCl/KCl eutectic mixture that has a melting temperature of 355 °C.¹¹ Developments in the area led to chloroaluminate salts based on pyridinium/imidazolium cations, which showed greater stability compared to the alkali halide systems.¹² 1-ethyl-3-methylimidazolium (EMIM) chloride mixed with AlCl₃ forms a liquid with a freezing point well below room temperature for a range of compositions and showing excellent solvent properties.^{11,13} Unfortunately, pyridinium/imidazolium chloroaluminates suffered from water sensitivity, and in the early 1990s research began on ILs derived from imidazolium cations coupled to water stable anions.⁵ Anions including tetrafluoroborate [BF₄]⁻, hexafluorophosphate [PF₆]⁻, nitrate [NO₃]⁻, sulphate [SO₄]²⁻ and acetate [OAc]⁻ have shown to be stable at room temperature towards hydrolysis.¹⁴

Protic ionic liquids (PILs) are a subset of ILs that are the adduct of a Brønsted acid and Brønsted base, which are liquids at ambient temperatures.¹⁵ The Watanabe group reported the development of Brønsted acid-base ILs from the addition of amines to bis(trifluoromethane sulfonyl) amide (HTFSI), and found many of the acid-base adducts were liquids at temperatures less than 100 °C.¹⁶ PILs can be prepared using many of the cationic species found in aprotic ILs but most importantly, the synthesis mechanism involves proton transfer from the Brønsted acid to the Brønsted base.¹⁵

There is an almost limitless combination of anions and cations that form ILs and the concept being adopted is to design a specific liquid with optimal properties for the application rather than choosing from a limited number of available solvents.¹⁷

1.3. Components of Ionic Liquids

There are countless cation and anion combinations that can form ILs, therefore it is simpler to categorise ILs by the cationic species, as shown in Figure 1.1.¹⁷ Protonation of a suitable: phosphine, sulphide, imidazole, amine or pyridine is the simplest method of for the formation of the desired cationic species in ILs.¹⁷ However, decomposition via deprotonation has restricted the use of such cationic species.¹⁷ Therefore, most ILs are formed from cations, which have R groups that are generally alkyl chains, as shown in Figure 1.1.¹⁸ The most common class cationic species in ILs are the N,N-dialkylimidazolium salts, of which, the 1-butyl-3-methylimidazolium (BMIM) and EMIM cations are the most generally studied.¹⁷ Although

alkylimidazolium salts are the most commonly investigated, they are also some of the most expensive ILs to produce with typical costs of € 25000-50000 per ton, whereas some ammonium based ILs can be produced for € 5000-15000 per ton.¹⁹

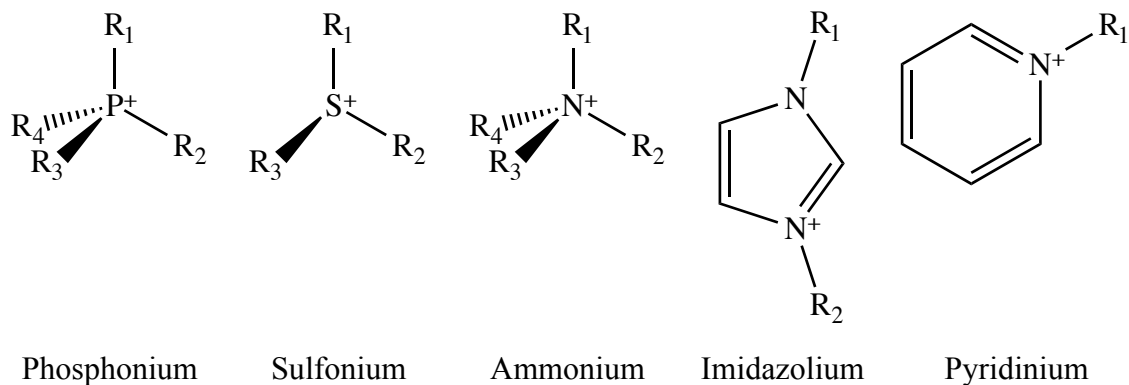


Figure 1.1 Categories of cations found in ILs

The cationic species used are generally very bulky and show high levels of asymmetry, whereas the anions are generally more symmetrical.¹⁷ Many anions are bulky inorganic species including: [BF₄]⁻, [PF₆]⁻, [NO₃]⁻, [SO₄]²⁻, [OAc]⁻ and [AlCl₄]⁻.¹⁴ Anions that are highly fluorinated such as bis(trifluoromethanesulfonyl)amide [(CF₃SO₂)₂N]⁻ appear to offer the lowest melting temperatures.²⁰ Although highly fluorinated anions allow significantly lower melting points, and improved stability, they are considerably more expensive than chloroaluminate or nitrate equivalents.²¹

1.4. Synthesis

The synthesis of ILs can be summarised into two parts, the formation of the preferred cation followed by anion exchange to provide the wanted product, as shown in the reaction scheme outlined in Figure 1.2.⁹ The reaction scheme in Figure 1.2 outline the general synthetic pathway for an ammonium salt based IL, but it is also applicable to all of the cationic species listed in Figure 1.1.⁹

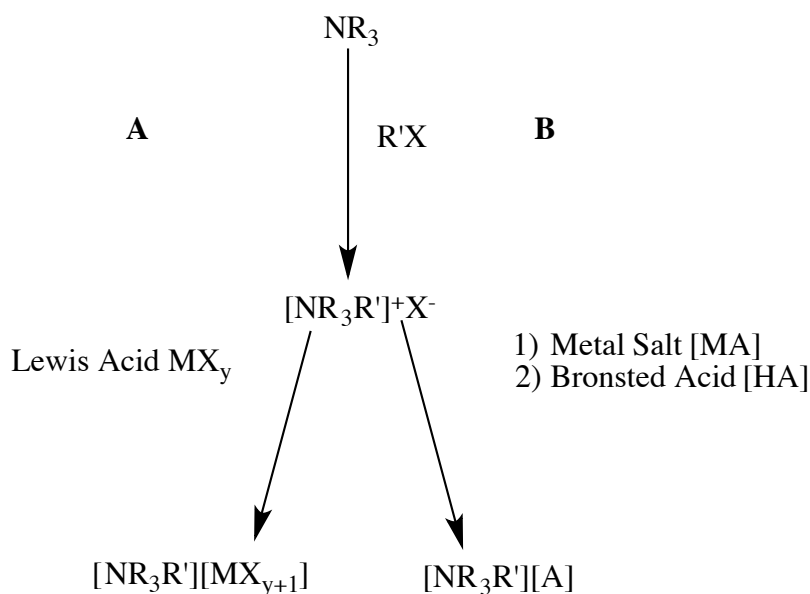


Figure 1.2 General synthetic pathways for ammonium salt based ILs: anion exchange pathway (A) and anion metathesis pathway (B)

The first part of IL synthesis is usually quaternisation of a pyridine, imidazole, phosphine, amine or sulfide utilising an alkylating agent such as a haloalkane.²² For some IL systems the quaternisation step is all that is required, as with the formation of ethylammonium nitrate from ethylamine and nitric acid.²³ The alkylation process has the advantages of a wide range of haloalkane starting chemicals, the substitution occurs easily at ambient temperatures, and the resulting halide salts are easily converted into the desired anion.¹⁷ The reaction mixture must be kept moisture free during the quaternisation process, as the products are generally hygroscopic.¹⁷

After the desired cation has been formed, there are two pathways for anion exchange: direct treatment with a Lewis acid, as shown in Figure 1.2 A, or via anion metathesis, as shown in Figure 1.2 B.¹⁷ The synthetic pathway outlined in Figure 1.2 A is dominated by the use of AlCl_3 , and generally leads to the formation of different anionic species depending on the Lewis acid mole fraction.^{24,25,26} When the halide salt is in molar excess over AlCl_3 , only one anionic species is observed and the IL is relatively basic, as shown by the equilibrium in equation 1.1.²⁷ When there is an excess of AlCl_3 , the IL becomes more acidic and the equilibria shown in equations 1.2 and 1.3 dominate giving rise to multiple anionic species.²⁷ The synthetic pathway outlined in Figure 1.2 A is not limited to the use of AlCl_3 , and ILs have been prepared in this way using BCl_3 , CuCl , and SnCl_2 .^{28,29,30} The formation of ILs using pathway outlined in Figure 1.2 A can be obtained simply by mixing the components together, but the process is

exothermic and care needs to be taken, as excess heat can result in decomposition.²⁷ The water sensitivity of chloroaluminate ILs means the synthesis process needs to be carried out in dry conditions in either in a dry-box, or under an unreactive alkane solvent.²⁷



The synthetic pathway outlined in Figure 1.2 B outlines the production of an IL by the addition of a metal salt or a Bronsted acid, which includes the desired anion.¹⁷ This method of IL synthesis was reported by Wilkes *et al.* with the metathesis reaction between [EMIM]I and a range of silver salts in aqueous solution, which formed insoluble silver iodide that could be easily filtered.³¹ The earliest reports of water insoluble ILs were for the preparation of [EMIM][PF₆] from [EMIM]Cl and HPF₆ in aqueous solution.³² Preparation of water-immiscible ILs is relatively straight forward as the by-products are easily removable by washing with water, whereas water-miscible ILs are more difficult to prepare as by-products are difficult to remove, unless an organic solvent system is employed.^{21,33} ILs prepared via this pathway will only have the one desired anionic species unlike ILs prepared through the pathway shown in Figure 1.2 A.¹⁷ However, anion metathesis methods generally result in impurities from remaining halide species, and due to relatively low vapour pressures, distillation methods used for the purification of conventional solvents are not applicable.¹⁷ As a consequence of impurity issues, distilled starting materials and solvents need to be used, which compromises the suitability of these systems being used on an industrial scale.³⁴

PILs are prepared through the proton transfer from a Brønsted acid to a Brønsted base, which can be improved by using stronger acids and/or bases due to greater driving forces for proton transfer.¹⁵ High purity starting materials are still required to avoid issues with impurities, but the proton transfer process does not result in formation of by-products when the correct reaction stoichiometry is used.¹⁵ Water is the most significant impurity, which strongly affects the physical properties of a PIL system, and its removal requires heating for several hours.¹⁵

1.5. Physical Properties

For any new material to be classified as technically useful, the chemical and physical properties must be well characterised such that processes and devices can be engineered efficiently.⁵ Conveniently, by selecting appropriate cations and anions, IL systems can be fine-tuned to suit a specific application. The characteristic ability to tune ILs to a specific application has led to ILs being branded as ‘designer solvents’.³⁵

1.5.1. Melting Point

ILs are defined as salts with melting points below 100 °C, therefore the melting point is one of the most defining properties of ILs.³⁶ It is well known that the charge distribution, structure and composition of the components in an IL impact strongly on its melting temperature and liquidus range.³⁶

Increasing the size of the anion results in a depression in the melting point through a disruption of the Coulombic interactions causing a decrease in the lattice energy.⁹ For the [EMIM] cation, changing the anion from Cl⁻ to NO₃⁻ results in a melting point change from 87 °C to 38 °C.²² Substituting the anion for a species that is highly fluorinated such as [CF₃CO₂]⁻ leads to a further melting point decrease to -14 °C.³⁷ It has been observed that highly fluorinated anions provide the greatest depression in melting point due to the greater delocalisation of charge.³⁸

The size and structure of the cation also plays a role in the melting point on an IL. Large cations with alkyl-shielded charge, such as tetraalkylammonium or phosphonium salts provide large depressions in melting point.⁹ Cation symmetry is also known to affect system melting point, as ions with higher symmetry have higher melting points due to more efficient ion packing in the crystal unit cell.³⁹ A reduction in cation symmetry leads to a distortion of charges in the crystal unit cell, which subsequently reduces the lattice energy and results in a decrease in melting temperature.³⁹ In imidazolium salts, substitutions on the imidazolium ring can both increase or decrease the melting temperature of the system by altering ion packing and aromatic stacking and methyl- π interactions between cations.³⁶ The melting point of the 1-alkyl-3-methylimidazolium tetrafluoroborate system was investigated as a function of the alkyl group chain length, and the melting point was found to decrease initially due to disruption of the lattice unit cell.⁴⁰ At alkyl chains greater than 10 carbon atoms, increases in melting point are observed, as van der Waals (VDW) interactions between the alkyl chains increase and contribute more to the local structure via the formation of

liquid crystalline phases.⁴⁰ Increasing the degree of alkyl chain branching in a 1-alkyl-3-methylimidazolium hexafluorophosphate system increases the melting point, which reflects the increase in packing efficiency due to the decrease in free rotation volume.⁴¹

1.5.2. Decomposition Temperature

The upper limit of the liquidus range of an IL is limited by the decomposition temperature of the system, as ILs are generally considered to be non-volatile.³⁶ Pyrolysis of ILs containing organic cations typically occurs over 350-450 °C, provided no other decomposition pathways are available for the system.⁴² The Grimmer group have studied the decomposition of imidazolium based ILs and found the degradation pathway to be the reverse of the reaction pathways used to form the ILs.⁴²

Research has shown IL stability is inversely proportional to the stability of the alkyl-anion species formed through the decomposition process, with decomposition temperature following the stability order: $\text{Cl}^- < [\text{BF}_4]^- < [\text{PF}_6]^- < [\text{NTf}_2]^-$.^{21,40,41,43} This stability trend suggests weakly coordinating anions provide the highest decomposition temperatures.³⁶

MacFarlane *et al.* have reported that determination of the degradation onset temperature via a step-tangent method, generally overestimates the thermal stability of ionic liquid compounds.^{44,45} Welton *et al.* have investigated the rate of thermal degradation of [EMIM][OAc] over long periods of time at temperatures below the onset of rapid thermal degradation.⁴⁶ The authors reported that even though the degradation temperature of [EMIM][OAc] was 214 °C, 1% thermal degradation was in less than 10 hours was observed at temperatures above 102 °C.⁴⁶ The authors analysed the degradation products and found Ionic liquids incorporating the acetate, octanoate or thioacetate anions decompose primarily via a $\text{S}_{\text{N}}2$ -type nucleophilic substitution mechanisms.⁴⁶

1.5.3. Vapour Pressure

ILs are generally reported to have nominal vapour pressures, which suggests it is possible to separate a reaction mixture from an IL solvent by distillation, as there is no azeotropic composition of the IL and the product.^{6,9} However, Seddon *et al.* showed that 1-ethyl-3-methylimidazolium bistriflamide [EMIM][(CF₃SO₂)₂N] and 1-decyl-3-methylimidazolium bistriflamide [DMIM][(CF₃SO₂)₂N] can be distilled at 300 °C with a pressure of 0.1 mbar, at a rate of 0.120 g h⁻¹ and 0.070 g h⁻¹ respectively.⁴⁷ Distillable

ILs have been developed based on mixtures of CO₂ and dialkylamines by mixing MeNH₂ with CO₂ in a ratio of 1.8:1, which yields dimethylammonium dimethyl carbamate (DIMCARB).^{12,13} During distillation, the IL breaks down into its dialkylamine and CO₂ components re-associates easily, with no permanent decomposition to the IL.^{12,13}

1.5.4. Density

The densities of ionic liquids generally vary from 1.12 g cm⁻³ for [(C₈H₁₇)(C₄H₉)₃N][(CF₃SO₂)₂N] to 2.4 g cm⁻³ for the 34 – 66 mol % [(CH₃)₃S]Br/AlBr₃ ionic liquid.^{48,49,50} System density is generally insensitive to variations in temperature, considering the 1:1 [EMIM]Cl/AlCl₃ system as an example, a 5 K change in temperature from 298 to 303 K results in a 0.3 % decrease in the density.²² Impurities also appear to have a nominal effect on system density when compared to impurity effects on system viscosity.^{36 51}

System density is heavily dependent on the size and structure of the ionic species.⁵² Generally, bulkier asymmetric cations give rise to lower densities, as steric bulk leads to poorer ion packing and greater molar volume compared to smaller symmetrical cations.⁴⁸⁻⁵⁰ Progressively increasing the imidazolium cation size in the presence of the triflate anion, resulted in a density decrease from 1.390 g cm⁻³ for the [EMIM] cation, to 1.270 g cm⁻³ for the 1-butyl-3-ethyl imidazolium [BEIM] cation.^{21,53} The anion usually contributes a greater effect than the cation, and increasing the anion mass generally results in an increase in system density.⁵⁴ Anion effects on density in haloaluminate systems can be observed by comparing [EMIM][AlBr₄] to [EMIM][AlCl₄], where the bromoaluminates are considerably more dense than the chloroaluminates.⁵⁵

1.5.5. Viscosity

The viscosity of a fluid is a consequence of internal friction that manifests itself as a resistance to flow.¹⁷ There are two general classes of fluid: Newtonian and non-Newtonian.³⁶ A Newtonian fluid has a viscosity that is independent of shear rate and is typically made from low molecular weight pure substances.³⁶ A non-Newtonian fluid has a viscosity that is dependent on shear rate, which are typically: polymers, colloidal suspensions and emulsions.⁵⁶ The concept of viscosity is discussed in more detail in

section 3.3.4. Historically, researchers have treated ILs as Newtonian fluids, as there was little data suggest non-Newtonian behaviour, but recent research suggests that some, but not all ILs, are non-Newtonian fluids.^{36,57,58}

Molecular solvents typically have viscosities of 1 – 20 cP, and ILs are generally more viscous than even the most viscous molecular solvents.⁵⁹ IL viscosities typically range from 8 cP, for the $[(\text{CH}_3)_3\text{S}][\text{HBr}_2]$ system, to in excess of 500 cP, for the $[(\text{C}_8\text{H}_{17})(\text{C}_4\text{H}_9)_3\text{N}][\text{TFSI}]$ system.^{17,48,49,60}

VDWs interaction strength and ability to form hydrogen bonding are the primary factors that contribute to the viscosity of an IL.²¹ Hydrogen bonding is the main interaction that contributes to the viscosity of the hydrophilic and chloroaluminate systems.³⁶ In chloroaluminate systems at low AlCl_3 mole fractions, viscosity is relatively high as there is greater hydrogen bonding between the cation and basic chloride anion.⁵² At higher AlCl_3 mole fractions, bulkier multi-nuclear anions form, as shown by the equilibria in equations 1.2 and 1.3, reducing the contributions from hydrogen bonding.^{61,62} In hydrophobic, highly fluorinated ILs, van der Waals interactions are the main contributor to viscosity, which can be seen when comparing $[\text{BMIM}][\text{CF}_3\text{SO}_3]$ with $[\text{BMIM}][\text{n-C}_4\text{F}_9\text{SO}_3]$, where viscosity increases from 90 cP to 373 cP at 25 °C.²¹

The size and shape of the cation also has a bearing on the viscosity of an IL, as cations with large, bulky side chains tend to have higher viscosities.²¹ Considering imidazolium based ILs, increasing the cation size from $[\text{EMIM}]$ to $[\text{BEIM}]$ in the presence of the trifluoroacetate anion increased the system viscosity from 35 cP to 89 cP.²¹

IL viscosity is sensitive to changes in temperature, the $[\text{BMIM}][\text{PF}_6]$ system for example, shows a 27 % viscosity increase by decreasing the system temperature from 25 to 20 °C.⁶³ Impurities are also known to have a drastic effect on the viscosity of an IL system, with chloride impurities up to 6 % increasing the viscosity of alkylimidazolium based ILs by 600 %.⁶⁴

1.5.6. Solubility in Ionic Liquids

ILs are a versatile solvent class, which can be developed as alternatives to organic solvents for: synthesis, liquid/liquid separations and electrochemical processes due to the distinctive properties that separate ILs from molecular solvents. ILs are generally considered to be polar solvents, with polarities similar to alcohols and polar, aprotic

solvents such as: dimethylsulfoxide (DMSO) and dimethylformamide (DMF).^{21,65,66,67} The polarity and the co-ordinating ability of an IL system can be varied depending on the components chosen.³⁶ IL miscibility with water can be varied from thorough miscibility to complete immiscibility by changing the system anion from Cl⁻ to [PF₆]⁻, and lipophilicity of an IL system can be tuned through cation substitution.³⁶ The solvent properties of an IL system are dependent on the H-bond donating, H-bond accepting abilities of the system components, and in aromatic ILs, the strength of CH₃ - π and π - π interactions.³⁶

Solubility of metal complexes in ILs depends on the system properties, but metal ions are generally more soluble in water than in ILs.³⁶ Metal compounds are sparingly soluble in ILs containing non-coordinating components, and ionic complexes tend to be more soluble than neutral complexes.^{68,69,70} Studies into the interactions of organic solutes with ILs have shown ILs with long alkyl side chains can act as low polarity phases, which interact strongly with non-polar solutes.⁷¹ Polar solutes containing proton donor functional groups have been shown to interact strongly with ILs, and solutes with weak proton acceptor/donor functional groups such as: aromatics, ketones and esters have shown to interact through ion-dipole or VDWs interactions.⁷¹

1.5.7. Ionic Conductivity

Most of the early research into ILs was dedicated to their development as electrochemical solvents, with one of the first reported applications for ILs was as an electrochemical solvent for the electrodeposition of aluminium.^{72,73} One would expect ILs to have high ionic conductivities, considering they are comprised primarily of ionic species. However, this is not the case and many ILs have conductivities that are comparable with non-aqueous electrolyte systems, with ionic conductivities up to approximately 20 mS cm⁻¹.⁷⁴ ILs are significantly less conductive than concentrated aqueous electrolytes, which can be linked to the reduction of free charge carrying species due to ion-pairing, and hindered ion mobility due to large ion sizes and high system viscosities.¹⁷ The temperature dependence of ionic conductivity in ILs is heavily dependent on the system temperature, for example, over the 375 – 275 K temperature range, [EMIM][BF₄] and [PMMIM][TFSI] decrease in ionic conductivity by factors of 10 and 30 respectively.⁷⁵ The temperature dependence of ionic conductivity in ILs involves complex long- and short-range interactions that are highly dependent on the components of the IL system, which makes accurate predictions of ionic conductivity

within an IL system not possible.⁷⁵ The concept of ionic conductivity is discussed in more detail in section 3.3.6.

1.6. Applications

ILs have been utilised in a wide variety of applications ranging from organic synthesis to transition metal catalysis and electrochemistry, to name but a few.^{76,77,78,79,80,81}

Utilisation of ILs in organic synthesis can be summarised by two key organic reactions: Diels-Alder and Friedel-Crafts.⁸² Ethylammonium nitrate was one of the first ILs recorded to be used in a Diels-Alder reaction between methyl acrylate and cyclopentadiene, as shown in Figure 1.3, and exhibited improved reaction kinetics compared to molecular solvents.⁷⁶ Welton *et al.* have used [EMIM] based ILs in the Diels-Alder reaction between methyl acrylate and cyclopentadiene, and found where faster reaction rates with better *endo:exo* selectivity compared to non-polar solvents, but still under performs compared to water.⁸³

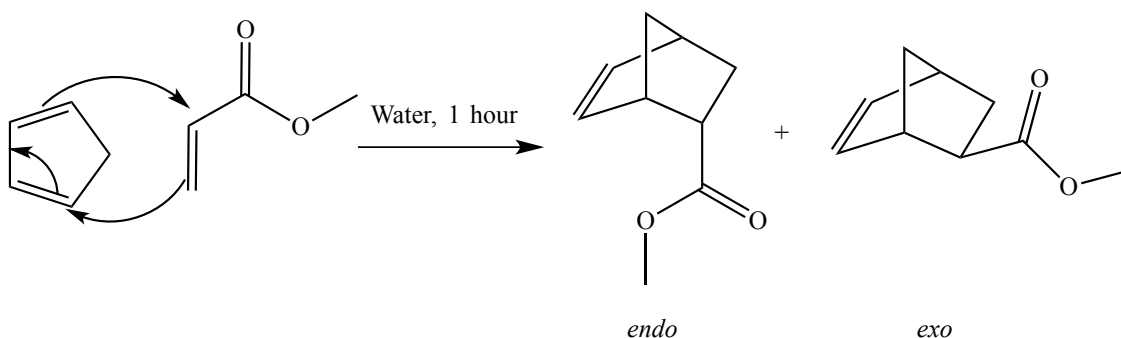


Figure 1.3 General reaction scheme for the Diels-Alder reaction

The Friedel-Crafts alkylation process is the reaction between an alkylation agent and an aromatic compound, of which the general reaction is shown in Figure 1.4. Fremantle *et al.* has shown that some chloroaluminate ILs can achieve conversions reaching 100% in as little as 30 seconds, whereas more than 6 hours are required to achieve 80 % conversion in organic solvents.³⁵ Keim *et al.* investigated alkylation of aromatic compounds in ILs, and found non-Lewis acidic ILs such as [BMIM][HSO₄] in conjunction with a sulphuric acid catalyst were capable of alkylating benzene with decene.⁸⁴ The same authors found the same acid-IL systems could also be used for esterification reactions.⁸⁴

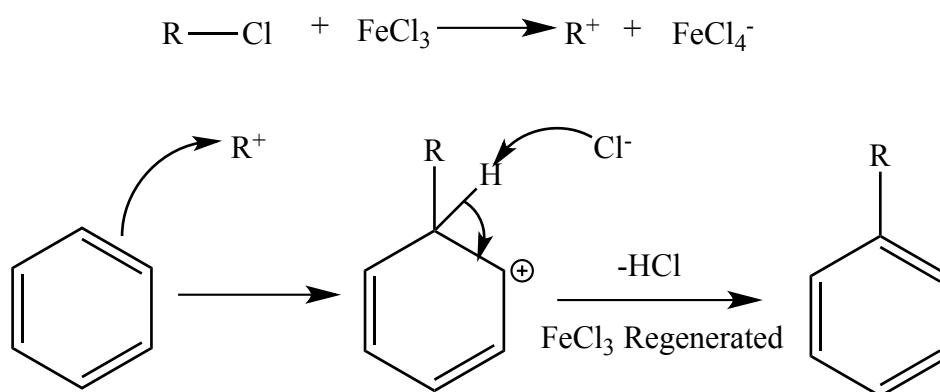


Figure 1.4 General reaction scheme for the Friedel-Crafts alkylation reaction

Transition metal complexes can be easily dissolved in ILs, and provide a versatile solvent system for homogeneous catalysis.⁸⁵ ILs were first tested as a solvent system for homogeneous catalysis in the platinum-catalysed hydroformylation of ethene using tetraethylammonium trichlorostannate.⁷⁹ ILs have been successfully employed in hydrogenation reactions by Chauvin and de Souza.^{78,86} De Souza used a rhodium-based catalyst in the hydrogenation of cyclohexene dissolved in [BMIM][BF₄], Chauvin however, used a range of [BMIM] based ILs to dissolve a rhodium catalyst to be utilised in the biphasic hydrogenation of 1-pentene.^{78,86}

Another widely investigated category of applications for ILs is in the realm of electrochemistry as ILs typically possess conductivities in the region of 1-10 mS cm⁻¹, which is comparable to many non-aqueous electrolyte systems.⁷⁶ Water and organic solvents require the addition of a background electrolyte to be able to pass an electric current. Most ILs have an electrochemical window of 2-4 V, which is much wider than some non-aqueous electrolyte systems, and allows ILs to be used in electrodeposition metals and semi-conductors.^{76,81}

Aluminium electrodeposition from chloroaluminate ILs has been investigated by many authors, and has been found to occur under acidic conditions, which yields deposits of greater quality compared to those achieved with organic solvents.^{87,88} Bulk aluminium deposits tend to look granular, but the addition of brighteners such as: toluene or benzene have been used to provide mirror-bright deposits.⁸⁹ Deposition of alloys of Al with Fe, Co, Ni, Cu and Ag have been investigated and found to exhibit complex electrodisolution.⁹⁰

Most of the metals that can be electrodeposited from aqueous solution can be deposited from ILs with the advantages of wider electrochemical windows, which limits

side processes during electrodeposition, access to higher temperatures, which can improve the kinetics of a process.⁹¹ Metals including: In, Sb, Te, Cd, Cu, Ag Ni, Co, Os, Au, Zn and Sn have been successfully electrodeposited from ILs onto a range of substrates.^{92,93,94,95,96,97,98,99,100,101,102}

Semiconductor electrodeposition has been conducted in aqueous, organic and IL media, but little research into the electrodeposition of compound semiconductors from ILs has been carried out.¹⁰³ GaAs, InSb, ZnTe and Ge compound semiconductors have been successfully electrodeposited from ILs.^{93, 104, 105, 106} Investigations into semiconductor materials require ultra-high vacuums (UHV), and ILs would be ideal due to the nominal vapour pressures of ILs resisting distillation at UHV.⁹¹ Kinetic barriers restrict the formation of many semiconductors, and most organic solvents would evaporate at the temperatures required to overcome the activation energies of the processes.⁹¹ ILs generally start to decompose at temperatures above 350 °C, thus potentially overcoming any activation energy barriers for semiconductor formation.⁹¹ However, studies into the slow thermal degradation of [EMIM][OAc] over long periods of time at temperatures below the onset of rapid thermal degradation have shown, 1% thermal degradation was in less than 10 hours was observed at temperatures 100 °C below the rapid onset degradation temperature⁴⁶

1.7. Deep Eutectic Solvents

ILs have some advantages over conventional solvents in a wide variety of applications, but ILs are not a solvent class without issues. The two main disadvantages of ILs are the cost of the starting materials and synthesis, and problems associated with sensitivity to impurities, especially water.¹⁰⁷ An alternative to ILs are Deep Eutectic Solvents (DESs), which are considered to be an extension of the IL model, and share many of the characteristics and physical properties.¹⁰⁷ DESs are a category of ionic solvents that are formed from a eutectic mixture of Brønsted or Lewis acids and bases, which contain a variety of anionic and cationic species, whereas ILs are systems that consist of one discrete cation and anion.¹⁰⁷

1.7.1. Synthesis and Phase Behaviour of DESs

DESs are formed via the complexation of an organic salt, typically a quaternary ammonium salt (QAS) with a: metal salt, metal salt hydrate or a hydrogen bond donor (HBD), referred to as type I, II and III DES respectively, as shown in Table 1.1.¹⁰⁷

Abbott *et al.* have shown DESs can also be prepared by mixing metal salt hydrates with HBDs to form type IV DESs, also shown in Table 1.1.¹⁰⁷ The general formulae of all four types of DES are presented in Table 1.2. Charge delocalization that follows complexation occurs between the organic salt anion and the HBD species, which lowers the lattice energy of the organic salt.¹⁰⁷ The reduction in lattice energy results in a decrease in the melting point of the mixture relative to that of the individual components.⁷⁷

Table 1.1 Categories of DESs

Type I	Organic salt + metal salt
Type II	Organic salt + metal salt hydrate
Type III	Organic salt + hydrogen-bond donor
Type IV	Metal salt + hydrogen-bond donor

Table 1.2 General formulae of DESs¹⁰⁷

Type	General formula	Terms
Type I	$\text{Cat}^+\text{X}^-\cdot z\text{MCl}_x$	M = Zn, Sn, Fe, Al
Type II	$\text{Cat}^+\text{X}^-\cdot z\text{MCl}_x\cdot y\text{H}_2\text{O}$	M = Cr, Co, Cu, Ni, Fe
Type III	$\text{Cat}^+\text{X}^-\cdot z\text{RZ}$	Z = COOH, CONH ₂ , OH
Type IV	$\text{MCl}_{x-1}^+\cdot\text{RZ} + \text{MCl}_{x+1}^+$	M = Al, Zn, Cr Z = CONH ₂ , OH

Type I DESs are systems that comprise of metal halides, such as ZnCl₂, mixed with an organic salt, typically a QAS.^{77,108,109,110} A variety of metal halides including: SnCl₂, ZnCl₂ and FeCl₃ have been mixed with ChCl in a 1:2 respective molar ratio, and all were found to form mixtures, which have freezing points below 100 °C¹⁰⁸⁻¹¹⁰ The freezing temperature of a Type I DES system is dependent on the metal species in the system at a given concentration ratio.¹⁰⁸⁻¹¹⁰ Considering the ZnCl₂: ChCl DES system as an example, at low concentrations of ZnCl₂, the amount of ZnCl₃⁻ is high, and as the molar ratio of ZnCl₂ increases, the larger Zn₂Cl₅⁻ species becomes more prevalent, and the concentration of ZnCl₃⁻ decreases.¹¹¹ The prevalence of the Zn₂Cl₅⁻ species results in weaker electrostatic interactions with the chloride anion, which decreases the lattice energy of the system resulting in a decrease in the freezing temperature.¹¹¹ Upon further

addition of ZnCl_2 an increase in the freezing point observed due to the formation of the Lewis basic Zn_3Cl_7^- anion.¹¹¹ Type I DESs are comparable to the chloroaluminate-imidazolium salt melts and ILs formed with imidazolium salts and various metal halides including: AgCl , CuCl , LiCl , CdCl_2 , CuCl_2 , SnCl_2 , ZnCl_2 , LaCl_3 , YCl_3 , and SnCl_4 .^{112,113} However, the range of anhydrous metal halides which have a suitably low melting point to form type I DESs is limited.¹⁰⁷

Type II DESs substitute the anhydrous metal salt with a metal salt hydrate as the anionic component, which allows access to a wider range of metal salt systems, and removes problems with moisture sensitivity and the necessity for dryness.³⁸ Type II DESs do not require the IL synthesis methods, which in conjunction with moisture insensitivity, potentially enables their use in large scale industrial applications.³⁸ $\text{CrCl}_3 \cdot 6\text{H}_2\text{O}$ can be mixed with ChCl to form a type II DES, but it is not possible to form a DES with anhydrous CrCl_3 even if 6 molar equivalents of H_2O are added, which indicates the hydrate waters are part of the Cr speciation.¹¹⁴ Type I and type II DESs do not solely interact through ionic interactions, but through the formation of a hydrogen-bonding interaction between the quaternary ammonium salt and metal salt.¹⁰⁷ In contrast, ILs network through ionic interactions, therefore type I and type II DESs cannot be truly regarded as ILs.¹⁰⁷

Type III DESs are eutectic mixtures of an organic salt with a HBD including: polycarboxylic acids, polyamides and polyalcohols, which are simple to prepare, and unreactive with water, and many systems being low cost and biodegradable.^{115,116,117} One of the first type III DES systems to be studied involved ChCl and urea in a 1:2 respective molar ratio, which had a freezing temperature of 12°C .¹¹⁵ Abbott *et al.* have used phenolic dicarboxylic acids to form DESs with ChCl and demonstrated a 2:1 respective molar ratio for the eutectic composition as observed for the ChCl : urea DES system, which indicates that 2 carboxylic acid molecules complex with the chloride ion.¹¹⁶ Monocarboxylic acids were also tested in the studies by the Abbott group, but found DES formation was not possible in many cases.¹¹⁶ In general, the freezing point of a type DES is dependent on: the magnitudes of the lattice energies of organic salt and the HBD, and also the interaction between that anion and the HBD.¹¹⁵⁻¹¹⁷ A strong anion-HBD interaction results in a weaker interaction between the cation and the anion of the organic salt, which gives rise to a more disordered system, thus a lower freezing point.¹¹⁵⁻¹¹⁷

Type IV DESs use a metal salt hydrate as a replacement for the organic salts used in the type I, II and III DESs, where the HBD complexes to the anion, thus extracting them from the metal centres.¹⁰⁷ Early investigations into type IV DESs by the Abbott group studied ZnCl_2 with HBDs including: acetamide, 1,6-hexanediol, urea and 1,2-ethanediol, and found the eutectic composition was dependent on: the strength and size of the HBD species and the metal halide species.¹¹⁸ Abbott *et al.* have built upon the initial studies with ZnCl_2 , and have shown that a range of transition metals can be incorporated into ambient temperature eutectic mixtures.¹¹⁶ $\text{CrCl}_3 \cdot 6\text{H}_2\text{O}$ has been shown to form a type IV DES when complexed with: urea, glycerol or ethylene glycol, and were found to be liquid at room temperature when combined in a 2:1 respective molar ratio.¹¹⁹

The term DES originates from the eutectic behaviour of this class of ionic solvent, where the two components are mixed together results in a depression in the freezing temperature of the system, as shown in Figure 1.5.¹⁰⁷ The difference between the freezing temperatures of the eutectic composition of a two-component system compared to the theoretical freezing temperature of the ideal mixture is dependent on the strength of the interactions between the two components.¹¹⁶ Strong interactions result in larger deviations from the ideal freezing temperature, whereas weak interactions result in less pronounced deviations from ideality.¹⁰⁷

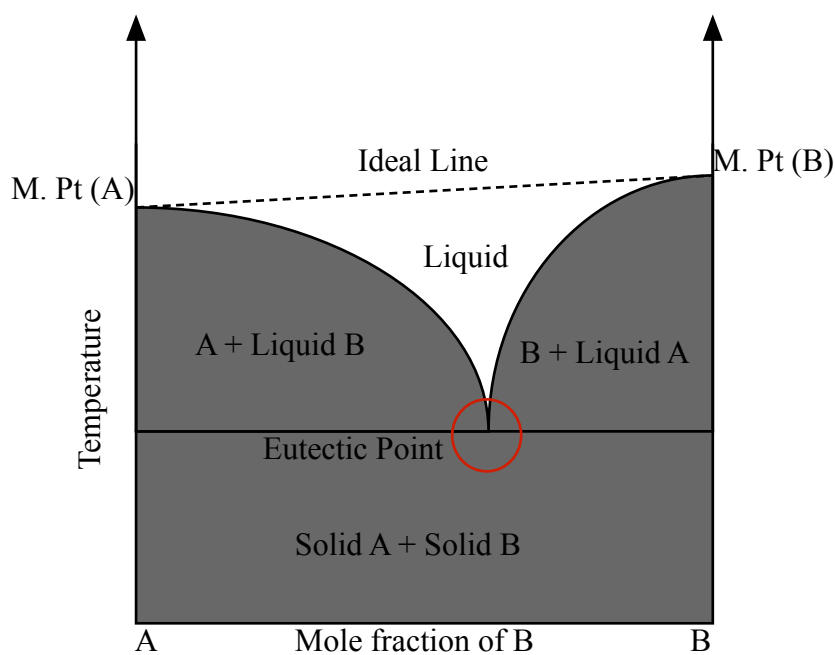


Figure 1.5 Typical freezing point behaviour of DESs

The interactions between metal halides and the halide anion from a QAS in type I DES systems form halometallate species with comparable enthalpies of formation, which implies depressions in freezing temperature are between 200 and 300 °C.¹⁰⁷ For type I DESs to be liquid at ambient temperatures the metal halide needs to have a melting temperature of approximately 300 °C or less.¹⁰⁷ This phenomenon is observed for: AlCl₃, FeCl₃, SnCl₂, ZnCl₂ and GaCl₃, which have melting temperatures of: 193, 308, 247, 290 and 78 °C respectively.^{52,112,113,120} The same rationale can also be extended to the organic salt where large, asymmetrical cations have lower melting temperatures, and therefore lead to lower melting point DESs.¹⁰⁷ This phenomenon is observed when comparing large, asymmetrical QAS cations such as [N₉₆₄₁]⁺ with symmetrical analogues such as [N₅₅₅₅]⁺, which have melting temperatures of below 20 °C, and 101 °C respectively, and show superior phase behaviour compared to ChCl, with a melting temperature of 301 °C.^{36,107}

Metal halide hydrates have melting points lower than the anhydrous analogue, which results in a smaller depression in freezing point when combined with an organic salt.¹⁰⁷ This occurrence is due to salts with lower melting temperatures, and therefore lower lattice energies, having smaller interactions with the anion of the organic salt.¹⁰⁷ The only system fully described thus far is the CrCl₃·6H₂O: ChCl DES, although others systems including: CaCl₂·6H₂O, MgCl₂·6H₂O, CoCl₂·6H₂O, LaCl₃·6H₂O, and CuCl₂·2H₂O are described in the patent literature.¹⁰⁸⁻¹¹⁰ The eutectic behaviour of type III DESs is dependent on the formation of hydrogen bonds between the anion of the salt and the HBD.¹⁰⁷ HBDs that are multifunctional tend to show eutectic compositions near a 1:1 molar ratio of organic salt and HBD.¹¹⁶

1.7.2. Applications of DESs

DESs have been trialled in a wide range of applications including: lubrication of steel/steel contacts, alternative electrolyte to water and organic solvents for the study of conducting polymers, use in analytical devices, drug solubilisation vehicles, electrolyte for dye-sensitized solar cells, and the synthesis of carbon electrodes for capacitors.^{121,122,123,124,125,126,127} Research has been focused on replacement solvents for metal finishing applications, although in recent years investigations into DESs as alternative solvents for organic synthesis have also increased.¹⁰⁷

The most significant applications of DESs involve the incorporation of metal ions in solution for metal deposition, metal dissolution, or metal processing.¹⁰⁷ Utilisation of DESs allows: high solubility of metal salts, without the limiting chemistry of water, and obtain higher ionic conductivities compared to organic solvents.¹⁰⁷ A range of metal reduction processes have been studied in DESs including: Zn, Sn, Cu, Ni, Ag, Cr, Al, Co, and Sm.^{119,128,129,130,131,132,133} Metal deposits have been achieved under current density-limited and potential-limited regimes, and the morphology and adhesion of metal deposit have been found to be dependent on current density, as observed in aqueous electrolytes.¹⁰⁷ The Abbott group have reported Zn–Sn alloy have been deposited onto mild steel substrates using ChCl: ethylene glycol, or ChCl: urea DESs, and shown Zn and Sn can be electrodeposited individually.¹³⁴ Stainless steel can be electropolished using a ChCl: ethylene glycol DES.¹⁰⁷ The acidic solutions typically used electropolishing show a passivation response at 1.3 V, which is followed by a polishing response between 1.5 and 1.6 V.¹³⁵ The ChCl: ethylene glycol DES showed no passivation response suggesting the dissolution process activation controlled, and found that a passive oxide film did not develop at large over-potentials, allowing the efficient electrodisolution of the stainless steel.¹³⁵ Abbott *et al.* have shown that a highly polished surface can be obtained with current densities between 50 and 70 mA cm⁻² at 40 °C, with a current efficiency of 92 %.¹³⁵ The solubilities of metal oxides have been investigated in a range of DESs, and type III DESs have been shown to dissolve a wide range of metal oxides.¹³⁶ Ligands including: urea, thiourea, and oxalate are well-known complexants for a variety of metals and can be made part of a DES, and allow metals to be separated from a complex mixture using electrochemistry.¹³⁷ Abbott *et al.* have demonstrated iodine can be used as a reversible electro- catalyst for the dissolution of a range of metals, as the redox potential of I₂/I⁻ in a ChCl: ethylene glycol DES is more positive than that of most common metals, and has been shown to oxidise and allow recovery of gold.¹⁰⁷ A ChCl: ethylene glycol: urea type III DES has been trialled in the extraction of lead and zinc from electric arc furnace dust, showing selectivity towards zinc and lead oxides, although the process was not economically viable due to lead and zinc being relatively inexpensive metals.¹³⁸ Type III DESs including: ChCl: urea and ChCl: malonic acid have been trialled for pilot scale metal extraction, and have shown to be effective in the removal of copper oxides and fluorides from etching process residues.^{139,140}

1.7.3. Use of Organic Salts in DESs

The most common organic salts used in preparing DESs are QASs, of which ChCl is the most commonly studied QAS, as shown in Figure 1.6.¹⁰⁷ When mixed with most metal halides or HBDs, the resulting eutectic mixtures demonstrated much improved physical properties over the use of most other QASs.¹⁰⁷ The depression in freezing point was noted to be one of the largest with one of the lowest viscosities, due to the asymmetry and polar hydroxyl group of the choline cation.³⁸ ChCl is non-toxic, is also known as pro-vitamin B4 and has been used in chicken feed for many years.³⁸

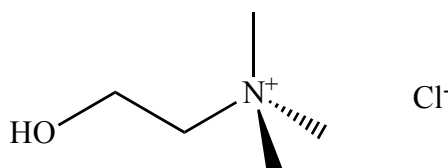


Figure 1.6 Structure of choline chloride, also referred to as hydroxyethyl trimethyl ammonium chloride

The use of QASs in DESs is limited to relatively small scale processes (c.a. 1 tonne) due to the cost of ChCl steadily increasing and now typically between 5-15 \$ kg⁻¹, which makes use of DESs more expensive than some conventional solvents, although in some applications such as metal deposition where the cost of the metal salt is the major factor this can be insignificant. Substituting the organic salts typically used in DESs with a metal salt that can be mined directly would significantly reduce the cost of a DES system. Type IV DESs are an alternative to the DES systems that utilise an organic salt, however studies into have mostly been limited to using hydrated salts of transition metal for use in metal processing applications.¹⁰⁷ Expansion of the type IV DES model to include metal salts, which are inexpensive and relatively redox inactive is required to make DESs more applicable in processes beyond laboratory scale.

1.8. Aims

The aim of this project was to expand the DES model to include alkali metal salts, which were investigated by studying the thermophysical properties including: electrical conductance, density and viscosity of concentrated alkali metal salt:glycerol mixtures. From understanding the thermophysical properties, an insight into the structures occurring in solution could be obtained, and investigations into mass and charge transport mechanisms could be conducted. It was hypothesised that by replacing the

bulky organic cations commonly found in DESs and ILs with small alkali metal cations, comparable trends in physical properties, ion speciation and ion transport properties could be achieved.

Investigations into the thermophysical properties could only provide a partial insight into species structure, and the role of water in ion mobility in non-aqueous ionic systems. Pulse field gradient nuclear magnetic resonance (PFG NMR) techniques were used to provide an insight into the diffusion regimes present in these systems as a function of temperature. The details gained from PFG NMR experiments were used to further explain the macroscopic thermophysical properties of sodium salt:glycerol systems, and explain deviations from ideal mechanisms. Voltammetric techniques were used to probe the diffusion and mobility of electroactive species dissolved in sodium salt:glycerol mixtures, and were cross-referenced with the self-diffusion behaviour observed for the background sodium salt:glycerol systems using PFG NMR. Sodium salt:glycerol mixtures were hypothesised to follow similar ion speciation and ion transport regimes to what was observed in DESs and ILs.

DESs and ILs have previously been shown to effectively plasticise starch providing a versatile thermoplastic material, which have been successfully trialled as novel formaldehyde-free binders for medium density fibreboard (MDF). Utilisation of inorganic salts as part of a DES binder system were conjectured to provide a sustainable method of: reducing free formaldehyde and other volatile organic compound (VOC) emissions, improving biodegradability and recyclability, and minimising the need for petroleum derived binders of engineered woods. The final aim was to develop a suitable binder system that could be easily integrated into the current infrastructure, which was tested by running pilot scale trials of MDF production.

The aims of each aspect of the work discussed in this thesis are presented in more detail at the beginning of each thesis chapter.

1.9. References

-
- ¹ F. M. Kerton, *Alternative Solvents for Green Chemistry*, RSC Publishing, Cambridge, 2009, Ch 1, 1
 - ² F. M. Kerton, *Alternative Solvents for Green Chemistry*, RSC Publishing, Cambridge, 2009, Ch 3, 44
 - ³ K. Izutsu, *Electrochemistry in Non-aqueous Solutions*, Wiley-VCH, Weinheim, 2002

-
- ⁴ F. M. Kerton, *Alternative Solvents for Green Chemistry*, RSC Publishing, Cambridge, 2009, Ch 2, 23
- ⁵ P. Wasserscheid and T. Welton, *Ionic Liquids in Synthesis*, Wiley-VCH, Weinheim, 2003, Ch 1, 1
- ⁶ T. Welton, *Chem. Rev.*, 1999, **8**, 2071
- ⁷ D. J. Adams, P. J. Dyson and S. J. Taverner, *Chemistry in Alternative Reaction Media*, John Wiley & Sons, Chichester, 2004
- ⁸ F. M. Kerton, *Alternative Solvents for Green Chemistry*, RSC Publishing, Cambridge, 2009, Ch 6, 118
- ⁹ P. Wasserscheid and W. Keim, *Angew. Chem. Int. Ed.* 2000, **39**, 3773
- ¹⁰ H. Ohno, *Electrochemical Aspects of Ionic Liquids*, Wiley-Interscience, New Jersey, 2005
- ¹¹ S. Sugden and H. Wilkins, *J. Chem. Soc.* 1929, 1291
- ¹² A. I. Bhatt and A. M. Bond, *J. Electroanal. Chem.*, 2008, **619**, 1
- ¹³ A. I. Bhatt, A. M. Bond and J. J. Zhang, *Solid State Electrochem.*, 2007, **11**, 1593
- ¹⁴ F. Hurley, *U.S. Patent*, 4 446 331, 1948
- ¹⁵ T. L. Greaves and C. J. Drummond. *Chem. Rev.* 2008, **108**, 206
- ¹⁶ M. A. B. H. Susan, A. Noda, S. Mitsushima and M. Watanabe, *Chem. Commun.*, 2003, 938
- ¹⁷ P. Wasserscheid and T. Welton, *Ionic Liquids in Synthesis*, Wiley-VCH, Weinheim, 2003, Ch 2, 7
- ¹⁸ R. M. Pagni, *Advances in Molten Salt Chemistry 6*, Elsevier, New York, 1987, 211
- ¹⁹ Alibaba, www.alibaba.com, (accessed August 2015)
- ²⁰ C. M. Forsyth, J. J. Golding, J. Huang, D. R. MacFarlane, M. Forsyth and J. Sun, *Chemistry of Materials*, 2002, **14**, 2103
- ²¹ P. Bonhôte, A. P. Dias, N. Papageorgiou, K. Kalyanasundaram and M. Grätzel, *Inorg. Chem.*, 1996, **35**, 1168
- ²² J. S. Wilkes, J. A. Levisky, R. A. Willson and C. L. Hussey, *Inorg. Chem.*, 1982, **21**, 1263
- ²³ D. F. Evans, A. Yamouchi, G. J. Wei and V. A. Bloomfield, *J. Phys. Chem.*, 1983, **87**, 3537
- ²⁴ M. Tinkl, *Chem. Rundschau*, 1999, **2**, 59
- ²⁵ N. Imizuka and T. Nakashima, *Japan Patent*, JP 002003478, 2002

-
- ²⁶ M. Schmidt, U. Heider, W. Geissler, N. Ignatyev and V. Hilarius, *European Patent*, EP 1162204, 2001
- ²⁷ H. A. Øye, M. Jagtoyen, T. Oksefjell and J. S. Wilkes, *Mater. Sci. Forum*, 1991, **73-75**, 183
- ²⁸ P. Bonnet, E. Lacroix and J. P. Schirmann, *International Patent*, WO 0181353, 2001,
- ²⁹ P. Wasserscheid, W. Keim, C. Bolm and A. Boesmann, *International Patent*, WO 0155060, 2001
- ³⁰ M. H. Valkenberg, E. Sauvage, C. P. De Castro-Moreira and W. F. Holderich, *International Patent*, WO 0132308, 2001
- ³¹ J. S. Wilkes and M. J. Zaworotko, *Chem. Commun.*, 1992, 965
- ³² J. Fuller, R. T. Carlin, H. C. DeLong and D. Haworth, *Chem. Commun.*, 1994, 299
- ³³ L. Cammarata, S. Kazarian, P. Slater and T. Welton, *Phys. Chem. Chem. Phys.*, 2001, **3**, 5192
- ³⁴ W. L. F. Armarego and D. D. Perrin, *Purification of Laboratory Chemicals*, Butterworth-Heinemann, Oxford, 4th Ed., 1997
- ³⁵ M. Fremantle, *Chem. Eng. News*, 1998, **76**, 32
- ³⁶ P. Wasserscheid and T. Welton, *Ionic Liquids in Synthesis*, Wiley-VCH, Weinheim, 2003, Ch 3, 41
- ³⁷ J. Caja, T. D. J. Dunstan, D. M. Ryan and V. Katovic, *Proceeding of the Twelfth International Symposium on Molten Salts*, The Electrochemical Society, New Jersey, 2000, **41-99**, 273
- ³⁸ R. C. Harris, Ph. D. Thesis, University of Leicester, 2008
- ³⁹ J. E. Gordon and G. N. SubbaRao, *J. Am. Chem. Soc.*, 1978, **100**, 7445
- ⁴⁰ J. D. Holbrey and K. R. Seddon, *J. Chem. Soc., Dalton Trans.*, 1999, 2133
- ⁴¹ H. L. Ngo, K. LeCompte, L. Hargens and A. B. McEwan, *Thermochim Acta*, 2000, **357-358**, 97
- ⁴² B. K. M. Chan, N.-H. Chang and M. R. Grimmett, *Aust. J. Chem.*, 1977, **30**, 2005
- ⁴³ J. G. Huddleston, A. E. Visser, W. M. Reichert, H. D. Willauer, G. A. Broker and R. D. Rogers, *Green Chem.*, 2001, 156
- ⁴⁴ K. J. Baranyai, G. B. Deacon, D. R. MacFarlane, J. M. Pringle and J. L. Scott, *Aust. J. Chem.*, 2004, **57**, 145.
- ⁴⁵ J. Wooster, K. M. Johanson, K. J. Fraser, D. R. MacFarlane and J. L. Scott, *Green Chem.*, 2006, **8**, 691

-
- ⁴⁶ M. T. Clough, K. Geyer, P. A. Hunt, J. Mertes and T. Welton, *Phys. Chem. Chem. Phys.*, 2013, **15**, 20480
- ⁴⁷ M. J. Earle, J. M. S. S. Esperanca, M. A. Gilea, J. N. Canongia Lopes, L. P. N. Rebelo, J. W. Magee, K. R. Seddon and J. A. Widegren, *Nature*, 2006, **439**, 831
- ⁴⁸ J. Sun, M. Forsyth and D. R. MacFarlane, *Molten Salt forum*, 1998, **5-6**, 585
- ⁴⁹ J. Sun, M. Forsyth and D. R. MacFarlane, *J. Phys. Chem. B.*, 1998, **102**, 8858
- ⁵⁰ H. Matsumoto, T. Matsuda and Y. miyazaki, *Chem. Lett.*, 2000, 1430
- ⁵¹ R. L. Perry, K. M. Jons, W. D. Scott, Q. Liao and C. L. Hussey, *J. Chem. Eng. Data*, 1995, **40**, 615
- ⁵² A. A. Fannin Jr., D. A. Floreani, L. A. King, J. S. Landers, B. J. Piersma, D. J. Stech, R. L. Vaughn, J. S. Wilkes and J. L. Williams, *J. Phys. Chem.* 1984, **88**, 2614
- ⁵³ E. I. Cooper and E. J. M. O'Sullivan, *Proceedings of the Eighth International Symposium on Molten Salts*, The Electrochemical Society, New Jersey, 2000, **92-16**, 386
- ⁵⁴ H. Stegemann, A. Rhode, A. Reiche, A. Schnittke and H. Fullbier, *Electrochim. Acta* 1992, **37**, 379
- ⁵⁵ J. R. Sanders, E. H. Ward and C. L. Hussey, *J. Electrochem. Soc.*, 1986, **133**, 325
- ⁵⁶ J. R. Van Wazer, J. W. Lyons, K. Y. Kim and R. E. Colwell, *Viscosity and Flow Measurement: A Laboratory Handbook of Rheology*, Wiley-Interscience, New Jersey, 1963
- ⁵⁷ M. Moosavi, A. Daneshvar, *Journal of Molecular Liquids*, 2014, **190**, 59
- ⁵⁸ J. A. Smith, G. B. Webber, G. G. Warr and R. Atkin, *J. Phys. Chem. B*, 2013, **117**, 13930
- ⁵⁹ D. R. Lide, *CRC Handbook of Chemistry and Physics*, CRC press, Florida, 89th Ed., 2008, Ch. 3
- ⁶⁰ M. Ma and K. E. Johnson, *Proceedings of the Ninth International Symposium on Molten Salts*, The Electrochemical Society, New Jersey, 1994, **94-13**, 179
- ⁶¹ C. J. Dymek, D. A. Grossie, A. V. Fratini and W. W. Adams, *J. Mol. Struct.*, 1989, **213**, 25
- ⁶² C. J. Dymek and J. J. Stewart, *Inorg. Chem.*, 1989, **28**, 1472
- ⁶³ S. N. Baker, G. A. Baker, M. A. Kane and F. V. Bright, *J. Phys. Chem. B.*, 2001, **105**, 9663
- ⁶⁴ K. R. Seddon, A. Stark and M. –J. Torres, *Pure Appl. Chem.*, 2000, **72**, 2275

-
- ⁶⁵ A. J. Carmichael and K. R. Seddon, *J. Phys. Chem.*, 2000, **13**, 591
- ⁶⁶ M. J. Muldoon, C. M. Gordon and I. R. Duncan, *J. Chem. Soc., Perkin Trans. 2*, 2001, 433
- ⁶⁷ S. N. V. K. Aki, J. F. Brennecke and A. Samanta, *Chem. Commun.*, 2001, 413
- ⁶⁸ Y. Chauvin, L. Mussmann and H. Oliver, *Angew. Chem. Int. Ed.*, 1996, **34**, 2698
- ⁶⁹ S. Einloft, F. K. Dietrich, R. F. Desouza and J. Dupont, *Polyhedron*, 1996, **15**, 3257
- ⁷⁰ P. J. Dyson, D. J. Ellis, D. G. Parker and T. Welton, *Chem. Commun.*, 1996, 25
- ⁷¹ D. W. Armstrong, L. He and Y. S. Lui, *Anal. Chem.*, 1999, **71**, 3873
- ⁷² F. H. Hurley and T. P. Weir, *J. Electrochem. Soc.*, 1951, **98**, 203
- ⁷³ F. H. Hurley and T. P. Weir, *J. Electrochem. Soc.*, 1951, **98**, 207
- ⁷⁴ A. Noda and M. Watanabe, *Electrochem. Acta*, 2000, **45**, 1265
- ⁷⁵ C. A. Angell, *Molten Salts: From Fundamentals to Applications*, Kluwer Academic Publishers, London, 2002, 305
- ⁷⁶ D. A. Jaeger and C. E. Tucker, *Tet. Lett.*, 1989, **30**, 1785
- ⁷⁷ A. P. Abbott, G. Capper, D. L. Davies, R. K. Rasheed, H. L. Munro and V. Tambyrajah, *Chem. Commun.*, 2001, 2010
- ⁷⁸ P. A. Z. Suarez, S. Einloft, J. E. L. Dullius, R. F. de Souza and J. Dupont, *Polyhedron*, 1996, **15**, 1217
- ⁷⁹ G. W. Parshall, *J. Am. Chem. Soc.*, 1972, **94**, 8716
- ⁸⁰ F. Endres, *Chem. Phys. Chem.*, 2002, **3**, 144
- ⁸¹ M. C. Buzzeo, R. G. Evans and R. G. Compton, *Chem. Phys. Chem.*, 2004, **5**, 1106
- ⁸² F. M. Kerton, *Alternative Solvents for Green Chemistry*, RSC Publishing, Cambridge, 2009, Ch 5, 174
- ⁸³ T. Fisher, A. Sethi, T. Welton and J. Woolf, *Tetrahedron Lett.*, 1999, **40**, 793
- ⁸⁴ W. Keim, W. Korth and P. Wasserscheid, *World Patent*, WO0016902, 2000
- ⁸⁵ P. Wasserscheid and T. Welton, *Ionic Liquids in Synthesis*, Wiley-VCH, Weinheim, 2003, Ch 5, 174
- ⁸⁶ Y. Chauvin, L. Mußman and H. Olivier, *Angew. Chem.*, 1995, **107**, 2941
- ⁸⁷ P. K. Lai and M. Skyllas-Kazacos, *J. Electroan. Chem.*, 1988, **248**, 431
- ⁸⁸ Y. Zhao and T. J. VanderNoot, *Electrochim. Acta.*, 1997, **42**, 1639
- ⁸⁹ Q. Liao, W. R. Pitner, G. Stewart and C. L. Hussey, *J. Electrochem. Soc.*, 1997, **144**, 936

-
- ⁹⁰ R. T. Carlin, H. C. De Long, J. Fuller and P. C. Trulove, *J. Electrochem. Soc.*, 1998, **145**, 1598
- ⁹¹ P. Wasserscheid and T. Welton, *Ionic Liquids in Synthesis*, Wiley-VCH, Weinheim, 2003, Ch 6, 289
- ⁹² J. S.-Y. Liu and I. -W. Sun, *J. Electrochem. Soc.*, 1997, **144**, 140
- ⁹³ M. K. Carpenter and M. W. Verbrugge, *J. Mater. Res.* 1994, **9**, 2584
- ⁹⁴ E. G.-S. Jeng and I. -W. Sun, *J. Electrochem. Soc.*, 1997, **144**, 2369
- ⁹⁵ M. A. M. Noel and R. A. Osteryoung, *J. Electroan. Chem.*, 1996, **293**, 139
- ⁹⁶ C. L. Hussey, L. A. King, R. A. Caprio, *J. Electrochem. Soc.*, 1979, **126**, 1029
- ⁹⁷ X. -H. Xu and C. L. Hussey, *J. Electrochem. Soc.*, 1992, **139**, 1295
- ⁹⁸ W. Schindler, D. Hofmann and J. Kirschner, *J. Electrochem. Soc.*, 2001, **148**, C124
- ⁹⁹ H. C. De long, J. S. Wilkes and R. T. Carlin, *J. Electrochem. Soc.*, 1994, **141**, 1000
- ¹⁰⁰ X. -H. Xu and C. L. Hussey, *Proc. Electrochem. Soc.*, 1992, **16**, 445
- ¹⁰¹ W. R. Pitner and C. L. Hussey, *J. Electrochem. Soc.*, 1997, **144**, 3095
- ¹⁰² X. -H. Xu and C. L. Hussey, *J. Electrochem. Soc.*, 1993, **140**, 618
- ¹⁰³ R. K. Pandey, S. N. Sahu and S. Chandra, *Handbook of Semiconductor Electrodeposition*, Marcel Dekker, New York, 1996
- ¹⁰⁴ S. P. Wicelinski and R. J. Gale, *Proc. Electrochem. Soc.*, 1987, **134**, 262
- ¹⁰⁵ M. -C. Lin, P. -Y. Chrn and I. -W. Sun, *J. Electrochem. Soc.*, 2001, **148**, C653
- ¹⁰⁶ F. Endres and C. Schrodt, *Phys. Chem. Chem. Phys.*, 2000, **24**, 5517
- ¹⁰⁷ E. L. Smith, A. P. Abbott and K. S. Ryder, *Chem. Rev.*, 2014, **114**, 11060
- ¹⁰⁸ A. P. Abbott, G. Capper, D. L. Davies, R. Rasheed and V. Tambyrajah, *International Patent*, WO 2002026701.
- ¹⁰⁹ A. P. Abbott, G. Capper, D. L. Davies, R. Rasheed and V. Tambyrajah, *International Patent*, WO 2002026381.
- ¹¹⁰ A. P. Abbott and D. L. Davies, *International Patent*, WO 2000056700.
- ¹¹¹ A. P. Abbott, G. Capper, D. L. Davies and R. Rasheed, *Inorg. Chem.*, 2004, **43**, 3447
- ¹¹² M. S. Sitze, E. R. Schreiter, E. V. Patterson and R. G. Freeman, *Inorg. Chem.* 2001, **40**, 2298.
- ¹¹³ T. B. Scheffler and M. S. Thomson, *Seventh International Conference on Molten Salts*, The Electrochemical Society, Montreal, 1990, 281
- ¹¹⁴ A. P. Abbott, G. Capper, D. L. Davies and R. K. Rasheed, *Chem. Eur. J.*, 2004, **10**, 3769

-
- ¹¹⁵ A. P. Abbott, G. Capper, D. L. Davies and R. K. Rasheed and V. Tambyrajah, *Chem. Commun.*, 2003, 70.
- ¹¹⁶ A. P. Abbott, D. Boothby, G. Capper, D. L. Davies and R. Rasheed, *J. Am. Chem. Soc.*, 2004, **126**, 9142.
- ¹¹⁷ A. P. Abbott, G. Capper, B. G. Swain and D. A. Wheeler, *Trans. Inst. Met. Finish.*, 2005, **83**, 51.
- ¹¹⁸ A. P. Abbott, J. C. Barron, K. S. Ryder and D. Wilson, *J. Eur. Chem.*, 2007, **13**, 6495
- ¹¹⁹ A. P. Abbott, A. A. Al-Barzinjy, P. D. Abbott, G. Frisch, R. C. Harris, J. Hartley and K. S. Ryder, *Phys. Chem. Chem. Phys.*, 2014, **16**, 9047
- ¹²⁰ J. -Z. Yang, Y. Jin, W. -G. Xu, Q. -G. Zhang and S. -L. Zang, *Fluid Phase Equilib.*, 2005, **227**, 41.
- ¹²¹ S. D. A. Lawes, S. V. Hainsworth, P. Blake, K. S. Ryder and A. P. Abbott, *Tribol. Lett.* 2010, **37**, 103.
- ¹²² M. A. Skopek, M. A. Mohamoud, K. S. Ryder and A. R. Hillman, *Chem. Commun.*, 2009, 935
- ¹²³ A. P. Abbott, G. W. Barker, A. J. Walter and P. Kocovsky, *Analyst*, 2003, **128**, 245
- ¹²⁴ H. G. Morrison, C. C. Sun and S. Neervannan, *Int. J. Pharm.*, 2009, **378**, 136.
- ¹²⁵ M. C. Serrano, M. C. Gutierrez, R. Jimenez, M. L. Ferrer and F. del Monte, *Chem. Commun.*, 2012, **48**, 579.
- ¹²⁶ H. -R. Jhong, D. S. -H. Wong, C. -C. Wan, Y. -Y. Wang and T. -C. Wei, *Electrochem. Commun.*, 2009, **11**, 209.
- ¹²⁷ M. C. Gutierrez, D. Carriazo, A. Tamayo, R. Jimenez, F. Pico, J. M. Rojo, M. Ferrer and F. del Monte, *Chem. Eur. J.*, 2011, **17**, 10533.
- ¹²⁸ A. P. Abbott, J. C. Barron, G. Frisch, K. S. Ryder and A. F. Silva, *Electrochim. Acta*, 2011, **56**, 5272.
- ¹²⁹ A. M. Popescu, A. Cojocar, C. Donath and V. Constantin, *Chem. Res. Chin. Univ.*, 2013, **29**, 991.
- ¹³⁰ A. P. Abbott, K. El Ttaib, K. S. Ryder and E. L. Smith, *Trans. Inst. Met. Finish.*, 2008, **86**, 234.
- ¹³¹ A. P. Abbott, K. El Ttaib, G. Frisch, K. S. Ryder and D. Weston, *Phys. Chem. Chem. Phys.*, 2012, **14**, 2443.

-
- ¹³² H. M. A. Abood, A. P. Abbott, A. D. Ballantyne and K. S. Ryder, *Chem. Commun.*, 2011, **47**, 3523.
- ¹³³ E. Gomez, P. Cojocar, L. Magagnin and E. Valles, *J. Electroanal. Chem.* 2011, **658**, 18.
- ¹³⁴ A. P. Abbott, G. Capper, K. McKenzie and K. S. Ryder, *J. Electroanal. Chem.*, 2007, **599**, 288
- ¹³⁵ A. P. Abbott, G. Capper, K. J. McKenzie and K. S. Ryder, *Electrochim. Acta*, 2005, **51**, 4420.
- ¹³⁶ A. P. Abbott, G. Capper, D. L. Davies, R. Rasheed and P. Shikotra, *Inorg. Chem.* 2005, **44**, 6497
- ¹³⁷ A. P. Abbott, G. Capper and P. Shikotra, *Trans. Inst. Min. Metall., Sect. C*, 2006, **115**, 15
- ¹³⁸ A. P. Abbott, J. Collins, I. Dalrymple, R. C. Harris, R. Mistry, F. Qiu, J. Scheirer and W. R. Wise, *Aust. J. Chem.*, 2009, **62**, 341
- ¹³⁹ J. Taubert and S. Raghavan, *Microelectron. Eng.*, 2014, **114**, 141.
- ¹⁴⁰ J. Taubert, M. Keswani, S. Raghavan, *Microelectron. Eng.*, 2013, **102**, 81

2. Experimental

2.1. Introduction	31
2.2. Chemicals and Materials	31
2.2.1. Chemicals.....	31
2.2.2. Materials	32
2.3. Preparation of Ionic Solutions	32
2.3.1. Synthesis of solutions	32
2.3.2. Inorganic ionic solutions	32
2.3.3. Deep Eutectic Solvents.....	33
2.3.4. Copper Solutions in Ionic Solvents	33
2.4. Physical Properties	33
2.4.1. Viscosity	33
2.4.2. Conductivity	34
2.4.3. Density.....	34
2.4.4. Surface Tension.....	34
2.4.5. Infrared Spectroscopy.....	34
2.4.6. Nuclear Magnetic Resonance Spectroscopy	35
2.5. Thermal properties	36
2.5.1. Differential Scanning Calorimetry	36
2.5.2. Thermogravimetric Analysis.....	36
2.6. Electrochemical Measurements.....	36
2.6.1. Voltammetry.....	37
2.6.2. Bulk Deposition.....	37
2.6.3. Electropolishing of Stainless Steel	38
2.7. Surface Analysis.....	38
2.7.1. Scanning Electron Microscopy and Energy-Dispersive X-Ray Spectroscopy	38
2.7.2. 3D Microscopy	39
2.7.3. Microscopy	39
2.8. Preparation of Thermoplastic Starch.....	39
2.9. Preparation of Resinated Wood Fibre	39
2.9.1. Large Scale Preparation of Plasticiser	39
2.9.2. In-house Resination Process.....	40

2.9.3. Aspirator Resination Process.....	40
2.10. Preparation of Fibreboards	42
2.10.1. 9 x 9 x 1.5 cm Fibreboards	42
2.10.2. 1 m x 1 m Fibreboards.....	42
2.11. Fibreboard Analysis	43
2.11.1. Density.....	43
2.11.2. Tensile Stress Testing.....	43
2.11.3. Differential Scanning Calorimetry	44
2.12. References	44

2.1. Introduction

This thesis chapter presents the experimental conditions and procedures used throughout this project. The background theories for the standard analytical techniques are not defined in detail.

2.2. Chemicals and Materials

2.2.1. Chemicals

Table 2.1 List of reagents used in the project. All chemicals were used as received.

Chemical	Purity (%)	Supplier
Choline chloride	≥98.0	Sigma-Aldrich
Ethylene glycol	≥99.0	Sigma-Aldrich
Urea	≥98.0	Sigma-Aldrich
Glycerol	≥98.0	Fisher Scientific
Sodium acetate	99.0	Fisher Scientific
Sodium chloride	99.7	Fisher Scientific
Sodium bromide	99.5	Sigma-Aldrich
Sodium tetraborate anhydrous	99.5	Alfa-Aesar
Sodium tetraborate decahydrate	≥99.0	Sigma-Aldrich
Calcium chloride dehydrate	99.0	Sigma-Aldrich
Magnesium chloride hexahydrate	98.0	Sigma-Aldrich
Potassium ferrocyanide trihydrate	98.0	Acros Organics
Copper (II) chloride anhydrous	98.0	Acros Organics
Copper (II) bromide anhydrous	99.0	Sigma-Aldrich
Copper (II) acetate anhydrous	99.0	Sigma-Aldrich
Ammonium Persulfate	>98.0	Sigma-Aldrich
Sulfuric acid	95.0	Fisher Scientific
Ammonium Nitrate	98.0	Sigma-Aldrich

2.2.2. Materials

Table 2.2 List of materials used in the project. All materials were used as received.

Material	Supplier	Notes
Corn starch	Weikfield	Food grade
Wood fibre	Norboard	
Anopol cleaner C	Anopol Ltd	
Stainless steel	Goodfellow	AISI 316
Brass	Goodfellow	Cu 63 %, Zn 37 %
Melamine urea formaldehyde pre-polymer	Hexion Speciality Chemicals Ltd	Sample number: MMD 6195

2.3. Preparation of Ionic Solutions

The ionic solvents investigated were mixtures of glycerol with; NaOAc, NaBr or $\text{Na}_2\text{B}_4\text{O}_7 \cdot 10\text{H}_2\text{O}$. These systems were compared with deep eutectic solvents (DESs) previously reported by Abbott *et al.*¹ Solutions of CuCl_2 , CuBr_2 and CuOAc_2 are prepared from these ionic solvents and were compared to the solutions of the same salts dissolved in DES.²

2.3.1. Synthesis of solutions

Glycerol was heated to 50 °C using a thermostatically controlled hotplate (IKA, RCT Basic). Salt was added to the glycerol whilst being stirred mechanically using an overhead stirrer (Stuart Scientific, ss10, 500 RPM) until all of the salt had dissolved. All ionic solvents were stored at 50 °C (Thermo Scientific, Heraeus oven).

2.3.2. Inorganic ionic solutions

Ionic solvents prepared by mixing glycerol with: NaOAc, NaBr or $\text{Na}_2\text{B}_4\text{O}_7 \cdot 10\text{H}_2\text{O}$, were made over the concentration range 20 mM - 4 M using the method outlined in section 2.3.1. The quantities of the reagents used and the densities of the concentrations prepared are shown in Table 7.1

2.3.3. Deep Eutectic Solvents

Deep eutectic solvents were prepared by mixing Choline chloride (ChCl) with either glycerol or ethylene glycol, were made over the concentration range 20mM- 4M with the method outlined in section 2.3.1. The quantities of the reagents used and the densities of the concentrations prepared are shown in Table 7.2

2.3.4. Copper Solutions in Ionic Solvents

Solutions of CuCl_2 , CuBr_2 and CuOAc_2 were prepared at the required concentration (5 - 500 mM) in the ionic solvents specified in section 2.3.1. The copper salt was added to the ionic solvent, which is heated to 50 °C using a thermostatically controlled hotplate (IKA, RCT Basic) whilst being stirred magnetically, for three hours to allow complete dissolution of the copper salt. The quantities of the reagents used and the concentrations prepared are shown in Table 7.30.

2.4. Physical Properties

2.4.1. Viscosity

The viscosities of all the ionic solvents were measured using a rotational viscometer (Brookfield DV-II+PRO), fitted with a temperature probe, and linked to a computer with a data logging software package (Rheocalc, version 3.3). Samples were heated to 45 °C and viscosity measurements were taken down to 25 °C with an accuracy ± 1 °C. The beaker used in all viscosity experiments had a diameter of 5.65 cm and a height of 11.60 cm. An average of three readings of viscosity were used for analysis.

Ionic solvents were tested for non-Newtonian fluid behaviour using the above instrument and apparatus over the viscometer rotation speed range 10-200 RPM. Samples were kept in a thermostatically controlled water bath (Techne, Tempette Junior TE-8J) at 25 °C for 30 minutes before measurement. Sample viscosity was recorded for 10 minutes for each rotation speed as to provide a stable measurement.

2.4.2. Conductivity

The electrical conductivities of all the ionic solvents were measured using a conductivity probe (Jenway 4510, cell constant $K = 0.96$), which was fitted with an integral temperature probe. Conductivity was measured over the temperature range 45-25 °C with an accuracy of ± 1 °C.

2.4.3. Density

Density measurements were made using a bench top tensiometer (Krüss, K9 Tensiometer) over the temperature range 45- 25 °C with the tensiometer fitted to a thermostatically controlled water circulator (Techne, Tempette Junior TE-8J). Measurements were taken, using a Si log mounted in a Pt cradle (Krüss, part number: DE01), which was submerged for 1 minute to reach equilibrium before a measurement was taken. The Pt cradle was washed with deionised water followed by heating to red hot in the flame of a Bunsen burner to remove any surface material.

2.4.4. Surface Tension

Surface tension measurements were made using the same apparatus outlined in section 2.4.3. Surface tension measurements were taken using a Pt-Ir alloy plate (Krüss, part number: PL21), which was in contact with the sample for 1 minute to reach equilibrium before a measurement was taken. The Pt-Ir plate was washed with deionised water followed by heating to red hot in the flame of a Bunsen burner to remove any surface material.

2.4.5. Infrared Spectroscopy

The infrared (IR) spectra of solutions and component materials were collected using a Fourier transform (FT) IR spectrometer (Perkin-Elmer, Spectrum 1) fitted with an attenuated total reflection (ATR) sampling accessory, and controlled by Spectrum version 10.03 software. A scan range of 400 - 4000 cm^{-1} , and all final spectra are the sum of 4 repeat scans.

2.4.6. Nuclear Magnetic Resonance Spectroscopy

Diffusion coefficients of ionic solvents were investigated using pulsed field gradient (PFG) nuclear magnetic resonance (NMR) experiments, which were carried out with a Bruker DMX300 equipped with a diffusion probe capable of producing a magnetic field gradient pulse of 11.6 T m^{-1} .³ The measurements were performed over the temperature range from 298 K to 338 K in steps of 10 K using a Bruker variable temperature unit (BVT 300). Samples were prepared in 5 mm NMR tubes filled with liquid to a height of approximately 20 mm. For each temperature, the sample was left for 15 minutes before starting the measurement to achieve thermal equilibrium. Diffusion measurements were carried out using the pulsed gradient stimulated echo (PGSTE) pulse sequence, as shown in Figure 2.1, holding the gradient pulse duration (δ) constant and varying the magnetic field gradient strength (g). A homospoil gradient between the second and the third 90° radiofrequency pulse was applied in order to remove any residual magnetisation on the transverse plane. The observation time (Δ) was set to 50 ms, and the numerical values of the diffusion coefficient (D) were obtained by fitting the NMR signal decay (E_g/E_o) to the echo attenuation equation, as shown in equation 2.1, where the gyromagnetic ratio (γ_H) is of the ^1H nucleus.

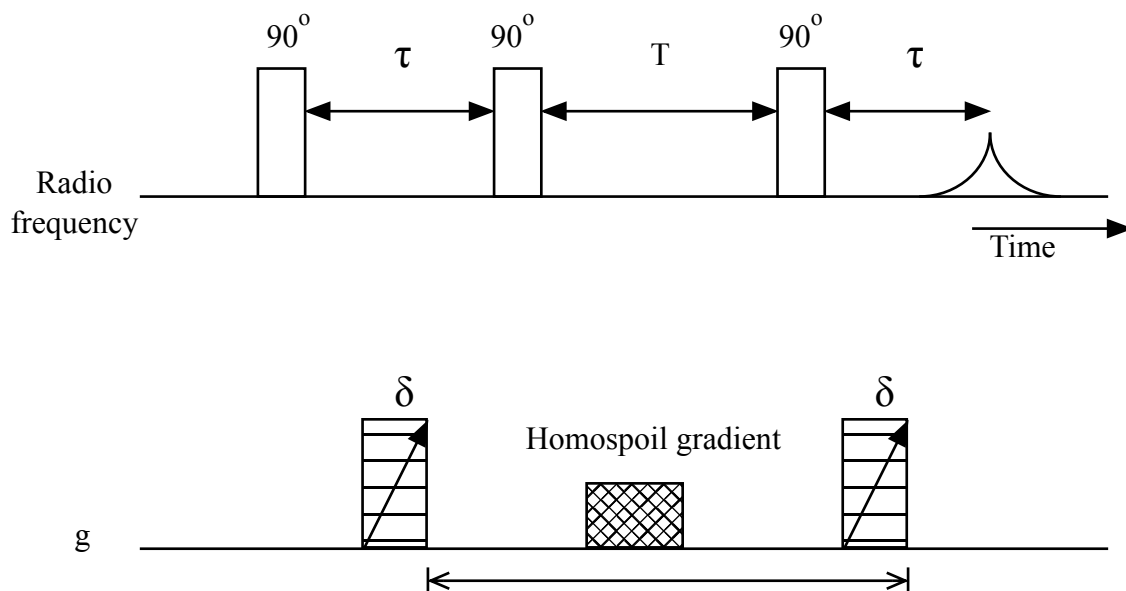


Figure 2.1 PGSTE pulse sequence showing gradient pulse duration (δ), echo time (τ), storage interval (T) and homospoil gradient and magnetic field gradient strength (g).³

$$\frac{E_g}{E_o} = e^{-D\gamma_H^2 g^2 \delta^2 \Delta} \quad 2.1^3$$

2.5. Thermal properties

2.5.1. Differential Scanning Calorimetry

Glass transition temperatures were determined using a Differential Scanning Calorimeter (Mettler Toledo, DSC1) controlled by STARe version 12.10 software. The mass of each sample ranged between 5 - 20 mg, and was sealed inside a 40 μl aluminium pan (Mettler Toledo) with a vent hole pierced into the lid. Samples were cooled to $-140\text{ }^{\circ}\text{C}$ at a rate of $10\text{ }^{\circ}\text{C min}^{-1}$, then held at $-140\text{ }^{\circ}\text{C}$ for 10 min and then heated up to $25\text{ }^{\circ}\text{C}$ at a rate of $5\text{ }^{\circ}\text{C min}^{-1}$. All experiments were carried out under a N_2 atmosphere. The resulting thermograms showed an endothermic peak corresponding to the glass transition of the samples.

2.5.2. Thermogravimetric Analysis

Thermogravimetric analysis (TGA) was carried out using a bench top thermogravimetric analyser (Mettler Toledo, TGA/DSC1) controlled by STARe version 12.10 software. The mass of each sample in the range 10-35 mg, and is sealed in a 70 μl aluminium pan with a vent hole pierced into the lid. Boiling temperatures, decomposition temperature and volatile loss were studied by heating from room temperature to $550\text{ }^{\circ}\text{C}$ at a rate of $10\text{ }^{\circ}\text{C min}^{-1}$, then the samples were held at $550\text{ }^{\circ}\text{C}$ for 10 minutes.

2.6. Electrochemical Measurements

All electrochemical measurements were carried out using a potentiostat (Metrohm Autolab, $\mu\text{AutolabIII}$), which is controlled by GPES version 4.9 software. A three-electrode system consisting of a platinum working electrode (0.5 mm diameter), a platinum flag counter electrode (1 cm^2 area) and a silver wire pseudo-reference electrode were used for all experiments. The working electrode was mechanically polished with $0.05\text{ }\mu\text{m}$ alumina paste (Buehler) and rinsed with deionised water and dried before each measurement.

A two-electrode system consisting of a platinum microelectrode (IJ Cambria Scientific, $10\text{ }\mu\text{m}$ diameter), a platinum wire counter electrode (IJ Cambria Scientific) were used for all experiments, and the electrical connection for the reference electrode

was connected to the counter electrode for all experiments. The working electrode was mechanically polished with 0.05 μm alumina paste (Buehler) and rinsed with deionised water and dried before each measurement.

2.6.1. Voltammetry

All samples were degassed using oxygen-free nitrogen gas (BOC Ltd) for 10 minutes, and then the sample was placed in an ultrasound bath (Decon, F5100b) for 15 minutes to remove any N_2 bubbles. All cyclic voltammetry experiments were conducted with a scan rate in the range 1-50 mV s^{-1} .

2.6.2. Bulk Deposition

Electrodeposition of copper onto brass was carried out in a two-electrode cell with an inert titanium mesh anode and 175 W power supply (TTi, EX355R) setup on a hotplate (Tefal, Vita compact Pro), as shown in Figure 2.2.

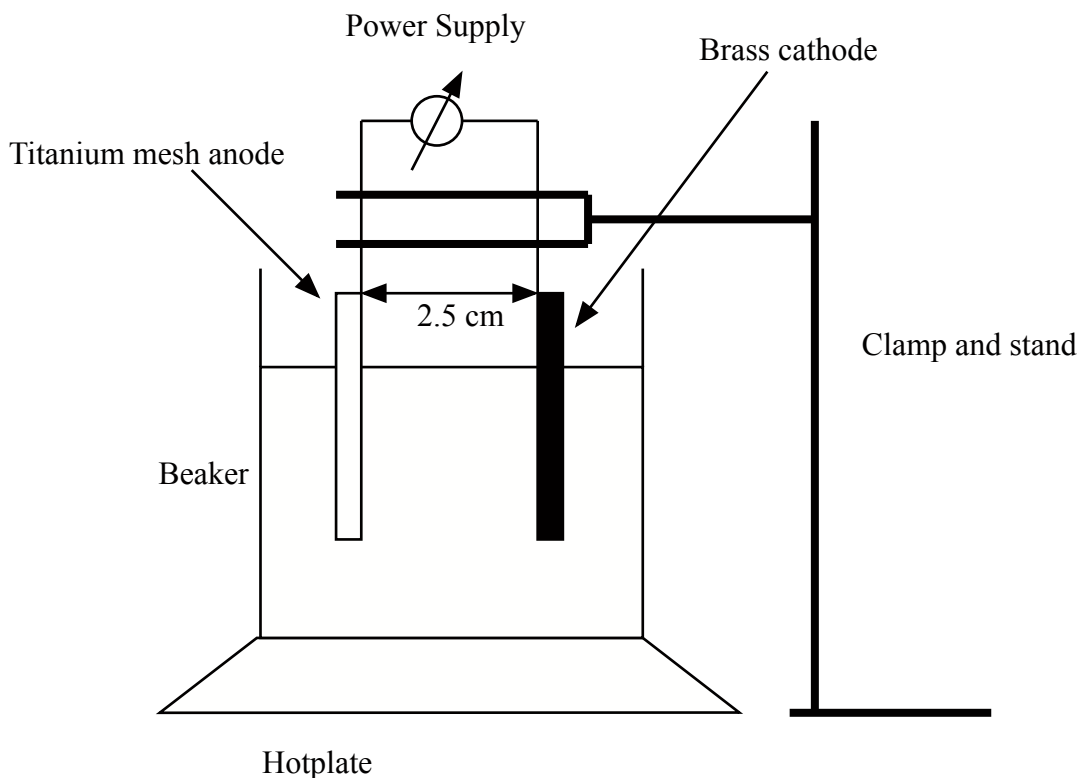


Figure 2.2 Cell setup for electrodeposition of Cu onto brass

2 x 5 cm brass pieces were pre-treated by first submersing into an acidified solution of ammonium persulfate (0.65 M, 2 % H_2SO_4) for 2 minutes, and then washed

with deionised water and acetone, then allowed to dry. Pre-treated samples were taped with a heat resistant adhesive tape to give a working surface area of 2 cm^2 . The electrolyte is heated to $80 \text{ }^\circ\text{C}$ and allowed to equilibrate for 10 min, and the power supply is set to current limited mode with the current density set to 50 mA cm^{-2} . Samples were exposed to a cathodic current for 1 hour, and then were washed with deionised water and acetone, and the heat resistant tape was removed.

2.6.3. Electropolishing of Stainless Steel

Electropolishing of stainless steel was carried out in the two-electrode cell outlined in Figure 2.2. $2 \times 5 \text{ cm}$ stainless steel pieces were pre-treated by first submersing into a 10:1 respective solution of deionised water and Anopol cleaner C for 10 minutes, then washed with deionised water and acetone, and then allowed to dry. Pre-treated samples were taped with a heat resistant tape to give a working surface area of 2 cm^2 . The electrolyte is heated to the required temperature ($25\text{-}80 \text{ }^\circ\text{C}$) and allowed to equilibrate for 10 minutes, and the power supply is set to current limited mode with the required current density ($2\text{-}50 \text{ mA cm}^{-2}$). Samples were exposed to an anodic current for the required amount of time (20 minutes- 2 hours), and then were washed with deionised water and acetone, and the heat resistant tape was removed.

2.7. Surface Analysis

2.7.1. Scanning Electron Microscopy and Energy-Dispersive X-Ray Spectroscopy

The surface morphology and composition has been studied using scanning electron microscopy (SEM), and elemental analysis by energy dispersive X-ray (EDX) spectroscopy. All analyses were conducted with a Phillips XL30 ESEM with an accelerating voltage of 20 keV. The ESEM was also fitted with an EDX analyser (Oxford Instruments, 6650) controlled by Inca Suite version 4.09 software.

2.7.2. 3D Microscopy

3D micrographs were taken using an optical profiler (Zeta Instruments, Zeta 2000) controlled by Zeta3D version 1.8.5 software. Micrographs were taken with a lens capable of 50x magnification and micrographs were stitched in sequence to achieve the complete image area. Surface dimensions and roughness were calculated using the Zeta3D software.

2.7.3. Microscopy

Micrographs were taken using an optical microscope (Meiji Techno, MT7100), which is fitted with a digital recorder (uEye) controlled by uEye version 3.20 software.

2.8. Preparation of Thermoplastic Starch

Corn flour was placed in a food processor (Tefal, Vita compact Pro). Ionic solvent, as prepared in section 2.3.1, was preheated to 50 °C and added to the corn flour whilst under constant mixing. The corn flour-ionic solvent mixtures were dried for 3 hours at 50 °C (Thermoscientific, Heraeus oven). The dried mixtures were stored in sealed plastic bags.

20 g of corn flour-ionic solvent mixture was placed in a square copper mould of 9 x 9 x 0.1 cm internal dimensions and 13 x 13 x 0.1 cm external dimensions lined with non-stick paper (Bake-o-glide). The mould was sealed with two 13 x 13 x 0.2 cm copper plates and pressed in a hydraulic press (Fontune, TH400) at 120 kN and 145 °C for 10 minutes. Samples were cooled to room temperature using water-cooling whilst maintaining a compressive force of 120 kN. Samples were stored in sealed plastic bags until needed.

2.9. Preparation of Resinated Wood Fibre

2.9.1. Large Scale Preparation of Plasticiser

25 kg batch productions of a 1:4 molar mixture of sodium tetraborate decahydrate and glycerol were carried out for pilot scale trials of medium density fibreboard (MDF) production. Glycerol was added to a 20 L steel drum container with the lid removed.

The drum was then fitted with a 1000 W heating element (Braude, Polaris Popular Cylindrical), thermometer and overhead mechanical stirrer (Stuart Scientific, SS10, 500 RPM), then heated to 80 °C under constant stirring. Sodium tetraborate decahydrate was added in small quantities to aid dissolution under constant stirring. The resulting plasticisers were stored in airtight containers.

2.9.2. In-house Resination Process

Wood fibre and corn flour were mixed together in a food processor (Tefal, Vita compact Pro). Ionic solvent, as prepared in section 2.3.1, was preheated to 50 °C and added to the corn flour-wood fibre mixture whilst under constant mixing. The resinated wood fibres were stored in sealed plastic bags and used when required. All resinated wood fibres made with this method contained 40% (w/w) ionic solvent, 45% (w/w) wood fibre and 15% (w/w) corn flour.

2.9.3. Aspirator Resination Process

5 kg batches of resinated wood fibre were prepared at the BioComposites Centre (Bangor University, Wales). Wood fibre and corn flour were weighed and placed in a large rotating drum equipped with a pressurised spray system, as shown in Figure 2.3 A and B respectively. The drum was set to rotate at 13 RPM for 2 minutes to mix the corn flour and wood fibre thoroughly.



A



B

Figure 2.3 The rotating mixing drum (A) and internal spray system (B) used at the BioComposites Centre

The plasticiser was preheated to 70 °C, was added to a 1900 cm³ metal container, which was preheated to 70 °C using an electric heating ribbon (Omegalux, HTWC102-010). The metal container was fitted to an air compressor, which was pressurised to 5 bar and the spraying process commenced, whilst the drum was rotating at 13 RPM. Certain batches of resinated wood fibre were dried using a flash drier preheated to 70 °C. Resinated wood fibres were emptied in to plastic bags and sealed until needed. The mixtures prepared are shown in Table 2.3.

Table 2.3 Resinated wood fibre mixtures prepared using the aspiration method

Corn flour (%)	Wood fibre (%)	Plasticiser (%)
10	40	50
10	45	45
10	47.5	42.5
10	50	40
10	52.5	37.5
10	55	35

2.10. Preparation of Fibreboards

2.10.1. 9 x 9 x 1.5 cm Fibreboards

90 g of resinated wood fibre was placed in a square steel mould of 9 x 9 x 1.5 cm internal dimensions and 13 x 13 x 1.5 cm external dimensions lined with non-stick paper (Bake-o-glide). The mould was sealed with two 13 x 13 x 0.2 cm copper plates and pressed in a hydraulic press (Fontune, TH400) at 120 kN and 145 °C for 30, 10 or 5 minutes. Boards were cooled to room temperature using water-cooling whilst maintaining a compressive force of 120 kN. Samples were stored in sealed plastic bags until needed.

2.10.2. 1 m x 1 m Fibreboards

For producing fibreboards that are 1.05 x 1.05 x 0.015 m, 12 kg of resinated wood fibre was put into a 1 x 1 x 0.53 m pre-mould and pressed into a 0.020 m thick mattress using a hydraulic pre-press (Mackey Bowley), as shown in Figure 2.4.

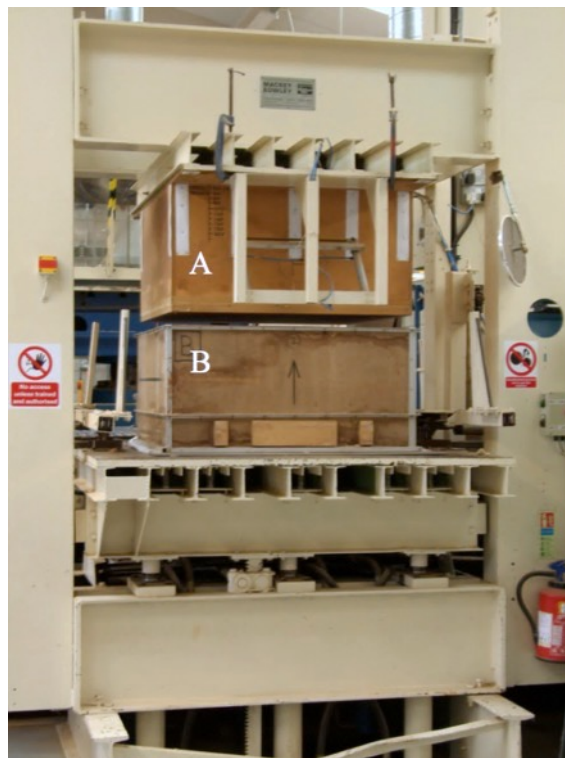


Figure 2.4 The hydraulic pre-press used to form moulded mattresses (A) and the mould (B)

The pre-formed mattress was then pressed inside a 1 x 1 m hydraulic press (manufacturer unknown), controlled by PressMAN version 0.78 software. The press plates were held 15mm apart at 145 °C for 30, 10 or 5 min. After the desired pressing time, the press plates were opened to allow the formed board to be removed and cool to room temperature before storing on 1 x 1 m pallet.

The same method was used for producing fibreboards that are 0.018 m thick, except 15.5 kg of resinated wood fibre was added to the pre-mould and was pre-pressed to a thickness of 0.025 m.

2.11. Fibreboard Analysis

2.11.1. Density

Fibreboards were weighed with a bench top balance (Denver Instruments, SI-6002) and then the dimensions were measured so the sample volume could be determined. From the weight and dimension measurements, the densities of the fibreboards were calculated, as shown in Table 7.37.

2.11.2. Tensile Stress Testing

9 x 9 x 0.1 cm sheets of thermoplastic starch were cut into dog bone shaped specimens using a bench top punch press (Ceast, punch number: 8047-020). The specimens had a test area of 0.04 cm² and a test length of 3 cm. Thermoplastic starch samples were tensile stress tested using a bench top mechanical stress tester (Instron, 3343 tensiometer), controlled by Bluehill version 2.0 software, at an extension rate of 2 mm min⁻¹.

9 x 9 x 1.5 cm fibreboards were cut into dog bone shaped specimens using a milling machine (Balding Engineering, Beaver milling machine). Each specimen had a test area of 2.25 cm² and a test length of 3 cm. Fibreboard samples were tensile stress tested using a bench top mechanical stress tester (Hounsfield, HTE Tensiometer, QMAT version 2.3 software) at an extension rate of 10 mm min⁻¹.

2.11.3. Differential Scanning Calorimetry

Corn starch gelation temperatures were determined using DSC (see section 2.5.1). Corn starch and ionic solvent is mixed in the mass ratio 1:4.5 respectively. The mass of each sample ranged between 5-20 mg, and was sealed inside a 40 µl aluminium pan with a vent hole pierced into the lid. Samples held at 25 °C for 10 minutes, then heated to 185 °C at a rate of 5 °C min⁻¹. The resulting thermograms showed an endothermic peak corresponding to the onset of corn starch gelation.

The polymerisation activation temperature of a melamine urea formaldehyde (MUF) pre-polymer (Hexion Speciality Chemicals Ltd, sample number: MMD 6195) was investigated using the same method above. Before addition of the sample to the DSC, 20 mg of aqueous ammonium nitrate solution (43 % w/w) was added to 2 g of MUF pre-polymer and thoroughly stirred at room temperature.

2.12. References

-
- ¹ E. L. Smith, A. P. Abbott and K. S. Ryder, *Chem. Rev.*, 2014, **114**, 11060
 - ² G. C. H. Forrest, PhD thesis, University of Leicester, 2015
 - ³ A. P. Abbott, R. C. Harris, K. S. Ryder, C. D'Agostino, L. F. Gladden and M. D. Mantle, *Green Chem.*, 2011, **13**, 82

3. Physical Properties of Novel Ionic Solvents

3.1. Introduction.....	46
3.1.1. Glycerol	46
3.1.2. Use of Glycerol in Deep Eutectic Solvents	48
3.1.3. Aims.....	49
3.2. Component Selection.....	50
3.3. Thermophysical Properties of Novel Ionic Solvents	52
3.3.1. Phase Behaviour	53
3.3.2. Density	57
3.3.3. Surface Tension and Free Volume.....	58
3.3.4. Viscosity	62
3.3.5. Fluid Behaviour	72
3.3.6. Ionic Conductivity	74
3.3.7. Molar Conductivity.....	79
3.4. Application of Walden's Rule	83
3.5. Future Developments.....	88
3.6. Conclusions.....	90
3.7. References.....	91

distillation to recover unreacted methanol.² The crude glycerol is then purified by electro dialysis and nanofiltration to yield glycerol of technical grade purity.²

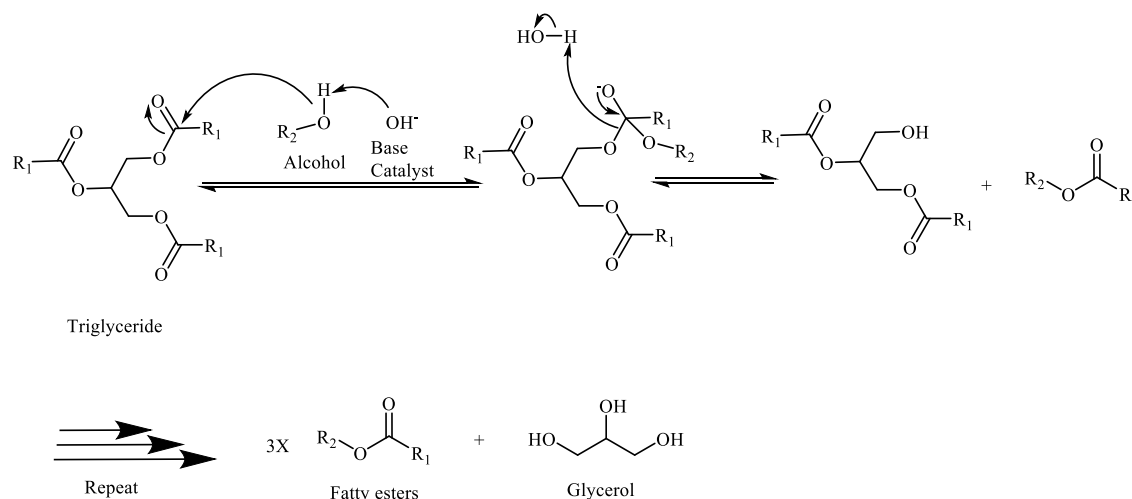


Figure 3.2 Mechanism of plant oil transesterification with methanol

Synthetic glycerol can be manufactured from a number of synthetic pathways from propylene. The most common of which, is the epichlorohydrin process; involving the chlorination of propene to yield allyl chloride, which is then oxidised with sodium chlorate and treated with a base to give epichlorohydrin, which upon hydrolysis yields glycerol, as shown in Figure 3.3.⁶ Due to the surplus of glycerol generated from biodiesel production, most of the traditional synthetic pathways are no longer economically viable, and glycerol is being researched as a potential feedstock for epichlorohydrin and acrolein.⁷

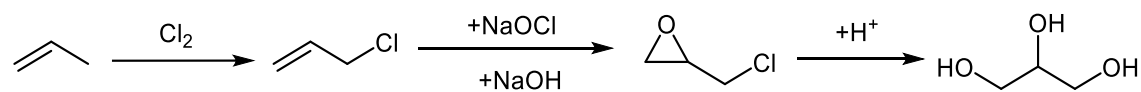


Figure 3.3 Mechanism for the epichlorohydrin process

Glycerol has been utilised in wide variety of environmentally friendly technologies including: hydrogen and hydrocarbon fuel production, selective reduction to industrially useful glycols, etherification to polyglycerol and additives for cement.² Although glycerol is being employed in novel green technologies, supply far exceeds demands and further investigation into applications is needed.⁸ Glycerol is poorly combustible due to its high flash point and low heat energy of combustion, and use as a

solvent is restricted due to the high boiling point and low vapour pressure limiting filtration and distillation processes.⁹

3.1.2. Use of Glycerol in Deep Eutectic Solvents

Abbott *et al.* showed that the addition of choline chloride (ChCl) decreases the viscosity of glycerol forming a non-toxic, environmentally friendly deep eutectic solvent (DES), known as Glyceline.¹⁰ Glyceline has been investigated by the Abbott group in a range of applications including: purification of biodiesel, sustainable solvent systems, plasticisers for salt modified starches, and lubricants.^{10,11,12,13}

Research by the Abbott group found that addition of a Lewis basic mixture of ChCl and glycerol to a crude biodiesel mixture resulted in the formation of the Glyceline 200 DES (1:2 molar ratio of ChCl and glycerol respectively), which extracted free glycerol from the biodiesel phase.¹¹ Addition of pure ChCl was ineffective at extracting glycerol and it was thought to be due to the enthalpy of formation of the DES being too large, and addition of Glyceline 200 proved to be inefficient as the eutectic composition between ChCl and glycerol had already been achieved.¹¹ Research has shown DESs consisting of ChCl and ethylene glycol, or 2,2,2-trifluoroacetamide are also capable of extracting glycerol from biodiesel, where the ethylene glycol system was successful in removing all free glycerol from palm-oil-based biodiesel.^{14,15,16} Although the processes have shown to be efficient at extracting glycerol from biodiesel, the separation of ChCl from glycerol was not successful and further research was required to develop glycerol recovery.^{11,16}

Studies into the physical properties of glycerol-based DESs show the viscosity of the mixtures decreases with increasing ChCl content, which is a result of the disruption of the 3D intermolecular hydrogen bonding network, causing a loss of order in the system.¹⁰ In the same research, density is shown to decrease with increasing ChCl content and free volume increases with ChCl content, supporting the loss of system order.¹⁰ Several polarity parameters including: transition energy of Reichardt's dye 30 $E_T(30)$, hydrogen-bonding acidity (α), hydrogen-bonding basicity (β) and polarizability (π^*) have been obtained for glycerol based DESs, and suggests DES polarity is similar to many imidazolium ionic liquids.¹⁰

Thermoplastic starch (TPS) has been investigated as a sustainable alternative to oil derived polymers, and is formed by the ingress of small polar molecules, such as

glycerol, into native starch, which breaks down the intermolecular hydrogen-bonding network, thus making the material structure more amorphous.¹⁷ TPS materials produced with conventional plasticisers show poor mechanical properties and tend to recrystallize over time and become increasingly brittle.¹⁸ Abbott *et al.* showed that glycerol based DESs can be used to efficiently plasticise starch that: have tensile strength comparable to polyolefin-based thermoplastics, do not recrystallise and can be recycled.¹² The same research group has demonstrated TPS plasticised with DESs can be used as a binder for wood particles to make a recyclable thermoplastic material.¹⁹

Ionic liquids (ILs) have recently been tested as lubricants and have shown viscosity indices superior to mineral base oils and comparable to many semi-synthetic base oils, as well as the capacity to form protective films under extreme wear conditions over bearing surfaces.²⁰ However, due to the complex synthesis required for ILs and cost of production, applications are limited to small-scale uses.¹³ DESs were investigated as potential alternatives, and glycerol based DES showed: promising viscosity indices, minimal wear and corrosion rates with respect to iron, aluminium and nickel, and low toxicity.¹³ These characteristics coupled with their miscibility with water and the ability to suppress corrosion when wet, suggests glycerol based DESs are particularly suitable for marine applications.¹³

Most DESs utilise an organic salt, typically a quaternary ammonium salt (QAS), and some research has been done utilising transition metal salt hydrates including zinc and chromium chloride, with hydrogen bond donors such as: urea, acetamide and ethylene glycol.^{21,22} This type of DES has been developed by the Abbott group, but have not extended the range of metals to include alkali metals due to the relatively high lattice energies of alkali metal salts.²³ However, previous studies have shown that mixtures of alkali metal halides with urea can form eutectic mixtures with melting points typically below 150 °C.²⁴ Electrical conductance, density and viscosity measurements of mixtures of alkali metal halides and glycerol have been previously carried out, but only concentrations up to 0.3 M had been investigated, which is not comparable to the 4 M salt concentrations found in many DESs.²⁵

3.1.3. Aims

The main aim of this aspect of the project was to expand the DES model to include alkali metal salts, and investigate the thermophysical properties including:

electrical conductance, density, viscosity and surface tension of concentrated alkali metal salt:glycerol mixtures, and compare these with the properties of DESs, ILs and other non-aqueous solutions. From understanding the thermophysical properties, an insight into the structures occurring in solution could be obtained, and investigations into mass and charge transport mechanisms could be conducted. The thermophysical properties of quaternary ammonium salts mixed with a variety of hydrogen bond donors have been well documented and suggest charge and mass transport regimes similar to what are applicable to ILs.²⁶ It was hypothesised that by replacing the bulky quaternary ammonium cation with a small alkali metal cation, similar conductivity and viscosity profiles would be found.

Glycerol is known to be a Newtonian fluid but it was unknown if the addition of alkali metal salts will change the fluid properties of glycerol by structuring the liquid. The systems investigated needed to be tested for a non-linear shear-stress shear-rate profile, as many of the theoretical methods used to define ionic solution and ionic liquid characteristics rely on a system expressing a constant dynamic viscosity.

After ascertaining a system's fluid behaviour and thermophysical properties, the effect of the addition of alkali metal salts on the structure of glycerol was investigated and compared to quaternary ammonium salts and ILs by probing changes in density, viscosity and free volume. Through understanding changes in structure, a deeper insight into charge and mass transport regimes could be gained.

3.2. Component Selection

Extensive research into DESs and ILs using QASs has been carried out by several groups.^{26,27,28} QASs are commonly used in DES as the quaternary ammonium cations can be easily synthesised to be large and non-symmetrical, which leads to a low salt lattice energy and melting point.²⁶ Complexation with a hydrogen-bond donor (HBD), such as a multi-functional alcohol or amide, results in charge delocalisation through hydrogen bonding between the QAS anion and the HBD, thus lowering the melting point of the mixture below that of its components.²⁹ Even though many DESs are easier to synthesis and more cost effective than many ILs, use of QASs in DESs is limited to small scale processes due to the cost of ChCl steadily increasing and now typically between 5-15 \$ kg⁻¹, which makes use of DESs more expensive than the costs of current industrial processes.³⁰

Abbott *et al.* has been successful in developing DESs that utilise a metal salt hydrates, as a substitute for the relatively more expensive QASs.^{21,22} However, studies into type IV DES have mostly been limited to using hydrated salts of transition metal for use in metal processing applications.²⁶ Gambino *et al.* have shown that mixtures of alkali metal halides with urea can form eutectic mixtures, but with typical melting points greater than 120 °C, the systems investigated proved to not be suitable for most domestic or industrial applications.²⁴ Mjalli *et al.* applied the same methodology to mixtures of potassium carbonate and glycerol, or ethylene glycol, and found that a 1:4 respective molar mixture of potassium carbonate and glycerol formed a colourless liquid at room temperature, with the potential application as a CO₂ capture medium.³¹

Ideally, a DES based on a concentrated mixture of NaCl and glycerol would be the most economically viable DES system as NaCl is naturally occurring and abundant, and glycerol can be collected as a waste product from biodiesel production and easily purified.² Unfortunately, NaCl is only partially soluble in glycerol with a solubility of 83 g kg⁻¹ of glycerol, which is not sufficiently concentrated enough to be compared against DES and ILs.³² Figure 3.4 shows a selection of group I and group II metal salts mixed with either: urea, xylitol an example of a complex sugar alcohol, and glycerol. All of the mixtures in Figure 3.4 were heated to 100 °C for 2 hours with intermittent shaking, and all systems were tested at a 1:4 respective molar ratio or salt to glycerol, except for NaCl and KCl, which was tested at a ratio of 1:8. Of the metal salts mixed with urea in Figure 3.4, only Na₂B₄O₇·10H₂O and MgCl₂·6H₂O showed signs of partial formation of a eutectic mixture, whereas all of the other salts tested remained as two separate solid phases. Marginally better miscibility was achieved when urea was substituted for xylitol, but none of the systems investigated completely formed liquids. When xylitol was substituted for glycerol, all of the systems investigated formed colourless liquids at 100 °C, and upon cooling to room temperature, the systems remained as colourless liquids of varying qualitative viscosities.

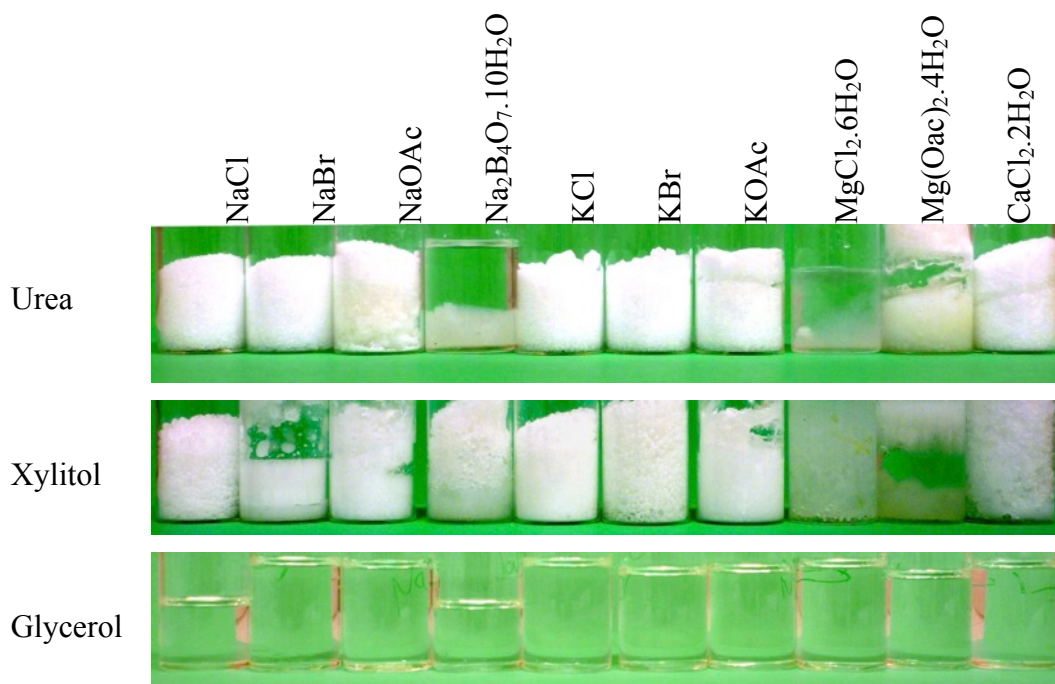


Figure 3.4 A selection of group I and group II metal salts mixed with either: urea, xylitol or glycerol. All systems tested were a 1:4 respective molar ratio or salt to glycerol, except for NaCl and KCl, which were tested at a ratio of 1:8.

Considering the research from Gambino *et al.*, many of the systems tested in Figure 3.4 may have fully formed if heated to over 150 °C, but further heating would have resulted in decomposition of urea.²⁴ Also, in cases where a colourless liquid formed at 100 °C, the system formed a hard glass at room temperature, which means thermophysical measurements at room temperature would be impractical. From the results shown in Figure 3.4, mixtures of: NaBr, NaOAc, NaOAc.3H₂O or Na₂B₄O₇.10H₂O with glycerol were investigated further and their thermophysical properties were studied as a function of salt concentration.

3.3. Thermophysical Properties of Novel Ionic Solvents

ILs and DESs have similar physical properties and are regarded as tuneable solvents that can be customised for a particular type of application.²⁶ For novel systems to be accepted as technically useful, the chemical and physical properties need to be understood.³³ Presented in this thesis chapter are the densities, dynamic viscosities,

ionic conductivities, phase behaviours and surface tensions for a selection of sodium salt:glycerol mixtures as a function of salt concentration. As well as providing information about the above thermophysical properties for an application's prospective, trends in thermophysical properties will be compared to glycerol-based DES, and the effect of exchanging a quaternary ammonium cation for a sodium cation will be quantified. Ion effects on the structure of glycerol will be considered and provide an insight into charge transport mechanisms occurring in solution.

3.3.1. Phase Behaviour

ILs generally show complex thermal behaviour as cooling from the liquid state results in the formation of glass at low temperature, typically 183 K for 1-alkyl-3-methylimidazolium salts, as solidification kinetics are slow.³⁴ A glass transition temperature (T_g) recorded up on cooling represent kinetic transitions and is not an accurate measurement of heating T_g values or melting points, therefore phase transitions must be measured on sample heating to obtain reliable data.³⁴ Mostly, heating from a glassy state, results in an exothermic crystallisation process followed by an endothermic melting transition.³⁴

A DES is a binary mixture of components, which at the eutectic composition, has a melting point that is lower than the melting points of the pure components.²⁶ The difference between the eutectic and ideal melting temperature of a mixture is related to the strength of the interactions between the components.³⁵ Figure 3.5 demonstrates a typical phase diagram of a two-component mixture showing a eutectic point, which applies to all types of DES.²⁶ The significant depression in melting point observed in DESs is a consequence of complexation of the anion of a halide salt, shown in Figure 3.6, as charge delocalisation through hydrogen bonding results in a decrease in the lattice energy, and thus decreasing the melting temperature of the halide salt.³⁶ Abbott *et al.* have shown that the melting points of ChCl and urea, 302 °C and 134 °C respectively, are reduced to 12 °C when mixed in a 1:2 respective molar ratio.³⁷

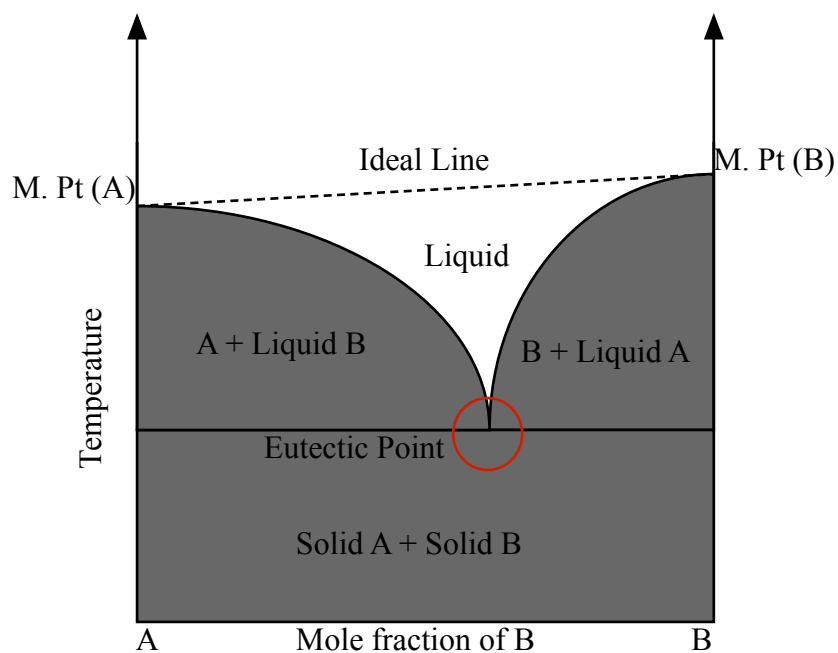


Figure 3.5 Typical phase diagram of a two-component mixture showing a eutectic point

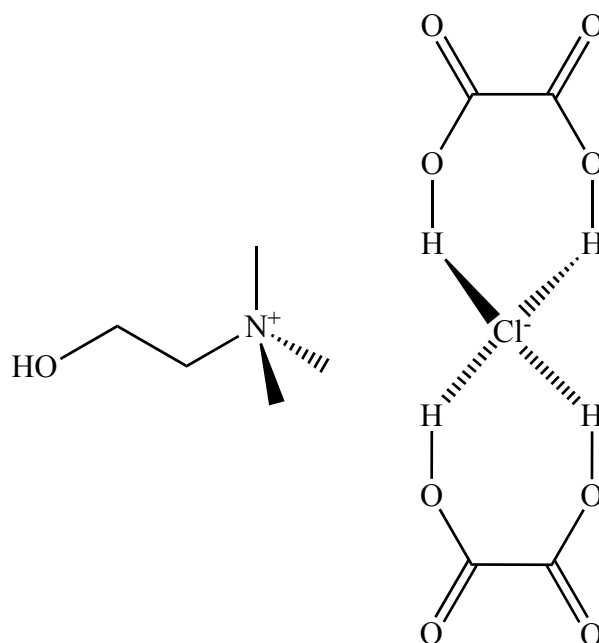


Figure 3.6 A possible DES structure demonstrating complexation of the organic salt anion

Figure 3.7 shows the glass transition temperatures for a range of sodium salts mixed with glycerol in the concentration range 20 mM – 4 M. All measurements were made using differential scanning calorimetry (DSC), and the melting temperature was

substituted for the onset of T_g as endotherms relating to material melting were not observed. This phenomenon is common in ILs and some DES as solidification kinetics are slow, and tend to only form glasses.³⁴ Glycerol is rarely found in the crystallised state as it has a tendency to supercool, and nominal amounts of water are known to have a pronounced depressing effect on the melting point.³⁸ Mixtures of NaOAc, NaBr, $\text{Na}_2\text{B}_4\text{O}_7 \cdot 10\text{H}_2\text{O}$ or $\text{NaOAc} \cdot 3\text{H}_2\text{O}$ with glycerol all showed a linear increase in T_g with increasing salt concentration, and did not show the characteristic depression, which is observed with DES, which is shown by the purple trend (ChCl) in Figure 3.7. Aqueous solutions of NaCl are known to show a depression in melting temperature with a eutectic composition of 23.3% w/w, which equates to a concentration of approximately 4 M.³⁹ Although a eutectic point is observed at approximately 4 M, the NaCl mole fraction is approximately 3.7 %, whereas in a 3.55 M NaBr solution in glycerol has a NaBr mole fraction of 22.5 % suggesting a eutectic composition might be observable at much lower salt concentrations, however at concentrations between 20 mM – 400 mM, a eutectic point still was not observed. Zaidi *et al.* developed an electrolyte based on sodium nitrate and N-methylacetamide and found a 1:9 respective molar ratio lead to a system with a melting point below that of the components, suggesting eutectic systems are possible with sodium salts, and an alternative method of determining melting points may be necessary.⁴⁰

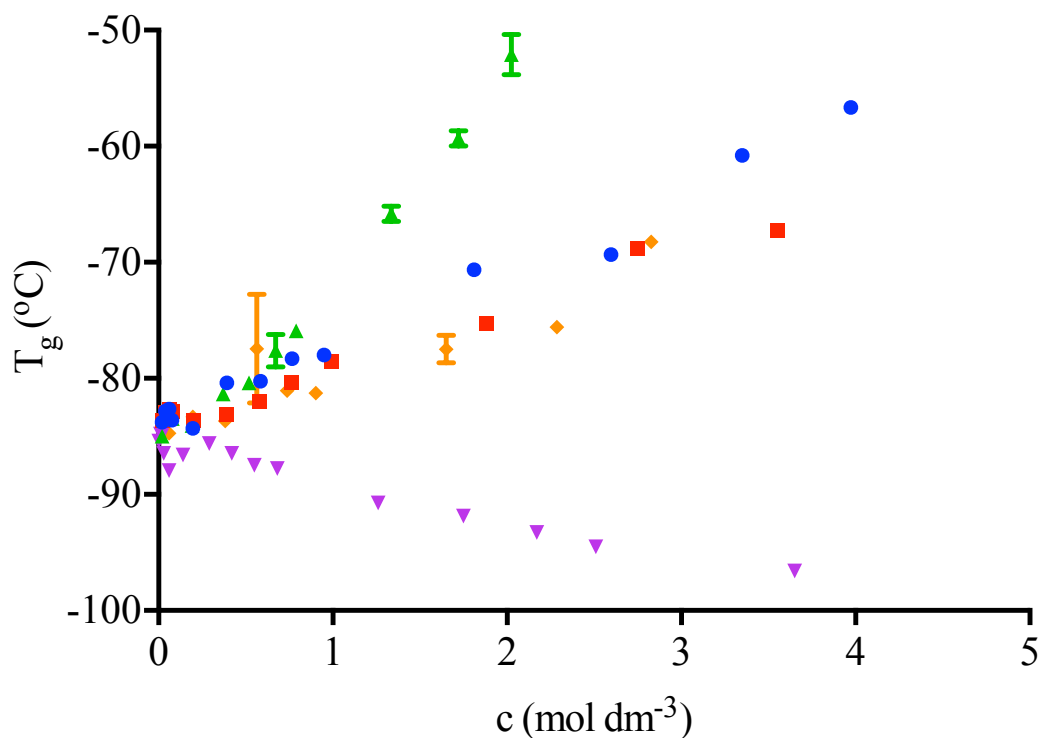


Figure 3.7 Glass transition onset temperature for a series of salt:glycerol mixture as a function of salt concentration: (blue) NaOAc, (red) NaBr, (green) Na₂B₄O₇·10H₂O, (purple) ChCl and (yellow) NaOAc·3H₂O

The positive trends in T_g in Figure 3.7 suggest the inorganic salts tested have a reinforcing effect (kosmotropic) on the structure of glycerol as the heat energy required to transfer into the molten state increases with salt concentration. In contrast, the QAS used in DES appear to have a structure disrupting (chaotropic) effect on glycerol as the heat energy required to transfer into the molten state decreases with salt concentration until the eutectic point.¹⁰ At low QAS concentrations, the T_g of glycerol appears to initially increase, which is surprising as a linear response is observed for the inorganic salts studied. The [EMIM]Cl/AlCl₃ system shows a eutectic maximum at an approximate AlCl₃ mole fraction of 0.5, due to the presence of different anionic species at different molar ratios of [EMIM]Cl to AlCl₃, which are outlined by the equilibria in section 1.4.^{41,42} The maximum at 0.2 M for the ChCl system in Figure 3.7 may be due to the presence of other anionic species, but this has not yet been observed for other DES systems and further work is required to understand this phenomenon.

3.3.2. Density

The density of an IL system is heavily dependent on the structure, charge density and functional groups of the ions, and have been reported to have densities ranging from 1.12 g cm^{-3} for $[(n\text{-C}_8\text{H}_{17})(\text{C}_4\text{H}_9)_3\text{N}][(\text{CF}_3\text{SO}_2)_2\text{N}]$ to 2.40 g cm^{-3} for a 1:2 molar ratio of a $[(\text{CH}_3)_3\text{S}]\text{Br}/\text{AlBr}_3$ eutectic system.^{43,44} IL densities are generally insensitive to changes in temperature, and the presence of impurities.^{45,46} The densities of DES are also dependant on the nature of the species present, with DES based on ChCl and a range of HBD typically displaying densities of $1.10 - 1.40 \text{ g cm}^{-3}$.^{47,48} Type IV DES are generally denser with densities ranging from 1.40 g cm^{-3} to 1.80 g cm^{-3} because of the larger masses of the metals in the salts.²¹ Figure 3.8 shows how the densities of a series of salt:glycerol mixtures vary as a function of salt content, and demonstrates for all of the sodium salts investigated, an increase in density. Sodium salt:glycerol mixtures appear to have densities similar to many of the ChCl: HBD DESs previously reported by the Abbott group, with a 3.55 M NaBr:glycerol mixture provided the highest density of $1.48 \pm 0.02 \text{ g cm}^{-3}$ due to the high mass of bromine.²⁶

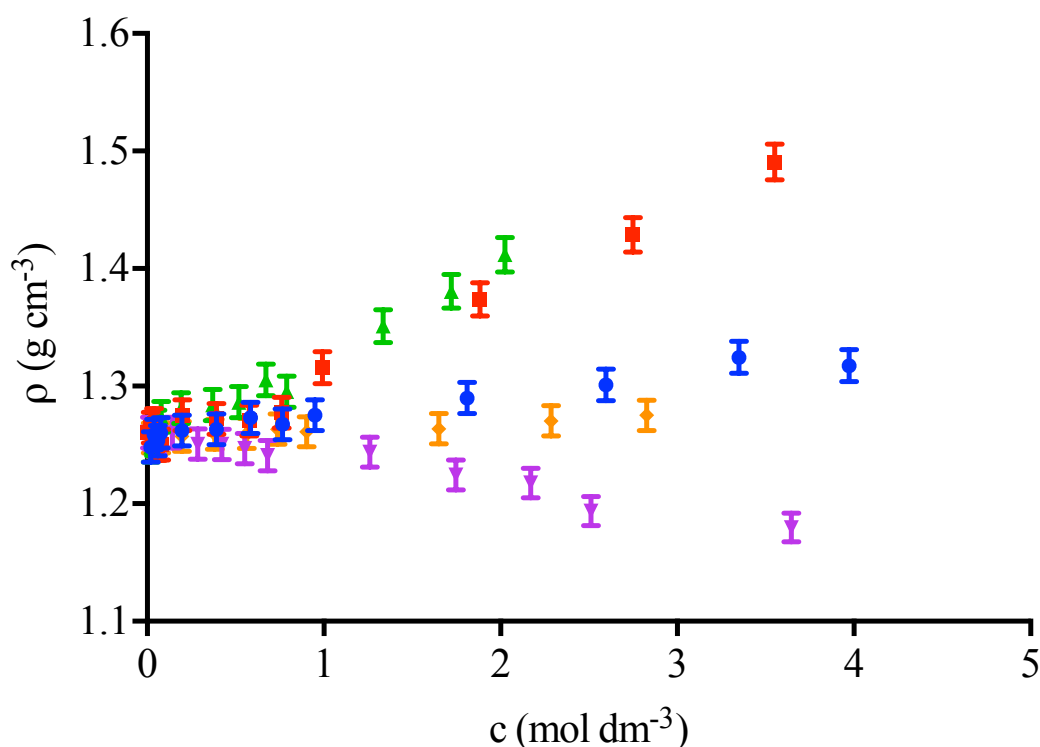


Figure 3.8 Density measurements for a series of salt:glycerol mixture as a function of salt concentration: (blue) NaOAc, (red) NaBr, (green) $\text{Na}_2\text{B}_4\text{O}_7 \cdot 10\text{H}_2\text{O}$, (purple) ChCl and (yellow) $\text{NaOAc} \cdot 3\text{H}_2\text{O}$, measured at 298 K

Abbott *et al.* found that for DESs based on ChCl and ethylene glycol, or 1,4 butanediol, showed an increase in density as a function of ChCl content, whereas when ChCl was mixed with glycerol, system density was found to decrease with ChCl content.⁴⁹ This phenomenon was explained by the fact that diol based HBD formed linear aggregates of hydrogen-bonded molecules, whereas the addition of ChCl to glycerol, breaks up the 3D structure of intermolecular hydrogen bonds through complexation to the chloride anion of the salt.⁴⁹ The significant breakdown in the glycerol structure suggests the surface tension of the ChCl:glycerol system decreases, accommodating an expansion in free volume, which leads to a decrease in density.⁴⁹

Addition of sodium salts to glycerol does not have the same effect as the addition of QASs, and suggests sodium salts have a kosmotropic effect of glycerol, which is due to the system volume not increasing by a significant amount, yet a large increase in the system mass occurs. The limited increase in system volume is likely to be caused by *electrostriction*: where the strong electrical forces on charge dense ions exert pressure on solvent molecules, which limit system expansion.⁵⁰ QASs are charge diffuse and the disruptive hydrogen bonding interactions between glycerol and ions dominate over electrostriction forces, thus accommodating a decrease in system density. Motin *et al.* found NaCl, CuCl₂, CuSO₄ and MgSO₄ to have a kosmotropic effect on water and water: urea mixtures, whereas NH₄Cl was found to have a chaotropic effect on the same solvent systems.⁵¹ Research by Trusler *et al.* also found that a range of group I and group II salts, and mixtures thereof, increased the density of water as a function of salt concentration.⁵²

3.3.3. Surface Tension and Free Volume

The density measurements shown in Figure 3.8 demonstrate that all of the salts tested have a strong influence upon the structure of glycerol. Further structural information can be taken from calculating the system *free volume* assuming a hard sphere model.¹⁰ From the density measurements in Figure 3.8, the molar volume (V_m) can be calculated with respect to density (ρ) as shown in equation 3.1.

$$V_m = \frac{M_r}{\rho} \quad 3.1$$

The relative molecular mass (M_r) of the mixture is calculated from the sum of partial relative molecular masses (M_{Salt}) of the components, where X_{Salt} is the mole fraction of the species concerned, as shown in equation 3.2.

$$M_r = x_{Salt}M_{Salt} + x_{Glycerol}M_{Glycerol} \quad 3.2$$

The mole fractions of the species concerned were calculated from the concentrations of the species within the mixtures using equation 3.3, where n signifies the moles of the species concerned.

$$x_{Salt} = \frac{n_{Salt}}{n_{Salt} + n_{Glycerol}} \quad 3.3$$

Combination of equations 3.1 - 3.3, coupled with the density measurements discussed in section 3.3.2, allow for the calculation of a system's molar volume using equation 3.4.

$$V_m = \frac{x_{Salt}M_{Salt} + x_{Glycerol}M_{Glycerol}}{\rho} \quad 3.4$$

The volume occupied by the components (V_{Comp}) can be treated as the sum of the molecular volumes (V_{Salt}) per mole of the system, where N_A is Avogadro's constant, as shown in equation 3.5. Molecular volumes were calculated using commercially available software.⁵³

$$V_{Comp} = (x_{Salt}V_{Salt} + x_{Glycerol}V_{Glycerol})N_A \quad 3.5$$

The relative difference between the V_m and V_{Comp} of a system can be treated its free volume (V_{Free}), as demonstrated by equation 3.6. Alternatively, V_{free} can be expressed as the difference between V_m and V_{Comp} , with units of inverse concentration, as shown in 3.7.

$$V_{free} = \frac{(V_m - V_{Comp})}{V_m} \quad 3.6$$

$$V_{free} = V_m - V_{Comp} \quad 3.7$$

V_{free} is known to have a strong influence on the transport properties of liquids and the Cohen-Turnbull equation, as shown in equation 3.8 where: A and γ are constants, and V_{free}^* is the minimum required void size, which links free volume with the self-diffusion coefficients (D) of species.⁵⁴ Combination of the Cohen-Turnbull equation with the Stokes-Einstein equation, as shown in equation 3.9 relates viscosity to free volume, and combination with the Nernst-Einstein equation, as shown in equation 3.10 relates ionic conductivity to free volume, and has been shown to be valid for ionic liquids.⁵⁵

$$D = A\sqrt{T}e^{\left(-\frac{\gamma V_{Free}^*}{V_{Free}}\right)} \quad 3.8$$

$$\eta = C_1\sqrt{T}e^{\left(\frac{\gamma V_{Free}^*}{V_{Free}}\right)} \quad 3.9$$

$$\kappa = \frac{C_2}{\sqrt{T}}e^{\left(-\frac{\gamma V_{Free}^*}{V_{Free}}\right)} \quad 3.1$$

0

Figure 3.9 outlines the theoretical volumes used to calculate V_{comp} in equation 3.5. Volumes were calculated by optimising the component molecular structure using a Hartree-Fock (HF) *ab initio* computational method coupled with a 3-21G basis set, followed by fitting a van der Waals (VDW) density surface. From the volumes calculated, hard sphere geometry was assumed and a corresponding hard sphere radius was calculated. All structure optimisation, surface fitting and component volume calculations were conducted using commercially available software.⁵³

Table 3.1 Table of theoretical hard sphere radii for the components studied

Species	Hard sphere radius (10^{-10} m)	Hard sphere volume (10^{-30} m ³)
Na ⁺	2.66	7.85
Ch ⁺	6.74	128
Cl ⁻	4.36	34.6
Br ⁻	4.66	42.3
OAc ⁻	5.29	62.0
B ₄ O ₇ ²⁻	6.35	107
H ₂ O	3.56	18.9
C ₃ H ₈ O ₃	6.02	91.5

Figure 3.9 shows the V_{free} values of a series of sodium salt:glycerol mixtures as a function of salt mole fraction, as well as the trend for a ChCl:glycerol system (purple trend). NaOAc, NaBr and NaOAc.3H₂O all show a decrease in V_{free} as a function of salt concentration, which is consistent with respect to observed changes in system density. In contrast, ChCl shows an increase in V_{free} , which is consistent with the decrease observed in system density. Abbott *et al.* also observed an increase in the V_{free} of a ChCl:glycerol mixture when compared with the fluidity of the system, and eluded the increase in V_{free} was a consequence of ChCl breaking down the structure of glycerol.¹⁰ Abbott *et al.* also demonstrated that mixtures of CrCl₃.6H₂O and urea showed an

increase in system free volume with increasing $\text{CrCl}_3 \cdot 6\text{H}_2\text{O}$ content, which coincided with decreases in viscosity and density.⁵⁶ The mechanism through which this phenomenon occurs can be related to the structural changes that occur in HBDs, as mentioned in section 3.3.2, which indicates disruptive hydrogen bonding interactions between the HBD and ions dominate over the ordering effect of electrostriction forces. The decrease in V_{free} observed in Figure 3.9 further reinforces the concept of NaOAc, NaBr and NaOAc. $3\text{H}_2\text{O}$ having a kosmotropic effect on glycerol, which may be due to the charge density of the ions promoting electrostriction.

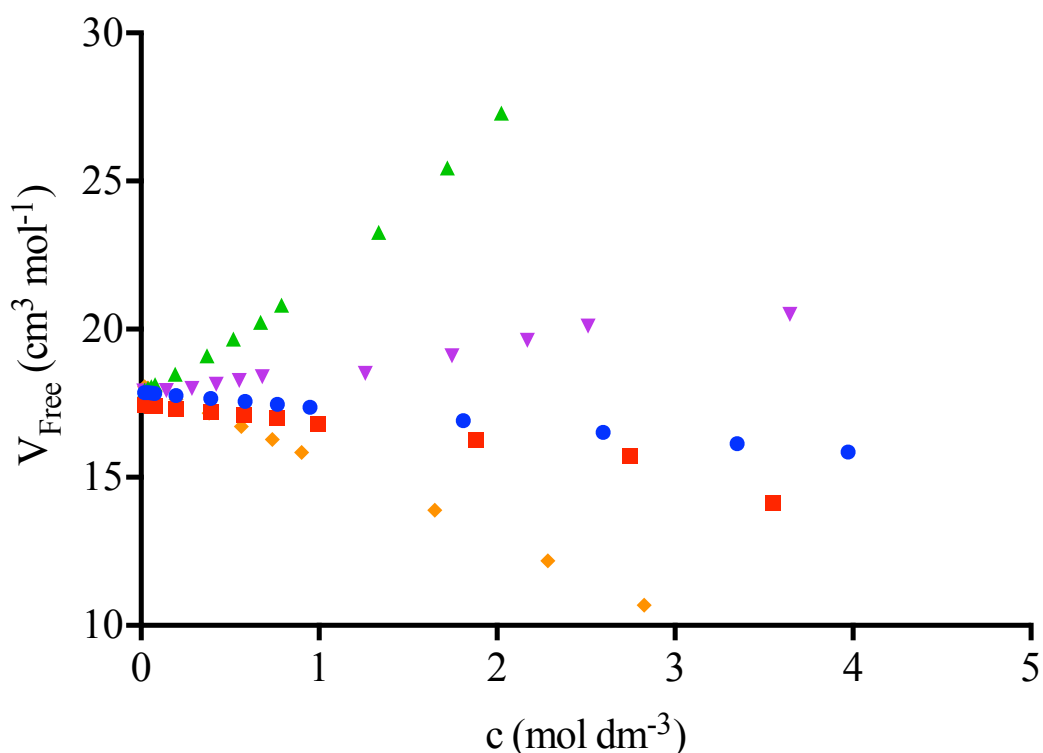


Figure 3.9 Free volume calculations for a series of salt:glycerol mixture as a function of salt concentration: (blue) NaOAc, (red) NaBr, (green) $\text{Na}_2\text{B}_4\text{O}_7 \cdot 10\text{H}_2\text{O}$, (purple) ChCl and (yellow) NaOAc. $3\text{H}_2\text{O}$, at 298 K

The role of waters of hydration is not clear from the data in Figure 3.9 as $\text{Na}_2\text{B}_4\text{O}_7 \cdot 10\text{H}_2\text{O}$ suggests a structure-breaking regime, whereas NaOAc. $3\text{H}_2\text{O}$ suggests a structure-making regime. It may be possible that water plays a different role in both systems but further studies are required to fully understand the role of water in these systems. The systems in Figure 3.9 are difficult to model as the speciation is still not fully understood, and even though the speciation of many DES have been previously

reported by the Abbott group using extended X-ray atomic fine structure (EXAFS), the speciation is dependent on the choice of components, and further research is required.⁵⁷

The HF computational method and 3-21G basis set used in the above analysis provide an introduction into the analysis of free volume measurements via computational methods. Further refinements can be made using higher levels of computational theory that account for electron correlation effects, which are otherwise neglected in the HF method.⁵⁸ Møller–Plesset perturbation theory (MP) is an advancement of the HF method that can contribute electron correlation effects via Rayleigh–Schrödinger perturbation theory.⁵⁹ Larger basis sets can improve the accuracy of computational methods, however, greater computing power is required as a consequence.⁶⁰

Density functional theory (DFT) is an alternative to traditional computational methods, which utilises functionals of spatially dependent electron density, as opposed to the complex many-electron wavefunctions used in HF methods.⁶¹ Computational requirements of DFT methods are relatively low when compared to HF methods and allow for relatively complex calculations without the need for specialist hardware.⁶¹

EXAFS could be utilised as a non-computational alternative to the determination of V_{comp} . Speciation determination using EXAFS allows for molecular volumes to be determined from the deduced species structure without the need for computational approximations.

3.3.4. Viscosity

The viscosity of a fluid is a quantification of the resistance to deformation via shear stress, which is due to internal friction within the fluid.³⁴ Dynamic viscosity of a fluid is specifically the resistance to shear flows, where parallel fluid layers move at different velocities, as shown in Figure 3.10, and mathematically represented in equation 3.11, where τ represents shear stress, η is the coefficient of dynamic viscosity and $(\delta u/\delta y)$ is the shear rate.⁶²

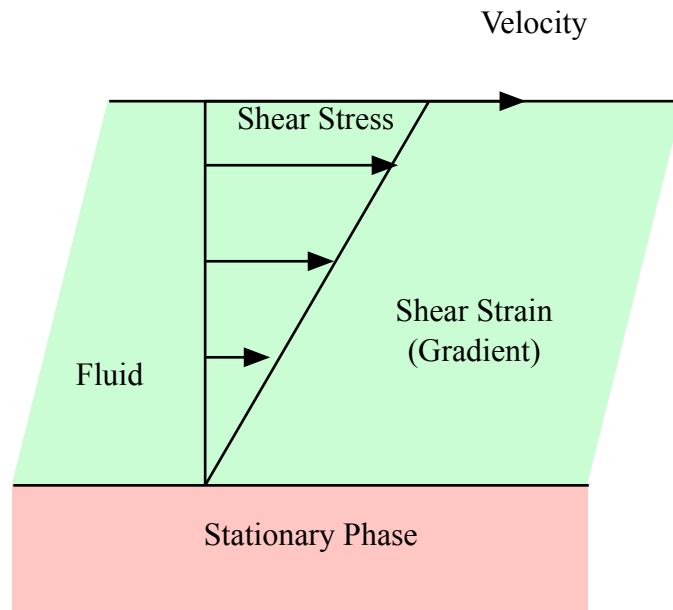


Figure 3.10 Laminar shear of a fluid demonstrating dynamic viscosity

$$\tau = \eta \frac{du}{dy} \quad 3.11$$

There are two broad classes of viscosity behaviour in fluids: *Newtonian* and *non-Newtonian*. Newtonian fluids have a constant viscosity coefficient regardless of the imposed shear rate, and low molecular weight pure liquids such as: water, glycerol and acetone are examples of liquids that express Newtonian fluid behaviour.³⁴ Non-Newtonian fluids have a variable viscosity coefficient depending on the imposed shear rate, and can either shear thicken or shear thin, which is graphically represented in Figure 3.11.³⁴ ILs were initially believed to be non-Newtonian fluids, as little research had been conducted to prove otherwise, however, recent research suggests that many, but not all ILs, are non-Newtonian fluids.^{34,63,64} There is some research to suggest some DESs behave as Newtonian fluids however, independent research suggests DESs behave as non-Newtonian fluids implying like ILs, the fluid behaviour is dependent on the components of the system.^{65,66,67}

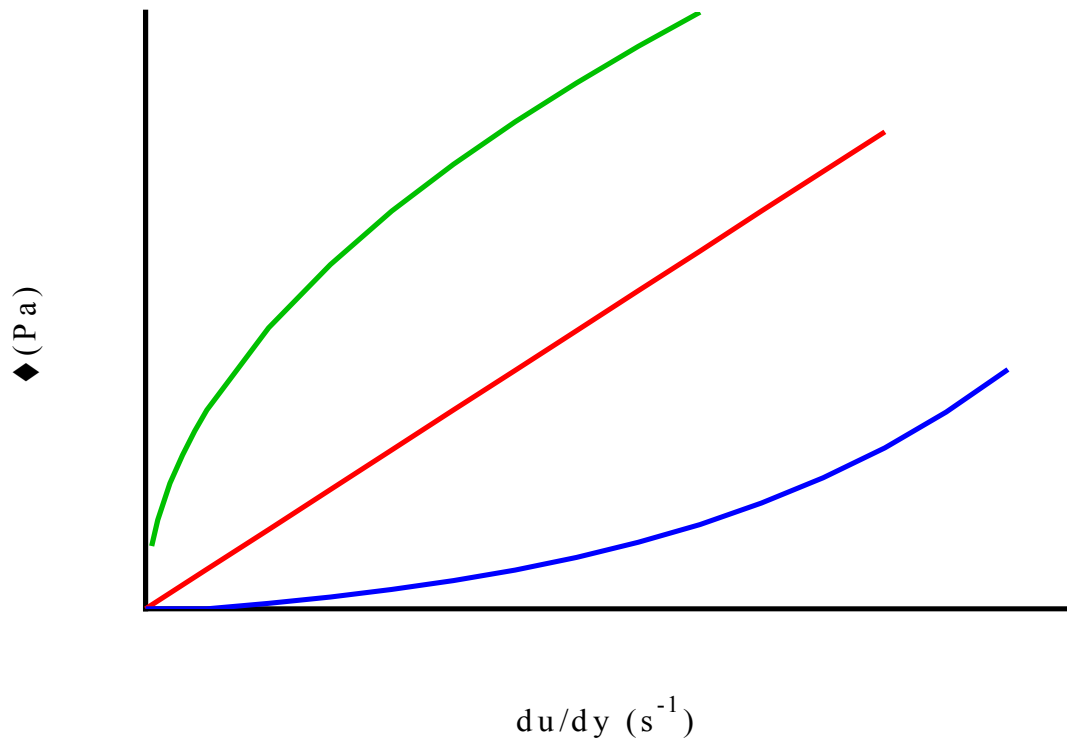


Figure 3.11 Typical shear stress (τ) vs. shear rate ($\delta u/\delta y$) profiles for Newtonian and non-Newtonian fluids: (Blue) Shear-thickening, (Red) Newtonian and (Green) Shear-thinning

Figure 3.12 shows how viscosity of a sodium salt:glycerol and ChCl:glycerol system varies as a function of temperature, and suggests both systems follow an Arrhenius model for dynamic viscosity. The trends presented in Figure 3.12 are representative of all of the systems tested, and have been omitted for clarity.

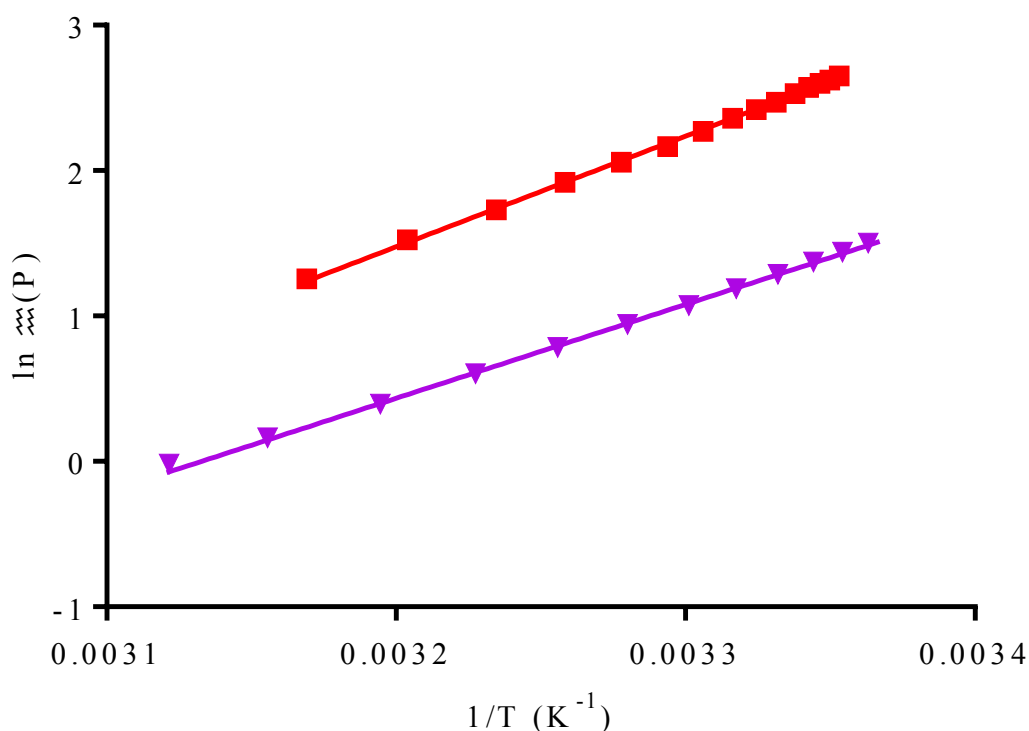


Figure 3.12 Natural logarithm of dynamic viscosity of salt:glycerol mixtures as a function of inverse temperature: (red) 1.88M NaBr and (purple) 2.17M ChCl

The Arrhenius model for dynamic viscosity assumes a fluid conforms to the Arrhenius equation of molecular kinetics, as expressed in equation 3.12 as the general form where: k is the rate constant, A is the pre-exponential factor, E_a is the activation energy of a process, R is the universal gas constant and T is absolute temperature.⁶⁸ Upon heating, the fraction of molecules that have kinetic energy greater than the E_a of a process, signified by the exponential factor in equation 3.12, increases, which leads to an increase in the rate constant of the process.⁶⁸ In the context of viscosity, heating results in a greater proportion of molecules having kinetic energy greater than the activation energy of viscous flow (E_η), which means more molecules are able to overpower the resistive interactions between shear planes.

$$k = Ae^{\frac{-E_a}{RT}} \quad 3.12$$

As temperatures tend towards the glass transition temperature of the system, viscosity deviates from Arrhenius behaviour, which is characteristic of glass-forming liquids.⁶⁹ The observed temperature dependence of IL viscosity can be defined using the

Vogel-Tammann-Fulcher (VFT) model, as shown in equation 3.13 where A and B are constants, and T_o is the temperature at which viscosity tends to zero.⁶⁹

$$\eta = Ae^{\frac{B}{T-T_o}} \quad 3.13$$

Figure 3.13 shows how viscosity of a sodium salt:glycerol and ChCl:glycerol system varies as a function of temperature, as fitted using the VFT model, and suggests both systems follow a VFT model for dynamic viscosity. Although the trends derived from fitting the Arrhenius model, Figure 3.12, showed acceptable linearity, fitting of the VFT model has allowed for better modelling at lower system temperatures. The trends presented in Figure 3.13 are representative of all of the systems tested, and have been omitted for clarity.

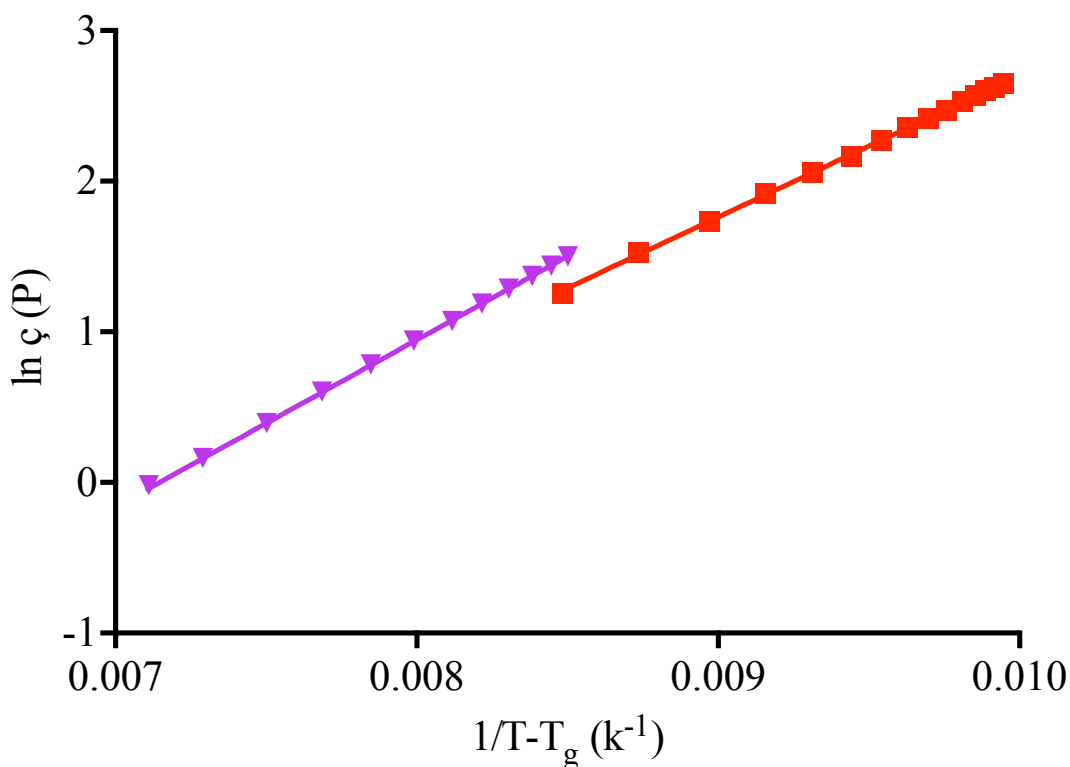


Figure 3.13 Natural logarithm of dynamic viscosity of salt:glycerol mixtures as a function of inverse temperature, fitted using the VFT model: (red) 1.88M NaBr and (purple) 2.17M ChCl

ILs are generally more viscous than molecular solvents, which at room temperature have viscosities ranging from 10 cP to over 500 cP, whereas: water,

ethylene glycol and glycerol have 0.890, 16.1 and 934 cP respectively.³² The viscosities of ILs are strongly dependent on temperature; for example, 1-butyl-3-methylimidazolium hexafluorophosphate experiences a viscosity change of 27 % over the temperature range 298-293 K.⁷⁰ As well as high temperature sensitivity, alkylimidazolium based ILs are adversely affected by the presence of impurities, with chloride impurity contents of between 1.5 and 6 % w/w resulting in a 30 – 600 % increase in system viscosity.⁷¹

The viscosities of DESs cover a much wider range than what is generally observed with ILs, with viscosities ranging from 36 cP, for a eutectic mixture of ChCl and ethylene glycol, to approximately 11000 cP for a eutectic mixture of ZnCl₂ and urea at 298 K.^{26,72} Abbott *et al.* found that viscosity followed the Arrhenius model with respect to temperature and found DESs had large values for E_η , which was shown to empirically correlate with the ratio of the ion size to the average radius of the voids in the liquid.³⁶

Figure 3.14 shows how viscosity of a series of salt:glycerol mixture varies as a function of salt concentration. At the highest concentrations measured for each sodium salt:glycerol system, viscosity varied from 487 ± 3 cP for a 2.83 M NaOAc.3H₂O mixture to 16300 ± 100 cP for a 3.98 M NaOAc mixture at 298 K. The range of viscosities measured is comparable with what is typically seen with DESs but are considerably more viscous than most commonly used ILs and molecular solvents.

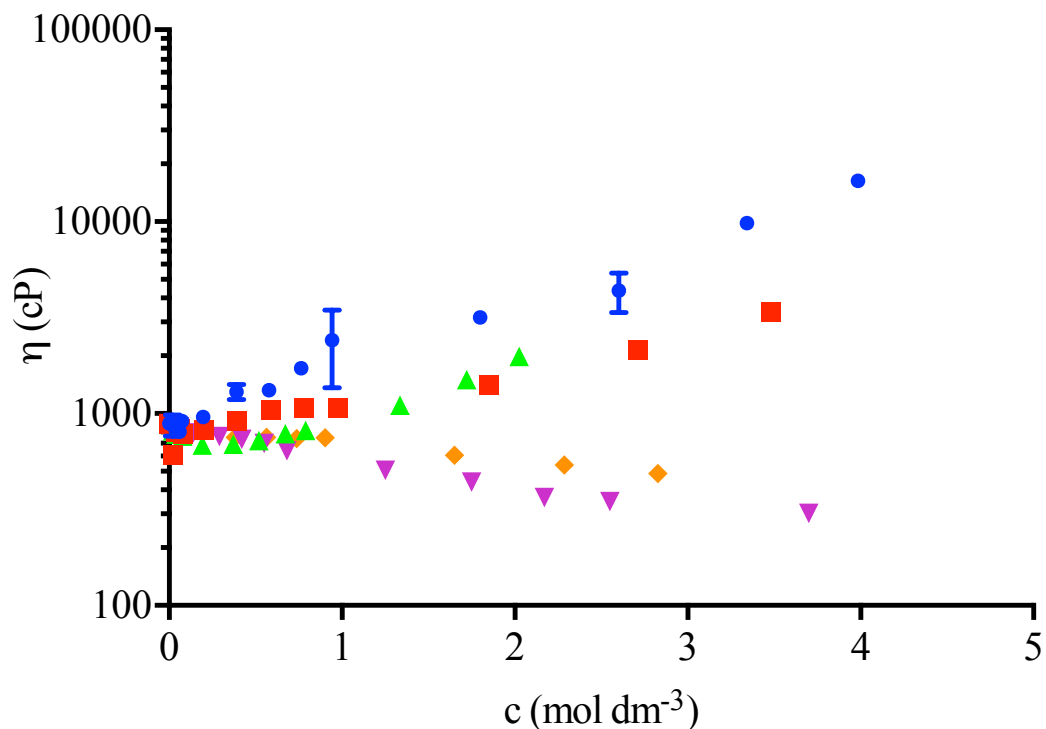


Figure 3.14 Viscosity measurements for a series of salt:glycerol mixture as a function of salt concentration: (blue) NaOAc, (red) NaBr, (green) $\text{Na}_2\text{B}_4\text{O}_7 \cdot 10\text{H}_2\text{O}$, (purple) ChCl and (yellow) $\text{NaOAc} \cdot 3\text{H}_2\text{O}$, at 298 K

Except for $\text{NaOAc} \cdot 3\text{H}_2\text{O}$, all of the sodium salts studied, at all concentrations, increased the viscosity of glycerol. Ionic species that have high charge densities are known to have a kosmotropic effect on polar solvents resulting in stronger solvent-solvent interactions, as shown in Figure 3.15 A.^{73,74} In the context of viscosity, stronger solvent-solvent interactions implies greater resistive forces between shear planes, which results in a greater E_η that leads to a greater dynamic viscosity. Not all inorganic salts have a structure forming effect on the viscosity of water, and the observed effect is dependent on the components of the salt.⁷⁵

The Abbott group have documented that QASs decrease the viscosity glycerol, oxalic acid, urea and other HBD as a function of QAS concentration.^{10,29,36} Abbott rationalised this phenomenon as the QAS disrupting the hydrogen bonding network, shown in Figure 3.15 B, which from a viscosity context, implies weaker resistive forces between fluid shear planes, which results in a lower E_η that leads to a decrease in dynamic viscosity.¹⁰ Chaotropic salts are known to show structure breaking effects via disruption of non-covalent intermolecular forces, which can result in the formation of ion-dipole interactions between ions and the hydrogen-bonding species, which is

thermodynamically more favourable compared to the solvent intermolecular interactions.⁷⁶

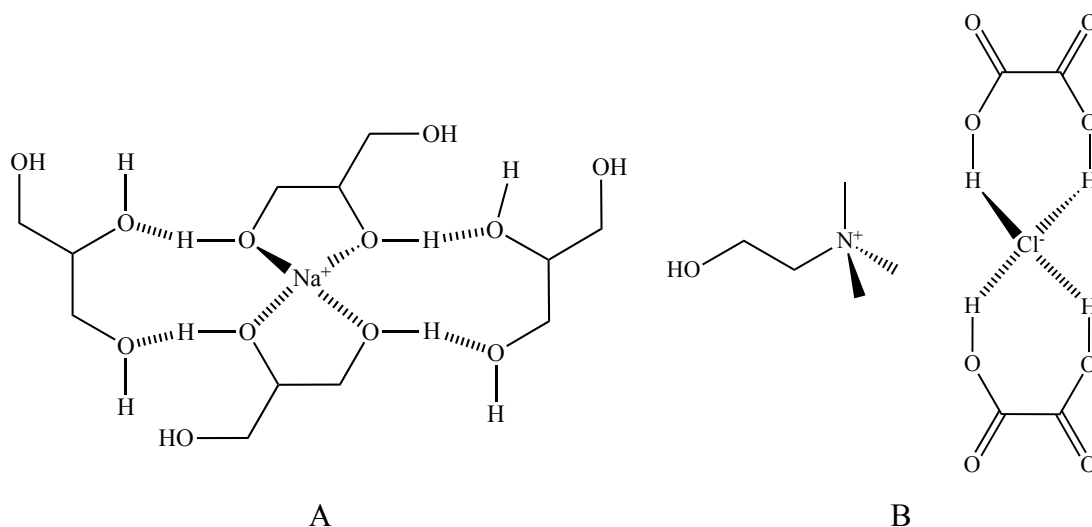


Figure 3.15 Salt effects on H-bonding network: Sodium salt (A) and QAS (B)

The role of water is not clear from the trends shown in Figure 3.14 as NaOAc.3H₂O shows a decrease in viscosity as a function of salt concentration, whereas Na₂B₄O₇.10H₂O indicates an increase in viscosity. Water could play a different role in both systems, but further work is needed to understand this phenomenon. A comparison between NaOAc.3H₂O and NaOAc suggests the waters of hydration may be relatively free, implying the free water could act as a diluent. Unfortunately, a comparison between Na₂B₄O₇.10H₂O and Na₂B₄O₇ could not be achieved, as Na₂B₄O₇ is insoluble in glycerol.

Arrhenius found that changes in solvent viscosity induced by the addition of salts were related through equation 3.14, where c is the salt concentration, and A is the *salt constant* at a given temperature.⁷⁷ At concentrations greater than 0.1 M the systems investigated in Figure 3.14 follow this model with typical R² values greater than 99 % however, at concentrations below 0.1 M significant deviations occur, which is well known for this model.⁷⁸

$$\eta = A^c \tag{3.14}$$

Dole and Jones expanded the Arrhenius model and found that the viscosity of a salt solution showed the dependence on ion concentration illustrated in equation 3.15, where (η/η_0) is the viscosity of the solution relative to the viscosity of the solvent, also known as relative viscosity (η_r), A and B are system specific constants.⁷⁹ The A constant

in equation 3.15 is independent of concentration and is a result of ion-ion interaction, whereas the B constant is related to the solute effect on the solvent.⁷⁹ Negative B values indicate the solute is behaving as a chaotrope, and a positive B values suggests the solute is behaving as a kosmotrope.⁷⁹

$$\eta_r = \frac{\eta}{\eta_o} = 1 + A\sqrt{c} + Bc \quad 3.15$$

Equation 3.15 can be rearranged to the simpler form shown in equation 3.16, which allows a linear plot of $(\eta_r - 1)/\sqrt{c}$ as a function of \sqrt{c} to be drawn, where A is the y-intercept and B is the slope of the plot.⁷⁸

$$\frac{\eta_r - 1}{\sqrt{c}} = A + B\sqrt{c} \quad 3.16$$

Figure 3.16 shows the Dole-Jones plots for a series of salt:glycerol mixtures as a function of the square root of salt concentration up to 1 M. The sodium salts investigated all showed an increase in the $(\eta_r - 1)/\sqrt{c}$ term, whereas the ChCl system showed a decrease, indicating positive and negative B constants respectively. The sodium salts investigated all demonstrated negative A values, whereas the ChCl:glycerol system showed an A value very close to zero. A and B values for all of the systems investigated have been listed in Table 3.2.

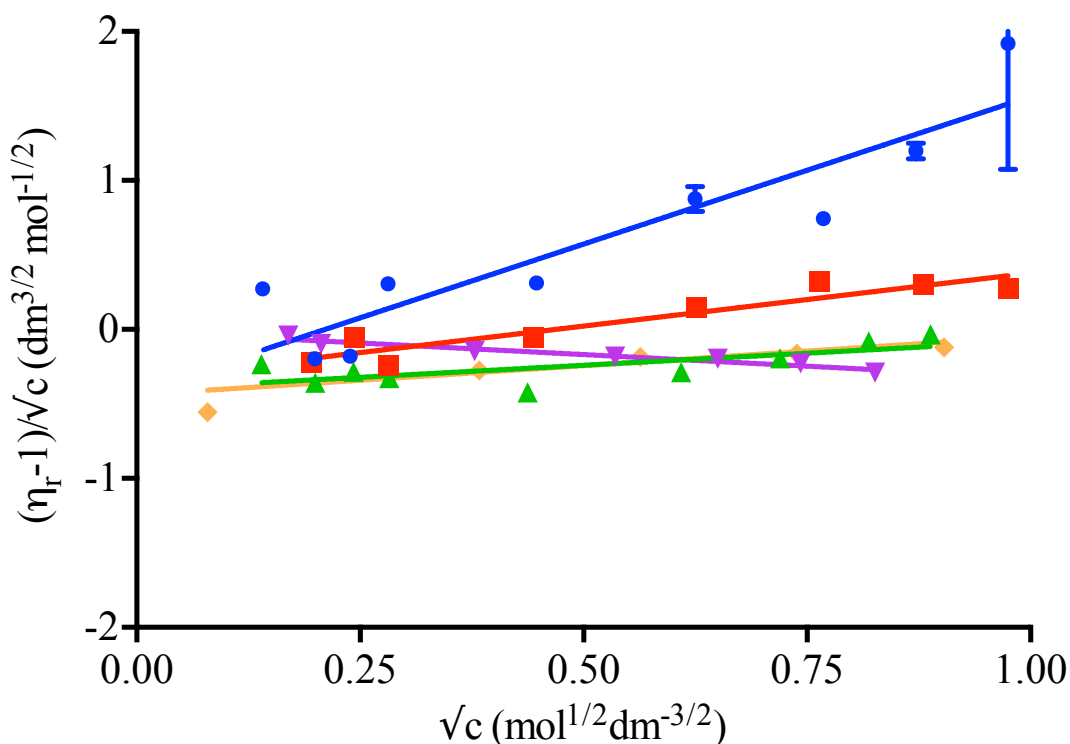


Figure 3.16 Dole-Jones plots for a series of salt:glycerol mixture as a function of salt concentration: (blue) NaOAc, (red) NaBr, (green) Na₂B₄O₇·10H₂O, (purple) ChCl and (yellow) NaOAc·3H₂O, at 298 K

Table 3.2 Dole-Jones A and B parameters for the systems investigated in Figure 3.16

Salt	A (dm ^{3/2} mol ^{-1/2})	B (dm ³ mol ⁻¹)
NaOAc	-0.42 ± 0.20	1.98 ± 0.33
NaBr	-0.33 ± 0.067	0.71 ± 0.11
Na ₂ B ₄ O ₇ ·10H ₂ O	-0.40 ± 0.064	0.32 ± 0.12
ChCl	-0.013 ± 0.019	-0.31 ± 0.034
NaOAc·3H ₂ O	-0.44 ± 0.086	0.39 ± 0.15

The values obtained for the *B* parameter give an insight into ion-solvent interactions and suggests the sodium salts investigated are acting as kosmotropes and reinforce the structure of glycerol, which in turn raises *E_η* of glycerol leading to an increase in the viscosity of the system.⁷⁸ The negative *B* parameter for the ChCl:glycerol system indicates a structure breaking effect on glycerol and implies ChCl acts as a chaotrope. Research by Dole and Jones showed the *A* parameter was negative

for all strong electrolytes and zero for non-electrolytes, which agrees with the values displayed by all of the systems investigated.⁷⁸ The A parameter can be calculated from equilibrium theory, which has been demonstrated by Falkenhagen, but additional investigations into the A parameter are required to further understand its qualitative significance.⁸⁰

3.3.5. Fluid Behaviour

There are conflicting arguments in the scientific literature regarding the fluid behaviour of ILs and DESs, but component choice has been repeatedly regarded as the deciding factor.⁵⁷⁻⁶⁷ Figure 3.17 shows how viscosity for a series of approximately 2 M salt:glycerol mixtures varied as a function of viscometer rotation speed (ω). A Newtonian fluid displays a linear relationship between shear stress and shear rate, whereas a non-Newtonian fluid can show any of the shear stress-rate relationships presented in Figure 3.11. When reviewing dynamic viscosity versus shear rate plots, a Newtonian fluid is represented by a linear trend of zero gradient, as shown by NaBr, Na₂B₄O₇·10H₂O, ChCl, NaOAc·3H₂O systems and pure glycerol in Figure 3.17. NaOAc showed a positive gradient, which suggests the NaOAc:glycerol system is behaving as a *shear-thickening* fluid.

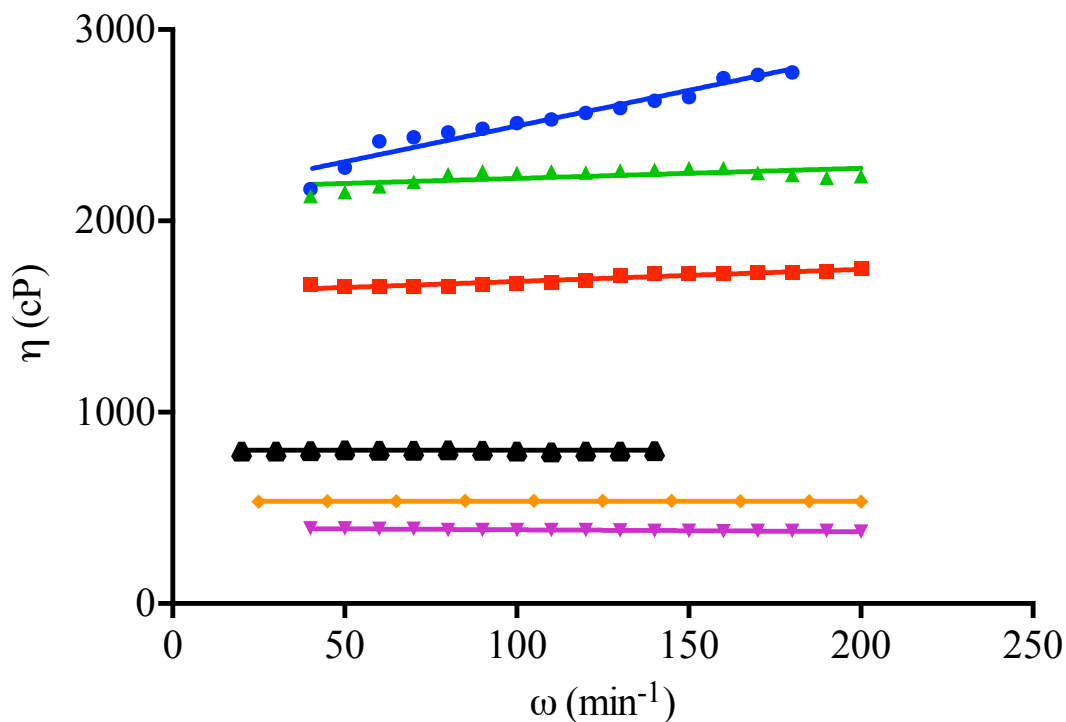


Figure 3.17 Viscosity for a series of salt:glycerol mixture as a function of viscometer rotation speed: (blue) 1.80 M NaOAc, (red) 1.88 M NaBr, (green) 2.02 M Na₂B₄O₇·10H₂O, (purple) 2.17 M ChCl, (yellow) 2.28 M NaOAc·3H₂O and (black) pure glycerol, at 298 K

Shear-thickening fluid behaviour is typical of many colloidal suspensions, and is a result of a system crystallising under stress and behaving more like a solid.⁸¹ ILs generally show shear thinning fluid characteristics at high shear rates, which has been attributed to the onset of stacking of polar and apolar layers that breaks down the hydrogen-bonded network, thus accommodating easier shear deformation.⁵⁸ Although, Jacquemin *et al.* found diisopropyl-ethylammonium based protic ionic liquids showed shear-thickening behaviour at shear rates greater than 4000 s⁻¹, but gave no indication as to why the phenomenon occurred.⁸² Abbott *et al.* found eutectic mixture of ChCl and urea showed non-Newtonian fluid properties in the pure state, but upon the addition of 2.5 % water was found to behave as a Newtonian fluid.⁸³ The pronounced effect of water on the fluid behaviour of the ChCl: urea mixture, was linked to the hydrogen bond donating parameter (α) of the system being lower compared to other ChCl: HBD systems and pure water, which suggested water was preferentially solvating the chloride anion.⁸³ Studies into the solvent parameters of sodium salt:glycerol mixtures have not

been investigated, and studies in this area may be needed to explain the uncharacteristic fluid behaviour in the NaOAc:glycerol system.

3.3.6. Ionic Conductivity

Initial development of ILs was concentrated on utilisation as electrolytes for capacitor and battery applications, as ILs have properties that are desirable for electrochemical processes including: good electrical conductivity and mass transport properties.³⁴ Ionic conductivity of ILs can be measured using an (AC) method that utilises a two-electrode cell to measure the impedance of a system (Z), which is dependent on resistance (R) and capacitance (C) and signal frequency (ω) as defined by equation 3.17.⁸⁴

$$z = \sqrt{\left(\frac{1}{\omega C}\right)^2 + R^2} \quad 3.17$$

As the AC signal frequency tends to infinity, capacitive contributions in Z tend to zero implying cell impedance becomes equal to the cell resistance. Therefore at high AC signal frequencies, the ionic conductivity of an IL (κ) can be deduced from resistance measurements with respect to the electrode separation (l) and area (A), as shown in equation 3.18.³⁴

$$\kappa = \frac{l}{AR} \quad 3.18$$

The conductivity of ILs follows the Arrhenius model above room temperature, which like the viscosity model, assumes the fluid conforms to the Arrhenius equation of molecular kinetics, as expressed in equation 3.12.³⁴ As temperatures tend towards the glass transition temperature of the system, ionic conductivity deviates from Arrhenius behaviour, which is characteristic of glass-forming liquids.⁶⁹ The observed temperature dependence of IL ionic conductivity can be defined using the VFT model, as shown in equation 3.19 where A and B are constants, and T_o is the temperature at which ionic conductivity tends to zero.⁶⁹

$$\kappa = A \frac{1}{\sqrt{T}} e^{\frac{-B}{T-T_o}} \quad 3.19$$

Figure 3.18 shows how the ionic conductivity of a NaBr:glycerol and ChCl:glycerol system varies as a function of temperature, and suggests both systems

follow the Arrhenius model. The trends presented in Figure 3.18 are representative of all of the systems tested, which have been omitted for clarity. The 1.88 M NaBr:glycerol system demonstrates the Arrhenius model breaking down at lower temperatures.

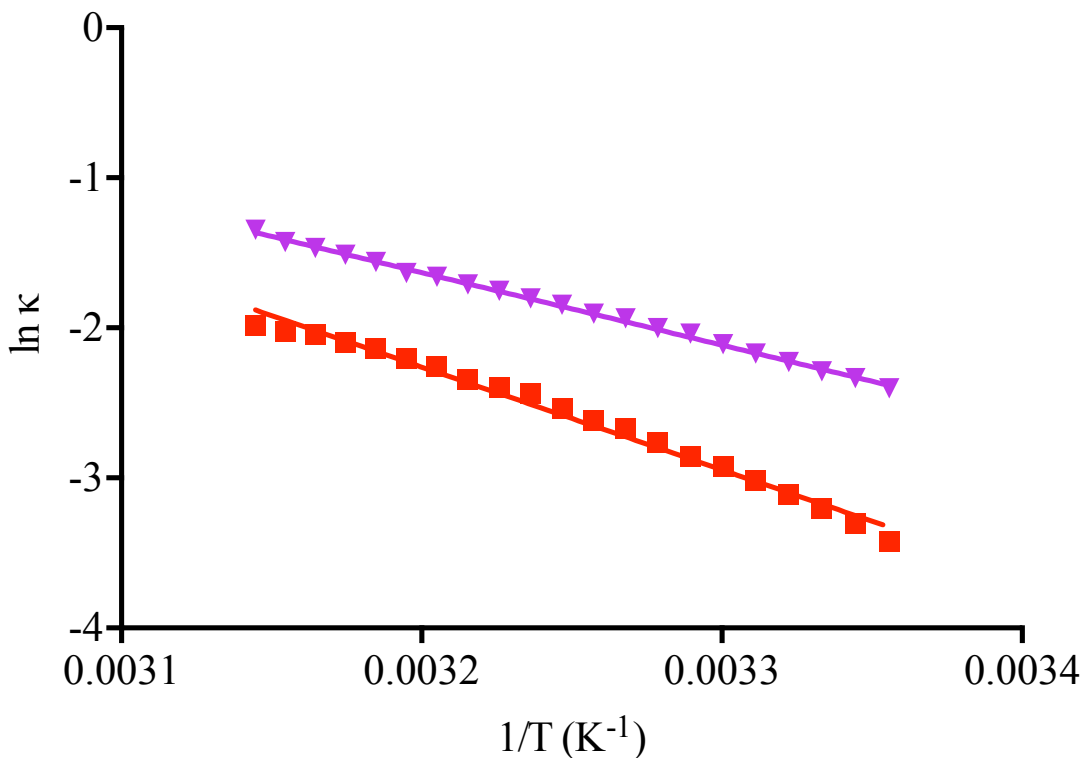


Figure 3.18 Natural logarithm of ionic conductivity of salt:glycerol mixtures as a function of inverse temperature: (red) 1.88M NaBr and (purple) 2.17M ChCl

Figure 3.19 shows how ionic conductivity of a sodium salt:glycerol and ChCl:glycerol system varies as a function of temperature, as fitted using the VFT model, and suggests both systems follow a VFT model for ionic conductivity. Although the trends derived from fitting the Arrhenius model, Figure 3.18, showed acceptable linearity, fitting of the VFT model has allowed for better modelling at lower system temperatures. The trends presented in Figure 3.19 are representative of all of the systems tested, and have been omitted for clarity.

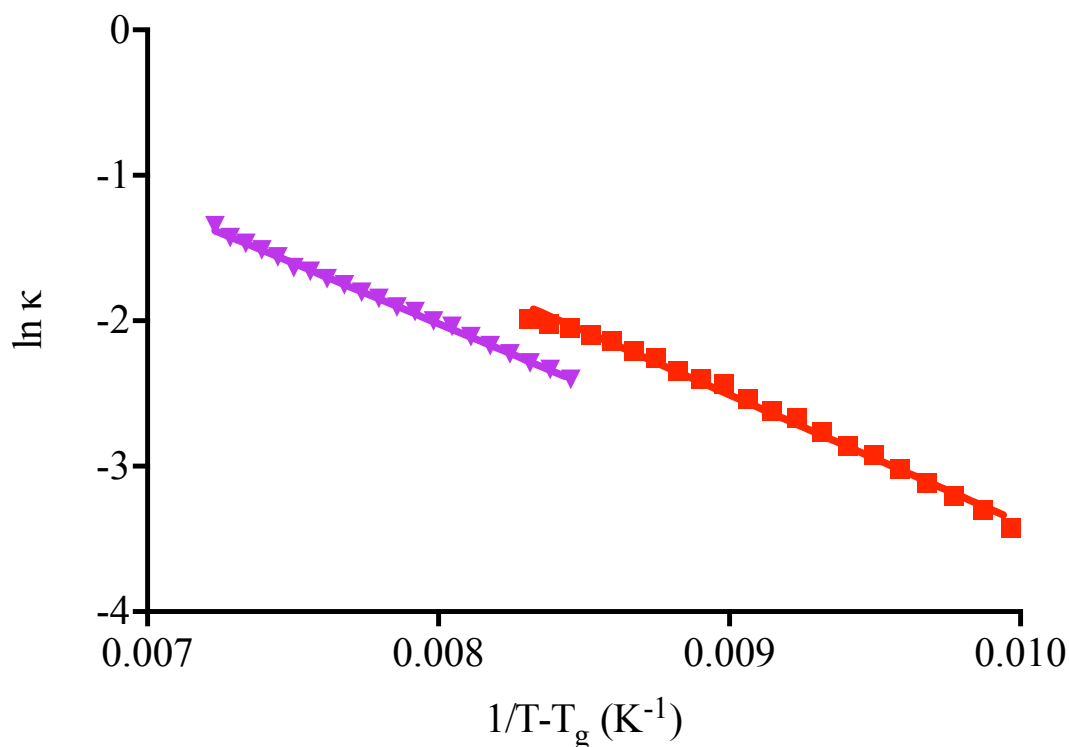
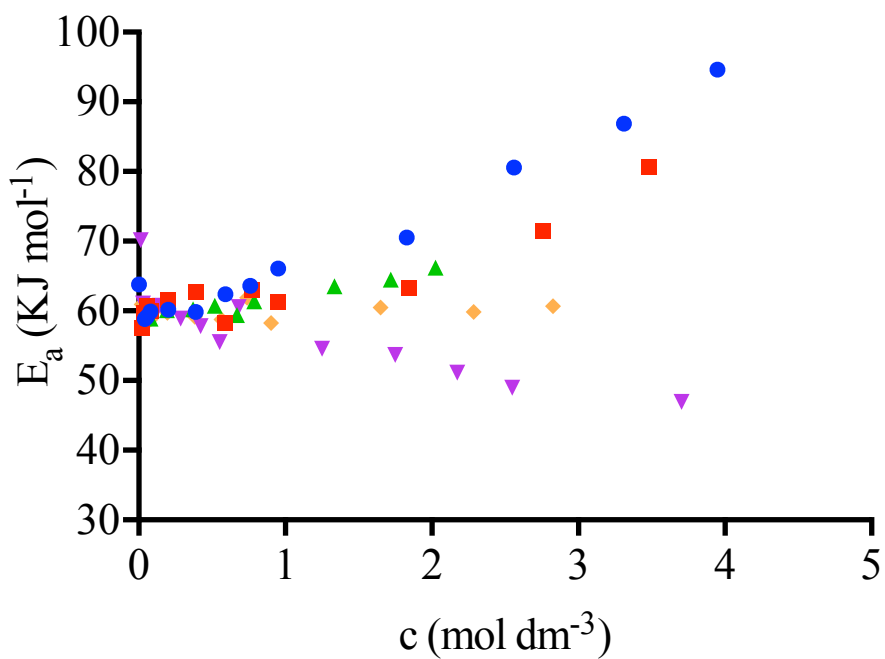
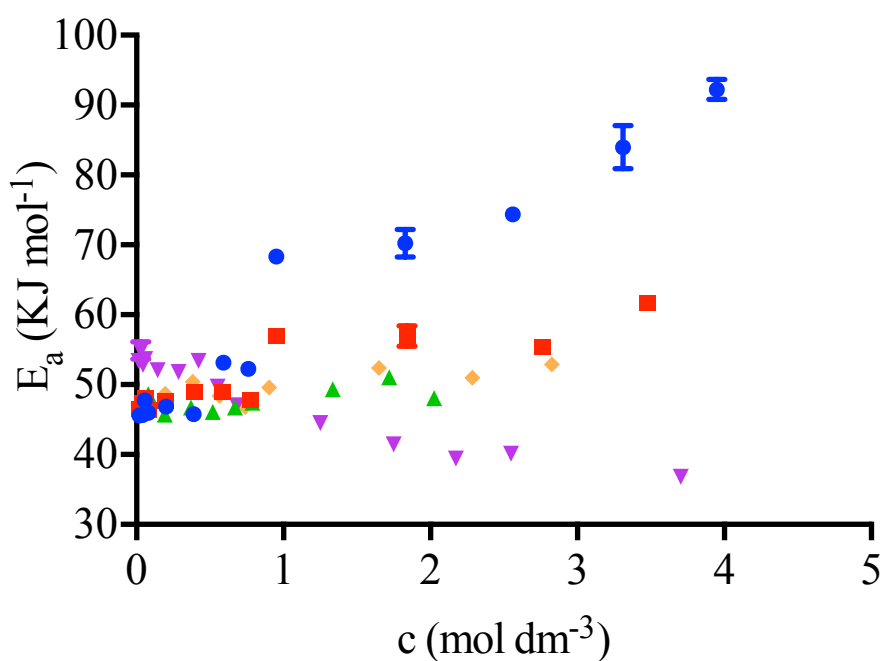


Figure 3.19 Natural logarithm of ionic conductivity of salt:glycerol mixtures as a function of inverse temperature, fitted using the VFT model: (red) 1.88M NaBr and (purple) 2.17M ChCl

From the Arrhenius model for dynamic viscosity and ionic conductivity the activation energy of viscous flow (E_η) and conductivity (E_κ) can be deduced respectively. E_η is normally quoted as a negative quantity due to the negative relationship between viscosity and temperature, as shown in Figure 3.12. To make a direct comparison with E_σ , viscosity is inverted to give the fluidity (φ) and the deduced activation energy of fluid flow (E_φ) is calculated using the formula outline in equation 3.12. Figure 3.20 A and B shows how E_φ and E_κ respectively vary with concentration as a function of salt concentration. The sodium salt:glycerol systems at their maximum concentrations show E_φ and E_κ values in the range 50-95 kJ mol⁻¹, which is significantly higher than most ILs and DES, and has been linked to low system free volume.^{36,85,86} For a given salt:glycerol system, at all concentrations, the E_φ and E_κ values are very similar and follow the same general trends, which further supports a link between the two parameters. Qualitatively, as the activation energy of fluid flow increases, the activation energy of conduction will also increase due to fewer charge carrying species having sufficient kinetic energy to engage in fluid flow, thus limiting charge carrier mobility.



A



B

Figure 3.20 Activation energy of: fluid flow (A), conductivity (B) for a series of salt:glycerol mixtures as a function of salt concentration: (blue) NaOAc, (red) NaBr, (green) $\text{Na}_2\text{B}_4\text{O}_7 \cdot 10\text{H}_2\text{O}$, (purple) ChCl and (yellow) $\text{NaOAc} \cdot 3\text{H}_2\text{O}$, at 298 K

The ionic conductivity of an electrolyte is a measure of charge carrier quantity and mobility.³⁴ Considering ILs are liquids comprised of ions, large ionic conductivities

would have been expected however, ionic conductivities are typically found to be in the 0.5-15 mS cm⁻¹ range at 298 K.³⁴ ILs possess significantly lower ionic conductivities compared aqueous electrolytes, as at high concentrations ions pair or form aggregates which reduces the concentration of charge carriers, and the generally large species size found in ILs results in reduced ion mobility.³⁴ DESs also possess lower than expected ionic conductivities due to the same limitations of ion aggregation and compromised ion mobility, but due to the generally higher dynamic viscosities further limiting ion mobility, DESs have ionic conductivities in the range 0.3-8.0 mS cm⁻¹.²⁶

Figure 3.21 shows the ionic conductivity for a series of salt:glycerol mixtures as a function of salt concentration. Of the sodium salt:glycerol systems investigated, a 2.83 M NaOAc.3H₂O:glycerol mixture achieved the highest conductivity of 0.77 ± 0.005 mS cm⁻¹, whereas the lowest ionic conductivity of a concentrated sodium salt:glycerol system was recorded at 6.55 ± 0.01 μS cm⁻¹ for the 2.28 M NaOAc:glycerol system. Compared to the ChCl:glycerol DES system, the sodium salt:glycerol mixtures in general showed significantly lower ionic conductivity.

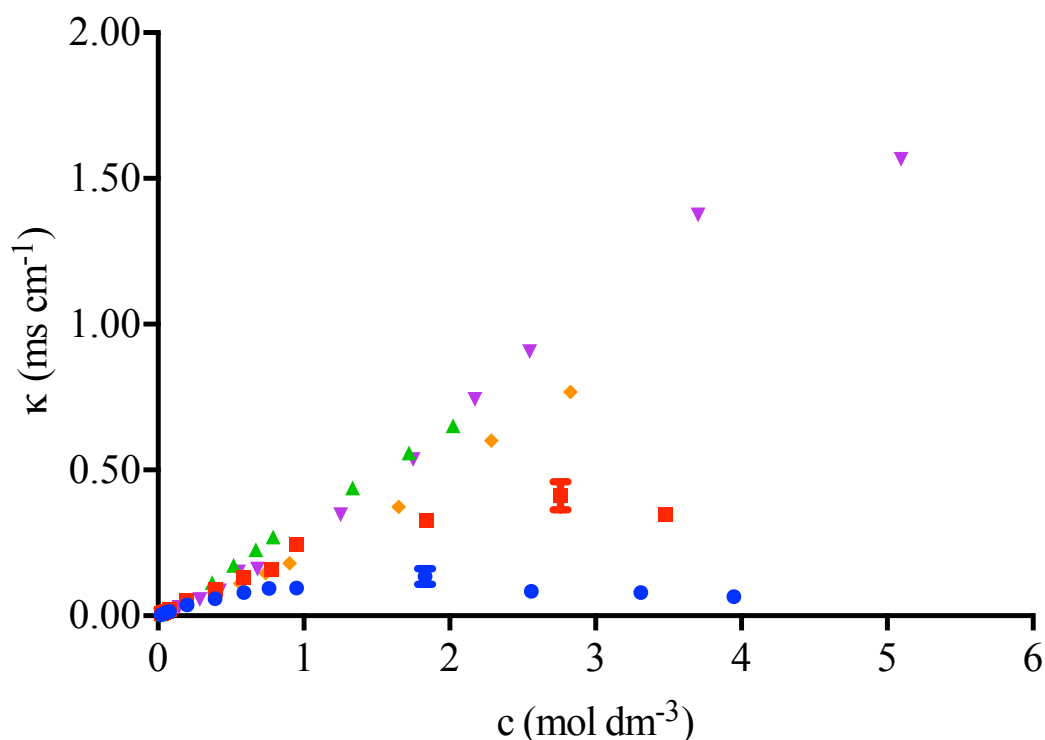


Figure 3.21 Ionic conductivity measurements for a series of salt:glycerol mixtures as a function of salt concentration: (blue) NaOAc, (red) NaBr, (green) Na₂B₄O₇·10H₂O, (purple) ChCl and (yellow) NaOAc·3H₂O, at 298 K

All of the systems investigated in Figure 3.21 showed initial increases in conductivity as concentration increased suggesting at lower concentrations, the number of charge carriers limits the ionic conductivity of the system. At concentrations above 2 M, the NaOAc and NaBr systems decrease in conductivity, suggesting ionic conductivity is no longer limited by charge carrier concentration. The Na₂B₄O₇·10H₂O, ChCl and NaOAc·3H₂O systems do not reach a maximum over the concentration range investigated, although extrapolation of the observed trends suggest a maximum would occur if the salt concentration were sufficiently high. Abbott *et al.* found that addition of ChCl to a variety of diols resulted in an increase in ionic conductivity of the system, and after a mole fraction of 15 % was achieved, the rate of change in ionic conductivity started to decrease suggesting a similar trend to what was observed in Figure 3.21.⁸⁷ However, the concentration range investigated in Abbott's research was not high enough to show a turning point.

Both Na₂B₄O₇·10H₂O and NaOAc·3H₂O increases the ionic conductivity of glycerol significantly more than NaOAc or NaBr at concentrations above 1 M. Considering both Na₂B₄O₇·10H₂O and NaOAc·3H₂O are hydrated salts, it may be possible the waters of hydration are relatively free, thus acting as a diluent to aid ion mobility and inhibit ion pair formation. However, further research into the speciation and role of water in these systems needs to be carried out to support this hypothesis.

3.3.7. Molar Conductivity

Considering ionic conductivity varies as a function of concentration, comparisons between systems can only be truly made when ionic conductivity is normalised with respect to the concentration of ions, as shown in equation 3.20.⁵⁰

$$\Lambda = \frac{\kappa}{c} = \frac{\kappa M_r}{\rho} \quad 3.20$$

Analysis of the conductivity behaviour of QAS in low dielectric solvents conducted by Fuoss and Kraus, found that conductivity went through four discrete regimes, which were dependent on the salt and solvent, as shown in Figure 3.22.^{88,89,90,91} Initially, conductance decreases proportionally with the square root of the concentration, which is linked to the equilibrium between single ions and neutral ion pairs, defined by the equilibrium in equation 3.21, where C and A are cations and anions respectively. A minimum was then observed resulting from the equilibrium

between triple ions and ion pairs, then at higher concentrations, an increase in conductance occurs due to the dominance of charged triple ions, defined by the equilibria in equations 3.22 and 3.23. Upon further increase in salt concentration a second maximum is observed followed by a decrease in conductance which has been attributed to a shift from a charge carrier limited regime to an ion-mobility-limited regime which is dominated by viscosity.^{92,93}

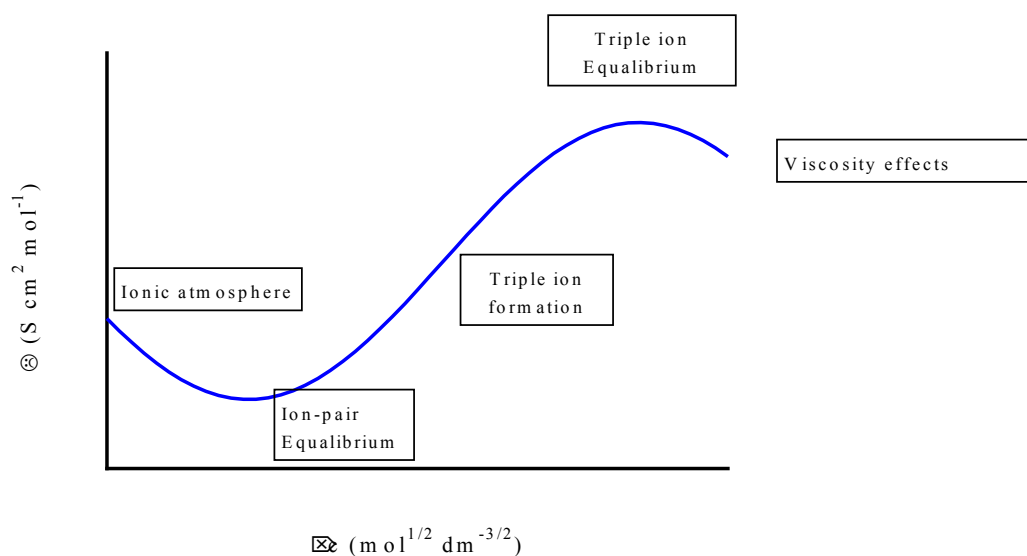


Figure 3.22 Schematic molar conductivity plot showing Fuoss and Kraus conductivity regimes



Figure 3.23 demonstrates how molar conductivity (Λ) for a series of salt:glycerol systems vary as a function of the square root of salt concentration. ChCl:glycerol mixtures (purple trend) show the four regimes Fuoss and Kraus defined for molar conductivity in ionic solutions: up to 0.25 M, molar conductivity decreases to a minimum suggesting formation of ion pairs, followed by an increase to approximately 4 M, which is indicative of triple ion formation, beyond 4 M a decrease is observed due to a shift to a ion mobility limited regime.⁹⁴ NaOAc and NaBr systems show a consistent

decrease in molar conductivity across the measured concentration range, which can be interpreted in two ways. Firstly, one could assume the initial stage of the Fuoss and Kraus model is dominating, and attribute the observed behaviour to the formation of neutral ion pairs, or, one could assume viscosity effects dominate over the observed concentration range. Fuoss showed that for ions of a finite size, ion pairing occurs regardless of the dielectric constant of the solvent, suggesting the trends observed for the NaOAc and NaBr system may not be totally attributed to a viscosity limited regime.⁸⁸ However, the conductivity trends for the same systems shown in Figure 3.21 show a clear maximum at approximately 2.5 M and subsequently decrease in conductivity suggests a shift to a viscosity limited regime does occur. The observed decrease in molar conductivity of these systems coincides with the increases observed in dynamic viscosity. The NaOAc:glycerol system, which was the most viscous system investigated, demonstrated the lowest molar conductivity; the NaBr:glycerol system, which was the second most viscous system studied, demonstrated the second lowest molar conductivity. Roy *et al.* found that the formation of triple ions is dependent on the ratio of ion pair, and triple ion formation constants, K_p and K_T respectively, and in some instances triple ion formation in mixtures of QAS and carbon tetrachloride was limited.⁹⁵ It may be possible that the NaBr and NaOAc systems show limited triple ion formation, and the transition from ion pair formation to a viscosity limited regime may not be observable, however further studies into K_p and K_T are required to investigate this hypothesis. It may be possible for all of the above factors to contribute to the overall trends observed for the NaOAc:glycerol and NaBr:glycerol systems in Figure 3.23, but ion pairing effects may be hidden due to large changes in system viscosity. Investigating concentrations lower than 0.2 M would help identify the dominating regime over the whole concentration range. If a maximum is noticed at concentrations less than 0.2 M, then it could be assumed that a shift from a charge carrier limited regime to an ion-mobility-limited regime occurs.^{92,93} However, if a maximum does not occur at concentrations less than 0.2 M, then it could be assumed that an ion-mobility-limited regime is dominant over the whole concentration range.

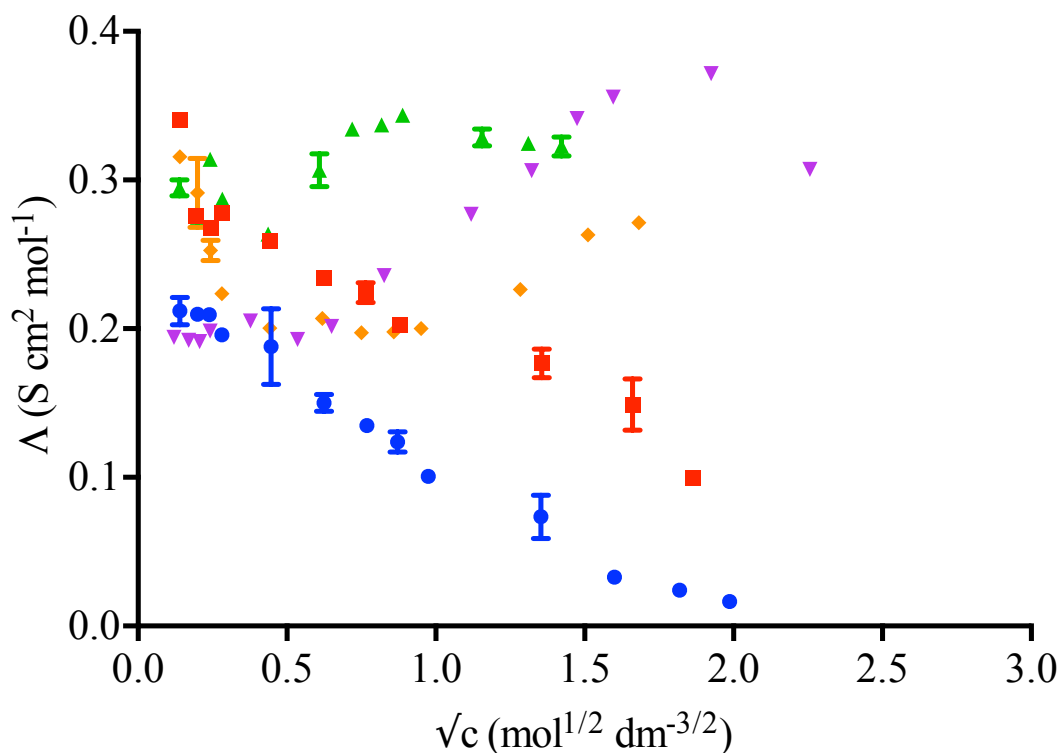


Figure 3.23 Molar conductivity measurements for a series of salt:glycerol mixtures as a function of the square root of salt concentration: (blue) NaOAc, (red) NaBr, (green) $\text{Na}_2\text{B}_4\text{O}_7 \cdot 10\text{H}_2\text{O}$, (purple) ChCl and (yellow) NaOAc. $3\text{H}_2\text{O}$, at 298 K

The NaOAc. $3\text{H}_2\text{O}$:glycerol system shows characteristic ion pair formation with a minimum at 0.25 M followed by triple ion formation up to approximately 3 M. The concentration range covered is insufficient to show the maximum and subsequent decrease due to viscosity effects, further studies at higher concentrations are needed to determine the conductivity maximum. The trend displayed by the NaOAc. $3\text{H}_2\text{O}$:glycerol system is very different to that of the anhydrous system and suggests water is contributing to the charge transport mechanisms in this system, which may be related to changes in dielectric constant that in turn may change the K_p : K_T ratio. Considering the viscosity of the NaOAc. $3\text{H}_2\text{O}$:glycerol system decreases as a function of NaOAc. $3\text{H}_2\text{O}$ concentration, the overall trend observed in Figure 3.23 is likely to be a consequence of the formation of ion pairs and triple ions. When this trend is compared with the anhydrous system, the dominating effect of dynamic viscosity in the anhydrous systems is made clear. The $\text{Na}_2\text{B}_4\text{O}_7 \cdot 10\text{H}_2\text{O}$:glycerol system does not show a clear trend in Figure 3.23, but molar conductivity is in the range 0.27 to 0.34 $\text{S cm}^2 \text{ mol}^{-1}$ implying little variance occurs. Considering the trend being very different compared to what is

seen for the NaOAc.3H₂O:glycerol system, it suggests water may be behaving differently. Abbott *et al.* found that addition of 5 % water to a range of ChCl:HBD systems significantly decreased viscosity and in turn increased molar conductivity.⁸³ At 0.08 M, and if the waters of hydration are assumed to be free, the water content of the Na₂B₄O₇.10H₂O:glycerol system is 5.5 %, and at 2.02 M, the water content is 69.2 %. Despite the significant water contents, little variance in molar conductivity occurs, which suggests the waters of hydration involved are likely to not be free and may be involved in a different charge transport mechanism.

At their maximum concentrations, the sodium salt:glycerol systems showed molar conductivities in the range 0.02 to 0.32 S cm² mol⁻¹, whereas ILs are typically in the 0.35 to 10 S cm² mol⁻¹ range, and DESs are 0.05 to 3 S cm² mol⁻¹.^{21,34,83} The sodium salt:glycerol systems measured are significantly lower than what are generally experienced for ILs however, ILs are normally less viscous than the sodium salt:glycerol mixtures and DESs allow for a much greater ion mobility.³⁴

3.4. Application of Walden's Rule

The Nernst-Einstein relationship relates the molar conductivity of an electrolyte at infinite dilution (Λ_m^0) to the diffusion coefficient (D^0) of the constituent ions, as shown in 3.24.⁹⁶ z is ion charge, F is Faraday's constant, R is the molar gas constant and T is absolute temperature. The Stokes-Einstein relationship links D^0 to the hydrodynamic radius of the species (r) and the dynamic viscosity of the system (η), as shown in equation 3.25.⁹⁶

$$\Lambda_m^0 = \left(\frac{z^2 F^2}{RT} \right) (D_+^0 + D_-^0) \quad 3.24$$

$$D^0 = \frac{RT}{6\pi\eta r} \quad 3.25$$

The model outlined by equations 3.24 and 3.25 assume spherical ion geometry at infinite dilution in a continuous medium where the diffusing species are larger than the solvent molecules.⁹⁶ Combination of equations 3.24 and 3.25 gives equation 3.26, where e is the fundamental charge of an electron.

$$\Lambda_m^0 = \frac{z^2 F e}{6\pi\eta} \left(\frac{1}{r_+} + \frac{1}{r_-} \right) \quad 3.26$$

From the relationship shown in equation 3.26, Walden derived the empirical rule for a given electrolyte shown in equation 3.27.⁹⁶ At high electrolyte concentrations,

viscosity effects dominate ion mobility, which can be compensated for by empirically applying a fractional equivalent of equation 3.27, as shown in equation 3.28.^{97,98,99} Walden's rule is based on observations of dilute aqueous electrolytes, but has since been applied to non-aqueous electrolyte solutions, molten salts and ILs.^{100,101,102,103}

$$\Lambda^0 \eta^0 = k \quad 3.27$$

$$(\Lambda \eta)^\alpha = k \quad 3.28$$

Angell *et al.* have used Walden's rule as a measure of ionicity in ILs, as shown in Figure 3.24, and provided a system can be represented as a medium of independent ions, the corresponding Walden plot will be close to an ideal line, which is established using a KCl solution at high dilution.^{104,105} Walden's rule neglects ion-ion interactions and is only truly applicable for ionic systems at infinite dilution, which is not a suitable assumption for molten salts, DES or ILs therefore, Walden plots only provide a qualitative method of understanding ionicity in DES and ILs.¹⁰⁶

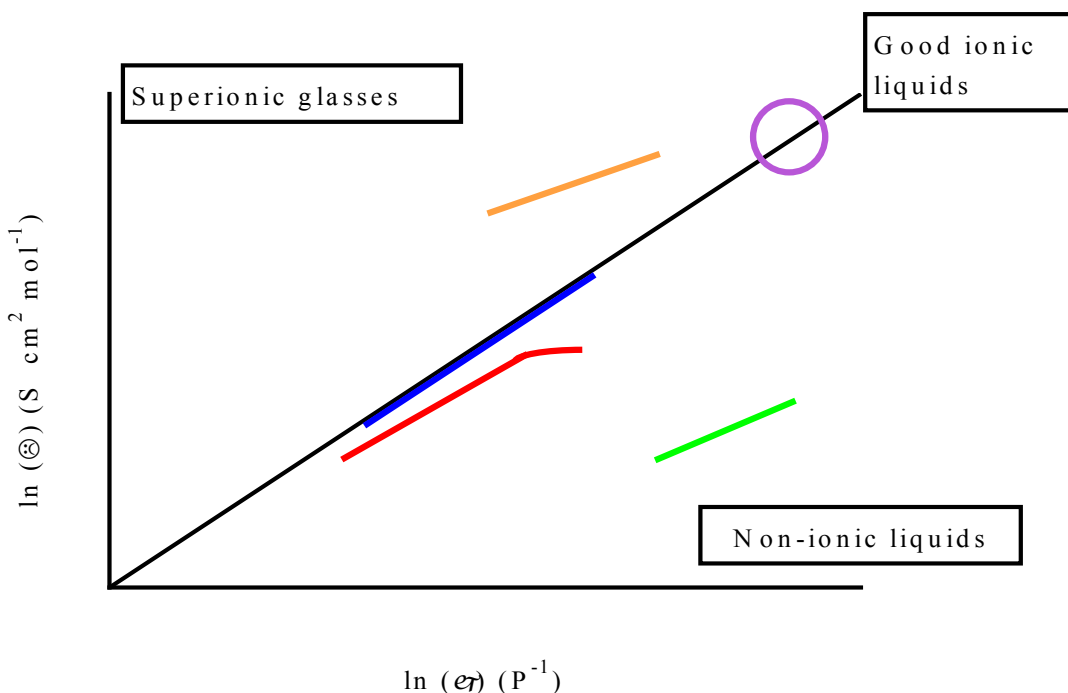


Figure 3.24 IL classification diagram according to the Walden rule: (blue) systems that follow the Walden Rule at all temperatures, (red) systems that show temperature dependent ion-pairing, (green) poor ILs, (purple) dilute KCl reference and (yellow) systems that show different charge transport mechanism.¹⁰⁴

Abbott *et al.* has suggested a model based on *hole theory* to explain the mechanism of motion in an IL that fits the behaviour of DES: it proposed that the

mechanism of charge transport is restricted by the migration of holes through the liquid.⁸⁵ Abbott *et al.* has quantified the meaning of Walden's rule in ILs and DESs using *hole theory*, and found the relationship occurs due to the low density of suitable sized voids in an IL or DES, which restrict ion mobility.⁸⁵ The void distribution is effectively at infinite dilution, thus validating the Nernst-Einstein relationship as shown in equation 3.26.⁸⁵ IL systems that are not modelled well by hole theory generally have cations which are asymmetrical, and adaptations made by Zhao *et al.* who took into account the cation symmetry and this significantly improved the prediction of the conductivity of long chain salts.¹⁰⁷

For ILs the Walden product ($\Lambda\eta$) is mostly independent of temperature, and the magnitude of the Walden product is for an IL is inversely proportional with respect to ion size.¹⁰⁸ The relationship between the Walden product and ion size is mostly seen with changes in cation size, and the size of the anion appears to have no correlation with the magnitude of the Walden product.³⁴ For DESs based on mixtures of ChCl and HBD, the Walden product also appears to be independent of temperature, however, in DESs based on mixtures for metal salt hydrates and HBD, non-linear behaviour has been observed and has been attributed to complex equilibria between the metal centre and the available ligands, suggesting charge carrying species of different sizes may be possible.^{21,49}

Figure 3.25 shows the Walden plots for a series of approximately 2 M sodium salt:glycerol systems as a function of temperature. Molar conductivity has been substituted for molal conductivity to provide an absolute concentration factor that did not vary with temperature. In all instances there is a linear relationship between molal conductivity and fluidity suggesting Walden's rule is applicable to sodium salt:glycerol. The associated Walden products are listed in Table 3.3.

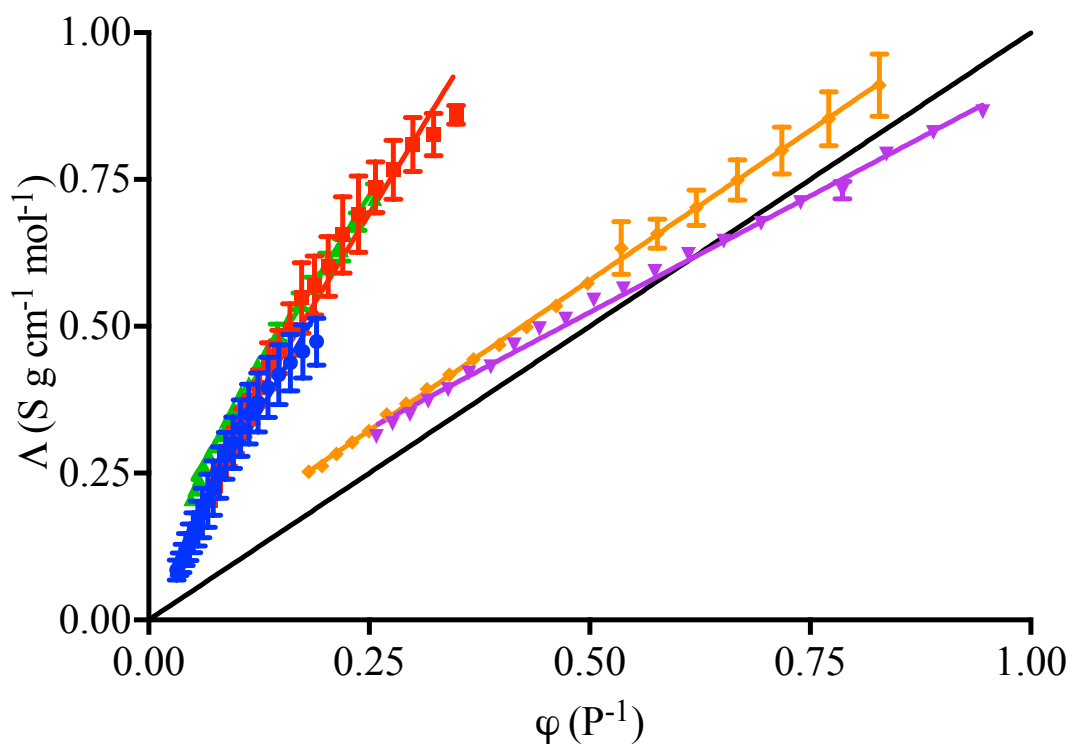


Figure 3.25 Walden plots for a series of salt:glycerol mixtures as a function of temperature: (blue) 1.80 M NaOAc, (red) 1.88 M NaBr, (green) 2.02 M $\text{Na}_2\text{B}_4\text{O}_7 \cdot 10\text{H}_2\text{O}$, (purple) 2.17 M ChCl and (yellow) 2.28 M NaOAc. $3\text{H}_2\text{O}$

Table 3.3 List of Walden products

Salt:glycerol system	Walden product ($\text{S g cm}^{-1} \text{ mol}^{-1} \text{ P}$)
1.80 M NaOAc	2.63 ± 0.10
1.88 M NaBr	2.45 ± 0.08
2.02 M $\text{Na}_2\text{B}_4\text{O}_7 \cdot 10\text{H}_2\text{O}$	2.42 ± 0.05
2.17 M ChCl	0.79 ± 0.01
2.28 M NaOAc. $3\text{H}_2\text{O}$	1.02 ± 0.01

The 1.80 M NaOAc, 1.88 M NaBr, 2.02 M $\text{Na}_2\text{B}_4\text{O}_7 \cdot 10\text{H}_2\text{O}$ systems all show very similar Walden products with a typical value of $2.50 \pm 0.91 \text{ S g cm}^{-1} \text{ mol}^{-1} \text{ P}$, which is in good agreement with the lack of correlation observed between the Walden product and anion size in ILs.³⁴ The 2.28 M NaOAc. $3\text{H}_2\text{O}$ system shows a surprisingly low Walden constant compared to the other sodium salt based systems, considering

anions appear not to affect the Walden product it was expected to have a Walden product of approximately $2.50 \text{ S g cm}^{-1} \text{ mol}^{-1} \text{ P}$. This unexpected result may be attributed to the role of water in this system, and further work is required to gain a deeper understanding of the effects of water in these systems. The 2.17 M ChCl system demonstrates a significantly lower Walden product compared to the sodium salt based systems, which is characteristic of the relationship between Walden product and cation size.³⁴ ILs typically have Walden products of the $0.30 - 1.00 \text{ S cm}^2 \text{ mol}^{-1} \text{ P}$ range, compared to the $1.00 - 2.50 \text{ S g cm}^{-1} \text{ mol}^{-1} \text{ P}$ range for the systems studied in Figure 3.25.³⁴ The Walden products of the sodium salt based systems are surprisingly high compared to what is generally achieved with ILs, and when reviewed using a logarithmic Walden plot, as shown in Figure 3.27, the sodium salt:glycerol systems are above the *ideal* line. When this occurrence is cross-referenced with Figure 3.24, it suggests there may be a Grotthuss type charge transport mechanism accommodating an uncharacteristically high mobility of charged species.^{104, 109} A Grotthuss type mechanism involves protons *hopping* within a hydrogen bonding network, shown in Figure 3.26, and is responsible for the high proton mobility in water, and it is speculated that a Grotthuss type mechanism might give rise to superprotonic behaviour in protic ionic liquids.^{110,111} However, the scientific literature focuses on this concept as a charge transport mechanism in protic ionic liquids, and further work is required to investigate the possibility of a Grotthuss type mechanism in sodium salt:glycerol mixtures and DES.

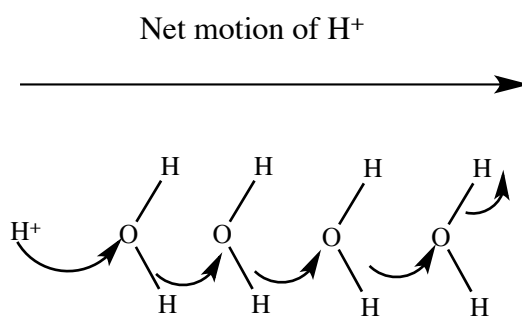


Figure 3.26 The Grotthuss mechanism

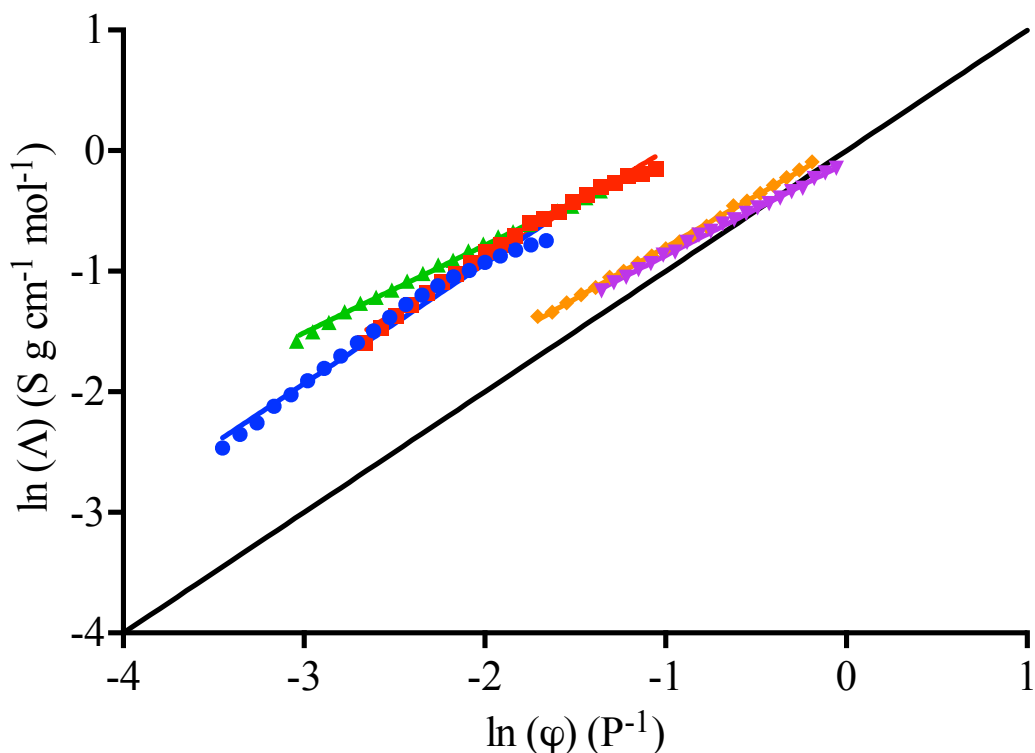


Figure 3.27 Logarithmic Walden plots for a series of salt:glycerol mixtures as a function of temperature: (blue) 1.80 M NaOAc, (red) 1.88 M NaBr, (green) 2.02 M $\text{Na}_2\text{B}_4\text{O}_7 \cdot 10\text{H}_2\text{O}$, (purple) 2.17 M ChCl and (yellow) 2.28 M NaOAc·3H₂O

At higher temperatures, the trends shown in Figure 3.27 deviate from a linear relationship, which is suggestive of temperature dependent ion-pairing forming neutral species that lowers the charge carrier concentration.¹⁰⁵ Torell *et al.* used Raman spectral analysis to differentiate between free anions and anions biased by cation interactions, and found that in NaCF_3SO_3 solutions in polypropylene glycol (PPG), the free ion content dropped from 86 % at 186 K to 39 % at 360 K.¹¹² However, when compare to LiClO_4 , an example of a stronger electrolyte, the free anion content dropped from 96 % at 200 K to 78 % at 340 K.¹¹² Angell *et al.* took Torell's research further and confirmed the positive temperature dependence of ion pairing through studying the ionic conductivity and viscosity of the systems.¹¹³

3.5. Future Developments

The investigations carried out in this section of the thesis require supplementary experimentation to give a deeper insight into the thermophysical properties of alkali

metal salt:glycerol mixtures, as well as to gain a better understanding of the properties of DES and ILs. The research carried out thus far has left some questions unanswered, and adoption of other analytical techniques could be used to support current analyses.

Phase behaviour was investigated using DSC with the intention to deduce the eutectic composition of salt:glycerol systems however, a depression in glass transition temperatures was not observed for any sodium salt:glycerol system. Research into the phase behaviour of glycerol: water mixtures suggest the eutectic trends seen in the melting points of mixtures may not be observed in changes in glass transition temperatures.¹¹⁴ Unfortunately, due to the super-cooling ability of glycerol, measurements of the melting points of glycerol solutions are not viable by DSC and an alternative method is required to confirm observed phase behaviour. As liquid water freezes into ice, a change in the density-temperature profile is observed, which is common in many liquids therefore, changes in density could be used as a probe for the freezing temperature of system.

A limited number of sodium salts have been investigated, which have been chosen according to the justifications in section 3.2. Anouti *et al.* has successfully made a DES from sodium nitrate and N-methyl acetamide, which suggests further investigations into other salt: HBD combinations are possible that may be useful as replacements for aqueous electrolytes.⁴⁰ IL and DES formation has utilised large, charge diffuse species, and using sodium salts with large, charge diffuse anions may also provide interesting systems.

The role of water in the systems investigated is still not understood. Studies into the thermophysical properties of sodium salt:glycerol systems support models where water is bound to other species, or free to act as a diluent. Abbott *et al.* has investigated the effect of added water on the transport properties of a range of DESs by utilising pulsed field gradient nuclear magnetic resonance (PFGNMR) spectroscopy to evaluate the effects of water on the self-diffusion coefficients of species.⁸³ Extended x-ray atomic fine structure (EXAFS) has been used to probe the speciation of charge carriers in DESs, and could be used to gain an insight into the structure of ions in the sodium salt:glycerol mixtures and ascertain if added water or waters of hydration are present in the charge carrier structures.⁵⁷

It is not clear as to why sodium salt:glycerol mixtures have molar conductivities greater than what is expected theoretically from the application of Walden's rule. Angell and other researchers have postulated a Grotthuss (proton hopping) type

mechanism may be contributing to charge transport in protic ionic liquids, and this mechanism may be applicable to sodium salt:glycerol mixtures.^{104,110} As well as conductivity and viscosity measurements, PFGNMR spectroscopy and *ab initio* molecular dynamics simulations have been employed to probe charge transport mechanisms.^{115,116}

3.6. Conclusions

It has been shown that concentrated non-aqueous ionic mixtures can be prepared using alkali metal salts and glycerol, which have: densities, viscosities and ionic conductivities comparable to DESs and ILs. All of the systems investigated showed Newtonian fluid behaviour over the shear rate range of the rotational viscometer used, except for the NaOAc:glycerol system where a shear thickening response was observed, which is also observed amongst protic ILs. The phase behaviour of all the sodium salt:glycerol mixtures do not show a eutectic composition, which may be linked to the super cooling ability of glycerol masking the true freezing points, and a non-calorimetric technique may be able avoid problems caused by super cooling.

Investigations into Dole-Jones viscosity relationships, density and system free volume have been used to study the effect of salts on the structure of glycerol. Alkali metal salts have been shown to have a kosmotropic, structure forming, effect on the structure of glycerol, which is linked to salts increasing solvent-solvent interactions, and electrostriction. In contrast, QASs have a chaotropic, structure breaking, effect on the structure of glycerol, which is linked to QASs disrupting the hydrogen bonding network in glycerol.

As a consequence of the kosmotropic properties of alkali salts, a characteristic decrease in conductivity is observed, which is supported by observed increases activation energy of fluid flow having a positive effect on the activation energy of conduction. At high salt concentrations, conductivity decreases upon salt addition suggesting a shift from an ion-concentration-limited, to a mobility-limited ionic conductivity regime. Molar conductivity trends with respect to salt content follow the pattern of regimes outlined by Fuoss and Kraus with the exception of the Na₂B₄O₇·10H₂O:glycerol system, where the waters of hydration are suspected to play an unknown role in the charge transport mechanism. The NaOAc:glycerol and NaBr:glycerol systems appear to only display the mobility-limited regime over the

concentration range investigated, and lower concentrations would need to be studied to observe ion pairing effects.

Sodium salt:glycerol systems have Walden products slightly higher than what is typically seen for DESs and ILs, and appear above the *ideal* line on a logarithmic Walden plot. Systems that appear above the *ideal* line on a Walden plot are suggestive of an unknown charge transport mechanism, but further investigations are needed to understand this phenomenon.

The role of water in hydrated sodium salt:glycerol systems is not clear, and further work is needed to investigate how water is involved in transport mechanisms.

3.7. References

-
- ¹A. Wolfson, C. Dlugy and Y. Shotland, *Environ. Chem. Lett.*, 2007, **5**, 67
- ²M. Pagliaro and M. Rossi, *The Future of Glycerol: New Usages for a Versatile Raw Material*, RSC Publishing, Cambridge, 2008
- ³F. M. Kerton, *RSC Green Chemistry, Volume 2: Alternative Solvents for Green Chemistry*, RSC Publishing, Cambridge, 2009, Ch. 5, 97
- ⁴J. N. Chheda, G. W. Huber and J. A. Dumesic, *Angew. Chem. Int. Ed.*, 2007, **46**, 7164
- ⁵S. Zhu Y. Zhu, S. Hao, H. Zheng, T. Mo and Y. Li, *Green Chem.*, 2012, **14**, 2607
- ⁶R. Christoph, B. Schmidt, U. Steinberner, W. Dilla, R. Karinen, *Ullmann's Encyclopedia of Industrial Chemistry*, Wiley-VCH, Germany, 2006
- ⁷B. Yu, *Synlett.*, 2014, **25**, 601
- ⁸R. Ciriminna, C D Pina, M Rossi and M Pagliaro, *Eur. J. Lipid Sci. Technol.* 2014, **116**, 1432
- ⁹H. K. Cammenga, F. W. Schulze, and W. Theuerl, *Journal of Chemical and Engineering Data*, 1977, **22**, 131
- ¹⁰A. P. Abbott, R. C. Harris, K. S. Ryder, C. D'Agostino, L. F. Gladden and M. D. Mantle, *Green Chem.*, 2011, **13**, 82
- ¹¹A. P. Abbott, P. M. Cullis, M. J. Gibson, R. C. Harris and E. Raven, *Green Chem.*, 2007, **9**, 868.
- ¹²A. P. Abbott, T. Z. Abolibda, S. J. Davis, F. Emmerling, D. Lourdin, E. Leroy and W. R. Wise, *RSC Adv.*, 2014, **4**, 40421
- ¹³A. P. Abbott, E. I. Ahmed, R. C. Harris and K. S. Ryder, *Green Chem.*, 2014, **16**, 4156

-
- ¹⁴ K. Shahbaz, F. S. Mjalli, M. A. Hashim and I. M. AlNashef, *J. Appl. Sci.*, 2010, **10**, 3349.
- ¹⁵ K. Shahbaz, F. S. Mjalli, M. A. Hashim and I. M. AlNashef, *Sep. Purif. Technol.*, 2011, **81**, 216.
- ¹⁶ K. Shahbaz, F. S. Mjalli, M. A. Hashim and I. M. AlNashef, *Energy Fuels*, 2011, **25**, 2671.
- ¹⁷ H. Liu, F. Xie, L. Yu, L. Chen and L. Li, *Prog. Polym. Sci.*, 2009, **34**, 1348.
- ¹⁸ L. P. B. M. Janssen and L. Moscicki, *Thermoplastic Starch*, Wiley-VCH, Weinheim, 2009, Ch 4., 77
- ¹⁹ A. P. Abbott, J. Palenzuela Conde, S. Davis and W. R. Wise, *Green Chem.*, 2012, **14**, 3067.
- ²⁰ A. E. Somers, P. C. Howlett, D. R. MacFarlane and M. Forsyth, *Lubricants*, 2013, **1**, 3.
- ²¹ A. P. Abbott, A. A. Al-Barzinjy, P. D. Abbott, G. Frisch, R. C. Harris, J. Hartley and K. S. Ryder, *Phys.Chem.Chem.Phys.*, 2014, **16**, 9047
- ²² A. P. Abbott, J. C. Barron, G. Frisch, S. Gurman, K. S. Ryder and A. F. Silva, *Phys. Chem. Chem. Phys.*, 2011, **13**, 10224
- ²³ J. C. Barron, PhD Thesis, University of Leicester
- ²⁴ M. Gambino, P. Gaune, M. Nabavian, M. Gaune-Escard, J. P. Bros, *Thermochimica Acta* 1987, **111**, 37.
- ²⁵ A. Hammadi, *International Journal of Thermophysics*, 2004, **25**, 89
- ²⁶ E. L. Smith, A. P. Abbott and K. S. Ryder, *Chem. Rev.*, 2014, **114**, 11060
- ²⁷ M. Hayyan, A. Abo-Hamad, M. A. AlSaadi and M. A. Hashim, *Nanoscale Research Letters*, 2015, **10**, 324
- ²⁸ S. Tang, G. A. Baker and H. Zhao, *Chem. Soc. Rev.*, 2012, **41**, 4030
- ²⁹ A. P. Abbott, G. Capper, D. L. Davies; H. L. Munro; R. K. Rasheed, V. Tambyrajah, *Chem. Commun.* 2001, **19**, 2010.
- ³⁰ Alibaba, www.alibaba.com, (accessed August 2015)
- ³¹ F. S. Mjalli, J. Naser, B. Jibril, S. S. Al-Hatmi and Z. S. Gano, *Thermochimica Acta*, 2014, **575**, 135
- ³² D. R. Lide, *CRC Handbook of Chemistry and Physics*, CRC press, Florida, 89th Ed., 2008, Ch. 3

-
- ³³P. Wasserscheid and T. Welton, *Ionic Liquids in Synthesis*, Wiley-VCH, Germany, 2003, Ch. 1, 7
- ³⁴P. Wasserscheid and T. Welton, *Ionic Liquids in Synthesis*, Wiley-VCH, Germany, 2003, Ch. 3, 41
- ³⁵A. P. Abbott, G. Capper, D. L. Davies and R. Rasheed, *Inorg. Chem.*, 2004, **43**, 3447
- ³⁶A. P. Abbott, D. Boothby, G. Capper, D. L. Davies and R. K. Rasheed, *J. Am. Chem. Soc.*, 2004, **126**, 9142
- ³⁷A. P. Abbott, G. Capper, D. L. Davies, R. K. Rasheed and V. Tambyrajah *Chem. Commun.*, 2003, 70
- ³⁸American Cleaning Institute
http://www.aciscience.org/docs/physical_properties_of_glycerine_and_its_solutions.pdf
(Accessed Sept 2015)
- ³⁹B. J. J. Verbeek, MSc Thesis, Delft University of Technology
- ⁴⁰W. Zaidi, L. Timperman and M. Anouti, *RSC Adv.*, 2014, **4**, 45647
- ⁴¹J. S. Wilkes, J. A. Levisky, R. A. Wilson and C. L. Hussey, *Inorg. Chem.*, 1982, **21**, 1263
- ⁴²A. A. Fannin, D. A. Floreani, L. A. King, J. S. Landers, B. J. Piersma, D. J. Stech, R. L. Vaughn, J. S. Wilkes and J. L. Williams, *J. Phys. Chem.*, 1984, **88**, 2614
- ⁴³M. Ma, K. E. Johnson, *Proceedings of the Ninth International Symposium on Molten Salts*, The Electrochemical Society, New Jersey, 1994, 94, 179
- ⁴⁴J. Sun, M. Forsyth, D. R. Macfarlane, *Molten Salt Forum*, 1998, **5**, 585
- ⁴⁵J. S. Wilkes, J. A. Levisky, R. A. Wilson and C. L. Hussey, *Inorg. Chem.*, 1982, **21**, 1263
- ⁴⁶R. L. Perry, K. M. Jons, W. D. Scott, Q. Liao and C. L. Hussey, *J. Chem. Eng. Data*, 1995, **40**, 615
- ⁴⁷M. S. Sitze, E. R. Schreiter, E. V. Patterson, R. G. Freeman, *Inorg. Chem.* 2001, **40**, 2298.
- ⁴⁸M. A. Kareem, F. S. Mjalli, M. A. Hashim, I. M. J. Al-Nashed, *Chem. Eng. Data*, 2010, **55**, 4632
- ⁴⁹A. P. Abbott, R. C. Harris and K. S. Ryder, *J. Phys. Chem. B*, 2007, **111**, 4910
- ⁵⁰J. O'M. Brockris and A. K. N. Reddy, *Modern Electrochemisyy I: Ionics*, Plenum, New York, 2nd ed. 1997, Ch2, 185
- ⁵¹M. A. Motin, *J. Chem. Eng. Data*, 2004, **49**, 94
- ⁵²S. Al Ghafri, G. C. Maitland and J. P. M. Trusler, *J. Chem. Eng. Data*, 2012, **57**, 1288

-
- ⁵³ *Spartan Pro*, Wavefunction Inc., Irvine, CA, 2000.
- ⁵⁴ M. H. Cohen and D. Turnbull, *J. Chem. Phys.*, 1959, **31**, 1164.
- ⁵⁵ Y. Yu, W. Beichel, G. Dlubek, R. Krause-Rehberg, M. Paluch, J. Pionteck, D. Pfefferkorn, S. Bulut, C. Friedrich, N. Pogodina and I. Krossing, *Phys. Chem. Chem. Phys.*, 2012, **14**, 6856.
- ⁵⁶ A. A. Al-Barzinjy, PhD Thesis, University of Leicester
- ⁵⁷ J. M. Hartley, I. Chung-Man, G. C. H. Forrest, K. Singh, S. J. Gurman, K. S. Ryder, A. P. Abbott and G. Frisch, *Inorg. Chem.* 2014, **53**, 6280
- ⁵⁸ C. F. Fischer, *Computer Physics Communications*, 1987, **43**, 355
- ⁵⁹ C. Møller and S. M. Plesset, *Phys. Rev.*, 1934, **46**, 618
- ⁶⁰ E. Davidson and D. Feller, *Chem. Rev.*, 1986, **86**, 681
- ⁶¹ K. Burke and L. O. Wagner, *International Journal of Quantum Chemistry*, 2013 **113**, 96
- ⁶² M. L. Berins, *Handbook of the Society of the Plastics Industry*, Kluwer Academic, Dordrecht, 5th ed., 1991, Ch. 5., 156
- ⁶³ M. Moosavi, A. Daneshvar, *Journal of Molecular Liquids*, 2014, **190**, 59
- ⁶⁴ J. A. Smith, G. B. Webber, G. G. Warr and R. Atkin, *J. Phys. Chem. B*, 2013, **117**, 13930
- ⁶⁵ L. L. Sze, S. Pandey, S. Ravula, S. Pandey, H. Zhao, G. A. Baker and S. N. Baker, *ACS Sustainable Chem. Eng.* 2014, **2**, 2117
- ⁶⁶ F. S. Mjalli, T. Al-Wahaibi and A. A. Al-Hashmi, *Journal of Molecular Liquids*, 2015, **206**, 256
- ⁶⁷ C. A. Nkuku and R. J. LeSuer, *J. Phys. Chem. B*, 2007, **111**, 13271
- ⁶⁸ P. Atkins and J. De Paula, *Elements of Physical Chemistry*, Oxford University Press, Oxford, 4th ed., 2007, Ch. 10, 244
- ⁶⁹ P. Stilbs, *Progress in NMR Spectroscopy*, 1987, **19**, 1
- ⁷⁰ S. N. Baker, G. A. Baker, M. A. Kane, F. V. Bright, *J. Phys. Chem. B.*, 2001, **105**, 9663
- ⁷¹ K. R. Seddon, A. Stark, M. J. Torres, *Pure Appl. Chem.* 2000, **72**, 2275
- ⁷² A. P. Abbott, J. C. Barron, K. S. Ryder and D. Wilson, *Chem. Eur. J.* 2007, **13**, 6495
- ⁷³ S. Moelbert, B. Normand, P. De Los Rios, *Biophysical Chemistry*, 2004, **112**, 45
- ⁷⁴ M. P. Applebey, *J. Chem. Soc., Trans.*, 1910, **97**, 2000
- ⁷⁵ J. L. M. Poiseuille, *Ann. chim. Phys.*, 1847, **21**, 76

-
- ⁷⁶K. D. Collins, *Biophysical Journal*, 1997, **72**, 65
- ⁷⁷S. Arrhenius, *Z. physik. Chem.*, 1887, **1**, 285.
- ⁷⁸G. Jones and M. Dole, *J. Am. Chem. Soc.*, 1929, **51**, 2950
- ⁷⁹G. Jones, S. K. Talley, *J. Am. Chem. Soc.*, 1933, **55**, 624
- ⁸⁰H. Falkenhagen, *Theory of electrolytes*.
- ⁸¹P. C. Coleman and M. M. Painter, *Fundamentals of Polymer Science: An Introductory Text*, Technomic, Pennsylvania, 2nd ed., 1997, 412
- ⁸²J. Jacquemin, M. Anouti and D. Lemordant, *J. Chem. Eng. Data*, 2011, **56**, 556
- ⁸³C. D'Agostino, L. F. Gladden, M. D. Mantle, A. P. Abbott, E., I. Ahmed, A. Y. M. Al-Murshedi and R. C. Harris, *Phys. Chem. Chem. Phys.*, 2015, **17**, 15297
- ⁸⁴F. J. Holler, C. G. Enke, *Laboratory Techniques in Electroanalytical Chemistry*, Marcel Dekker, New York, 1984, Ch. 8
- ⁸⁵A. P. Abbott, *ChemPhysChem*, 2004, **5**, 1242.
- ⁸⁶A. P. Abbott, G. Capper and S. Gray, *ChemPhysChem.*, 2006, **7**, 803
- ⁸⁷R. C. Harris, PhD Thesis, University of Leicester, 2008
- ⁸⁸R. M. Fuoss and C. A. Kraus, *J. Am. Chem. Soc.*, 1957, **79**, 3304.
- ⁸⁹R. M. Fuoss and C. A. Kraus, *J. Am. Chem. Soc.*, 1933, **55**, 21.
- ⁹⁰R. M. Fuoss and C. A. Kraus, *J. Am. Chem. Soc.*, 1933, **55**, 476.
- ⁹¹R. M. Fuoss, *Chem. Rev.*, 1935, **17**, 27
- ⁹²R. P. Seward, *J. Phys. Chem.*, 1958, **62**, 758.
- ⁹³M. Delsignore, H. E. Maaser and S. Petrucci, *J. Phys. Chem.*, 1984, **88**, 2405.
- ⁹⁴A. P. Abbott and D. J. Schiffrin, *J. Chem. Soc. Faraday Trans.*, 1990, **86**, 1453
- ⁹⁵M. N. Roy, P. K. Roy, R. S. Sah, P. Pradhan and B. Sinha, *J. Chem. Eng. Data* 2009, **54**, 2429
- ⁹⁶R. A. Robinson and R. H. Stokes, *Electrolyte Solutions*, Dover, New York, 2nd Rev. Ed., 2002
- ⁹⁷M. P. Longinotti and H. R. Corti, *J. Phys. Chem. B*, 2009, **113**, 5500
- ⁹⁸W. Bilz and W. Klemm, *Z. Anorg. Allg. Chem.*, 1926, **152**, 267
- ⁹⁹F. A. Pugsley and F. E. Westmore, *Can. J. Chem.*, 1954, **32**, 839
- ¹⁰⁰W. A. Adams and K. J. Laidler, *Can. J. Chem.*, 1968, **48**, 1977
- ¹⁰¹A. N. Campbell and E. T. van der Kouwe, *Can. J. Chem.*, 1968, **46**, 1294
- ¹⁰²S. I. Smedley, *The Interpretation of Ionic Conductivity in Liquids*, Plenum, New York, 1983, Ch. 3

-
- ¹⁰³P. Walden, *Z. Physik Chem.* 1906, **55**, 207
- ¹⁰⁴M Yoshizawa, W Xu and C. A. Angell, *J. Am. Chem. Soc.*, 2003, **125**, 15411
- ¹⁰⁵W. Xu, E. I. Cooper, C. A. Angell, *J. Phys. Chem. B.* 2003, **107**, 6170
- ¹⁰⁶D. R. MacFarlane, M. Forsyth, E. I. Izgorodina, A. P. Abbott, G. Annat and K. Fraser, *Phys. Chem. Chem. Phys.*, 2009, **11**, 4962
- ¹⁰⁷H. Zhao, Z-C. Liang and F. Li, *J. Mol. Liq.*, 2009, **149**, 55
- ¹⁰⁸A. B. McEwen, H. L. Ngo, K. LeCompte and J. L. Goldman, *J. Electrochem. Soc.*, 1999, **146**, 1687
- ¹⁰⁹C. J. T. de Grotthuss, *Ann. Chim.* 1806, **58**, 54
- ¹¹⁰L. Vilčiauskas, M. E. Tuckerman, G. Bester, S. J. Paddison and K.-D. Kreuer, *Nat. Chem.*, 2012, **4**, 461
- ¹¹¹Z. Wojnarowska, Y. Wang, K. J. Paluch, A. P. Sokolov and M. Paluch. *Phys.Chem.Chem.Phys.*, 2014, **16**, 9123
- ¹¹²M. Kakihana, S. Schantz and L. M. Torell, *J. Chem. Phys.* 1990, **92**, 6271
- ¹¹³M. G. McLint and C. A. Angell, *J. Phys. Chem.* 1991, **95**, 9464
- ¹¹⁴K. I Murata and H. Tanaka, *Nature Materials*, 2012, **11**, 436
- ¹¹⁵G. A. Luduena, T. D. Kühne and D. Sebastiani, *Chem. Mater.* 2011, **23**, 1424
- ¹¹⁶M. Anoutia, P. Porionb, C. Brigouleixa, H. Galianoc and D. Lemordant, *Fluid Phase Equilibria*, 2010, **299**, 229

4. Diffusion Studies and Electrochemical Properties of DES

Derived from Inorganic Salts

4.1. Introduction	98
4.1.1. NMR Techniques	99
4.1.2. Aims	103
4.2. Dynamics and Diffusion Investigations Using PFG NMR	104
4.2.1. Self-Diffusion Studies	105
4.2.2. NMR T ₁ Relaxation studies.....	112
4.2.3. Conclusions	117
4.3. Diffusion Studies of Solutes in Sodium Salt:Glycerol Mixtures by Electrochemical Methods	118
4.3.1. Introduction	118
4.3.2. Aims	123
4.3.3. Electrochemical Windows of Sodium Salt:Glycerol mixtures.....	124
4.3.4. Redox Behaviour of Copper in Sodium Salt:Glycerol Mixtures ...	126
4.3.5. Future Work	135
4.3.6. Conclusions	136
4.4. References	137

4.1. Introduction

Many thermophysical properties of a wide range of ionic liquids (ILs) and deep eutectic solvents (DESs) including: ionic conductivity, dynamic viscosity, density, surface tension, solubility and melting temperature have been extensively investigated.^{1,2,3} The thermophysical properties of ILs and DESs are heavily dependent on the components of the system, and are more complex than aqueous and non-aqueous solutions.⁴ Macroscopic measurements of thermophysical properties only provide a partial insight into the microscopic behaviour of ILs and DESs, and have shown that hydrogen bonding and ionic interactions play a crucial role.⁵ In DESs, the hydrogen bond donor (HBD) is known to associate with the anion of the salt that result in the formation of a bulky, charge diffuse anion, which decreases the lattice energy of the salt thus decreasing the freezing point of the system.⁶ However, the complexity of the model can be increased as some HBDs may also ionise leading to the presence of multiple ions within the mixtures.⁵ Macroscopic measurements provide little information on the speciation of a system and do not provide enough information to fully understand the role additives such as water. Limited knowledge of the system structure and, in the case of ILs and DESs, the role of water, restricts obtaining a deeper understanding of charge and mass transport at the molecular level.^{7,8}

The microscopic properties of ILs and DESs have been investigated using: nuclear magnetic resonance (NMR), electrochemical and X-ray techniques, which have been used to: further understand phenomenon that occur on the macroscopic scale, rationalise transport properties and deduce the local structure of species.^{7,9,10,11,}

Hartley *et al.* have employed extended X-ray absorption fine structure (EXAFS) to determine the speciation of a range of transition metal salts in DESs and ILs, and found diol based DESs prepared using choline chloride (ChCl) promoted metal chloro complexes, even in the presence of strong field ligands such as thiocyanate.⁹ Chloride co-ordination was also observed in urea based DESs for soft metals, whereas oxygen co-ordination was observed for hard metals following the hard and soft acids and bases (HSAB) model, which was rationalised by lower chloride activity in the urea based systems.⁹ Hydrate waters and added water were found to have either little or no effect on the speciation of metals in diol based DES, suggesting applications do not need a moisture-free environment.⁹

The diffusion behaviour of ferrocene, and derivatives thereof, in DESs and ILs have been investigated using voltammetric methods by Taylor *et al.*, who found that diffusion in ILs did not obey the Stokes-Einstein relationship as changes in the distance parameter were not directly related to the size of the electroactive species.⁷ It was suggested that the electroactive species moved between suitably sized holes within the IL medium, rather than the traditional *random walk* diffusion model used to describe non-ionic media.⁷ The electrochemical properties of ChCl based DESs at an electrified interface have been researched by the Silva group using impedance and voltammetric techniques.¹⁰ The electrode double layer difference capacitance depended heavily on the electrode material and was found to be similar to capacitance values obtained for many other ILs.¹⁰ The potential windows of DESs were found to decrease with temperature and be of a smaller range compared to conventional ILs but found proton reduction was not observed which is consistent with protons being strongly associated with chloride anions.¹⁰ The same authors proposed that at negative electrode potentials the electrode interface consisted of a layer of Ch cations separated by a layer of HBD molecules, whereas at positive electrode potentials the Ch cation is replaced by the adsorption of anions, thus suggesting a Helmholtz model for the electrode interface in DESs.¹⁰

4.1.1. NMR Techniques

NMR spectroscopy is an analytical technique that relies on the magnetic moment of a species being sensitive to its chemical environment to probe the chemical structure and dynamics of a system.¹² All magnetic nuclei have a quantum angular momentum known as *spin*, which is dependent on the number of unpaired protons and neutrons.¹² The magnetic moment (μ) of a nucleus is directly proportional to its angular momentum (I) through the gyromagnetic ratio (γ), as shown in equation 4.1.¹²

$$\mu = \gamma I \quad 4.1$$

In the absence of a magnetic field, all of the allowed quantum spin orientations are degenerate, which is negated by the presence of a magnetic field.¹² Upon exposure to a magnetic field, a magnetic nucleus orientates in to an allowed orientation of a different energy, where the difference in energy between the allowed orientations is dependent on the size of the nuclear magnetic moment and the magnetic field strength.¹² From the energy difference between allowed orientations, a resonant frequency for the

orientation transition can be deduced. The magnetic field experienced by a nucleus is slightly different from the applied external magnetic field, and the resulting resonant frequency depends on the chemical environment and its effect is known as the *chemical shift*.¹²

NMR has become a useful analytical tool for understanding the structure, dynamics and the presence of interactions, such as hydrogen bonding, within ILs in recent years.¹¹ As well as the overall structure, NMR can provide valuable information into the main charge carrying species, rheological properties and solute effects through observing changes in chemical shifts, magnetisation transfer and species relaxation times.¹¹ Unfortunately, the resolution of NMR techniques is compromised due to higher viscosity of ILs and DESs, which are typically 100 times more viscous than typical molecular systems.¹¹

Cremer *et al.* have investigated the effect of the anion on the ¹H and ¹³C chemical shifts of alkyimidazolium ILs and found that anions had the most noticeable effect on the relatively acidic proton and adjacent carbon atom between the two nitrogen groups.¹³ As well as anion location, Cremer *et al.* have shown a linear dependence between ¹H and ¹³C chemical shifts and anion size, and found that ¹H chemical shifts can be used as reliable measure of the Kamlet-Taft hydrogen bonding parameters.¹³

The phase behaviour of alkyimidazolium halides have been studied through NMR relaxation times by Imanari *et al.*, and have shown to have weak glass transitions upon cooling, whereas when heated they displayed a strong glass transition with broad crystallisation peaks.^{14,15} Through monitoring the ¹H transverse (T_2) relaxation times at the crystallisation temperature Imanari *et al.* were able to identify three separate stages of the crystallisation process: nucleation, linear crystal growth and saturation.^{16,17}

Pulse field gradient (PFG) NMR is regarded as one of the most reliable methods for the determination of self-diffusion of species in the liquid or solid state, and can be utilised for any spin active nuclei with sufficiently long enough relaxation times.^{11,18} Pulsed field gradients are spatially inhomogeneous magnetic fields, which dephase and rephase only the required coherences.¹⁹ NMR signals observed following an excitation pulse decays due to relaxation and non-homogeneous effects, which results in different spins to change rotational direction at different rates.²⁰ Relaxation is due to demagnetisation and is irreversible, however, non-homogeneous dephasing effects, caused by magnetic field gradients and chemical shift distributions, can be suppressed through application of an 180° inversion pulse, after which, the non-homogeneous

effects rephase as an *echo*.²⁰ This pulse sequence is known as a pulsed gradient spin echo (PGSE) sequence, and the echo decay is used to measure the T_2 transverse relaxation time by monitoring echo intensity as a function of pulse separation time.²¹ For systems that exhibit a rapid transverse relaxation, the loss of signal can be significant.²¹ Improvements can be made by utilising a pulsed gradient stimulated echo (PGSTE) sequence, where the single 180° inversion pulse is replaced with two successive 90° pulses, which causes the system to undergo slower longitudinal relaxation (T_1) during the storage period (T), as shown in Figure 4.1, to achieve an improved signal-to-noise ratio.^{22,23}

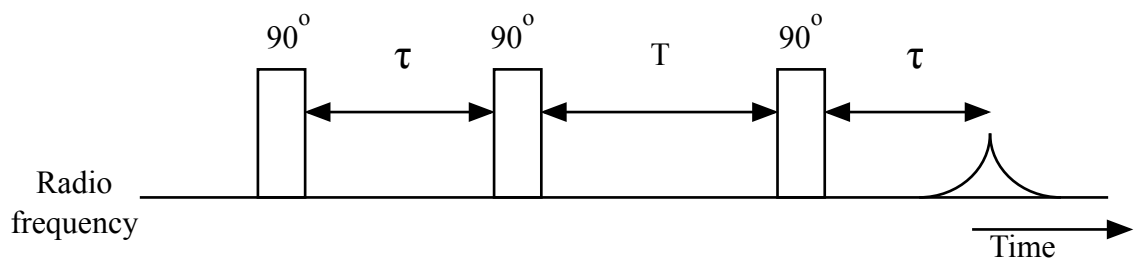


Figure 4.1 PGSTE pulse sequence showing echo time (τ) and storage interval (T)

In PFG NMR, under Brownian dynamics, signal attenuation (E_g/E_o) of gradient pulses is related to the strength of the gradient pulse g through equation 4.2, where D is the self-diffusion coefficient, Δ is the diffusion time, δ is the application time of the gradient pulse and γ is the gyromagnetic ratio of the nuclei concerned.¹¹ Diffusion times are typically set between 1 ms and several seconds due to limitations in the equipment and nucleus respectively, and in cases of low gyromagnetic ratio or slow diffusion a high field gradient is required.¹¹

$$\frac{E_g}{E_o} = e^{-D\gamma_H^2 g^2 \delta^2 \Delta} \quad 4.2$$

Due to the slow diffusion found in ILs, high field gradients are needed, which increases experimental difficulty as many high gradient probes are generally specifically tuned to one nucleus, and high field gradients can cause heterogeneous heating and cause convection.¹¹ A method to avoid these problems is to use a double

simulated spin echo sequence, which reduces the effect of convection as the pulse sequence separates the flux and self-diffusion aspects of molecular motion.²⁴

Self-diffusion coefficients derived PFG NMR have been used to study ion interactions by comparing measured molar ionic conductivity with theoretical molar ionic conductivity from self-diffusion coefficients in conjunction with the Nernst-Einstein relationship, which is shown in equation 4.3, where Λ_{NMR} is the molar ionic conductivity derived from PFG NMR, F is the Faraday constant, R is the universal gas constant, T is absolute temperature, ν and z are the stoichiometric and charge number of the ion respectively.²⁵ The Watanabe group found that for ILs in general, the ratio of Λ/Λ_{NMR} is approximately 0.5, whereas in high temperature molten salts the Λ/Λ_{NMR} ratio is approximately 0.9, and was attributed to differences in the degree of ion-pairing within the IL system.²⁶

$$\Lambda_{NMR} = \frac{F^2}{RT} (\nu_+ z_+^2 D_{NMR-Cation} + \nu_- z_-^2 D_{NMR-Anion}) \quad 4.3$$

As well as ILs, PFG NMR has been used to study DESs. D'Agostino *et al.* have investigated the molecular motion and ion diffusion in a range of ChCl based DESs and found that in many cases diffusion of the Ch cation was slower than the respective HBD, suggesting a link between molecular dimensions and the strength of hydrogen bonding interactions.²⁷ Self-diffusion coefficients were found to follow an Arrhenius temperature dependence, as shown in equation 4.4, where A is the Arrhenius pre-exponential factor and E_D is the activation energy of diffusivity, and the derived activation energies of diffusivity suggest the temperature dependence of the Ch cation was higher than the corresponding HBD.²⁷ When compared with viscosity behaviour, self-diffusion data indicated the diffusion mechanism where the diffusing species moves through nearby suitably sized voids in the medium, which is similar to what is observed in ILs, as opposed to the classical *random walk* diffusion mechanism seen in conventional liquids.²⁷

$$D = Ae^{\left(-\frac{E_D}{RT}\right)} \quad 4.4$$

The effect of added water on ionic diffusion within ChCl based DESs has also been studied by D'Agostino *et al.*²⁸ In the cases of anhydrous DESs, the HBD and

choline OH were found to be associated, and viscosity was found to be controlled by the hydrogen bonding interactions between the HBD and the chloride anion.²⁸ The addition of water reduced the viscosities of the systems tested, but at added water contents greater than 2.5 % w/w (greater than 1:1 molar ratio of water and ChCl respectively), there is a significant step in the overall trend.²⁸ PFG NMR experiments were employed and revealed the Ch cation diffuses according to the Stokes-Einstein relationship, and when a polyol is used as the HBD, the addition of water results in the exchange of the choline OH proton thus giving a mildly acidic solution, whereas when amides are used as the HBD exchange of the choline OH proton gives a mildly basic mixture.²⁸ Self-diffusion coefficients of water imply the systems investigated were not homogeneous on the microscopic scale, and water rich phases exist at higher added water contents.²⁸

PFG NMR is a powerful tool that provides a microscopic insight into macroscopic behaviour, and when used in conjunction with other characterisation methods gives a deeper understanding into complex liquid behaviour.¹¹

4.1.2. Aims

The main aim of this part of the project was to study the mobility of the different species in the systems, most notably the waters of hydration. To achieve this PFG NMR techniques were used to study the NMR T_1 relaxation times of: hydrate waters, glycerol aliphatic protons, glycerol hydroxyl groups, sodium cations and acetate anions of a series of sodium salt:glycerol systems as a function of temperature. Understanding the T_1 relaxation behaviour gave an insight into the diffusion regimes present in these systems as a function of temperature. As well as investigating T_1 relaxation times, ^1H and ^{23}Na PFG NMR measurements as a function of temperature were used to probe multi-component diffusion in the species outlined above. From the PFG NMR measurements, self-diffusion coefficients were deduced from which the activation energies of diffusivity could be interpreted. The activation energies of diffusivity and the self-diffusion coefficients were compared with molecular liquids, ILs and DESs to gain further knowledge of the transport properties of sodium salt:glycerol systems.

The details gained from PFG NMR experiments were used to further explain the macroscopic thermophysical properties of sodium salt:glycerol systems studied in section 3.3. From the self-diffusion data of hydrated sodium salt:glycerol systems, a better understanding of the role of water was achieved and used to explain deviations from ideal mechanisms.

4.2. Dynamics and Diffusion Investigations Using PFG NMR

NMR diffusion and relaxation investigations have been carried out to gain a greater insight into the dynamics of species in sodium salt:glycerol mixtures. ^1H PFG NMR diffusion and ^1H and ^{23}Na T_1 relaxation methods were used to probe translational and rotational dynamics of species and relate macroscopic behaviour correlates with microscopic NMR techniques. ^{23}Na PFG NMR diffusion studies were attempted, but due to the extremely short relaxation times and the quadrupolar interactions of the ^{23}Na species no PFG signal was observed, even when a minimised echo time was used in the NMR pulse sequence. Even though it was possible to measure the T_1 relaxation times, which were typically in the order of μs , it was not possible to detect any PFG NMR signals considering T_2 transverse relaxation times are less than T_1 relaxation times.²⁹

The PFG NMR signal decay, showing the diffusion attenuation for a 1.80 M NaOAc:glycerol mixture at 298 K is shown in Figure 4.2. The signal attenuation of the hydroxyl and aliphatic resonance of glycerol are shown at 4.54 ppm and 2.68 ppm, respectively, and the resonance of the acetate anion is indicated at 1.03 ppm. Figure 4.2 is also representative of the 1.88 M NaBr, 2.02 M $\text{Na}_2\text{B}_4\text{O}_7 \cdot 10\text{H}_2\text{O}$ and 2.28 M NaOAc $\cdot 3\text{H}_2\text{O}$:glycerol mixtures used in this study with the omission of the acetate resonance at 1.03 ppm. In all of the systems investigated the NMR resonances are broadened due to the relatively high viscosities of these systems.

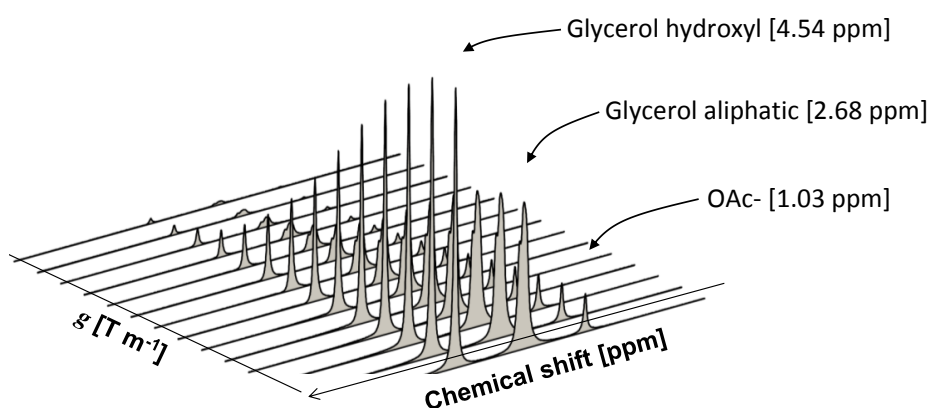


Figure 4.2 Typical PFG NMR signal decay for a 1.80 M NaOAc:glycerol mixture, which is applicable to all other sodium salt:glycerol mixtures investigated with the exception of the acetate peak at 1.03 ppm³⁰

4.2.1. Self-Diffusion Studies

Diffusion is defined as the spontaneous movement of a species under the influence of a concentration gradient, and mathematically defined by equation 4.5, where J is the flux of matter crossing a unit area perpendicular to the bulk flow, the concentration gradient (dc/dx) is the concentration increase with respect to the distance travelled in the direction of species flow, and D is the diffusion coefficient.³¹

$$J = D \frac{\partial c}{\partial x} \quad 4.5$$

The diffusion coefficient is dependent on temperature, viscosity of the fluid medium and the size and geometry of the diffusing species as defined by the Stokes-Einstein relationship. The Stokes-Einstein relationship is shown in equation 4.6, where k_B is the Boltzmann's constant, T is absolute temperature, η is dynamic viscosity and r is the hydrodynamic radius.³¹

$$D = \frac{k_B T}{6\pi\eta r} \quad 4.6$$

In a uniform liquid where the molecules are continually moving randomly, a given molecule has a definite probability of arriving at another location within a define time, which is known as self-diffusion.³² The self-diffusion coefficient (D^*) of a species is defined mathematically according to equation 4.7, where c is the concentration and a is the activity of the species.³² Self-diffusion is a process that is not detectable by traditional methods as all of the molecules of a species are indistinguishable, but can be approximated through isotopic substitution.³¹

$$D^* = D \frac{\partial \ln c}{\partial \ln a} \quad 4.7$$

NMR signal attenuation is directly proportional to gradient pulse strength, as shown in equation 4.2. By monitoring relative signal decay (E_g/E_0) as a function of gradient pulse strength ($\gamma^2 \delta^2 g^2 \Delta$) the self-diffusion coefficient of the species concerned can deduced from the negative of the slope. In all measurements taken, the relative error

was less than 3 %. Table 4.1 lists the self-diffusion coefficients for glycerol hydroxyl and aliphatic proton, water and the acetate anion deduced from PFG NMR for a range of sodium salt:glycerol mixtures as a function of inverse absolute temperature. In the cases where hydrate waters were present, the average diffusivity between water and glycerol hydroxyl groups was taken as the peaks for these species overlapped due to fast exchange.

Table 4.1 Self-diffusion coefficients derived from PFGNMR

Salt:glycerol system	Viscosity (cP)	1000/T (K ⁻¹)	Self-diffusion Coefficient (10 ⁻¹³ m ² s ⁻¹)			
			Glycerol OH	Glycerol OH/ Water	Glycerol aliphatic H	Acetate aliphatic H
1.80 M NaOAc	3169	3.35	6.30	-	5.95	6.34
	1250	3.25	15.4	-	14.0	15.0
	526	3.14	32.6	-	29.3	32.0
	252	3.05	66.0	-	57.2	65.7
	109	2.96	110	-	100	110
1.85 M NaBr	1420	3.35	9.10	-	9.10	-
	624	3.25	21.1	-	21.1	-
	287	3.14	43.1	-	43.2	-
	138	3.05	81.0	-	80.0	-
	70	2.96	142	-	143	-
2.02 M Na ₂ B ₄ O ₇ ·10H ₂ O	1982	3.35	-	140	9.00	-
	879	3.25	-	253	20.8	-
	390	3.14	-	520	42.0	-
	182	3.05	-	900	75.9	-
	89	2.96	-	1310	123	-
2.28 M NaOAc·3H ₂ O	538	3.35	-	75.9	29.9	32.0
	252	3.25	-	157	63.0	69.0
	121	3.14	-	300	118	130
	61	3.05	-	511	200	214
	32	2.96	-	780	330	354

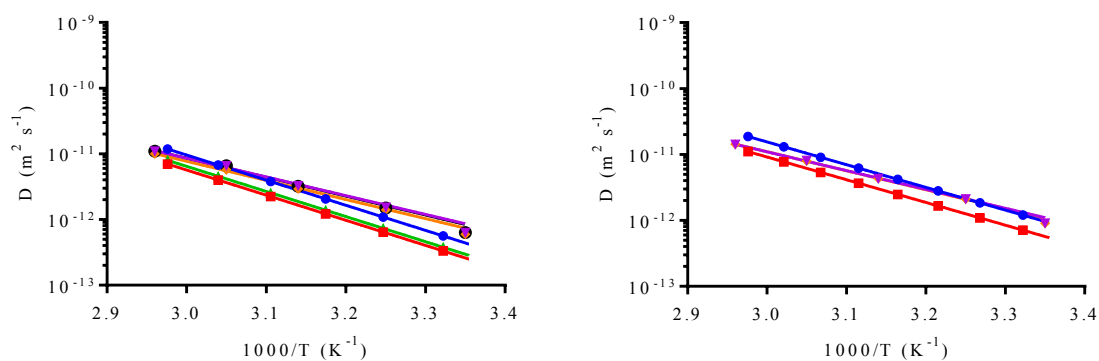
The NaOAc:glycerol system showed the lowest diffusivity values for all of the investigated species, which coincides with the NaOAc:glycerol system being the most viscous at any given temperature. The diffusivity of the glycerol hydroxyl protons, in exchange with water protons, in the $\text{Na}_2\text{B}_4\text{O}_7 \cdot 10\text{H}_2\text{O}$ system is comparatively fast, which suggests the hydrate waters are relatively free in the mixture. However, the $\text{Na}_2\text{B}_4\text{O}_7 \cdot 10\text{H}_2\text{O}$ system is noticeably more viscous than the NaBr:glycerol system even though a significant amount of free water is present, which suggests the hydrogen bonding network between the tetraborate anion and water plays a dominating role in reinforcing the structure of glycerol.

The NaOAc. $3\text{H}_2\text{O}$ glycerol system showed the lowest viscosity of all the systems tested, which results in faster diffusion coefficients for all of the species investigated. Despite the lower viscosity of the NaOAc. $3\text{H}_2\text{O}$ glycerol system, the diffusivity of the glycerol hydroxyl protons and water protons in fast exchange is noticeably lower than what was observed for the $\text{Na}_2\text{B}_4\text{O}_7 \cdot 10\text{H}_2\text{O}$:glycerol system. The hindered diffusivity of the NaOAc. $3\text{H}_2\text{O}$ glycerol system suggests the motion of the hydrate waters is more restrictive, even though the system is macroscopically less viscous than the other systems tested.

The aliphatic and hydroxyl protons of the NaBr:glycerol system show equal diffusivity over the temperature range tested, whereas in the NaOAc:glycerol system the glycerol hydroxyl protons appear to be diffusing slightly faster than the aliphatic protons with diffusion coefficients equal to that of the acetate anion. This phenomenon may be due to the acetate anion contributing to the dissociation of the hydroxyl proton from the parent molecule, however further studies are required to support this hypothesis.

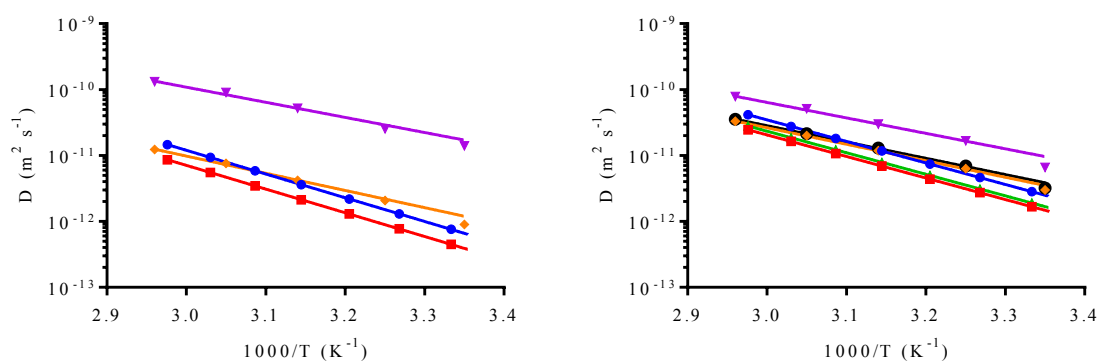
The Stokes-Einstein equation, (4.7), has commonly been used as a theoretical method for deriving the self-diffusion coefficient of a species from assuming a spherical geometry and knowing the size of the species, and knowing the dynamic viscosity of the fluid system.³¹ The Stokes-Einstein equation has been employed to derive theoretical self-diffusion coefficients of the sodium salt:glycerol systems being investigated, with the species being assumed to be hard spheres. Species volumes were calculated by optimising the component molecular structure using a Hartree-Fock (HF) computational method coupled with a 3-21G basis set, followed by fitting a van der Waal's (VDW) density surface, using commercially available software.³³ From the volumes calculated, hard sphere geometry was assumed and a corresponding hard

sphere radius was calculated. The theoretical self-diffusion coefficients derived from the Stokes-Einstein equation have been compared with the experimental values obtained using PFG NMR, with respect to inverse temperature, in Figure 4.3.



A) 1.80 M NaOAc

B) 1.88 M NaBr



C) 2.02 M $\text{Na}_2\text{B}_4\text{O}_7 \cdot 10\text{H}_2\text{O}$

D) 2.28 M $\text{NaOAc} \cdot 3\text{H}_2\text{O}$

Figure 4.3 Self-diffusion coefficients versus inverse temperature for a range of salt:glycerol mixtures. Within each plot there are trends from the Stokes-Einstein equation: (blue) glycerol/water OH, (red) glycerol aliphatic H, (green) acetate aliphatic H, and trends from PFGNMR: (purple) glycerol/water OH, (yellow) glycerol aliphatic H and (black) acetate aliphatic H

Figure 4.3 A shows the self-diffusion coefficient comparison for the NaOAc:glycerol system and suggests there is little difference between the theoretical and measured values. The Stokes-Einstein equation underestimates the glycerol hydroxyl and aliphatic protons values by approximately 13 % at 338 K and shows a more pronounced temperature dependence. The NaBr:glycerol system, as represented by Figure 4.3 B, shows the theoretical and measured self-diffusion coefficients to be in good agreement, suggesting the species in this system diffuse in a Stokesian manner.

The $\text{Na}_2\text{B}_4\text{O}_7 \cdot 10\text{H}_2\text{O}$:glycerol system, as shown in Figure 4.3 C, shows poor agreement for both the glycerol aliphatic and hydroxyl protons. The self-diffusion coefficients for the aliphatic protons are underestimated theoretically by 28 % at 338 K, however the hydroxyl protons are underestimated by one order of magnitude. This suggests water plays a significant role in delocalising the hydroxyl protons whilst having only a nominal effect on the aliphatic parent molecule, which agrees with the uncharacteristically high diffusivity of the hydroxyl protons in such a viscous medium.

The glycerol hydroxyl and aliphatic protons, and the acetate diffusivities are also underestimated by the Stokes-Einstein equation for the $\text{NaOAc} \cdot 3\text{H}_2\text{O}$:glycerol system, although the underestimation for the glycerol hydroxyl protons is not as large compared to the discrepancy observed in the $\text{Na}_2\text{B}_4\text{O}_7 \cdot 10\text{H}_2\text{O}$:glycerol system. Estimations by the Stokes-Einstein equation suggest the aliphatic glycerol parent species and the acetate anion are more mobile in the $\text{NaOAc} \cdot 3\text{H}_2\text{O}$:glycerol system, compared to the aliphatic glycerol parent species and the tetraborate anion in the $\text{Na}_2\text{B}_4\text{O}_7 \cdot 10\text{H}_2\text{O}$:glycerol system, hence the lower observed macroscopic viscosity. The diffusivity of the hydrate waters is more restricted than would be expected from a pure water phase, and so the role of water in the $\text{NaOAc} \cdot 3\text{H}_2\text{O}$:glycerol system is not obvious from this study and further research is required.

The above observations agree with the molar ionic conductivity behaviour reported in section 3.3.7 as the NaOAc :glycerol system appears to have the lowest molar ionic conductivity, followed by the NaBr :glycerol system. Of all of the systems tested, the $\text{Na}_2\text{B}_4\text{O}_7 \cdot 10\text{H}_2\text{O}$:glycerol system showed the highest molar ionic conductivity, which is reflected in the uncharacteristically high diffusivity of the glycerol/water exchange protons. The link between the diffusivity of the glycerol hydroxyl/water exchange protons and the molar ionic conductivity observed for the $\text{Na}_2\text{B}_4\text{O}_7 \cdot 10\text{H}_2\text{O}$:glycerol system suggests, the dominating charge transport mechanism involves a significant amount of free water. Cross-referencing the observations discussed in section 3.3.7 with Figure 4.3 shows in general that the molar ionic conductivities of the sodium salt:glycerol systems investigated appear to be dependent on the mobility of the glycerol hydroxyl protons. The relatively free nature of the hydrate waters in the $\text{Na}_2\text{B}_4\text{O}_7 \cdot 10\text{H}_2\text{O}$:glycerol system may answer why the free volume of this system increases with salt concentration, whereas the relatively restricted nature of the hydrate waters in the $\text{NaOAc} \cdot 3\text{H}_2\text{O}$ glycerol system may answer why the free volume of this system decreases with salt concentration, as discussed in section 3.3.3.

ILs typically possess self-diffusion coefficients in the range 10^{-9} to 10^{-12} $\text{m}^2 \text{s}^{-1}$ at 298 K, which is comparable with the diffusivity observed for the sodium salt:glycerol systems reported in section 4.2.1.^{34,35} The ionic species within an IL system generally show different self-diffusion coefficients depending of the relative size and charge density, which is also observed between the glycerol aliphatic and hydroxyl, and acetate protons.^{35,36} The effect of ion size and geometry has been investigated by Watanabe *et al.* and found that increasing the ion alkyl chain length of the decreased the diffusivity of both the cations and anions, suggesting a strengthening of the ionic network.³⁷ The same research group also investigated the effect of cation geometry whilst keeping the molecular mass similar to that of the anion and found the self-diffusivity of the cations obeyed the following order: imidazolium > pyridinium > pyrrolidinium > ammonium.³⁸

The physical properties of ILs are greatly affected by the presence of impurities with the absorption water being a significant issue due to the hygroscopic nature of ILs.³⁹ The effects of added water on the self-diffusivity coefficients of [BMIM][(CF₃SO₂)₂N] has been investigated by Rollet *et al.*, and found that the addition of 30 mol % water resulted in a 30 % increase in the self-diffusion coefficients of the anion and cation, as opposed to the 800 % increase in the self-diffusion coefficient of water, which did not correlate with the 30 % decrease in viscosity.⁴⁰ Hoffmann *et al.* made a similar observation with the [EMIM][CH₃SO₃] system and suggested within these systems, miscibility with water is not complete on a microscopic scale.⁴¹

The self-diffusion coefficients of ChCl: HBD based DESs have been studied by Abbott *et al.* and were found to be in the 10^{-11} - 10^{-13} $\text{m}^2 \text{s}^{-1}$ range at 298 K, which is similar to many ILs and the sodium salt:glycerol systems mentioned here.²⁷ In many cases, Abbott *et al.* found diffusion of the Ch cation was slower than the respective HBD, suggesting a link between molecular dimensions and the strength of hydrogen bonding interactions.²⁷ The same authors investigated the effect of added water and found the self-diffusion coefficients typically increased by 1-2 orders of magnitude upon the addition of 17.5 w/w % water compared to the anhydrous DES systems.²⁸ In the cases of anhydrous DESs, the HBD and choline OH were found to be associated, and viscosity was found to be controlled by the hydrogen bonding interactions between the HBD and the chloride anion.²⁸ The addition of water reduced the viscosities of the systems tested, but at added water contents greater than 2.5 % w/w (greater than 1:1 molar ratio of water and ChCl respectively) showed a significant step in the overall trend.²⁸ Experiments revealed the Ch cation diffuses according to the Stokes-Einstein

relationship, and when a polyol is used as the HBD, the addition of water results in the exchange of the choline OH proton thus giving a mildly acidic solution, whereas when amides are used as the HBD exchange of the choline OH proton gives a mildly basic mixture probably resulting from slight decomposition of urea into ammonia.²⁸ Self-diffusion coefficients of water imply the systems investigated were not homogeneous on the microscopic scale, and water rich phases exist at higher added water contents.²⁸

The diffusivity of a species follows the Arrhenius temperature dependence, and assumes the fluid conforms to the Arrhenius equation of molecular kinetics, as expressed in equation 4.4. As temperatures tend towards the glass transition temperature of the system, diffusivity deviates from Arrhenius behaviour, which is characteristic of glass-forming liquids.⁴² The observed temperature dependence of IL diffusivity can be defined using the Vogel-Tammann-Fulcher (VFT) model, as shown in equation 4.8, where A and B are constants, and T_o is the ideal glass-transition temperature.^{43,44,45}

$$D = Ae^{\left(-\frac{B}{T-T_o}\right)} \quad 4.8$$

The data represented in Table 4.1 and Figure 4.3 suggests the Arrhenius temperature dependence is applicable over the temperature range concerned for all of the species investigated. From the fitted Arrhenius trends, the activation energy of diffusivity (E_D) was deduced and listed in Table 4.2.

The activation energies of diffusivity are in the range of 40 – 55 kJ mol⁻¹, which are slightly higher than the 30 - 50 kJ mol⁻¹ observed for ChCl based DESs.²⁷ In the DESs investigated, the Ch cation was observed to have a larger activation energy compared to the HBD, whereas in the sodium salt:glycerol systems investigated there is little observable difference between the species.²⁷ Table 4.2 shows the presence of hydrate water noticeably reduces the activation energy barrier of diffusion for the glycerol hydroxyl and aliphatic protons, and the acetate species.

Table 4.2 Activation energies of diffusivity

Salt:glycerol system	Activation energy of diffusivity (kJ mol ⁻¹)			
	Glycerol OH	Glycerol OH/ Water	Glycerol aliphatic H	Acetate aliphatic H
1.80 M NaOAc	53.4±2.9	-	54.5±1.7	53.9±2.9
1.85 M NaBr	53.4±1.2	-	54.0±0.9	-
2.02 M Na ₂ B ₄ O ₇ ·10H ₂ O	-	42.9±3.0	48.8±2.1	-
2.28 M NaOAc·3H ₂ O	-	44.9±2.5	47.9±0.9	47.3±1.1

When Table 4.2 is compared with Table 4.1, larger self-diffusion coefficients are observed for species with lower activation energy barriers for diffusion. The Na₂B₄O₇·10H₂O:glycerol system showed a slightly higher activation energy for the glycerol aliphatic parent species compared to the NaOAc·3H₂O:glycerol system, which matches the differences observed in self-diffusion coefficients. However the relatively small difference in activation energy does not explain why the dynamic viscosity of the NaOAc·3H₂O:glycerol system is significantly lower than the Na₂B₄O₇·10H₂O:glycerol system, Further work is needed to fully understand the restricted role of water in this system.

The activation energies of diffusivity are noticeably lower than the activation energies of fluid flow and ionic conduction, as shown in section 3.3.6, which is surprising considering there appears to be a strong link between viscosity, ionic conductivity and self-diffusivity within the systems studied. The order from highest to lowest activation energy of diffusivity of the glycerol hydroxyl/water exchange protons follows the same trend observed for the activation energies of ionic conductivity, reinforcing the possibility of a link between the mobility of the glycerol hydroxyl groups and the ionic conductivity of the system.

4.2.2. NMR T₁ Relaxation studies

¹H and ²³Na T₁ relaxation were investigated as a function of absolute temperature using the inversion recovery pulse sequence, where an 180° pulse inverts the initial magnetisation followed by a 90° pulse allowing longitudinal relaxation to be recorded.^{46,47} The T₁ relaxation time constant was obtained by fitting the NMR signal

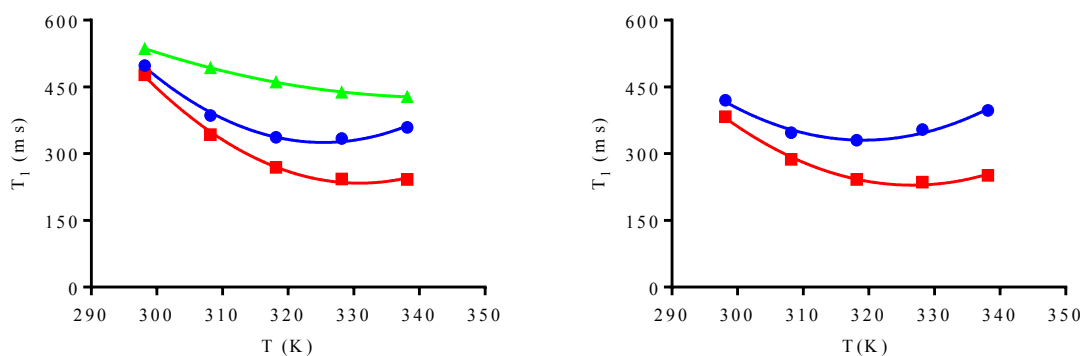
decay to equation 4.9 where S_t is the signal intensity after a decay time t , and S_o is the NMR signal intensity at equilibrium.³⁰

$$S_t = S_o \left[1 - 2e^{\left(-\frac{t}{T_1}\right)} \right] \quad 4.9$$

In liquids of low viscosity, T_1 relaxation times generally increase as a function of absolute temperature, as the rotational correlation times decrease as a consequence in the increased rate of species tumbling caused by elevations in temperature.⁴⁸ In high viscosity liquids, a minimum in T_1 can be detected, which signifies a transition from a slow tumbling (low mobility) relaxation regime to a fast tumbling (high mobility) relaxation regime.⁴⁸ Species that are more mobile will transition into the fast tumbling regime at lower temperatures.⁴⁸

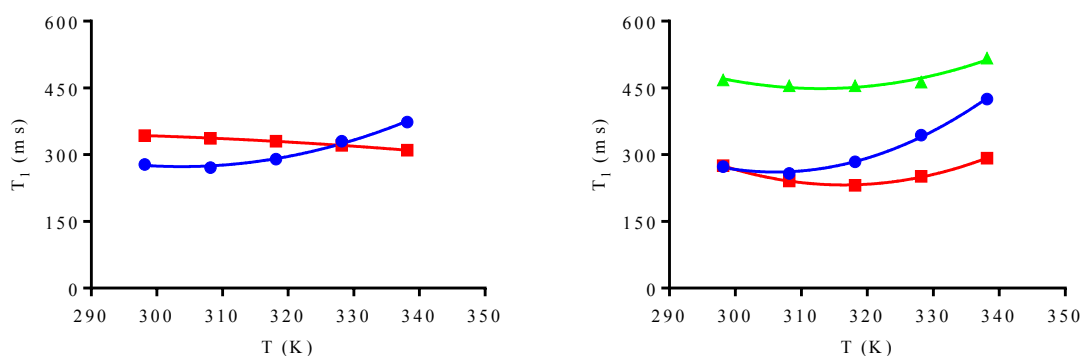
The ^1H T_1 NMR relaxation times for the glycerol hydroxyl and aliphatic protons, and acetate protons for all of the sodium salt:glycerol systems investigated are shown in Figure 4.4. The T_1 relaxation time-temperature profile for the NaOAc:glycerol system is shown in Figure 4.4 A. The transition into the fast tumbling regime for the glycerol hydroxyl protons occurred at 325 K, however the glycerol aliphatic and acetate protons did not transition into the fast tumbling regime over the temperature range investigated. This observation is consistent with the higher viscosity and lower species mobility displayed by the NaOAc:glycerol system. In contrast, the NaBr:glycerol system, shown in Figure 4.4 B, displays the transition into the fast tumbling regime at 319 K and 327 K for the glycerol hydroxyl and aliphatic protons respectively. The difference in transition temperature is surprising considering the self-diffusion coefficients for both species were equal at all of the temperatures investigated.

The $\text{Na}_2\text{B}_4\text{O}_7 \cdot 10\text{H}_2\text{O}$:glycerol system, represented by Figure 4.4 C shows the glycerol hydroxyl/ water exchange protons undergo the regime transition at 304 K, which is the lowest transition temperature recorded for the systems investigated, and reflects the higher self-diffusion coefficients of the glycerol hydroxyl/ water exchange protons. However, the glycerol aliphatic protons fail to transit and remain in the slow tumbling regime, which could explain the significantly higher dynamic viscosity of the $\text{Na}_2\text{B}_4\text{O}_7 \cdot 10\text{H}_2\text{O}$:glycerol system despite the presence of highly mobile water.



A) 1.80 M NaOAc

B) 1.88 M NaBr



C) 2.02 M $\text{Na}_2\text{B}_4\text{O}_7 \cdot 10\text{H}_2\text{O}$

D) 2.28 M $\text{NaOAc} \cdot 3\text{H}_2\text{O}$

Figure 4.4 T_1 relaxation times versus temperature for a range of salt:glycerol mixtures. Within each plot there are trends from: (blue) glycerol/water OH, (red) glycerol aliphatic H and (green) acetate aliphatic H

Figure 4.4 D shows the $\text{NaOAc} \cdot 3\text{H}_2\text{O}$:glycerol system, which displayed the highest self-diffusivity for the acetate and glycerol aliphatic protons. The transition into the fast tumbling regime occurs at 306 K, 316 K and 313 K for the glycerol hydroxyl/water exchange and aliphatic protons, and acetate protons respectively. The $\text{NaOAc} \cdot 3\text{H}_2\text{O}$:glycerol system shows the lowest transition temperature for the glycerol aliphatic parent species of all of the systems tested, and the acetate anion shows a transition into the fast tumbling regime. Whereas the anhydrous NaOAc :glycerol system shows the acetate anion remaining in the slow tumbling regime, suggesting the addition of water decreases the interactions between the aliphatic glycerol parent species and the acetate anion.

Hayamizu *et al.* studied the molecular motions and ion diffusions of 1,2-dimethyl-3-propylimidazolium bis(trifluoromethylsulfonyl)amide (DMPIImTFSA) and observed the T_1 of the ^1H NMR showed minima for the DMPIIm cation, but did not for the TFSA

anion.⁴⁹ The transitions from the slow to fast tumbling regimes occurred between 303 – 278 K depending on the proton environment due to different relaxation mechanism occurring.⁴⁹ Remsing *et al.* studied the dynamics of alkylimidazolium ILs and found the imidazolium carbon atoms underwent a transition from a slow tumbling regime to a fast tumbling, high mobility, regime in the 209 – 343 K temperature range, however, the carbon atoms on the imidazolium alkyl chains failed to show this transition suggesting the alkyl chains are more mobile than the imidazolium parent species.⁵⁰ The authors also observed a significant increase in the T_1 relaxation times of the chloride and acetate anions with increasing temperature, which correlates with reductions in viscosity and ion-ion interactions.^{50,51}

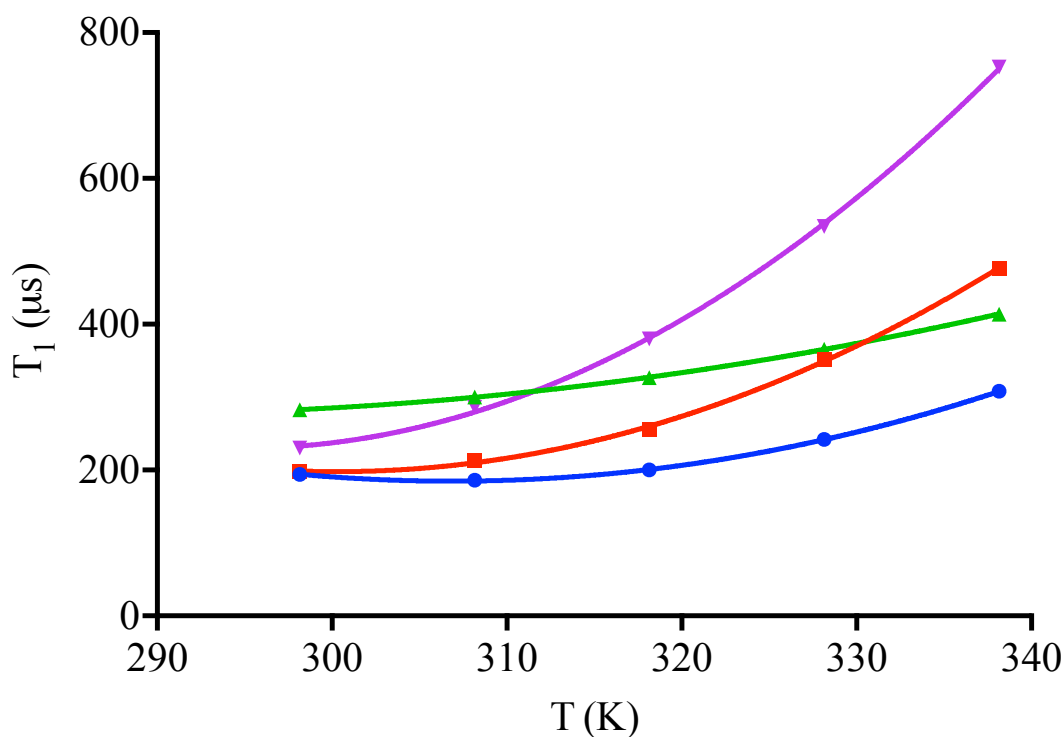


Figure 4.5 T_1 relaxation times ^{23}Na versus temperature for a range of salt:glycerol mixtures: (blue) 1.80 M NaOAc, (red) 1.88 M NaBr, (green) 2.02 M $\text{Na}_2\text{B}_4\text{O}_7 \cdot 10\text{H}_2\text{O}$ and (purple) 2.28 M $\text{NaOAc} \cdot 3\text{H}_2\text{O}$.

The ^{23}Na NMR T_1 relaxation times have also been studied as a function of absolute temperature for all of the sodium salt:glycerol mixtures being investigated and have been represented in Figure 4.5. The ^{23}Na NMR T_1 relaxation times are shorter compared to the ^1H T_1 NMR relaxation times, which is a consequence of quadrupolar nature of the ^{23}Na isotope exhibiting enhanced relaxation.³⁰

The NaOAc:glycerol system, shown as the blue trend in Figure 4.5, is the only system to show a minimum in the T_1 relaxation time-temperature profile signifying a transition from a slow tumbling to a fast tumbling regime. All of the other systems investigated suggest the fast tumbling regime is evident over the temperature range studied. The ^{23}Na T_1 relaxation times show a stronger temperature dependence compared to the glycerol and acetate protons, which correlates well with the observed changes in viscosity, and suggests a weakening of ion-ion interactions.^{50,51} The higher mobility of the ^{23}Na species suggests the dynamics of these ions are mostly independent from the other species. When the NaOAc.3H₂O:glycerol system is compared with the anhydrous counterpart, the ^{23}Na T_1 relaxation becomes much faster and reaches significantly higher values, which implies enhanced molecular dynamics in agreement with the dramatic decrease in dynamic viscosity. However, the Na₂B₄O₇.10H₂O:glycerol system shows less temperature dependence, and at 338 K, has a slower relaxation time than the ^{23}Na species in the NaBr:glycerol system, despite the high self-diffusion coefficient of the glycerol hydroxyl/ water exchange protons.

In the systems investigated, Na⁺ has to be solvated with glycerol, water or exist as an ionic aggregate. If the Na⁺ ions were solvated by glycerol in the same way in all of the systems, one would expect the T_1 relaxations times to be equivalent. However, all of the systems investigated showed different T_1 relaxations times at a given temperature, which suggests different types of solvation may be present. The significantly higher T_1 relaxations times of the NaOAc.3H₂O:glycerol and Na₂B₄O₇.10H₂O:glycerol systems show evidence of different types of solvation. The increase in T_1 relaxation times due to increases in temperature also suggest breakdown of ion aggregates may also be occurring.

Hoffmann *et al.* investigated the physical properties of aqueous solutions of 1-butyl-3-methylimidazolium methanesulfonate [BMIM][MeSO₃], and found that ion aggregation was significant even at IL mole fractions less than 10 %.⁵² The same authors also reported the [BMIM][MeSO₃]: water system transitioned from the slow tumbling regime to the fast tumbling regime at an IL mole fraction of 30 %, at 298 K.⁵² Murgia *et al.* studied the [BMIM][BF₄]: water system and found from ¹¹B NMR analysis, increasing water content progressively disrupted ion-pairing from molar water contents of 20 % up to 60 %, suggesting increasing ion dissociation occurs at high dilutions.⁵³ Umecky *et al.* have probed the effect of dissolved water on Li⁺ solvation in the [EMIM][TFSA] system and found the addition of water reduced the distance

between Li^+ and the solvating species, suggesting the change in the solvation structure.⁵⁴ The authors concluded $[\text{TFSA}]^-$ the solvating species for Li^+ in the IL solutions were replaced by water molecules at a water content of 0.1 mol kg^{-1} , which corresponded to a hydration number of 8, and that Li^+ diffuses in a water-rich domain.⁵⁴

4.2.3. Conclusions

PFG NMR has been utilised to probe the molecular dynamics and self-diffusion in sodium salt:glycerol systems, and has shown the systems investigated exhibit complex behaviour at the microscopic level. The self-diffusion coefficients of the systems investigated have been shown to be in the 10^{-11} - $10^{-13} \text{ m}^2\text{s}^{-1}$ range which is similar to many DES and IL systems. Within the NaBr:glycerol system, the glycerol aliphatic and hydroxyl protons appear to be diffusing together, whereas in the NaOAc:glycerol system the glycerol hydroxyl protons appear to be diffusing with the acetate anion.

There appears to be a clear link between system dynamic viscosity and the self-diffusivity of a species, however, the role of water complicates the diffusion mechanism. Hydrate waters increase species self-diffusivity, and reduces the viscosity of the NaOAc.3H₂O:glycerol system however, water in this system appears to be more restricted compared to the Na₂B₄O₇.10H₂O:glycerol system. Hydrate waters appear to preferentially increase the diffusivity of the glycerol hydroxyl protons in the Na₂B₄O₇.10H₂O:glycerol system resulting in higher dynamic viscosity yet higher ionic conductivity. The relatively free water in the Na₂B₄O₇.10H₂O:glycerol system may be the cause of the increase in the system free volume.

Comparisons between PFG NMR diffusion studies and theoretical self-diffusion coefficients from the Stokes-Einstein relationship have been made. In all of the systems investigated, the Stokes-Einstein relationship underestimated the self-diffusion coefficients of all of the ¹H species probed. The most significant deviation from theory was observed for the glycerol hydroxyl/water exchange protons, suggesting a non-Stokesian transport mechanism for the Na₂B₄O₇.10H₂O:glycerol system.

The self-diffusion coefficients determined from PFG NMR were fitted to an Arrhenius model, and the activation energies of diffusivity were calculated, which were found to be similar to many DES and IL systems. The activation energies of diffusivity were cross-referenced with the activation energies of fluid flow and conduction, and were found to be slightly lower in magnitude but followed the same general trend.

The ^1H longitudinal T_1 relaxation times have been investigated using an inversion recovery pulse sequence, and all systems showed a transition from a diffusion-limited, slow molecular tumbling regime to a fast molecular, high-mobility, tumbling regime. A link between the tumbling regime transition temperature, viscosity and ion-ion interactions has been observed and agrees with observations made with other IL systems.^{49,50} The ^{23}Na T_1 relaxation times were found to be significantly faster than the ^1H containing species, and were found to be in the fast tumbling, high mobility regime over the temperature range investigated. Water was found system to dramatically increase the ^{23}Na T_1 relaxation rate in the $\text{NaOAc}\cdot 3\text{H}_2\text{O}$:glycerol, whereas little effect was observed for the $\text{Na}_2\text{B}_4\text{O}_7\cdot 10\text{H}_2\text{O}$:glycerol system.

To study diffusion in more depth attempts were made to use electrochemical methods to study the movement of metal probe molecules. The diffusion of copper in choline based DESs has been studied in depth previously and this was thought to be a good model system to use. The speciation of CuCl_2 is known to be mostly $[\text{CuCl}_4]^{2-}$ in chloride based DESs and it is thought that changes in speciation could be observed through diffusional measurements.

4.3. Diffusion Studies of Solutes in Sodium Salt:Glycerol Mixtures by Electrochemical Methods

4.3.1. Introduction

Studying the thermophysical properties and the microscopic diffusion behaviour of the sodium salt:glycerol systems of interest have shown many of these systems have properties that are comparable with ChCl : HBD based DESs, and ILs.^{5,27,49,50}

Diffusion coefficients within a fluid system can deduced from a variety of methods including: steady-state, conductimetric, optical, NMR and electrochemical techniques.^{55,56,57,58} The two most common electrochemical techniques for studying diffusion coefficients are voltammetry and chronoamperometry.

Voltammetry is the collective term for a group of electroanalytical techniques where electrical current is measured as a function of electrical potential, from which the potential (E) indicates the Gibbs free energy (ΔG) of a process, as shown in equation 4.10, and the current represents the rate of a redox process.⁵⁹ Voltammetry techniques involve the application of an increase in potential from a starting potential where no redox process occurs to a potential where a redox process proceeds, and a further

increase in potential leads to diffusional control where a deficiency of reactant limits the rate of the redox process.⁵⁹ In the case of cyclic voltammetry, the potential scan is reversed to provide analysis of the products of the forward scan.

$$\Delta G = -nFE \quad 4.10$$

The diffusion coefficient (D) of an electroactive species in solution can be determined using cyclic voltammetry through the Randles-Sevcik relationship, as shown in equation 4.11 where: i_p is the peak current of a redox process, n is the number of electrons exchanged in the process concerned, F is the Faraday constant, A is the electrode surface area, c is the concentration of the species in solution and ν is the potential scan rate.⁵⁹

$$i_p = 0.4463nFAc \sqrt{\frac{nF\nu D}{RT}} \quad 4.11$$

For the Randles-Sevcik relationship to be valid, the species in solution must exhibit reversible, rapid electrochemistry, as shown in Figure 4.6.⁵⁹ For a voltmmetric response to be regarded as rapid and reversible, the kinetics of the redox process of interest must be rapid, and the concentrations of reactants and products at the electrode surface, signified by the reaction quotient (Q), must satisfy the Nernst equation under all potentials, as shown in equation 4.12, where E_{red} is the half-cell reduction potential, E°_{red} is the standard half-cell reduction potential, R is the molar gas constant.⁵⁹ As a consequence of rapid, reversible electrochemistry:⁵⁹

- Peak current is directly proportional to the square root of the potential scan rate.
- Process peak potential is independent of scan rate.
- Diffusion coefficients for the oxidative and reductive processes are equal.
- Difference in peak potential between the oxidative and reductive processes is defined by the Nernst equation, as shown in equation 4.12.

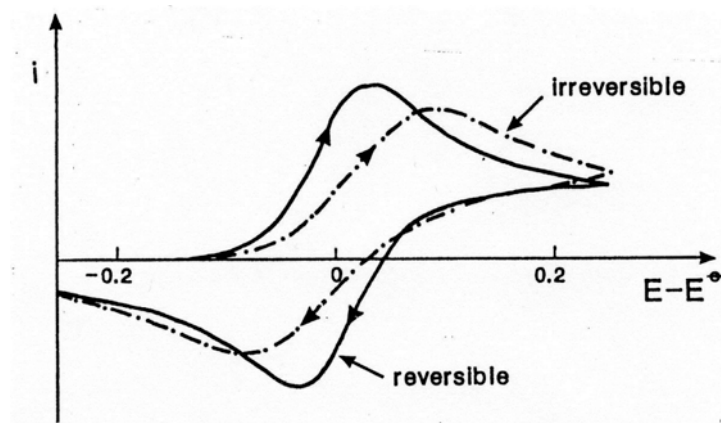


Figure 4.6 Main types of electrochemical response: reversible, rapid (solid line), and irreversible, slow (dashed line)⁶⁰

$$E_{red} = E_{red}^{\theta} + \frac{RT}{nF} \ln(Q_{red}) \quad 4.12$$

In cases where the species of interest in solution does not show rapid, reversible behaviour, as shown in Figure 4.9, equation 4.11 is not valid, and is described as irreversible, slow electrochemical behaviour.⁵⁹ Species that show this type of electrochemical response typically:⁵⁹

- Exhibit peak currents that are governed by diffusion.
- Show wave shapes controlled by kinetics
- Require a greater over-potential for a given process current.
- Peaks separate and show a hysteresis effect as a function of potential scan rate

Currents in electrochemical technique responses are with respect to a non-zero baseline and at low analyte concentrations, electrode double layer charging currents conflicting with Faradaic currents associated with the species concerned.⁶¹

The charge on an electrode at an electrode-electrolyte interface is dependent on the electrode material, electrolyte and applied potential.⁶² The charge on the electrode is balanced by ions of opposite charge being withdrawn from the bulk solution to form a surface regarded as the *electrical double layer*.⁶² There are three models of that describe the structure of the electrical double layer:⁶²

- Compact model
- Diffuse model
- Stern model

The compact model, also referred to as the Helmholtz model, suggests a highly ordered layer of ions of opposite charge to the electrode surface forms to balance the net charge, as shown in Figure 4.7.⁶³ The interactions between interface ions and bulk solution are considered to be electrostatic, and the counter ions are assumed to be fixed.⁶³ The Compact model does not consider diffusion of ions into solution or the possibility of adsorption onto the electrode surface.⁶² The Diffuse model, also referred to as the Gouy-Chapman model, suggests a region of ions is diffusely populated due to electrical forces and random thermal motion at the electrode surface, as shown in Figure 4.7.⁶² The Diffuse model suggests ions are not fixed and are in continuous flux within the diffuse region, which has a total charge equal to the electrode surface but opposite in sign.⁶² The model assumes the electrode surface is flat and ions behave as point charges.

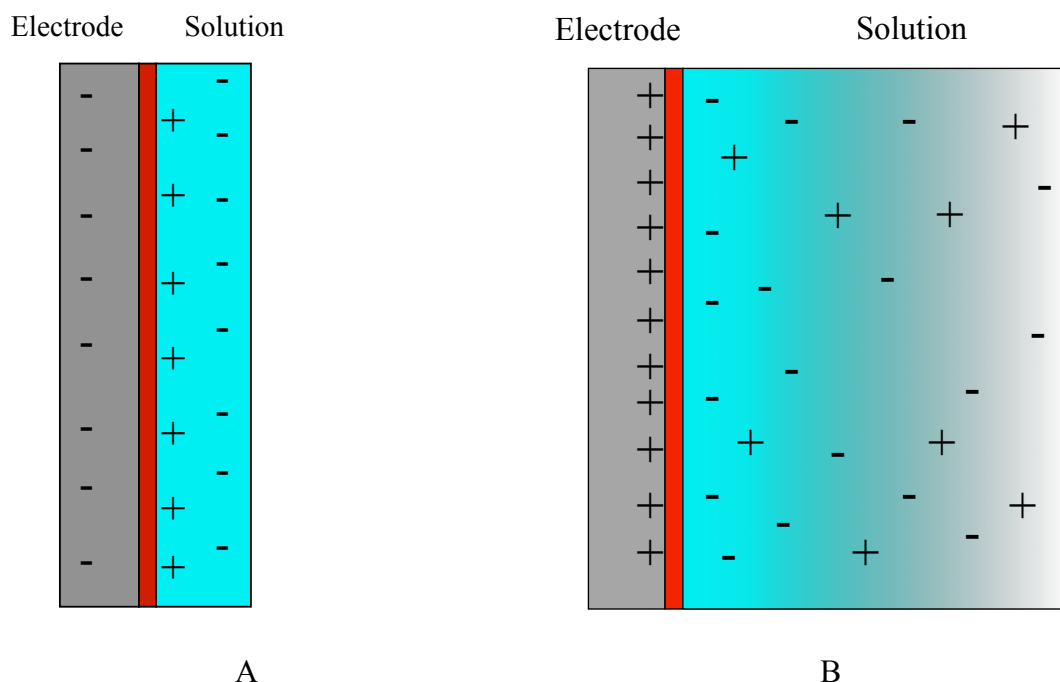


Figure 4.7 Electrical double layer diagrams: Compact model (A) and Diffuse model (B)

The Compact model overestimates the stiffness of the double layer, whereas the Diffuse model underestimates the double layer structure.⁶² The Stern model combines both the Compact model and Diffuse model, and describes the electrical double layer as two sections that are separated by a plane, known as the Stern plane as shown in Figure 4.8.⁶² Adsorbed ions are attached to the electrode surface through electrostatic interactions or VDW forces, and are said to be located in the Stern layer: between the electrode surface and the Stern plane, which is similar to the Compact model.⁶² Ions

outside of the Stern plane are diffuse and in continuous flux, as described by the Diffuse model.⁶²

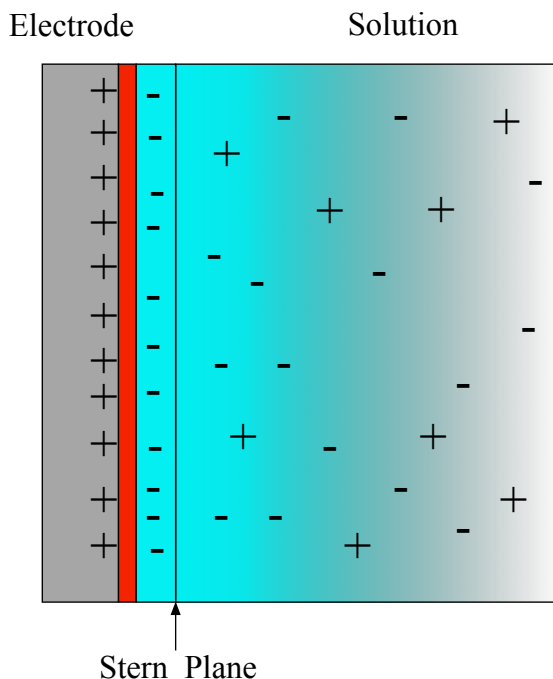


Figure 4.8 The Stern electrical double layer model

The electrode double layer has electrical capacitance when under the influence of a change in potential results in a change in charge, which consequently gives rise to a current flow, as shown in equation 4.13, where Q is charge and C_{DL} is double layer capacitance.⁶¹ The timescale of double layer charging current is dependent on the capacitance and the resistance of the electrode double layer, therefore a suitable scan rate must be determined to minimise contributions to overall measured current.⁶¹

$$Q = C_{DL}E \quad 4.13$$

Microelectrodes are electrodes that employ a working interface that is typically nanometres to micrometres in size, and results in a response that is dependent on electrode size.^{59,64} Due to the relatively small size, the microelectrode surface is assumed to be an edge that allows a steady state voltammetric response without the need to apply a convection current, which is required for a steady state response on a macroelectrode.^{59,64} Diffusion at a macroelectrode surface is regarded as linear and perpendicular to the electrode surface, which is defined by the Cottrell equation, as shown in equation 4.14, where t is defined as the time after a step potential has been

applied.^{59,64} Diffusion at a microelectrode is regarded as hemispherical and defined by the steady state equation shown in equation 4.15.^{59,64}

$$i_D = nFAc \sqrt{\frac{D}{\pi t}} \quad 4.14$$

$$i_D = 4nFDcr \quad 4.15$$

When current is flowing in an electrochemical cell, there is a potential drop, sometimes referred to as an ohmic drop, between the reference and working electrodes, as defined by Ohm's law in equation 4.16, where R is the ohmic resistance.^{64,65} The potential drop is caused by the electrolyte resistivity, the distance between the two electrodes and the magnitude of the current.^{64,65}

$$E = iR \quad 4.16$$

The use of microelectrodes reduces the potential drop between the working and reference electrodes as the high current densities are achieved with small absolute currents, which allow electrochemical measurements in resistive media.^{59,64} Utilisation of a microelectrode minimises the electrode double layer charging currents, as double layer charging currents decrease proportionally with electrode area, whereas Faradaic currents decrease proportionally with electrode radius.^{59,64}

4.3.2. Aims

The main aim of this aspect of the project was to utilise voltammetry techniques to probe the diffusion and mobility of electroactive species dissolved in sodium salt:glycerol mixtures, and cross-reference with the self-diffusion behaviour observed for the background sodium salt:glycerol systems using PFG NMR. From investigating the diffusion and mobility characteristics of dissolved species, transport mechanisms for ions in solution could be investigated and compared with DESs and ILs.

4.3.3. Electrochemical Windows of Sodium Salt:Glycerol mixtures

The electrochemical window of a conductive system is defined as the potential range where the background electrolyte is neither oxidised nor reduced, and is used to determine suitability of a background electrolyte for an electrochemical process.⁶⁶

The most common variety of DESs are the QAS: HBD mixtures referred to as type III DESs, which utilise a QAS as a source of ionic species.¹ Type III DESs have had their thermophysical properties extensively tested, and are known to be redox inactive within the electrochemical window of the DES.⁶⁷ Redox inactivity is a crucial requirement for a conducting medium to act as a background electrolyte in electrochemical processes, and as a consequence, type III DESs have shown to be versatile conducting solvents.^{68,69,70}

Type IV DESs are mixtures of metal salt hydrates with HBDs, and are a potential alternative to the QAS based type III DESs.⁷¹ Traditionally, type IV DESs have been prepared using transition metal salt hydrates, which can be more economically viable than QASs as transition metal salts often occur naturally and do not require synthesis.⁷² The thermophysical properties of many type IV DESs have also been investigated and have shown the transition metal to be redox active within the electrochemical window of the system.⁷² The redox activity of the transition metal can be a useful characteristic, as many type IV DESs are designed with a specific application in mind.^{71,72} The presence of a redox-active metal species limits the use of type IV DESs as background electrolytes.

The electrochemical windows of the sodium salt:glycerol systems of interest have been studied using: a platinum working electrode, a silver wire quasi-reference electrode, a scan rate of 5 mV s^{-1} at 293 K, and are reported in Figure 4.9.

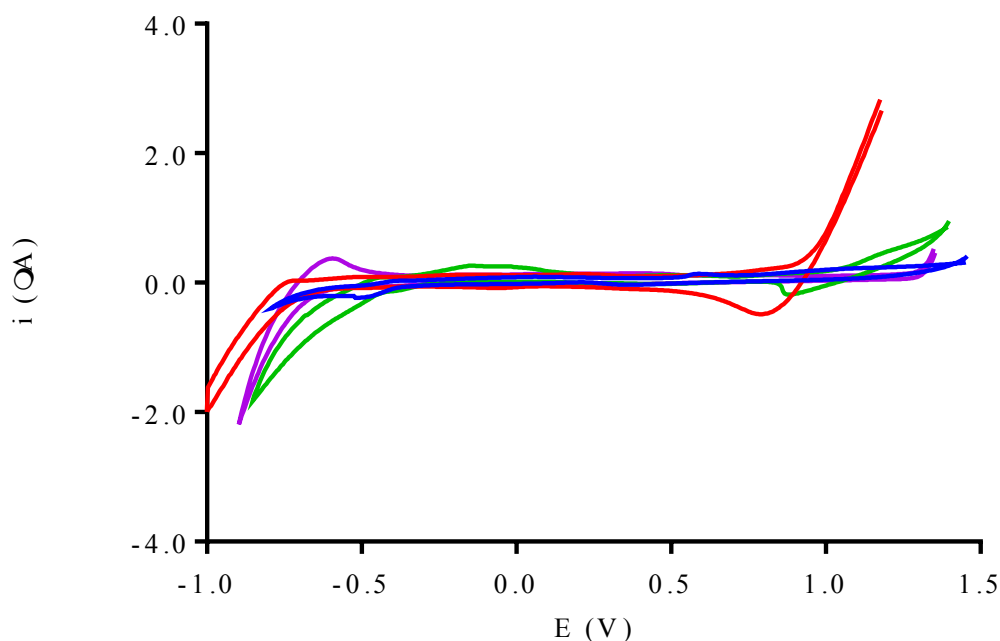


Figure 4.9 Potential windows of sodium salt:glycerol system with a scan rate of 5 mV s^{-1} at 293 K: 1.80M NaOAc (blue), 1.88M NaBr (red), 2.02M Borax (green) and 2.17M ChCl (purple)

All of the sodium salts investigated showed electrolyte breakdown at potentials greater than 1.2 V, which is representative of glycerol. The electrooxidation of glycerol has been studied in acidic and basic media at a platinum electrode, and has been found to undergo a complex oxidation reaction at approximately 1.2 V in the presence of absorbed oxygen.⁷³ Roquet *et al.* found that glycerol electrooxidised to glyceraldehyde at approximately 1.3 V in acidic media.⁷⁴ Electrolyte breakdown also occurred at potentials less than -0.7 V, which is suggestive of the production of hydrogen gas, as represented in equation 4.17.⁷⁵ The reduction process outlined in equation 4.17 suggests water is being reduced to hydrogen gas, but the glycerol hydroxyl groups are also capable of taking part in this reduction process. The systems tested were prepared using anhydrous starting materials that were not further purified or dried before use, and there may be some traces of water that will contribute to the electrolyte breakdown processes.



The NaBr:glycerol system shows the onset of an oxidation process at 0.85 V, which suggests the oxidation of the bromide anion to bromine is occurring, as outlined in equation 4.18.⁷⁵



The ChCl:glycerol DES system also shows an electrochemical window that is confined by similar limits to the sodium salt:glycerol systems investigated, which shows an oxidation process at approximately 1.3 V and a reduction process at approximately -0.7 V. The electrochemical windows of the ChCl: urea and ChCl: malonic acid DESs have also been investigated, and are known to undergo an oxidative process at approximately 1.3 V, which has been attributed to the oxidation of chloride.⁷⁶ Oxidation of chloride may also be coinciding with the oxidation of glycerol in the ChCl:glycerol system. The electrochemical windows of ILs have also been investigated and are generally found to be of the -3 V to 3 V range, on a platinum working electrode with respect to a Ag/AgCl reference electrode.^{4,77} The electrochemical window of ILs in general are much wider than those observed for the type 3 DES systems, and the anodic and cathodic limits of an IL system are dependent on the component ions.¹

The sodium salt:glycerol systems tested show to be redox inactive within their respective electrochemical windows, which suggests these systems are suitable to investigate the redox and diffusion behaviour of metal salts.

4.3.4. Redox Behaviour of Copper in Sodium Salt:Glycerol Mixtures

The redox properties, electrochemical behaviour and species solubility of metal salts in solution are known to be heavily dependent on the ion speciation, and through understanding the ion speciation, a deeper insight into microscopic behaviour can be achieved.⁹

The redox properties of copper have been investigated in aqueous solutions, DESs and ILs and are well described.^{9,78} Cu^{I} is known to not be stable in aqueous solution and undergoes disproportionation, where Cu^{I} is simultaneously oxidised and reduced to Cu^{II} and Cu^0 respectively, as shown in equation 4.19.⁷⁸ This phenomenon is due to the electrode potentials of the $\text{Cu}^{\text{II}}/\text{Cu}^{\text{I}}$, $\text{Cu}^{\text{I}}/\text{Cu}^0$ and $\text{Cu}^{\text{II}}/\text{Cu}^0$ redox couples being greater

than zero, which implies a negative, and therefore spontaneous, Gibbs free energy for all three redox processes.⁷⁸



In aqueous solutions, 3rd period transition metals generally exist as the metal aqua complexes ($[\text{M}(\text{OH}_2)_6]^{2+}$), and generally have octahedral geometry.⁷⁹ Cu^{II} ions exist as the $[\text{Cu}(\text{OH}_2)_6]^{2+}$ species in aqueous solution but show tetragonal distortions from an ideal octahedral geometry due to the Jahn-Teller effect.⁸⁰ The $[\text{Cu}(\text{OH}_2)_6]^{2+}$ species is an example of an octahedral d^9 transition metal complex, which exhibits unequal electron occupation of degenerate d orbitals, as shown in Figure 4.10.⁸⁰ Tetragonal distortions take place in one component direction to remove degeneracy between unequally occupied orbitals, thus lowering the energy of the species.⁸⁰

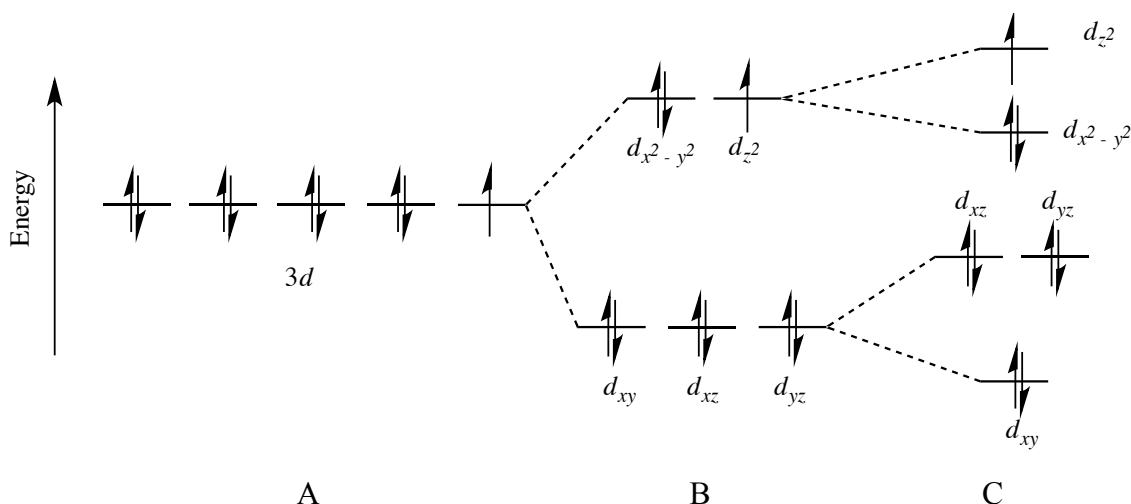


Figure 4.10 Crystal field splitting diagram for: non-ligated Cu^{2+} (A), Typical $[\text{M}(\text{OH}_2)_6]^{2+}$ ion complex (B) and $[\text{Cu}(\text{OH}_2)_6]^{2+}$ species exhibiting tetragonal distortions (C)

The dipositive ions of 3d metals can form four-coordinate complexes when in the presence of an excess of halide anions, and at high chloride concentrations, Cu^{II} ions exist as the $[\text{CuCl}_4]^{2-}$ complex.⁷⁹ The 3d metal tetrahalo complexes generally have a tetrahedral geometry due to the smaller ligand field splitting power of the halide anions, and copper tetrahalo complexes have a distorted tetrahedral geometry.^{79,80} The geometry distortion observed in the copper tetrahalo complexes is due to the d^9 electronic

configuration showing unequal occupation of degenerate d orbitals, and therefore displaying Jahn-Teller distortion to lower the energy of the complex.⁷⁹

Type 3 DESs based on ChCl typically have a 4 M chloride concentration at the eutectic molar ratio, and as a consequence, the $[\text{CuCl}_4]^{2-}$ complex is the dominant speciation of Cu^{II} ions.^{81,82} The cyclic voltammogram of CuCl_2 dissolved in the Glyceline DES measured with: a Pt working electrode, Ag wire quasi-reference electrode, at a scan rate of 10 mV s^{-1} at 293 K, is shown in Figure 4.11.⁸³ There are two separate redox couples in Figure 4.11, the first of which appears at 0.48 V and is representative of the $\text{Cu}^{\text{II}}/\text{Cu}^{\text{I}}$ redox process, the second occurs at -0.33 V and is a consequence of the $\text{Cu}^{\text{I}}/\text{Cu}^0$ redox process.^{83,84} The high chloride environment in the Glyceline DES is thought to stabilise the Cu^{I} species, but other type 3 DESs have shown that disproportionation of the Cu^{I} can occur.^{83,84} CuCl_2 dissolved in the Glyceline DES, or dilute HCl, is a dark green colour, as shown in Figure 4.12 A, and is indicative of the presence of the $[\text{CuCl}_4]^{2-}$, whereas CuCl_2 dissolved in water provides a blue solution due to the presence of $[\text{Cu}(\text{OH}_2)_6]^{2+}$.⁸⁰

The cyclic voltammogram of 5 mM CuCl_2 dissolved in a 1.88 M NaBr:glycerol mixture is represented by Figure 4.13 and shows two separate redox couples, as shown by the Glyceline DES system in Figure 4.11. The first redox process at 0.59 V could be due to a $\text{Cu}^{\text{II}}/\text{Cu}^{\text{I}}$ redox process. However the deep brown colour of the solution is characteristic of Br_2 and could result the $\text{Br}_3^-/\text{Br}^-$ couple.⁸⁵ The anodic limit for the liquid shown in figure 4.9 is +0.6 V confirming this could be a possibility. Considering the NaBr:glycerol mixture has a 1.88 M concentration of the bromide anion, the speciation of Cu^{II} ions would be expected to be $[\text{CuBr}_4]^{2-}$ and that of the Cu^{I} is $[\text{CuBr}_2]^-$ but the $[\text{CuBr}_4]^{2-}$ anion is known to be typically dark green in solution.

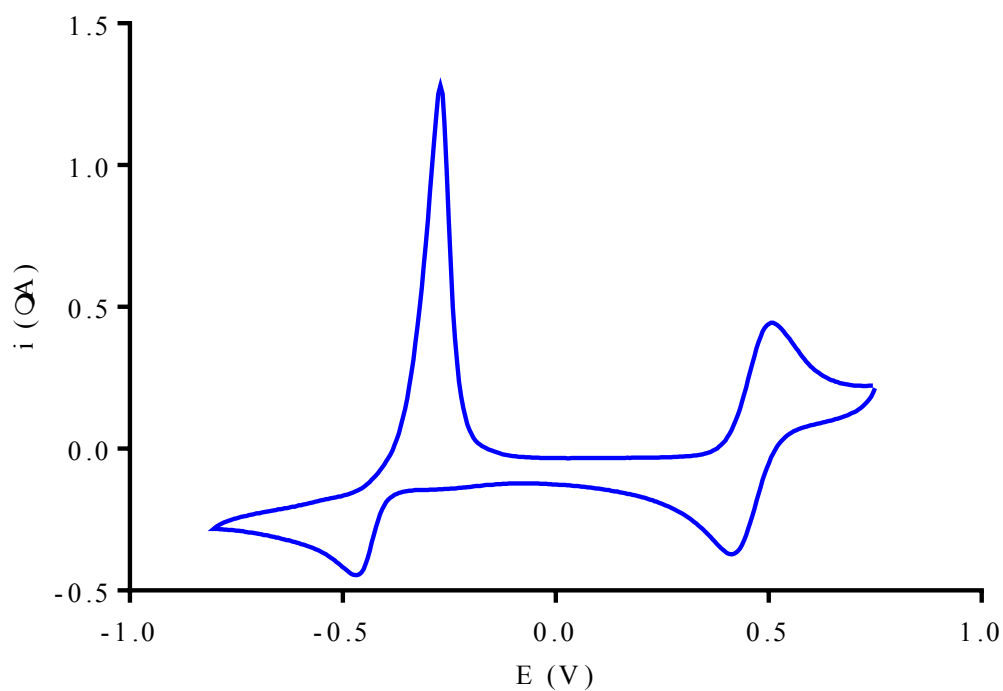


Figure 4.11 Cyclic voltammogram of 10 mM CuCl_2 dissolved in the Glyceline DES measured with: a Pt working electrode, Ag wire quasi-reference electrode, as scan rate of 10 mV s^{-1} at 293 K⁸³

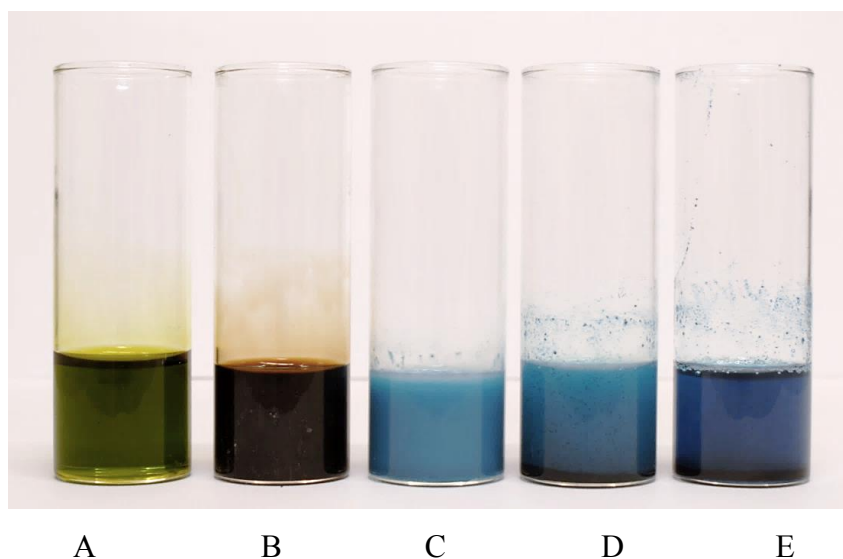


Figure 4.12 Photograph of 0.5 M solutions of CuCl_2 dissolved in different salt:glycerol systems: 2.17 M ChCl (A), 1.88 M NaBr (B), 2.02 M $\text{Na}_2\text{B}_4\text{O}_7 \cdot 10\text{H}_2\text{O}$ (C), 1.80 M NaOAc (D), 2.28 M $\text{NaOAc} \cdot 3\text{H}_2\text{O}$ (E)

The second process occurs at approximately -0.25 V, may be due to the Cu^1/Cu^0 redox process, suggesting the NaBr:glycerol mixture stabilises the Cu^1 species. From the cyclic voltammogram in Figure 4.13 double layer charging currents are evident, which has resulted in poor resolution of the redox process peaks due to the absolute currents of the redox processes being of a similar magnitude to the double layer charging currents. This occurrence is not surprising considering the NaBr:glycerol is more viscous, and less conductive than the Glyceline system.

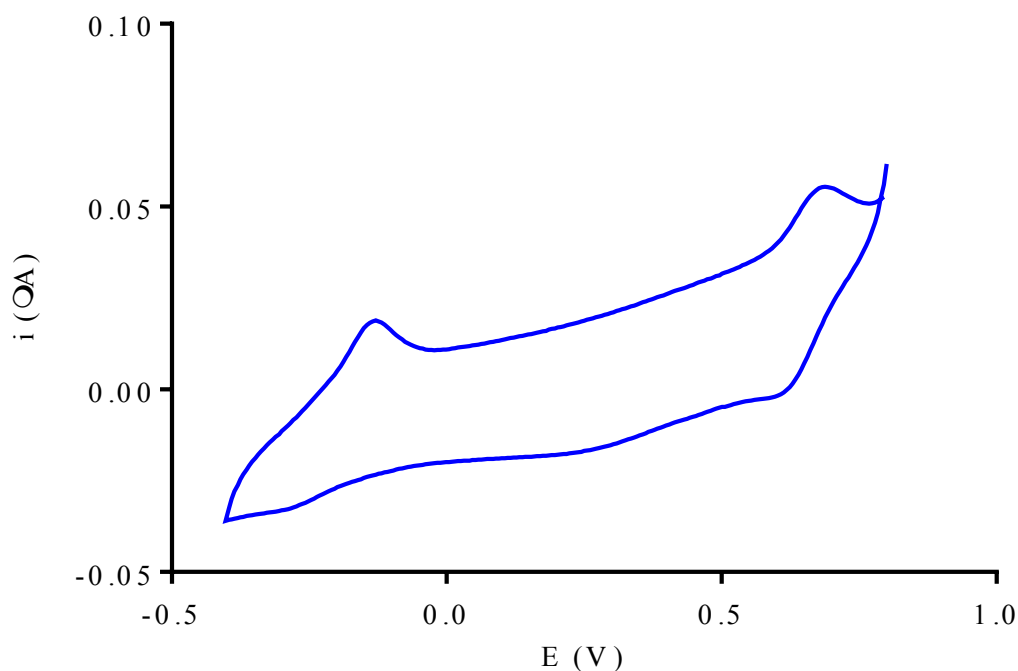


Figure 4.13 Cyclic voltammogram of 5 mM CuCl_2 dissolved in a 1.88 M NaBr:glycerol mixture measured with: a Pt working electrode, Ag wire quasi-reference electrode, as scan rate of 10 mV s^{-1} at 293 K

Figure 4.14 shows the cyclic voltammogram of 5 mM CuCl_2 in a 2.02 M $\text{Na}_2\text{B}_4\text{O}_7 \cdot 10\text{H}_2\text{O}$:glycerol mixture, which unlike the NaBr:glycerol and Glyceline systems, shows only a single redox process at approximately 0.1 V. Looking at figure 4.12 it is evident that the copper is not dissolved as a solution but rather it is colloidal and it is therefore not surprising that a classical diffusion limited response is not obtained.

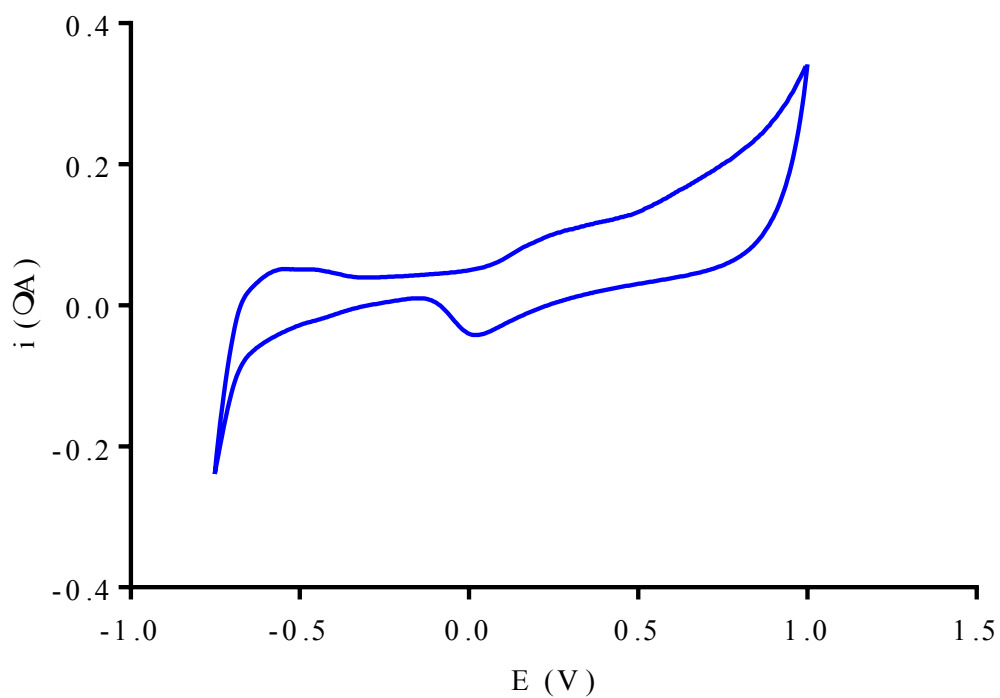


Figure 4.14 Cyclic voltammogram of 5 mM CuCl₂ dissolved in a 2.02 M Na₂B₄O₇·10H₂O:glycerol mixture on a Pt working electrode, at a scan rate of 10 mV s⁻¹ at 293 K

Figure 4.15 shows the cyclic voltammogram of 5 mM CuCl₂ dissolved in a 2.28 M NaOAc:glycerol mixture, which shows a single redox process occurring at 0.25 V. As observed with the Na₂B₄O₇·10H₂O:glycerol system, the copper complex is not fully soluble.

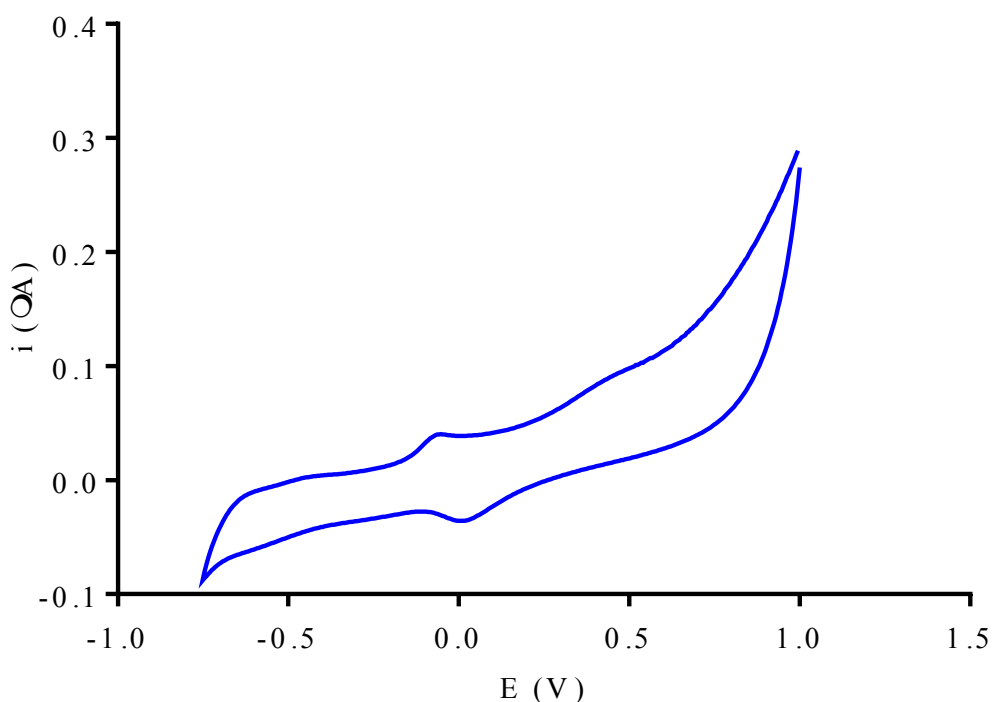


Figure 4.15 Cyclic voltammogram of 5 mM CuCl₂ dissolved in a 1.80 M NaOAc:glycerol mixture on a Pt working electrode, at a scan rate of 10 mV s⁻¹ at 293 K

The acetate anion is known to act as a monodentate, bidentate or a bridging ligand depending on the metal centre it is ligated to.⁸⁶ Considering acetate has a field ligand strength similar to that of chloride, a tetrahedral complex geometry would be energetically favourable, but due to the steric bulk of the acetate anion monodenticity is unlikely.⁸⁷ Acetate acting as a bidentate ligand with a tetrahedral geometry for the Cu^{II} core would give as speciation as outlined in Figure 4.16 A, which is a neutral species. Assuming the speciation outlined in Figure 4.16 A, poor solubility in the NaOAc:glycerol mixture would be likely, and a suspension of Cu^{II} species is expected to form, which can be observed in Figure 4.12 D. The NaOAc.3H₂O:glycerol mixture also forms a suspension with CuCl₂, as shown in Figure 4.12 E, but shows slightly better solubility as the presence of water may allow the acetate to act as a bridging ligand, as shown in Figure 4.16 B, which is observed in the hydrated Cu(OAc)₂ salt.⁸⁸

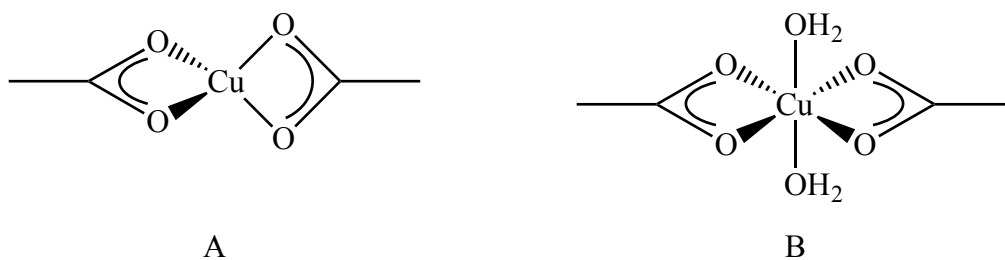


Figure 4.16 Proposed speciation of Cu^{II} in a: 1.80 M NaOAc:glycerol mixture (A) and 2.28 M NaOAc.3H₂O:glycerol mixture (B)

Abbott *et al.* recently found the anodic dissolution of copper into a ChCl: ethylene glycol DES mixture resulted in the formation of an insoluble CuCl layer that oxidised to CuCl₂.⁸⁹ If the anodic dissolution was carried out in non-quiet conditions the CuCl layer does not form suggesting the insoluble layer forms due to insufficient solubilising ligand at the electrode surface.⁸⁹ The insolubility of the Cu^{II} species found in the Na₂B₄O₇.10H₂O, and NaOAc:glycerol systems may be due to insufficient ligation occurring due to the steric bulk acetate and borate anions.

The sodium salt:glycerol systems investigated show different speciation for the Cu^{II} ions in solution, indicating the anion of the salt plays a dominating role in controlling ion speciation and solubility. The different speciation for Cu^{II} ions in sodium salt:glycerol mixtures have shown to have a noticeable effect on the electrochemical behaviour of copper. Research by Hartley *et al.* has shown that a range of copper (II) salts dissolved into 1-ethyl-3-methylimidazolium thiocyanate showed the $[\text{Cu}(\text{NCS})_2(\text{SCN})]^-$, suggesting the anion of the IL system plays the dominating role in controlling speciation, and therefore electrochemistry of ions in solution.⁹

To test if the poor solubility of metal salts in these liquids was a generic issue a variety of salts were added to the NaOAc:glycerol system, as shown in Figure 4.17. The equivalent masses required to produce 50mM solutions of FeCl₃.6H₂O, Zn(NO₃)₂.6H₂O, CrCl₃.6H₂O, AgCl, were prepared. All of these salts would be fully soluble in Ethaline or Glyceline but as can be seen in Figure 4.17 A-D respectively, all formed colloidal dispersions and precipitates suggesting limited solubility.

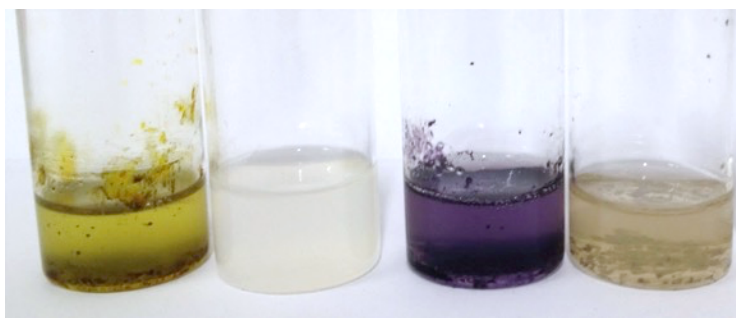


Figure 4.17 Photograph of 50mM solutions of different transition metal salts in a 1.80 M NaOAc:glycerol mixture: $\text{FeCl}_3 \cdot 6\text{H}_2\text{O}$ (A), $\text{Zn}(\text{NO}_3)_2 \cdot 6\text{H}_2\text{O}$ (B), $\text{CrCl}_3 \cdot 6\text{H}_2\text{O}$ (C), AgCl (D)

The purple colour exhibited by the $\text{CrCl}_3 \cdot 6\text{H}_2\text{O}$ solution in Figure 4.17 C suggests water is not part of the Cr^{III} species in solution. Abbott *et al.* found that DESs based on $\text{CrCl}_3 \cdot 6\text{H}_2\text{O}$ and urea changed from a dark green solution to a dark purple solution when heated up to $180\text{ }^\circ\text{C}$, which was attributed to removal of the waters of hydration from the Cr^{III} complex structure.⁷¹ Further work by Hartley *et al.* has shown that in a high oxygen donor environment the Cr^{III} species has the $[\text{CrCl}_2(\text{R})_4]^+$ speciation, where R is an oxygen donor such as water.⁹ A possible speciation for Cr^{III} in the NaOAc:glycerol system could be a $[\text{CrCl}_2(\text{OAc})_4]^{3-}$ if the acetate anion acts as a monodentate ligand, or $[\text{CrCl}_2(\text{OAc})_2]^+$ if the acetate anion acts as bidentate ligand.

Fe^{III} in an aqueous environment typically forms an $[\text{Fe}(\text{OH}_2)_6]^{2+}$, if this speciation were to be assumed for the NaOAc:glycerol system, the speciation of Fe^{III} could be $[\text{Fe}(\text{OAc})_6]^{3-}$ if monodentate behaviour is prevalent, or $[\text{Fe}(\text{OAc})_3]$ if bidentate behaviour is prevalent.⁸⁰ Considering the poor solubility of the Fe^{III} complex in the NaOAc:glycerol system, the neutral $[\text{Fe}(\text{OAc})_3]$ species would be more likely. The Zn^{II} also forms the hexaaqua complex in solution and may follow a similar speciation to Fe^{III} .⁸⁰

The NaOAc:glycerol system has been observed to change colour from a colourless solution to an orange solution, as shown in Figure 4.18 A, which is suggestive of the glycerol being oxidised.⁹⁰ The oxidation of the NaOAc:glycerol system suggests it can act as a mild reducing agent, which may be capable of reducing AgCl to silver nanoparticles, explaining the translucent solution seen in Figure 4.17 D. AgCl dissolved in the $\text{Na}_2\text{B}_4\text{O}_7 \cdot 10\text{H}_2\text{O}$:glycerol system forms a brown transparent solution, as shown in Figure 4.18 B A reduction of Ag^{I} does not occur, but solubility is still poor. AgCl in the NaBr:glycerol system shows a colourless transparent solution

with yellow solid suggests halide exchange is occurring to yield AgBr, which does not dissolve, as shown in Figure 4.18 C.⁹¹



A

B

C

Figure 4.18 Photographs of: 1.80 M NaOAc that has oxidised over a period of 3 years (A) a 0.5 M solution of AgCl in a 2.02 M Na₂B₄O₇·10H₂O:glycerol mixture (B) and a 0.5 M solution of AgCl in a NaBr:glycerol mixture (C)

The limited solubility of transition metals in the NaOAc:glycerol system may be related to insufficient ligation occurring due to the size of the acetate anion, which is similar to the observations made by the Abbott group when investigating the anodic dissolution of transition metals in DESs.⁸⁹ From Figure 4.12 and Figure 4.17, the speciation of transition metal salts in sodium salt:glycerol mixtures appears to be complex, and limits solubility of a range of transition metals, which limits their use as electrochemical probes to study diffusion in these systems. The proposals for ion speciation within sodium salt:glycerol mixtures need to be validated, which requires further research into structure determining methods.

4.3.5. Future Work

Complex metal speciation has restricted the application of electrochemical methods to probe the dynamics and diffusion behaviour of transition metals in sodium salt:glycerol mixtures. Copper, chromium, iron, zinc and silver all have spin active nuclei that could potentially be probed by PFG NMR, which could provide a non-electrochemical method of investigating ion dynamics and diffusion.

Ion speciation must be known to allow a deeper understanding of phenomena in physical properties, which can be investigated using EXAFS. To provide a preliminary insight into ion structure in solution, fast atom bombardment mass spectrometry (FAB-MS) can be used until synchrotron access can be granted. As well as providing detailed

speciation for novel systems, the knowledge gained can be used to predict the speciation of unknown systems.

Selection of the system components plays a critical role in determining physical properties, and alternatives are required. The Abbott group have successfully investigated the microscopic properties of transition metals in type III DESs, and found using low viscosity HBDs including ethylene and propylene glycols gave DESs that allowed quantitative analysis of transition metals in solution.^{82,83} Utilisation of glycols with sodium salts may provide more electrochemically useful systems, with properties that may allow better speciation of transition metal salts, and may consequently be more suitable for electrochemical applications.

4.3.6. Conclusions

Sodium salt:glycerol mixtures have been shown to have electrochemical windows similar to type 3 DESs where a polyol has been utilised as a HBD. The positive limit of electrochemical windows of the systems investigated was restricted by the oxidation of glycerol at approximately 1.2 V, which is likely to be oxidised to glyceraldehyde. The negative limit of the electrochemical window is due to the reduction of hydroxyl groups to give hydrogen gas, which occurred at -0.7 V. Significant oxidation of the NaBr:glycerol system was observed at 0.85 V, which is due to the oxidation of the bromide anion to elemental bromine.

The redox behaviour of copper has been investigated in sodium salt:glycerol systems and compared with a ChCl:glycerol DES. The NaBr:glycerol system was shown to stabilise the Cu^I species, which allowed the resolution of separate Cu^{II}/Cu^I and Cu^I/Cu⁰ redox couples. Stabilisation of the Cu^I species observed in chloride concentrated DESs and is a consequence of the [CuCl₄]²⁻ speciation, which suggests a [CuBr₄]²⁻ speciation for Cu^{II} in the NaBr:glycerol system. Both the Na₂B₄O₇·10H₂O and NaOAc:glycerol systems showed a single redox couple suggesting a Cu^{II}/Cu⁰ process, which implies the Cu^I species is not stabilised by these systems. The instability of the Cu^I species and lack of halide concentration suggests the [CuX₄]²⁻ speciation does not exist in these systems, and a more complex ion structure relating to the [Cu(OH₂)₆]²⁺ is expected.

Cu^{II} in a ChCl:glycerol DES shows a rapid, reversible electrochemical response and through application of the Randles-Sevcik relationship, the diffusion coefficient of the Cu^{II} species was deduced to be $1.55 \pm 0.07 \times 10^{-12} \text{ m}^2 \text{ s}^{-1}$. The Cu^{II} species in all of

the sodium salt:glycerol mixtures of interest showed slow, irreversible electrochemistry, and as a consequence the Randles-Sevcik relationship is not valid, therefore deduction the diffusion coefficient was not possible. A microelectrode was employed in an attempt to generate a steady-state electrochemical response as an alternative method of determining the Cu^{II} diffusion coefficient, but absolute currents were smaller than the resolution of the potentiostat used, and diffusion coefficients were not determinable.

The low absolute peak currents during electrochemical experiments were a consequence of poor solubility of the Cu^{II} probe in the sodium salt:glycerol systems of interest, which has been attributed to the complex speciation resulting from the presence of borate and acetate ligands. The speciation of Cu^{II} in the Na₂B₄O₇·10H₂O:glycerol system is unknown, but a complex structure involving Cu-O-B bonds is likely due to the Cu²⁺ being Lewis acidic. The acetate anion probably acts as a bidentate ligand for Cu^{II} in the NaOAc:glycerol system and give a [Cu(OAc)₂] speciation, which is neutral and therefore poorly soluble. Poor solubility was experienced with a range of transition metal salts, which was also attributed to complex ion speciation in the Na₂B₄O₇·10H₂O and NaOAc:glycerol systems.

Poor solubility of a range of electrochemical probes suggests the sodium salt:glycerol systems studied are not ideal for electrochemical investigation, and adjustment of the system components is needed to provide media that are suitable for electrochemical processes.

4.4. References

-
- ¹ E. L. Smith, A. P. Abbott and K. S. Ryder, *Chem. Rev.*, 2014, **114**, 11060
 - ² V. Losetty, B. K. Chennuri and R. L. Gardas *J. Chem. Thermodynamics*, 2015, **90**, 251
 - ³ S. Tang, G. A. Baker and H. Zhao, *Chem. Soc. Rev.*, 2012, **41**, 4030
 - ⁴ P. Wasserscheid and T. Welton, *Ionic Liquids in Synthesis*, Wiley-VCH, Germany, 2003, Ch. 3
 - ⁵ C. D'Agostino, L. F. Gladden, M. D. Mantle, A. P. Abbott, E. I. Ahmed, A. Y. M. Al-Murshedi and R. C. Harris, *Phys.Chem.Chem.Phys.* 2015, **17**, 15297
 - ⁶ A. P. Abbott, D. Boothby, G. Capper, D. L. Davies and R. K. Rasheed, *J. Am. Chem. Soc.*, 2004, **126**, 9142
 - ⁷ A. W. Taylor, P. Licence and A. P. Abbott, *Phys. Chem. Chem. Phys.*, 2011, **13**, 10147

-
- ⁸ D. Lloyd, T. Vainikka, L. Murtomaki, K. Kontturi and E. Ahlberg, *Electrochim. Acta*, 2011, **56**, 4942–4948
- ⁹ J. M. Hartley, I. Chung-Man, G. C. H. Forrest, K. Singh, S. J. Gurman, K. S. Ryder, A. P. Abbott and G. Frisch, *Inorg. Chem.*, 2014, **53**, 6280
- ¹⁰ M. Figueiredo, C. Gomes, R. Costa, A. Martins, C. M. Pereira and F. Silva, *Electrochimica Acta*, 2009, **54**, 2630
- ¹¹ A.-L. Rollet and C. Bessada, *Annual Reports on NMR Spectroscopy*, Elsevier, Cambridge, 2013, Ch. 4, 149
- ¹² P. J. Hore, *Nuclear Magnetic Resonance*, Oxford Science Publications, Oxford, 1995, Ch. 1
- ¹³ T. Cremer, C. Kolbeck, K. R. J. Lovelock, N. Paape, R. Wölfel and P. S. Schulz, *J. Eur. Chem*, 2010, **16**, 9018
- ¹⁴ M. Imanari, M. Nakakoshi, H. Seki and K. Nishikawa, *Chem Phys Lett* 2008, **459**, 89
- ¹⁵ M. Imanari, H. Tsuchiya, H. Seki, K. Nishikawa and M. Tashiro, *Magn Reson Chem*, 2009, **47**, 67
- ¹⁶ M. Imanari, K. Uchida, K. Miyano, H. Seki, K and Nishikawa, *Phys Chem Chem Phys* 2010, **12**, 2959
- ¹⁷ M. Imanari, K. Fujii, T. Endo, H. Seki, K. Tozaki and K. Nishikawa, *J Phys Chem B*, 2012, **116**, 3991
- ¹⁸ P. T. Callaghan, *Translational dynamics and magnetic resonance: principles of pulsed gradient spin echo NMR*. Oxford University Press, New York, 2011.
- ¹⁹ P. J. Hore, J. A. Jones and S. Whipperis, *NMR: The Toolkit*, Oxford Science Publications, Oxford, 2000, Ch. 6
- ²⁰ M. H. Levitt and R. Freeman, *Journal of Magnetic Resonance*, 1979, **2**, 473
- ²¹ H. Y. Carr, E. M. Purcell, *Physical Review*, 1954, **94**, 630
- ²² E. L. Hahn, *Physical Review*, 1950, **80**, 580
- ²³ J. E. Tanner, *J. Chem. Phys.*, 1970, **52**, 2523
- ²⁴ A. Jerschow and N. Müller, *J Magn Reson* 1997, **125**, 372
- ²⁵ H. Tokuda, K. Hayamizu, K. Ishii, A. B. H. Susan Md and M. Watanabe, *J Phys Chem B*, 2004, **108**, 16593
- ²⁶ H. Tokuda, S. Tsuzuki, A. B. H. Susan Md, K. Hayamizu and M. Watanabe, *J Phys Chem B*, 2006, **110**, 19593

-
- ²⁷ C. D'Agostino, R. C. Harris, A. P. Abbott, L. F. Gladden and M. D. Mantle, *Phys. Chem. Chem. Phys.*, 2011, **13**, 21383
- ²⁸ C. D'Agostino, L. F. Gladden, M. D. Mantle, A. P. Abbott, E. I. Ahmed, A. Y. M. Al-Murshedi and R. C. Harris, *Phys.Chem.Chem.Phys.*, 2015, **17**, 15297
- ²⁹ T. N. Mitchell and B. Costisella, *NMR - From Spectra to Structures: An Experimental Approach*, Springer, New York, 2007
- ³⁰ C. D'Agostino, Cambridge University, private communication.
- ³¹ R. A. Robinson and R. H. Stokes, *Electrolyte Solutions*, Dover, New York, 2nd Rev. Ed., 2002, Ch. 2, 45
- ³² A. D. McNaught and A. Wilkinson, *Compendium of Chemical Terminology*, Blackwell Science, New Jersey, 2nd Ed., 1997
- ³³ *Spartan Pro*, Wavefunction Inc., Irvine, CA, 2000.
- ³⁴ K. R. Harris, L. A. Woolf, M. Kanakubo and T. Rüther, *J Chem Eng Data*, 2011, **56**, 4672.
- ³⁵ K. R. Harris, M. Kanakubo, N. Tsuchihashi, K. Ibuki and M. Ueno, *J Phys Chem B*, 2008, **112**, 9830.
- ³⁶ A. Noda, K. Hayamizu, M. Watanabe, *J Phys Chem B*, 2001, **105**, 4603.
- ³⁷ H. Tokuda, K. Hayamizu, K. Ishii, A. B. H. Susan Md and M. Watanabe, *J Phys Chem B*, 2005, **109**, 6103.
- ³⁸ H. Tokuda, K. Ishii, A. B. H. Susan Md, S. Tsuzuki, K. Hayamizu and M. Watanabe, *J Phys Chem B*, 2006, **110**, 2833.
- ³⁹ K. R. Seddon, A. Stark and M. J. Torres, *Pure Appl Chem*, 2000, **72**, 2275
- ⁴⁰ A. -L. Rollet, P. Porion, M. Vaultier, I. Billard, M. Deschamps and C. Bessada, *J Phys Chem B*, 2007, **111**, 11888.
- ⁴¹ A. Stark, A. W. Zidell and M. M. Hoffmann, *J Mol Liq*, 2011, **160**, 166.
- ⁴² P. Stilbs, *Progress in NMR Spectroscopy*, 1987, **19**, 1
- ⁴³ H. Vogel, *Z. Phys*, 1921, **22**, 645.
- ⁴⁴ G. S. Fulcher, *J Am Ceram Soc*, 1923, **8**, 339.
- ⁴⁵ G. Tamman, W. Hesse, *Z Anorg Allg Chem*, 1926, **156**, 245.
- ⁴⁶ D. D. Stark, W. G. Bradley and W. G. Bradley, *Magnetic resonance imaging*, C.V. Mosby, Missouri, 3rd ed., 1999

-
- ⁴⁷ J. T. Bushberg, J. A. Seibert, E. M. Leidholdt Jr. and J. M. Boone, *The Essential Physics of Medical Imaging*, Lippincott Williams & Wilkins, Philadelphia, 2nd ed., 2002
- ⁴⁸ N. Bloembergen, E.M. Purcell, R.V. Pound, *Physical Review*, 1948, **73**, 679
- ⁴⁹ K. Hayamizu, S. Tsuzuki and S. Seki, *J. Phys. Chem. A*, 2008, **112**, 12027
- ⁵⁰ R. C. Remsing, G. Hernandez, R. P. Swatloski, W. W. Masefski, R. D. Rogers, and G. Moyna, *J. Phys. Chem. B*, 2008, **112**, 11071
- ⁵¹ R. C. Remsing, R. P. Swatloski, R. D. Rogers and G. Moyna, *Chem. Commun.* 2006, 1271
- ⁵² M.M. Hoffmann, E. D. Sylvester and J. W. Russo, *Journal of Molecular Liquids*, 2014, **199**, 175
- ⁵³ S. Murgia, M. Monduzzi F, Lopez and G. Palazzo, *J Solution Chem.*, 2013, **42**, 1111
- ⁵⁴ T. Umecky, T. Takamuku, T. Matsumoto, E. Kawai, M. Takagi and T. Funazukuri, *J. Phys. Chem. B*, 2013, **117**, 16219
- ⁵⁵ R. H. Stokes, *J. Am. Chem. Soc.*, 1950, **72**, 763
- ⁵⁶ J. S. Anderson and K. Saddington, *J. Chem. Soc.*, 1949, **S**, 381
- ⁵⁷ H. S. Hardened and R. L. Nuttall, *ibid*, 1947, **69**, 736
- ⁵⁸ L. J. Gosting, E. M. Hanson, G. Kegeles and M. S. Morris, *Rev. Sci. Instrum.*, 1949, **20**, 209
- ⁵⁹ A. J. Bard and L. R. Faulkner, *Electrochemical Methods: Fundamentals and Applications*, John Wiley & Sons, New York, 2nd ed., 2001, Ch. 6, 226
- ⁶⁰ D. Pletcher, R. Greef, R. Peat, L. M. Peter and J. Robinson, *Instrumental Methods in Electrochemistry*, Horwood Publishing Ltd, Chichester, 2001, Ch. 6, 186
- ⁶¹ A. J. Bard and L. R. Faulkner, *Electrochemical Methods: Fundamentals and Applications*, John Wiley & Sons, New York, 2nd ed., 2001, Ch. 13, 534
- ⁶² D. J. Shaw, *Introduction to Colloid and Surface Chemistry*, Elsevier Limited, Amsterdam, 4th ed., 1992
- ⁶³ H. Helmholtz, *Annalen der Physik und Chemie*, 1853, **165**, 211
- ⁶⁴ A. J. Bard and L. R. Faulkner, *Electrochemical Methods: Fundamentals and Applications*, John Wiley & Sons, New York, 2nd ed., 2001, Ch. 5, 156
- ⁶⁵ A. J. Bard and L. R. Faulkner, *Electrochemical Methods: Fundamentals and Applications*, John Wiley & Sons, New York, 2nd ed., 2001, Ch. 1, 1

-
- ⁶⁶ M. Hayyan, F. S. Mjalli, M. A. Hashim and I. M. AlNashef, *Journal of Industrial and Engineering Chemistry*, 2013, **19**, 106
- ⁶⁷ R. Costa, M. Figueiredo, C. Pereira and F. Silva, *Electrochim. Acta*, 2010, **55**, 8916
- ⁶⁸ D. Lloyd, T. Vainikka, L. Murtomaki, K. Kontturi and E. Ahlberg, *Electrochim. Acta*, 2011, **56**, 4942
- ⁶⁹ A. P. Abbott, K. El Ttaib, K. S. Ryder and E. L. Smith, *Trans. Inst. Met. Finish.* 2008, **86**, 234
- ⁷⁰ A. P. Abbott, J. C. Barron and K. S. Ryder, *Trans. Inst. Met. Finish.* 2009, **87**, 201
- ⁷¹ A. P. Abbott, A. A. Al-Barzinjy, P. D. Abbott, G. Frisch, R. C. Harris, J Hartley and K. S. Ryder, *Phys.Chem.Chem.Phys*, 2014, **16**, 9047
- ⁷² A. P. Abbott, J. C. Barron, K. S. Ryder and D. Wilson, *Chem. – Eur. J.*, 2007, **13**, 6495.
- ⁷³ R. S. Gonçalvesab, W. E. Triacaac and T. Rabockaia, *Analytical Letters*, 1985, **18**, 957
- ⁷⁴ L. Roquet, E. M. Belgsir, J.-M. Léger and C. Lamy, *Electrochimica Acta*, 1994, **39**, 2387
- ⁷⁵ D. R. Lide, *CRC Handbook of Chemistry and Physics*, CRC press, Florida, 89th Ed., 2008, Ch. 4
- ⁷⁶ A.-M. Popescu, V. Constantin, A. Florea and A. Baran, *Rev. Chim.* 2011, **62**, 531
- ⁷⁷ M Hayyan, F. S. Mjalli, M. A. Hashim, I. M. AlNashef and T. X. Mei, *Journal of Industrial and Engineering Chemistry*, 2013, **19**, 106
- ⁷⁸ D. F. Shriver, P. W. Atkins and C. H. Langford, *Inorganic chemistry*, Oxford University Press, Oxford, 2nd ed., 1996, Ch. 7, 199
- ⁷⁹ D. F. Shriver, P. W. Atkins and C. H. Langford, *Inorganic chemistry*, Oxford University Press, Oxford, 2nd ed., 1996, Ch. 8, 223
- ⁸⁰ D. F. Shriver, P. W. Atkins and C. H. Langford, *Inorganic chemistry*, Oxford University Press, Oxford, 2nd ed., 1996, Ch. 6, 179
- ⁸¹ A. P. Abbott, G. Frisch, S. J. Gurman, A. R. Hillman, J. Hartley, F. Holyoak, and K. S. Ryder, *Chem. Commun.*, 2011, **47**, 10031
- ⁸² J. Hartley, Ph.D. Thesis, University of Leicester, 2013
- ⁸³ G. C. H. Forrest, Ph.D. Thesis, University of Leicester, 2015
- ⁸⁴ A. P. Abbott, K. El Ttaib, G. Frisch, K. J. McKenzie and K. S. Ryder, *Phys. Chem. Chem. Phys.*, 2009, **11**, 4269

-
- ⁸⁵ A. Luque, J. Sertucha, O. Castillo and P. Román, *New J. Chem.*, 2001, **25**, 1208
- ⁸⁶ G. S. Groenewold, W. A. de Jong, J. Oomens and M. J. Van Stipdonk, *J Am Soc Mass Spectrom*, 2010, **21**, 719
- ⁸⁷ P. J. van der Put, *The Inorganic Chemistry Of Materials: How To Make Things Out Of Elements*, Springer, New York, 1998, Ch. 2, 54
- ⁸⁸ R.A. Mackay and W. Henderson, *Introduction to Modern Inorganic Chemistry*, NT Ltd, Cheltenham, 6th. Ed, 2002, Ch. 14, 346
- ⁸⁹ A. P. Abbott, G. Frisch, J. Hartley, W. O. Karim and K. S. Ryder, *publication submitted*
- ⁹⁰ American Cleaning Society,
http://www.aciscience.org/docs/chemical_properties_and_derivatives_of_glycerol.pdf, (accessed October 2015)
- ⁹¹ J. J. Zuckerman, *Inorganic Reactions and Methods Volume 3: The Formation of Bonds to Halogens (Part 1)*, Wiley-VCH, Weinheim, 1989, Ch. 5, 277

5. Application of Novel Ionic Solvents as Modifiers for Bio-composite Materials

5.1. Introduction	144
5.1.1. Engineered Wood	144
5.1.2. Synthetic Adhesives	146
5.1.3. Thermoplastic Starch Adhesives	153
5.1.4. Aims	157
5.2. Preparation of Plasticised Starches.....	158
5.2.1. Choice of Ionic Solvent.....	158
5.2.2. Thermal Properties of Plasticised Starch.....	160
5.2.3. Mechanical Properties of Plasticised Starch	161
5.3. Plasticised Starch as a Binder for Fibreboards.....	168
5.3.1. Effect of Ionic Solvent on Structure.....	169
5.3.2. Effect of Ionic Solvent on mechanical properties	171
5.3.3. Effect of Ionic solvent on Thermal properties.....	192
5.3.4. Pilot Scale production Medium Density Fibreboard.....	195
5.3.5. Future Developments	196
5.4. Conclusions	198
5.5. References	199

5.1. Introduction

5.1.1. Engineered Wood

Engineered wood is the collective term for any man-made wood product that is prepared by binding: particles, strands, fibres or veneers of natural wood with an adhesive.¹ Engineered woods are an inexpensive and practical alternative to solid wood, and have become a popular building material since the production of particleboard (PB) began after World War II.² The manufacture of PB was initially implemented as a cost effective alternative to solid wood in the furniture industry, but now has diversified into industrial products and the construction industry.³ Since 2000, production of medium density fibreboard (MDF) and PB grew significantly, as more solid wood and plywood products are replaced with cheaper engineered wood alternatives.² As of 2006, MDF production in Europe is 14.9 million m³ per year.⁴

Wood is mainly composed of cellulose, hemicellulose and lignin; each of these materials contributes differently towards wood's natural structure and dictates its physical properties.⁵ Cellulose contributes to 40-45 % of the total weight, and is a polysaccharide composed of linear chains of D-glucose monomer units, which are linked together by β -1,4 glycosidic linkages, as shown in Figure 5.1.⁵ The vast array of hydroxyl groups allow the ability to form a strong network of inter- and intra-molecular hydrogen bonds between polysaccharide chains, which provides stiffness, and results in the formation of fibres.⁶

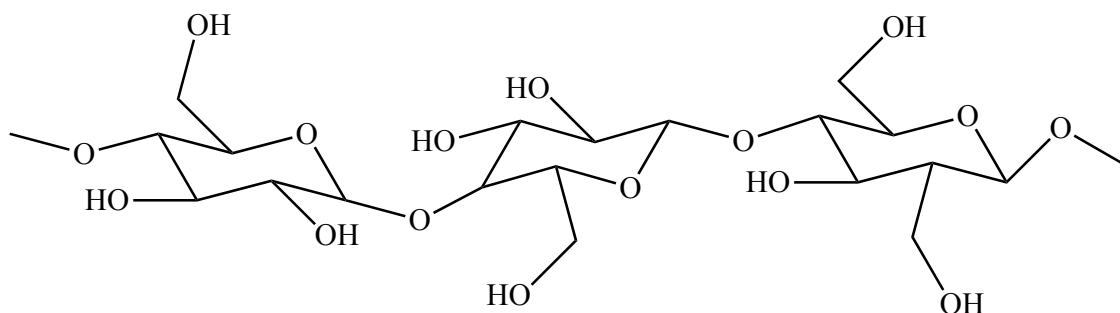


Figure 5.1 Structure of cellulose

Hemicellulose is also a polysaccharide, but hemicelluloses are mixed polymers of different sugar base units.⁷ Whilst cellulose is strong, crystalline and hydrolysis resistant, hemicellulose is amorphous, weak and is easily hydrolysed.⁷ Hemicellulose makes up 15-35 % of the total weight and typically has a degree of polymerisation (DP) of 150.⁷

Lignin is a naturally occurring aromatic polymer, which has a random polymeric structure consisting of a range of phenyl propane monomer units, as shown in Figure 5.2.⁸ Lignin normally makes up 15-25 % of the total weight, and binds cellulose and hemicellulose together and acts to reduce the ingress of water through cell walls.⁸

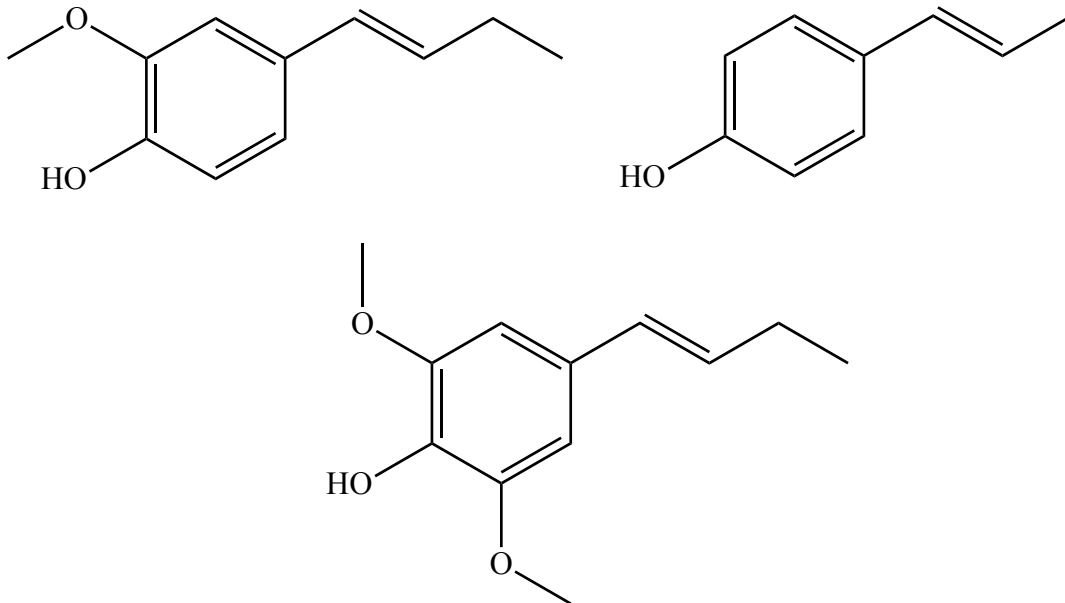


Figure 5.2 Phenolic monomer units of lignin

Engineered woods are manufactured from the same soft and hardwoods that are used to make lumber, the main subcategories of engineered wood are:

- Particleboard
- Fibreboard
- Oriented Strand board
- Plywood

Particleboard is manufactured from wood chips, sawdust and saw mill shavings, doped with a synthetic resin and heated under pressure into boards.² Particleboard is generally manufactured with finer wood particles or veneers at the surfaces, and the core comprising of a coarser grade of wood particle.⁹ Particleboard is cheaper and more uniform than solid woods, but is weaker and more susceptible to moisture than other forms of engineered wood.¹⁰ Due to the limitations of the material, it is mainly used in the indoor furniture and flooring industries.²

Fibreboard refers to a range of engineered woods that are manufactured by breaking down solid wood into wood fibres, which is then doped with a synthetic resin and pressed into sheets.⁴ There are three subcategories of fibreboard: low-density, medium-density and hardboard. Low-density fibreboard has a typical density range of

160-450 kg m⁻³, it is the weakest of the fibreboards, and is generally used for low quality indoor furniture.¹¹ MDF has a typical density range of 600-800 kg m⁻³, it is the most common form of fibreboard, and is mainly used by the indoor furniture and cabinet industries.¹² Hardboard has a typical density range of 800-900 kg m⁻³, it is the strongest of all the types of fibreboard, and is typically used for high quality furniture, and in the construction industry.¹²

Oriented strand board (OSB) is manufactured from cross-orientated layers of shredded wood strips, which are doped with a synthetic resin and pressed into boards.¹³ OSB possesses excellent mechanical properties along the strand axis, and makes OSB suitable for load-bearing applications including: roof, wall and floor sheathing in the construction industry.¹³ OSB is water-resistant, but requires additional coatings to make OSB impermeable.¹³

Plywood is manufactured from thin layers of wood veneer, where the veneer grains of adjacent layers are perpendicular, which are glued together.¹⁴ The changing direction of the grain is known as *cross-graining*, which minimises the chances of the wood splitting when being nailed, provides enhanced dimensional stability and gives isotropic mechanical properties.¹⁵ Plywood has a variety of uses in the construction industry including: floors, roofs, fencing and insulation.¹⁶

5.1.2. Synthetic Adhesives

An adhesive is a substance that when applied to bearing surfaces, it binds them together and resists separation.¹⁷ Adhesives are organised by method of adhesion and are then categorised as either reactive or mechanical adhesives: where reactive adhesives chemically react to harden. Mechanical adhesives rely on the penetration of adhesive material into crevasses and pores, whereas reactive adhesives involve intermolecular forces between surfaces to act as the binding mechanism.¹⁷ There are three main requirements for an adhesive to be effective:

1. Efficiently wet the substrates
2. It must harden
3. Effectively transmit load between the adhered substrates

Engineered woods require an adhesive in the presence of temperature and pressure to bind the individual woods particles.¹⁸ Synthetic thermosetting polymers are used in the manufacture of all varieties of engineered wood, the commonly used adhesives are:

- Urea formaldehyde (UF)
- Melamine formaldehyde (MF)
- Phenol formaldehyde (PF)

Thermosetting polymers are a class of polymer that irreversibly cure to form a resin that cannot be softened or melted on the application of heat, as the polymer chains are chemically linked via covalent bonds.¹⁹ As a consequence, thermoset resins are stronger, more resistant to creep, and better suited to high temperature environments than similar thermoplastics.¹⁹ In contrast, thermoplastic polymers can soften on application of heat, as the high molecular weight polymer chains interact through intermolecular forces, as opposed to interacting via covalent bonds.²⁰

Synthesis of UF involves two stages. The first step involves nucleophilic addition of urea to formaldehyde, as shown in Figure 5.3 to form oligomeric UF species.²¹ The UF network structure is formed in the second step by the condensation of oligomeric derivatives, as shown in Figure 5.4.²² UF resins are a popular binding agent in the engineered woods industry due to: lack of colour, hardness, non-flammability, resistance to abrasion and cost.²³ UF resins do have limited resistance to moisture and undergo hydrolytic degradation, consequently UF resins are used in materials for indoor applications.²⁴

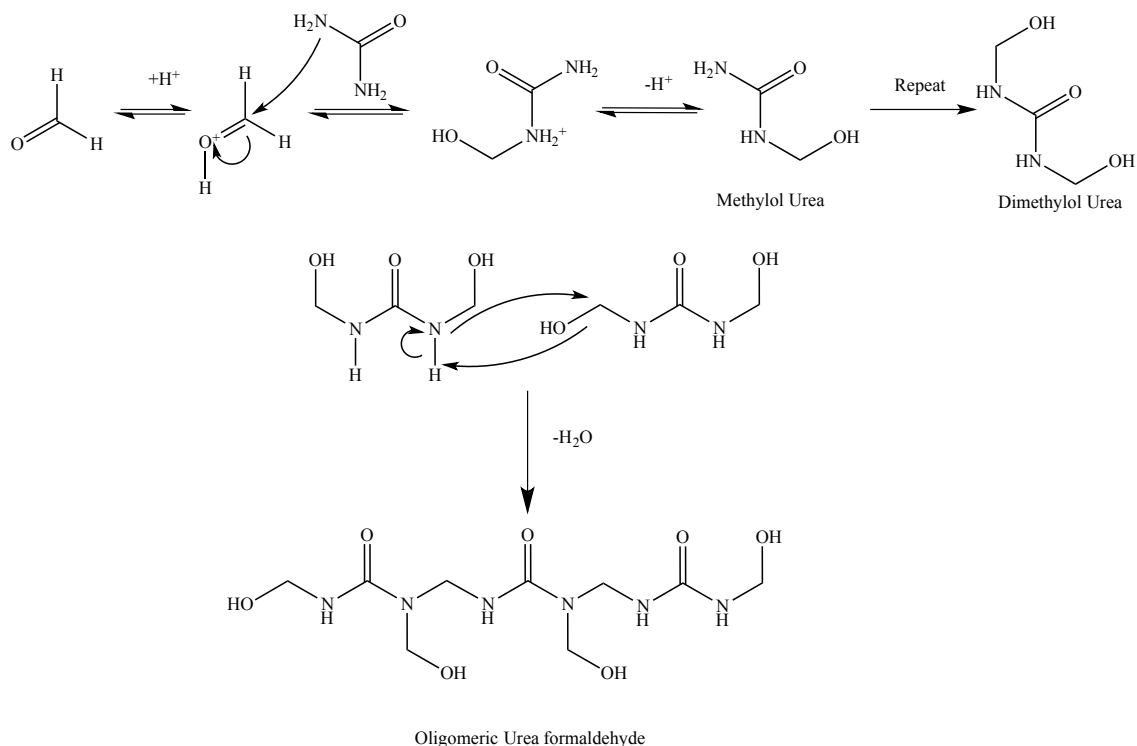


Figure 5.3 Synthesis of oligomeric urea-formaldehyde

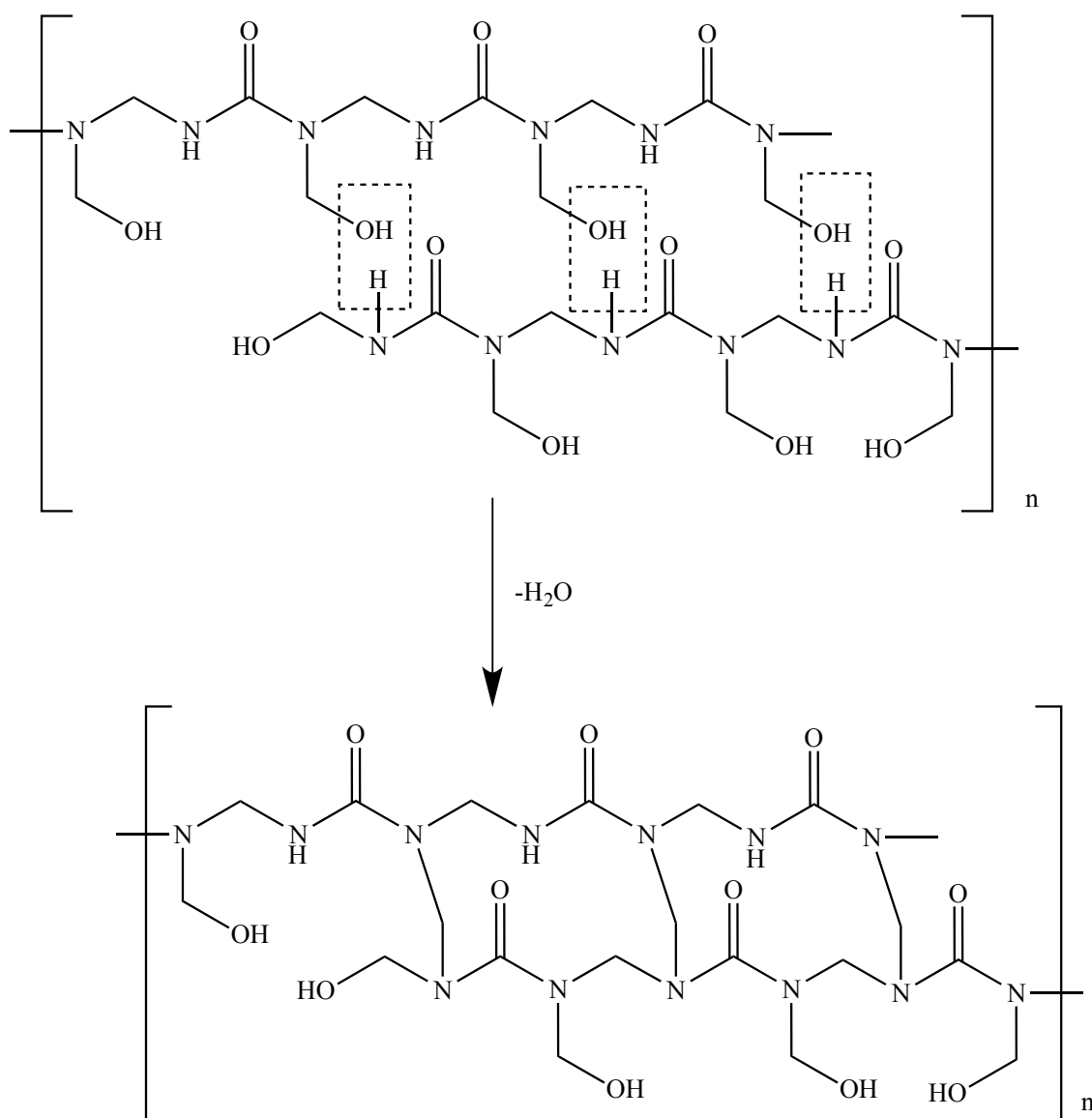


Figure 5.4 Condensation of oligomeric UF. Condensation mechanism is shown in Figure 5.3

The synthesis of MF involves a condensation reaction between melamine and formaldehyde that is similar to the reaction between urea and formaldehyde, but is more efficient and can occur over a wide range of pH.²¹ Firstly melamine is reacted with formaldehyde to form the methylol derivatives of melamine, as shown in Figure 5.5.¹⁹ MF is then formed by further reaction between methylol derivatives, melamine and formaldehyde, as shown in Figure 5.6.¹⁹

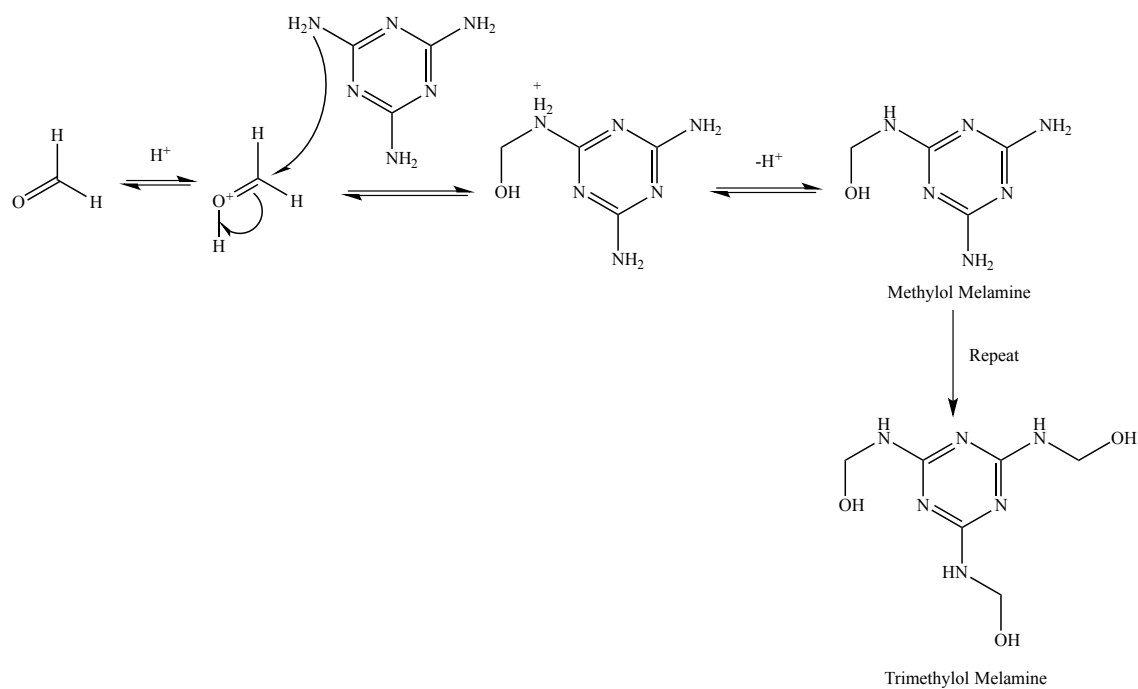


Figure 5.5 Synthesis of methylol melamine derivatives

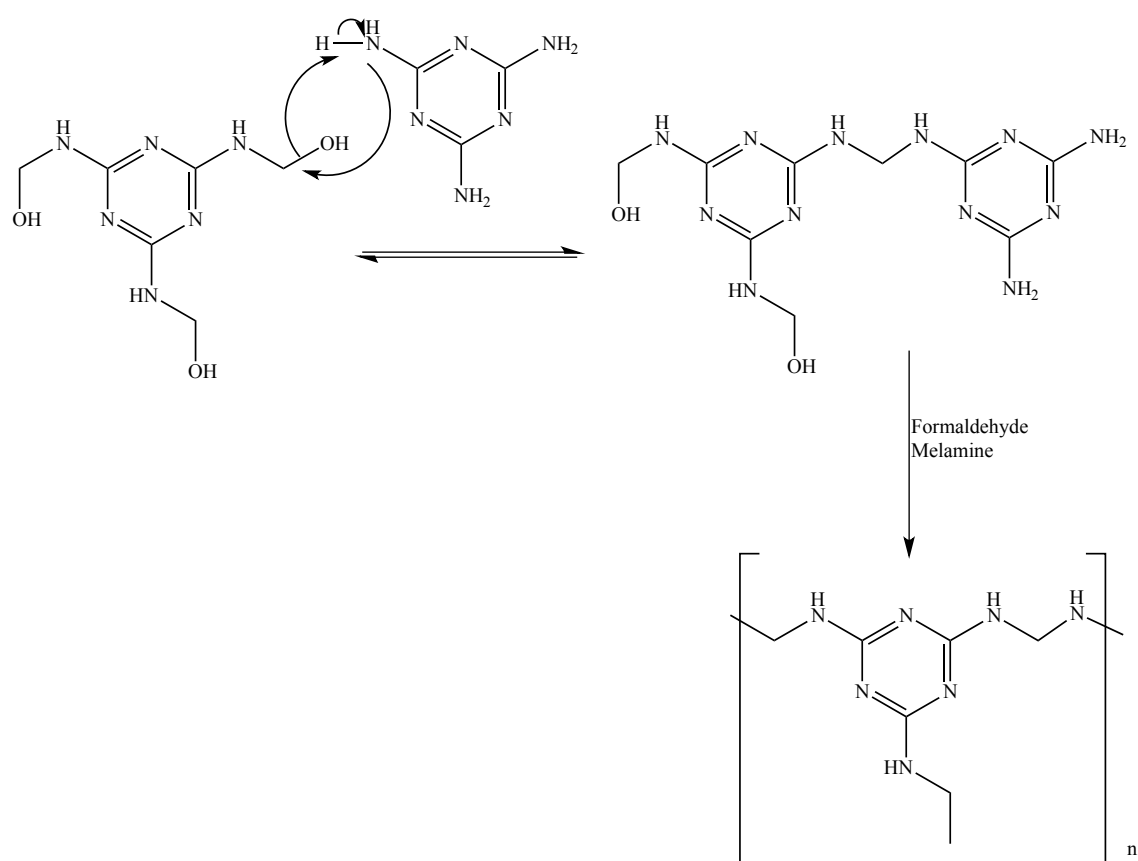


Figure 5.6 Methylol melamine condensation

MF resins are more durable, harder and show enhanced water and heat resistance making MF more suited to exterior applications, but MF resins are considerably more expensive than UF resins.²⁵ Formaldehyde emissions are known to decrease as the melamine content in MF increases, making MF an environmentally safer alternative to UF resins.²⁶

PF resins are formed by a two stage condensation reaction between phenol and formaldehyde in the presence of an acidic or basic catalyst, as shown in Figure 5.7.²¹ When prepared with a basic catalyst and an excess of formaldehyde, oligomeric PF is prepared in the first stage with a typical M_n of 500-1000. The PF network formed in the second step by the condensation of oligomeric derivatives at a higher temperature, typically 450 K.²¹ PF resins prepared in this way are referred to as *resole*, and predominantly consist of ether linkages between monomer units, as shown in Figure 5.8.²¹ When phenol and formaldehyde are co-polymerised under acidic conditions, a different type of PF resin known as *novolac* is made. Novolacs generally have a higher M_n , typically 1000-2000, compared to resoles, and require an excess of phenol.²¹ After the first stage of preparation, all of the functional groups in novolac have reacted, and further addition of formaldehyde is required for the novolac to fully cure at 450K.²¹ Novolacs predominately consist of methylene linkages between monomer units, as shown in Figure 5.9.

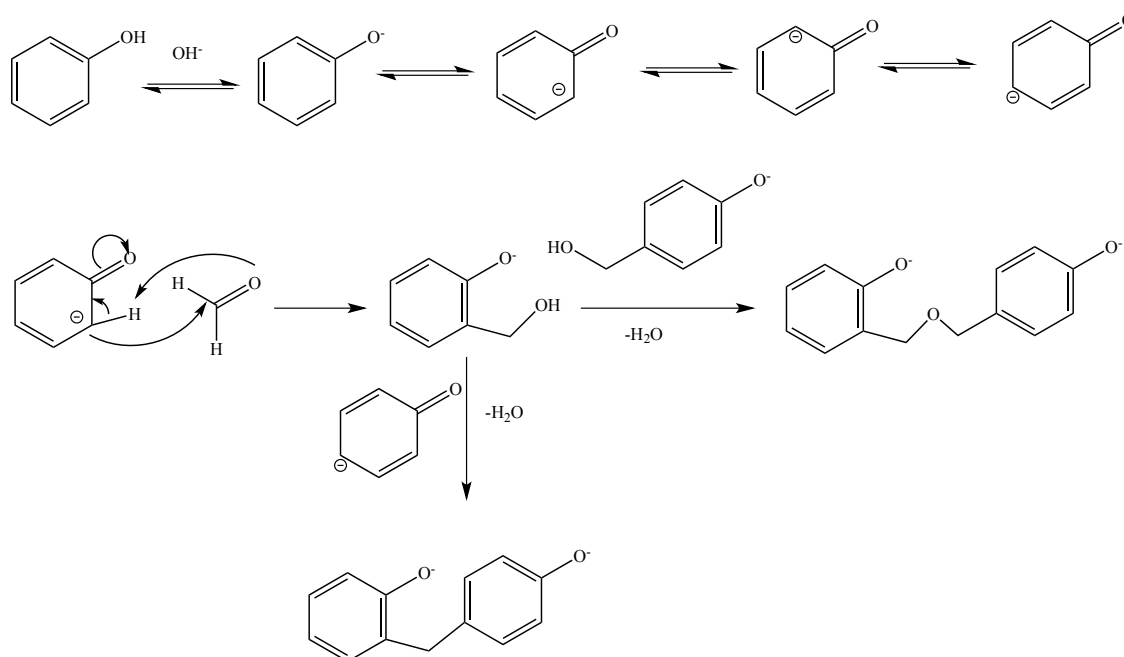


Figure 5.7 Synthesis of PF oligomers

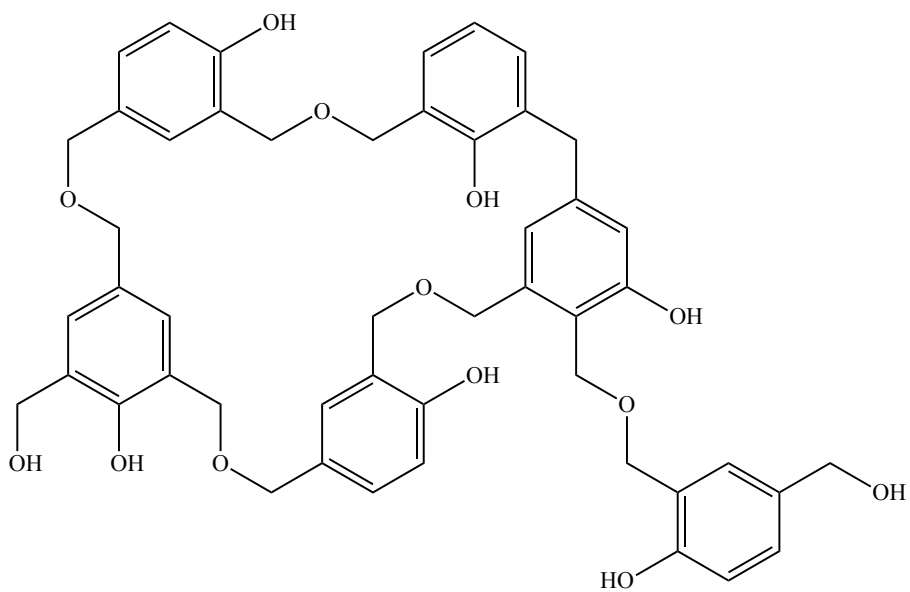


Figure 5.8 Structure of resole

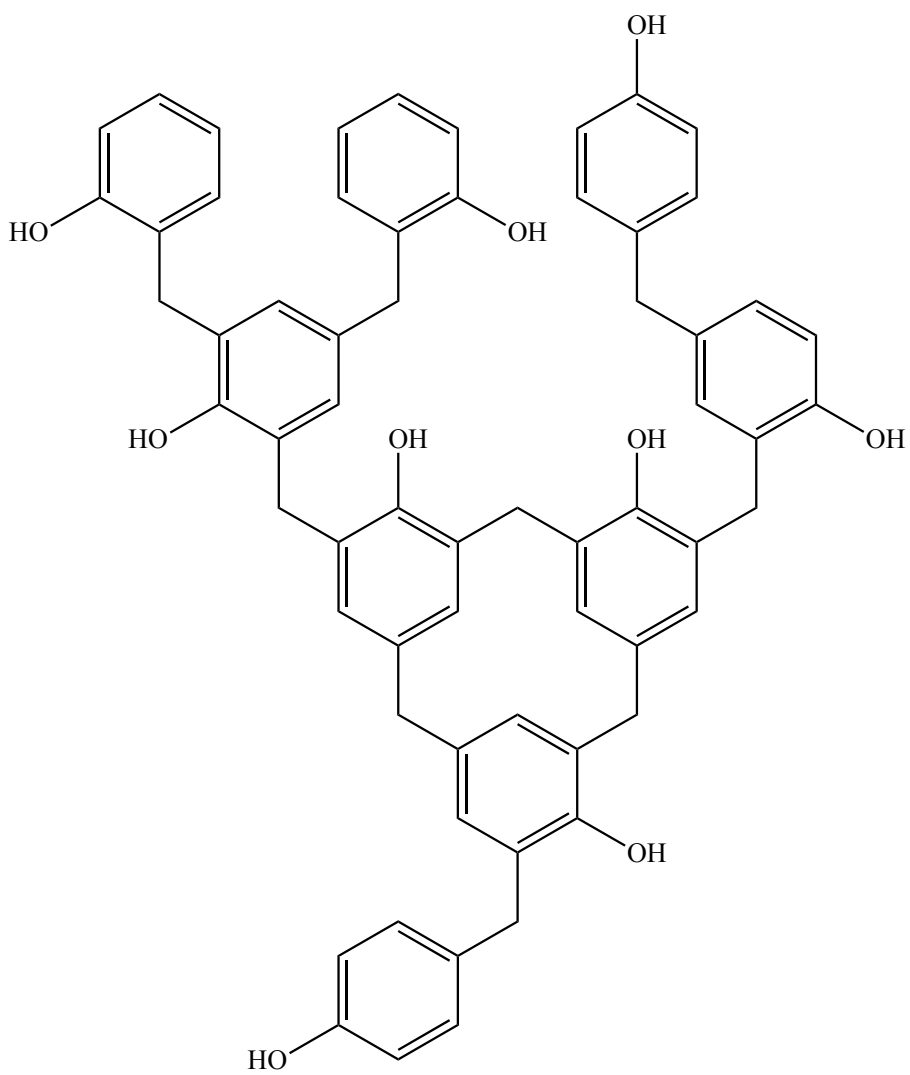


Figure 5.9 Structure of novolac

Engineered woods that have outdoor applications are normally manufactured with PF resins, as they have excellent weather, water and heat resistance.²² Unfortunately, PF resins are brittle, costly and have a naturally dark colour, which limits applications compared to UF based resins.²²

UF-bonded woods slowly emit formaldehyde, especially when temperature and relative humidity are high.²⁷ At manufacture, wood particles absorb and retain some hot formaldehyde during the hot pressing stage as *free* formaldehyde, and release it in low concentration environments.^{28,29} As well as vapour emission, further issues are caused by the dust made through machining engineered woods, which is linked to skin, eye and nose irritation.³⁰ Formaldehyde emissions are a health concern as formaldehyde is claimed to cause inflammation of mucous membranes.³¹ Formaldehyde is categorised as a group 1 human carcinogen, and its exposure is linked to nasopharyngeal cancer.³² These underlying health issues have led to restrictions on the amount of free formaldehyde present in engineered woods, with the World Health Organisation (WHO) stipulating less than 7.0 mg of formaldehyde per 100 g of wood product³³

Formaldehyde-based resins have many advantages as binders for engineered woods including: high bonding strength, high moisture resistance and low cost, but the environmental and health issues associated with formaldehyde emissions have forced the development of alternative binders.³⁴ The main categories of alternative are:

1. Reduction the formaldehyde-urea ratio
2. Addition of formaldehyde scavengers
3. Substitution for a formaldehyde free alternative

Reducing the formaldehyde- urea ratio within a UF resin is known to reduce the amount of free formaldehyde emitted from an engineered wood.³⁵ After a certain limit, the reactivity of the UF resin is compromised, which also compromises the internal bond strength, water absorption and thickness swelling.³⁵

A variety of amine compounds have been tested as “free” formaldehyde scavengers in UF bound MDF.³⁶ Amine compounds including: methylamine, ethylamine and cyclopentylamine were more effective as formaldehyde scavengers compared to further addition of urea, however significant increases in water absorption within the tested boards.³⁶ Tannins, naturally occurring phenolic polymers, can be used as environmentally sustainable formaldehyde scavengers however, tannins, like many other types of formaldehyde scavenger, compromise internal bond strength and increase water absorption rates.³⁷

Substituting formaldehyde-based resins for formaldehyde free alternatives has been focused on employing naturally occurring: polyphenolics such as tannins and lignins, starches, and proteins.^{38,39,40,41}

Soy protein has been investigated by several groups, and requires modification to overcome the inherent low bonding strength and poor water resistance.⁴¹ There have been many attempts at breaking down the internal bonds to promote protein unfolding, improve the adhesion potential of the protein complexes and give better interactions with cellulosic material.⁴²

Tannins are the naturally occurring polyphenolics found in many plant species, which regulate plant growth, and have been trialled with some industrial success.⁴³ However, tannins are known to be brittle, suffer from poor wood penetration, and poor wetting power.⁴⁴ Tannins shortcomings are attributed to two key problems, firstly, tannin molecules are relative large and exhibit poor rotation about the molecular backbone resulting in the characteristic brittleness.⁴⁴ Secondly, the reactivity of tannin molecules often results in premature curing, which causes incomplete crosslinking resulting loss of structural integrity.⁴⁴

Lignins are a class of naturally occurring polyphenolics, which are found in natural wood to bind together cellulose and hemicellulose fibres.⁸ Widsten *et al.* found that enzymatically activating the natural lignin within wood fibres could produce MDF with excellent board properties, and utilise the current industrial infrastructure.⁴⁵ In the same research, enzymatically activated technical lignins were also investigated as potential binders for MDF, but were found to be impractical and uneconomical due to the cost of technical lignins and the complexity of synthesis.⁴⁵

5.1.3. Thermoplastic Starch Adhesives

Starch is a complex mixture of polysaccharides composed of D-glucose units linked together by α -1,4 and α -1,6 glycoside linkages into two different forms; amylose the linear form, and amylopectin the highly branched form, as shown in Figure 5.10 A and B respectively.⁴⁶

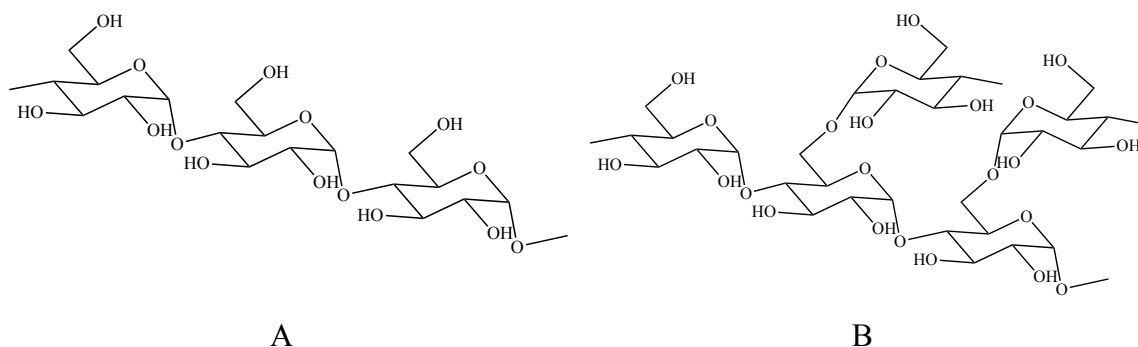


Figure 5.10 The structures of amylose (A) and amylopectin (B)

Amylopectin consists of α -1,4 bonded glucose sections linked by α -1,6 bonds at branching sites.⁴⁷ Approximately 4-6 % of bonds in typical amylopectin are of the α -1,6 type.⁴⁸ The branched chains of amylopectin behave like amylose, but amylopectin chains can be twisted to form a spiral.⁴⁹ Amylopectin is the dominant polysaccharide found in most sources of starch.⁵⁰

The DP of amylose depends on the source, but is typically 1500-6000.⁵⁰ From this variability and the M_w of glucose (180), the M_w for the amylose chains can vary between 240k-1000k, with an average of 500k. The M_w of amylopectin is 10000k-500000k, with a typical value of 250000k.⁵⁰

Starch granules contain both amorphous and crystalline regions, where the crystalline regions are formed from short amylopectin chains forming clusters.⁵⁰ Starch is classified as A, B or C type depending on the crystallographic structure, which depends on the starch source.⁵⁰ A-type starches exhibit an A-type polymorphic structure where orthogonal packing of double helices occurs.⁵¹ B-type starches show a B-type polymorphic structure with a more open hexagonal packing of double helices.⁵¹ C-type starch displays both polymorphic A and B patterns.⁵¹

Plasticised starch (PS) can be obtained when thermal and mechanical processing breaks down the semi-crystalline starch granules.⁵⁰ The melting temperature of starch is higher than its sublimation temperature, hence the necessity for a plasticiser to disrupt the crystalline structure of starch granules and form a continuous polymer phase, as shown in Figure 5.11.⁵²

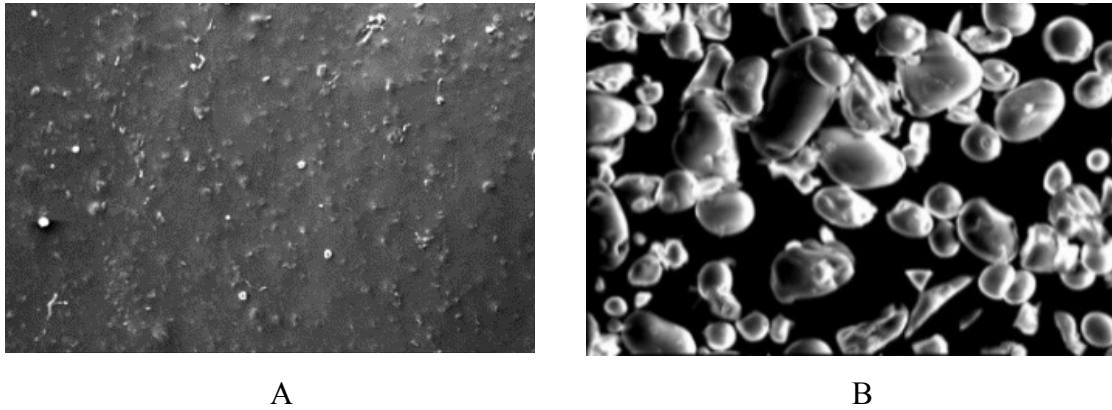


Figure 5.11 Scanning electron micrographs of plasticised starch (A) and native starch (B)⁵³

The simplest method of plasticising starch is by heating with water.⁵⁰ Heating to 57-72 °C, starch granules first swell, and then open up to give a viscous paste.⁵⁰ Addition of sodium hydroxide can lower the gelation temperature to room temperature.⁶⁷ Small additions of an aqueous mineral acid and heating the starch mixtures to approximately 50 °C followed by neutralisation, tends to lower the paste viscosity for a given starch content.⁶⁷ PS plasticised by water alone becomes brittle at room temperature so, in an effort to improve flexibility, other plasticisers including: glycerol, glucose and sorbitol have been used.⁵⁴ If inadequate thermal energy is provided, then the non-molten granules will still show characteristic polymorphic structures.⁵⁰ A lack of plasticiser can also result in incomplete elimination of the starch crystal structure.⁵⁵

The crystal structure of PS is based on single helices of amylose and manifests in three types; V_A (non-hydrated), V_H (hydrated) and E_H .⁵⁶ The E_H type is not stable and converts to V_H under the influence of moisture.⁵⁶ When starch has been plasticised by glycerol, the amylose and amylopectin can recrystallise into A and B type polymorphs, the rate depends upon the starch source and the moisture conditions.⁵⁷ The PS granulate surface structure depends heavily on the starch source.⁵⁰ PS formed from wheat or corn starch shows a porous structure with a uniform distribution of granulate masses.⁵⁰ The pores form due to granulate expansion under pressure and elevated temperatures, making a characteristic honeycomb structure.⁵⁸

Most plasticisers of starch including: water, urea, sorbitol, xylitol and glycerol have polar functional groups that are compatible with the functional groups within starch granules, which can breakdown the internal hydrogen bonding network of D-

glucose rings.^{59,60,61,62} For a plasticiser to be effective, it needs to be: polar, hydrophilic and able to penetrate starch granules, as well as a boiling point sufficiently high enough to minimise evaporation during processing.⁶³ Glycerol and water are the most common plasticisers, as penetration into the starch granule can be easily achieved, although molecules with the amide functionality have also been shown to be effective plasticisers.^{64, 65}

Degradation of the polysaccharides within plasticised starches occurs by enzymatic attack at the glycosidic linkages between the various sugar groups. This causes the starch chains to break into smaller oligosaccharides, disaccharides or monosaccharides, therefore plasticised starches can be described as fully compostable.⁵⁰

PS adhesives have been utilised since 1500 BC, and are still used in the packaging industry today.^{66,67} The adhesive properties of starch are attributed to its polymeric nature, and the vast collection of hydroxyl groups distributed along the polymeric structure resulting in an array of polar functional sites.⁶⁸ Starch adhesives tend to recrystallise upon drying, which results in a loss of adhesion.⁶⁸ Starch can be modified in a variety of ways to improve its adhesive properties including: heat treatment, acid and base treatments, functional group modification and enzyme treatment.⁶⁹

Due to natural abundance, low cost, biodegradability and good adhesion to cellulose, starch-based adhesives make attractive binding agents for the engineered wood industry.⁷⁰ Many research groups have investigated the use of plasticised starches as adhesives for engineered woods, but due to their inherent weakness and high moisture affinity, the majority of the research conducted focuses on plasticised starches with modified functional groups.^{71,72,73} Amini *et al.* found that corn starch modified with a 25 % glutardaldehyde (GA) solution could be used to prepare particleboards from rubber wood that conformed to Japanese industrial standards, however the addition of moisture repellents were still required to make the board suitable for external use.⁷¹ Baishya *et al.* studied the effect of GA, dimethyloldihydroxyethyleneurea (DMDHEU) and N-methylol acrylamide (NMA) to crosslink methylacrylate-grafted starch with wood flour.⁷³ Although starch-based wood composites could be achieved with this method, the synthesis of many of the cross linkers and co-polymers required significant amounts of formaldehyde and preparation limiting the industrial viability of the process.⁷³

Agnantopoulou *et al.* developed a low cost biodegradable composite material from wood flour mixed with a glycerol-plasticised starch.⁷⁴ Tondi *et al.* showed that a

carbohydrate-based adhesive prepared with sodium hydroxide as a catalyst, where the alkaline environment denatures the starch leading to an increase in penetration into the wood, can produce engineered woods.⁷⁵

Abbott *et al.* have successfully used a eutectic mixture of choline chloride (ChCl) and urea to plasticise corn starch, which showed superior mechanical properties compared to corn starch plasticised solely with urea.⁷⁶ Leroy *et al.* have shown that deep eutectic solvents (DESs) and ionic liquids (ILs) can plasticise starch more efficiently than glycerol.⁷⁷ Abbott *et al.* has since taken eutectic mixtures of choline chloride with a range of hydrogen bond donors to form plasticised starches, which could successfully take up to 45% w/w wood flour to form a thermoplastic composite material with mechanical properties comparable to MDF.⁷⁸

Due to the range of cheap and sustainable sources of starch and the lack of any petroleum-based materials, plasticised starch adhesives have the advantages of being economical, biodegradable and sustainable binding system that can rival formaldehyde-based resins in engineered wood manufacture.⁷⁸ Plasticised starches are thermoplastic implying they are recyclable, which is a significant advantage over the thermosetting resins currently used.⁷⁸

5.1.4. Aims

The main aim of this part of the project was to develop novel adhesives that are formaldehyde free and based on a novel plasticised starch. As a method of reducing free formaldehyde and other volatile organic compound (VOC) emissions, improving biodegradability and recyclability, and minimising the need for petroleum-derived chemicals, the developed adhesives were trialled as binders for MDF. The binders investigated were designed to be thermoplastic as opposed to thermosetting to provide mechanisms through which product degradation and material recycling could be achieved.

A range of inorganic salts were trialled with the intention of utilising more economically viable alternatives to the quaternary ammonium salts used in DESs that have previously been used as binders for MDF. The tensile strength and thermophysical properties of the plasticised starches were investigated and compared to a range of alternative binders.

The engineered woods prepared from the novel adhesives used industry grade wood fibre instead of the laboratory grade wood flour previously used. The tensile

strength and thermophysical properties of fibreboards were tested and compared to the current industrial standards. The final aim was to develop a suitable binder system that can be easily integrated into the current infrastructure, which was tested by running pilot scale trials of MDF production.

5.2. Preparation of Plasticised Starches

Native starch granules cannot completely melt simply by increasing temperature.⁷⁹ Due to an extensive network of inter- and intra-molecular hydrogen bonds, the melting temperature of starch is higher than its sublimation temperature, hence the necessity for a plasticiser to disrupt the crystalline structure of starch granules and form a continuous polymer phase.⁵² Native starch granules can be plasticised in the presence of water or other polar molecules such as alcohols and amides, which breakdown the native crystalline structure and lower the melting temperature.⁵⁰

Starches plasticised by glycerol have been used as binders for wood flour of varying particle sizes, however, particle sizes of less than 150 μm were required to achieve physical properties similar to that of a commercial product.⁷⁴ Many research groups have attempted to use glycerol-plasticised starch due to its natural abundance, biodegradability and economic viability, but have required the chemical modification of starch to avoid the disadvantages poor mechanical properties and fast water absorption rates.^{39, 73,80}

5.2.1. Choice of Ionic Solvent

Abbott *et al.* have taken eutectic mixtures of choline chloride with glycerol, ethylene glycol or urea to form plasticised starches, which could successfully take up to 45% w/w wood flour to form a thermoplastic composite material with mechanical properties comparable to MDF.⁷⁸ However, the use of choline chloride, and many other suitable quaternary ammonium salts, is limited to small scale processes due to the costs of being larger than that of the current industrial process. The cost of ChCl steadily increasing and is now typically 5-15 \$ kg^{-1} .⁸¹

NaCl would be ideal as alternative to choline chloride, as it is the cheapest and most naturally abundant salt. NaCl is also known to alter the glass transition temperature, gelation temperature and the gelatinisation enthalpy of plasticised starches at high concentrations.⁸² Unfortunately, solubility of NaCl within glycerol, and other

sugar alcohols, is limited, and NaCl does not form a eutectic mixture when combined with urea, as shown in section 3.2. NaBr has far better solubility in glycerol, but costs of \$ 2500 per ton would limit its use to smaller scales.⁸¹

NaOAc was trialled as a choline chloride substitute in previous work conducted by the Abbott group, and found the mechanical properties of fibreboards prepared were an order of magnitude lower compared to fibreboards prepared with glycerol plasticised starch (0.2MPa, 2.0 MPa respectively).⁸³

$\text{Na}_2\text{B}_4\text{O}_7 \cdot 10\text{H}_2\text{O}$, also known as sodium tetraborate or borax, Figure 5.12, is commonly used as an additive in plasticised starch adhesives used in paper and card manufacture.⁸⁴ Borax is known to act as a crosslinking agent, which forms covalent bonds between polymer chains, which improves material strength and rigidity, as opposed to a plasticiser, which forms temporary interactions between polymer chains.⁸⁵ Outside of the paper industry, little research has been conducted in utilising borax as an additive in plasticised starch for binding engineered woods. In the handful of documented cases, either the starch component of the binder or the cellulose in the wood component had been chemically modified before being cross-linked by borax.^{86,87,88}

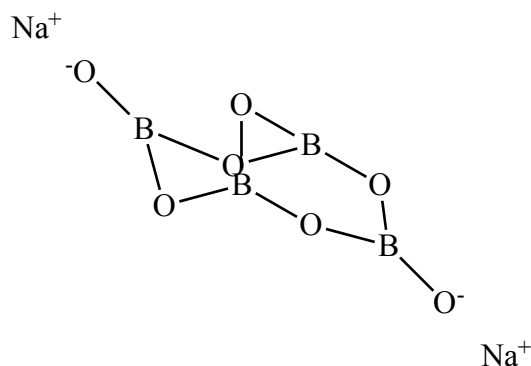


Figure 5.12 Structure of sodium tetraborate

Borax has the ability to cross-link polymer chains as it is an example of a multifunctional molecule that is capable of interacting with multiple polymer chains at once.⁸⁵ Being dicationic, it was thought that calcium and magnesium could have the same cross-linking abilities. CaCl_2 has been used in conjunction with sodium alginate as a crosslinking agent for gelatine oxidised-starch networks.⁸⁹ CaCl_2 has also been used as a plasticiser for starch/ polyvinyl alcohol (PVA) films, CaCl_2 was found to improve interactions between PVA and starch chains, and lower the glass transition temperature

of the composite materials.⁹⁰ CaCl₂ and MgCl₂ have yet to be utilised as potential cross-linking agents for binders in the engineered wood industry.

5.2.2. Thermal Properties of Plasticised Starch

The formation of plasticised starch is an irreversible, normally endothermic process that requires a plasticiser such that the process occurs at temperatures below the decomposition temperature of the starch polysaccharides.⁹¹ The hydrogen-bonding networks of the starch polysaccharides are disrupted by introduction of the plasticiser in the presence of heat, and a new network of inter- and intra-molecular hydrogen bonds is formed.⁹²

The gelation onset temperature of starch in the presence of a range of salt: plasticiser mixtures were measured by differential scanning calorimetry (DSC), as shown in Table 5.1

Table 5.1 Gelation onset temperatures, measured by DSC, of corn starch mixed with salt: plasticiser in the proportions 18% corn starch and 82% salt mixture.

Salt	Plasticiser	Concentration (mol dm ⁻³)	Gelation onset temperature (°C)
-	Ethylene Glycol	-	124.7
Choline Chloride	Ethylene Glycol	2.15	123.9
-	Glycerol	-	99.9
Choline Chloride	Glycerol	2.17	122.5
NaOAc	Glycerol	1.80	114.3
NaOAc.3H ₂ O	Glycerol	2.28	103.9
NaBr	Glycerol	1.88	116.5
Na ₂ B ₄ O ₇ .10H ₂ O	Glycerol	2.02	114.5
CaCl ₂ .2H ₂ O	Glycerol	2.52	147.4
MgCl ₂ .6H ₂ O	Glycerol	2.27	140.3
NaCl	Glycerol	1.30	96.6
MUF			107.1

The gelation onset temperatures for all of the systems investigated were within the range of 95-150 °C, with the CaCl₂.2H₂O:glycerol mixture and NaCl:glycerol mixture showing onset temperatures of 147.4 °C and 96.6 °C respectively. In all cases, except NaCl, the addition of salt to glycerol resulted in a noticeable increase in the gelation temperature of corn starch. Even though in most cases the salt concentration within the salt: plasticiser mixture was approximately 2 M, the change in gelation temperature varied significantly, suggesting both the cation and anion are interacting with the polysaccharide hydrogen bond network. Ahmed *et al.* found that a variety of Na, K, Mg and Cl salts increased the gelation temperature of sago starch at lower concentrations, and after reaching a maximum, typically at 2 M, the gelation temperature decreased with increasing salt concentration.⁹³ The complex effect salts appear to have on the gelation of properties of starch was attributed to two factors: firstly, the effect of the salt on the polymer-plasticiser interactions, where anions were observed to have a greater influence, and secondly, the interaction of cations with polysaccharide hydroxyl groups to hinder polymer chain aggregation.⁹³

In most instances, the gelation temperature of the salt: plasticiser mixtures were higher than the curing onset temperature MUF resins used in the engineered wood industry. Also, the curing of MUF is an exothermic process, whereas the gelation of starch is generally endothermic process with a typical gelation enthalpy of 15 J g⁻¹.^{21, 93} This may be an issue when considering an industrial scale, as extra heat energy will be required to maintain the starch gelling process. Glycerol and the NaCl:glycerol mixture showed gelation temperatures more than 10 °C lower than the curing temperature of MUF, although the gelation processes are still endothermic, having a lower onset temperature is favourable for industry as a measure of reducing processing costs.

Although the gelation temperature of salt: plasticiser mixtures were generally higher compared to the curing onset temperature MUF, starches plasticised with salt:glycerol mixtures were deemed suitable to test further as binders for MDF.

5.2.3. Mechanical Properties of Plasticised Starch

The extent to which a structure deforms is dependent on the imposed stress, and at relatively low loads, stress and strain are proportional through the relationship expressed in equation 5.1.⁹⁴ The relationship between stress (σ) and strain (ϵ) is referred to as Hooke's law and the proportionality constant (E) is the modulus of elasticity, also known as, the *Young's modulus*.⁹⁴

$$\sigma = E\epsilon$$

5.1

Deformation where the stress and strain are proportional is known as elastic deformation. Plots of stress versus strain result in a straight line, where the slope is equal to the modulus of elasticity, as shown in Figure 5.13.⁹⁴ The modulus of elasticity can be regarded as a material's resistance to elastic deformation, or as a material stiffness. Elastic deformation is not permanent: when the applied load has been released, the specimen will return to its original dimensions. Some polymers show a non-linear relationship between stress and strain hence, to be able to determine the modulus of elasticity, a tangential or a chordal modulus is normally used.⁹⁴ Young's modulus is also referred to as the modulus of elasticity (MOE), and is the most commonly quoted tensile measurement in scientific literature.

Deformation where the stress and strain are not proportional is known as plastic deformation, and occurs at a strain point beyond the proportionality limit of the material, where Hooke's law is no longer valid.⁹⁴ The proportionality limit is known as the yield point, and is generally regarded as the point at which departure from linearity occurs.⁹⁴ After deviation from linearity, the stress required to force further plastic deformation increases to a maximum, and then decreases until sample failure, as shown in Figure 5.13.⁹⁴ The ultimate tensile strength (UTS) of a specimen is defined as the maximum stress that can be sustained whilst under tension, which implies that failure will result if the stress is maintained.⁹⁴

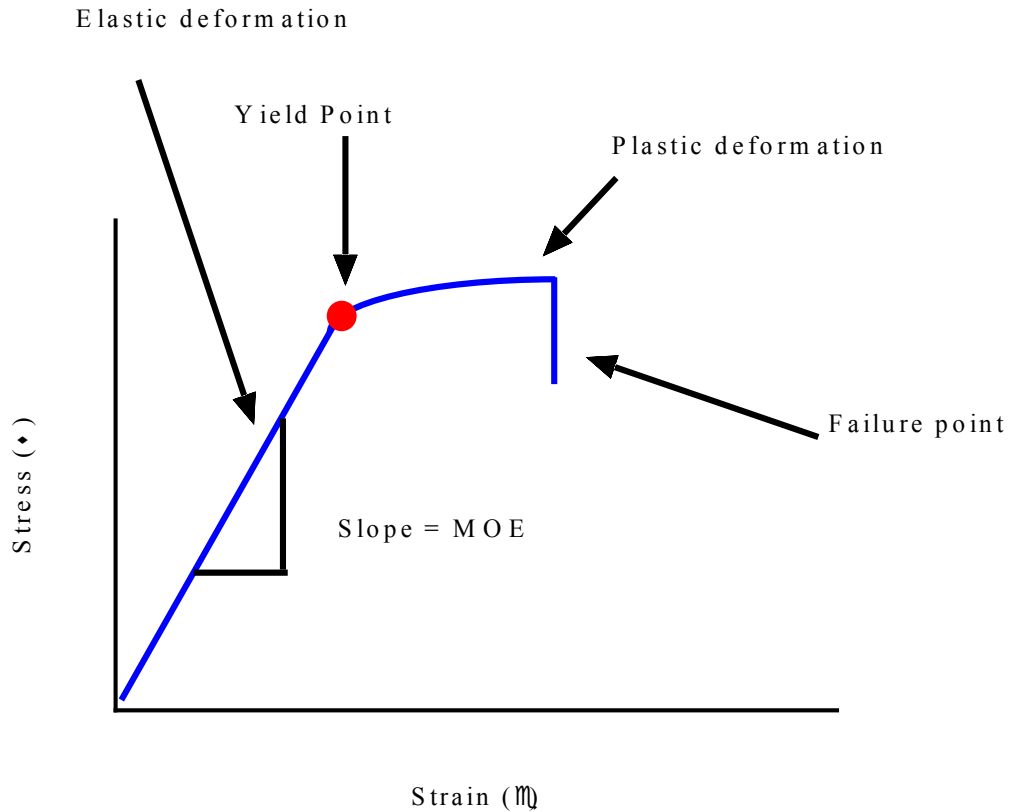


Figure 5.13 A typical tensile stress strain plot

Ductility is a measure of the amount of deformation that occurred at material failure, and can be expressed as either *percent elongation* (ϵ) or *percent reduction in area* (RA).⁹⁴ Mathematical representations of ϵ and RA are shown in equations 5.2 and 5.3 respectively, where l_0 and l_f are the initial and failed length respectively, and A_0 and A_f are the initial and failed specimen areas respectively. A material that experiences very little deformation at failure is considered to be a *brittle* material, whereas a material that experiences a large amount of deformation at failure is considered to be a *ductile* material.⁹⁴

$$\epsilon (\%) = \left(\frac{l_f - l_0}{l_0} \right) \times 100 \quad 5.2$$

$$RA (\%) = \left(\frac{A_0 - A_f}{A_0} \right) \times 100 \quad 5.3$$

Polymers typically show three different types of mechanical behaviour, as shown in Figure 5.14.⁹⁵ Profile A depicts the characteristic behaviour of a brittle polymer, where failure occurs during elastic deformation. Profile B shows the characteristic

behaviour of a polymer that performs like many metallic materials, where the early stages of deformation are elastic, and deformation at higher stresses is plastic. Profile C is representative of a material that is rubber-like, and can achieve large non-permanent strains at low stresses, polymers with this type of stress-strain profile are known as *elastomers*.⁹⁵

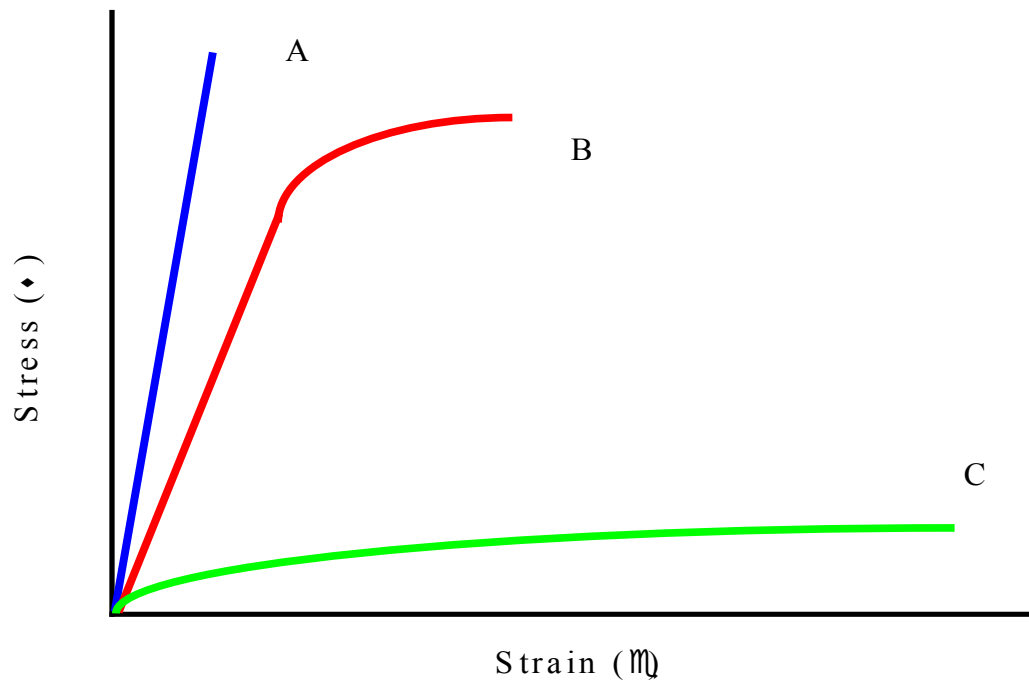


Figure 5.14 Typical stress-strain responses of polymeric materials: Brittle polymer response (A), metal-like response (B) and elastomer response (C)

Previous research by the Abbott *et al.*, utilising a choline chloride:glycerol mixture, prepared plasticised corn starch with the optimum ratio of starch to salt:glycerol mixture of 3:1 respectively.⁷⁶ The same ratio was initially used, but the salt:glycerol mixtures used were found to not fully plasticise starch, as shown in Figure 5.15.



Figure 5.15 Incomplete plasticisation of starch

Ahmad *et al.* found the addition of inorganic group I and group II generally reduced the gelation rate constant of sago starch.⁹³ Considering it may be possible the salt content is hindering the gelation process, it was decided to lower the corn starch content to 60 % w/w and maintain 10 minute process time. Lowering the corn starch content to 60% w/w resulted in materials that were fully plasticised and completely homogeneous, as shown in Figure 5.16.



Figure 5.16 Complete plasticisation of starch

The UTS, ϵ and E of a selection of plasticised corn starch based materials, where salt:glycerol mixtures were used as plasticisers, were measured using a tensiometer, the results of which are shown in Figure 5.17.

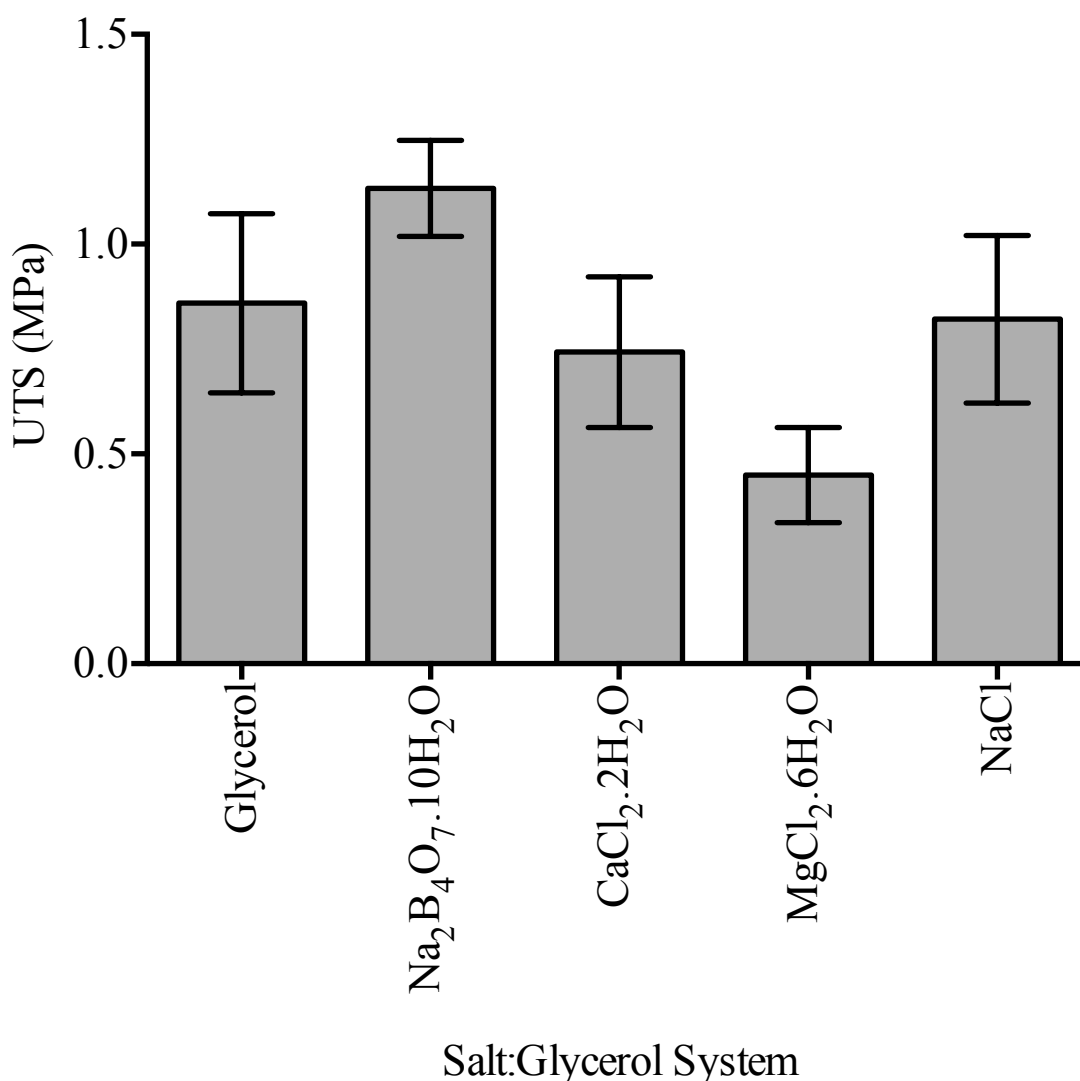


Figure 5.17 UTS values of corn starch plasticised with different salt:glycerol mixtures

Corn starch plasticised by glycerol mixed with borax showed the highest UTS of 1.13 ± 0.11 MPa, although the borax system was expected to have a larger UTS compared to glycerol, which gave a UTS of 0.86 ± 0.21 MPa. Borax is known to be an effective cross-linking agent, and may be possible that the waters of hydration associated with borax are further plasticising the starch in addition to the plasticiser effect of glycerol and the cross-linking effect of the borax.^{84,96} Further plasticisation can result in separation of polymer chains that can lead to compromised mechanical properties.⁹⁷ CaCl₂·2H₂O, MgCl₂·6H₂O appeared to decrease the UTS of starch plasticised with glycerol, and indicated UTS values of 0.74 ± 0.18 and 0.45 ± 0.11 MPa respectively. CaCl₂·2H₂O and MgCl₂·6H₂O have been used as additives within the paper industry to reduce starch gel viscosity, which reduces structural integrity.⁶⁷ Ahmad *et al.* found a 1 - 2 M NaCl solution had very little effect on the gel strength of

plasticised sago starch, suggesting why NaCl had little effect on the UTS of the plasticised corn starch.⁹³

Previous work by Abbott *et al.* found corn starch plasticised by a range of choline chloride: hydrogen bond donor (HBD) mixtures had UTS values of the 1.0 – 2.5 MPa.⁵³ When propylene glycol was utilised as the HBD, a UTS of 2.40 ± 0.13 MPa was achieved, whilst a UTS of 1.17 ± 0.07 MPa was achieved with ethylene glycol as a HBD.⁵³ The plasticised starches shown here and by Abbott *et al.* are relatively weak, and may be limited by the mechanism through which the components were combined. Extrusion is a technique that is commonly used to homogenise polymer mixtures, and Abbott *et al.* found choline chloride:glycerol mixtures that was extruded at temperatures greater than 120 °C had UTS values greater than 12 MPa, whereas the non-extruded equivalent had an UTS of about 4.62 ± 0.31 MPa.⁹⁸ The shear forces experienced during extrusion process were found to further breakdown the native starch structure and promote additional mixing and penetration of the plasticiser, which greatly improved structural integrity.⁵³ Considering the extrusion process significantly improves the mechanical properties of a plasticised starch, it would seem suitable to extrude starches plasticised with salt:glycerol mixtures to improve the material UTS. However, the extrusion process facilitates the starch gelation process, which forms a starch product that cannot be aspirated. The current industrial process utilises a blowline to aspirate pre-cured adhesive onto a high-pressure flow of steam saturated wood fibres, hence a pre-gelled starch cannot be used in conjunction with current industrial process.⁹⁹

The borax system also showed the highest ϵ at 234 ± 36 %, shown in Figure 5.18, which is surprising considering the borax system also showed the highest UTS value, and expected an ϵ of less than 50 %. Glycerol and the NaCl system displayed poor UTS values in conjunction low ϵ values of 55.0 ± 2.81 and 68.9 ± 12.9 % respectively suggesting weak polymer- polymer interactions. The $\text{CaCl}_2 \cdot 2\text{H}_2\text{O}$ systems produced a material with properties of an elastomer with an ϵ of 232 ± 35.0 %.

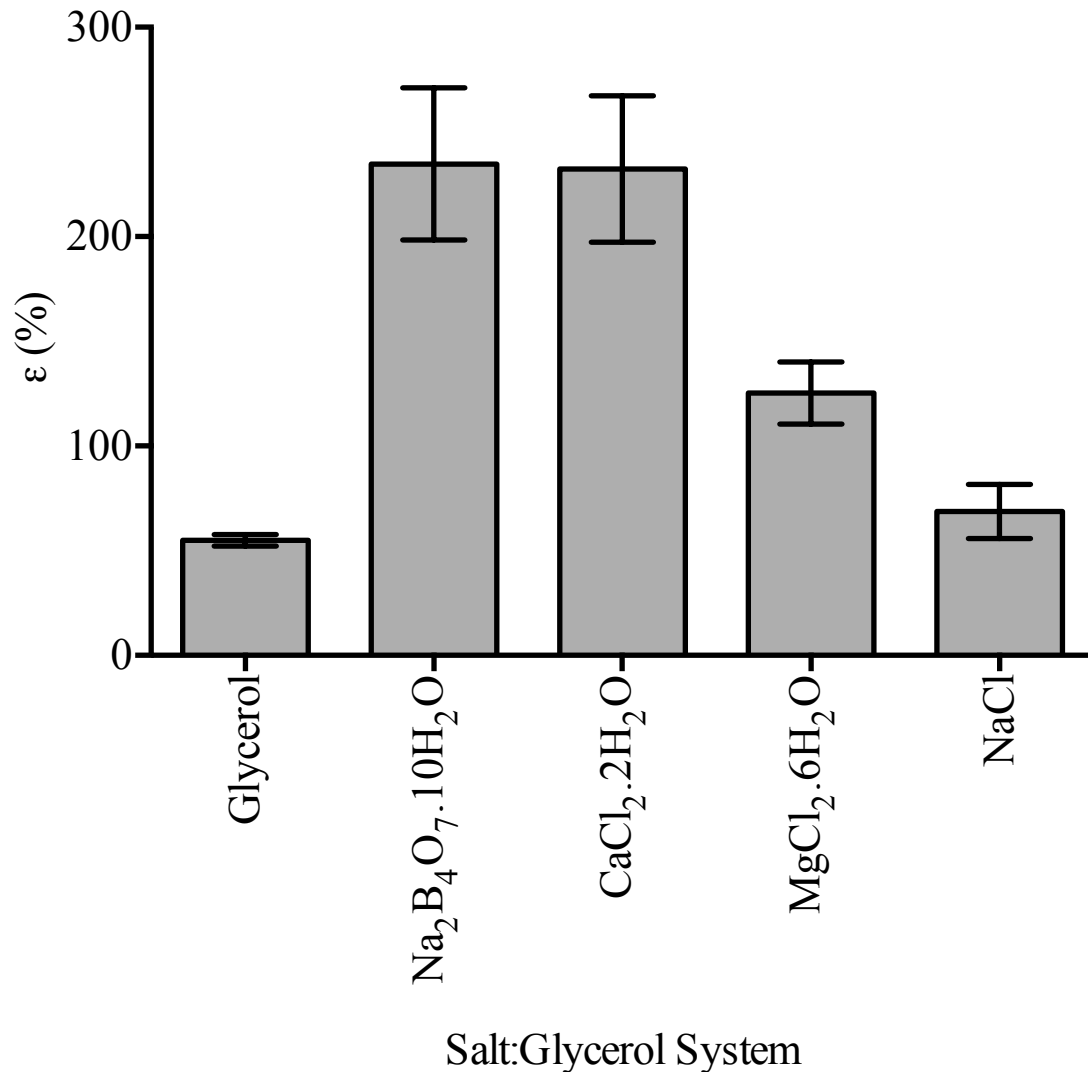


Figure 5.18 ϵ values of corn starch plasticised with different salt:glycerol mixtures

The UTS of a UF resin was found to be 2.10 MPa with an ϵ of 110.0%, which is comparable to the UTS of the plasticised starches tested here.¹⁰⁰ However, the mechanical properties of UF resins are dependent on the process method, as the average molecular weight, molecular weight distribution and degree of polymerisation.¹⁰¹

5.3. Plasticised Starch as a Binder for Fibreboards

Since the UTS and ϵ values of the plasticised starches tested in section 5.2.3 were generally comparable to that of a UF resin, they were trialled as potential binders for MDF. The initial method of preparation involved mixing together wood fibre, corn starch and a plasticiser in the proportions 45 %, 15 % and 40 % w/w respectively. From previous work, Abbott *et al.* found corn starch loadings of greater than 15 % resulted in boards where some starch present was not plasticised suggesting insufficient mixing,

also, plasticiser loads of at least 40 % were required to produce a particleboard with suitable aesthetics.⁸³ The fibreboard components were mixed together using a food processor, with the plasticiser heated to 50 °C before being poured into the wood fibre-corn starch mixture. The fibreboard mixture was packed into a steel mould and formed in a hydraulic press at 145 °C and 120 kN of pressing force for 30 minutes.

5.3.1. Effect of Ionic Solvent on Structure

Figure 5.19 shows the physical appearance of a typical fibreboard prepared using the method outlined in section 2.9.2. All fibreboards prepared using this method displayed regions that were salt:glycerol mixture rich and deficient, represented in Figure 5.19 by the dark and light regions respectively. The non-homogeneous nature of the sample appearance suggests the plasticiser is not being efficiently dispersed throughout the sample, even though the plasticisers are heated to 50 °C before adding to the wood fibre-corn starch blend to minimise mixture viscosity. Abbott *et al.* found particleboards prepared with over 40 % salt:glycerol mixture had a physical appearance that closely resembled commercially produced particleboard.⁸³



Figure 5.19 Photograph of a fibreboard prepared using the method outlined in section 2.9.2, showing the mixing limitations of the method

The surface area of the wood flour used by Abbott *et al.* would have been far greater than the surface area of the wood fibre used here as the particle length of the wood flour was less than 500 µm, whereas the wood fibre used typically had a fibre

length greater than 5mm.⁸³ The larger surface area would allow greater coverage by the controlled quantity of plasticiser, and give a more homogeneous appearance.

In the lighter, relatively dry regions of the fibreboards, there appears to be an excess of native starch, as shown in Figure 5.20 and Figure 5.21 A.

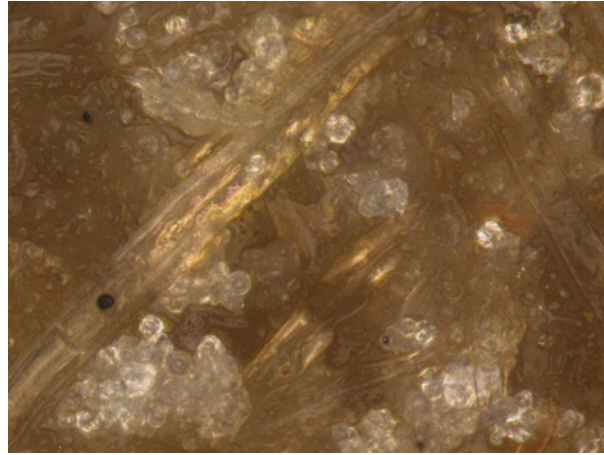
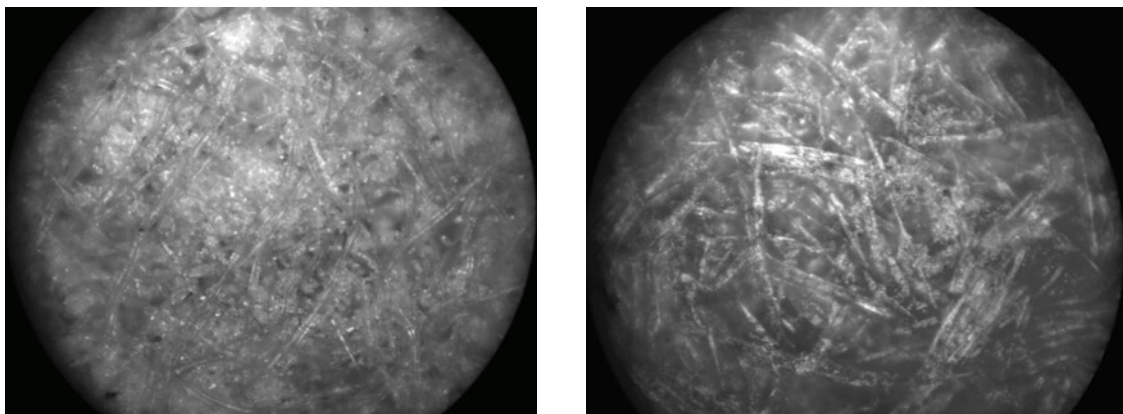


Figure 5.20 Micrograph of dry region of a fibreboard showing the abundance of native starch crystals



A

B

Figure 5.21 Micrograph of dry region of a fibreboard showing the abundance of native starch crystals (A), and Micrograph of wet region of a fibreboard showing the starch present is mostly plasticised (B)

This observation suggests that as well as poor binder-wood fibre mixing, there is also poor starch-plasticiser mixing, as the plasticiser needs to be present in sufficient quantity to lower the starch melting temperature below its decomposition temperature to facilitate plasticisation of starch.⁵² The darker, relatively wet regions fibreboards, there appears to be much less native starch, as shown in Figure 5.21 B. The lack of native

starch suggests much better starch-plasticiser mixing, but the process is completely random and varies from board to board.

5.3.2. Effect of Ionic Solvent on mechanical properties

Engineered woods are examples of composite materials, where composite material is generally defined as any multiphase material that possesses the properties individual component phases.¹⁰² Many composites are comprised of two phases: the matrix phase, which is homogeneous and encases the other phase, referred to as the dispersed phase.¹⁰² The scheme shown in Figure 5.22 outlines three main categories of composite material: particle-reinforced, fibre-reinforced and structural composites, where particleboards are examples of particle-reinforced composites, fibreboards and orientated strand boards are examples of fibre-reinforced composites, and plywood is an example of structural composites.¹⁰²

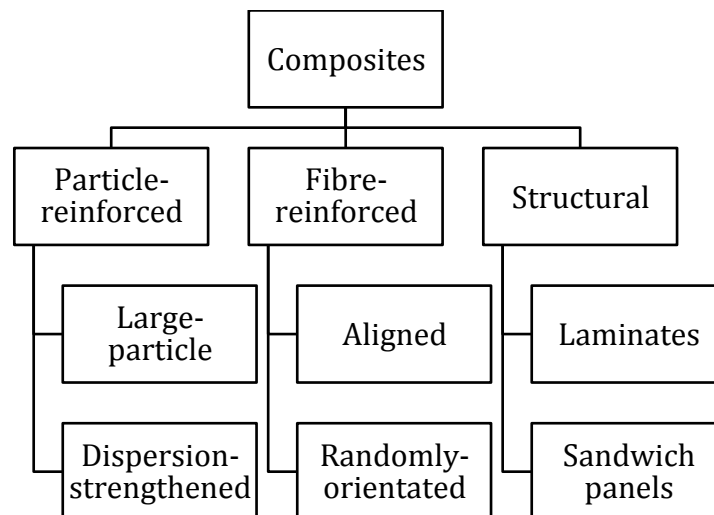


Figure 5.22 Groupings of composite materials

Particle-reinforced composites can be subcategorised into large-particle and dispersion-strengthened composites where: large-particle refers to matrix-particle interactions that are larger than the atomic scale, and dispersion-strengthened composites display strengthening on a molecular scale.¹⁰² Considering particleboards are examples of large-particle reinforced composite, dispersion-strengthened composites will not be considered here.

In large-particle reinforced composites, the particulate (dispersed) phase is generally stronger than, and restricts movement of, the matrix phase.¹⁰² The matrix phase transfers some of the applied mechanical load to the particulate phase to provide additional support: where the extent of the reinforcement is dependent on the strength of the matrix particle interface.¹⁰²

Structural composites can be sub-categorised in to laminar composites and sandwich panels where: laminar composites are comprised of sheets that possess directional strength that are stacked and bound in alternating directions; sandwich panels consist of a thick core material enclosed by thin, stiff panels.¹⁰² Considering the focus of this research is about fibre-reinforced composite, Structural composites will not be considered further.

The mechanical properties of fibre-reinforced composites are dependent on both the nature of the reinforcing fibre and the degree of mechanical load transfer from the matrix to the reinforcing fibre phase, which is reliant on the interface between the matrix and fibres.¹⁰² Under stress, the fibre-matrix bond stops at the ends of the fibres, suggesting no transfer of mechanical load occurs at the fibre edges, as shown in Figure 5.23.

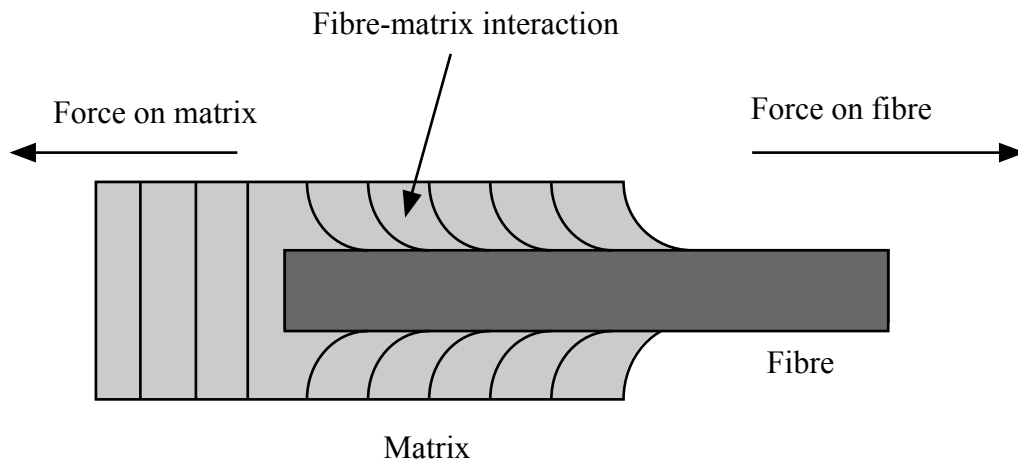


Figure 5.23 Diagram explaining matrix-fibre interactions

The relative orientation of fibres has a noticeable effect on the mechanical properties of a fibre-reinforced composite material.¹⁰² There are two extremes of fibre orientation: a parallel alignment of fibres along the load axis, and a totally random arrangement of fibre orientations, as shown in Figure 5.24 A and B respectively. A parallel arrangement allows a composite material to behave anisotropically as the reinforcement only truly occurs along the longitudinal axis of the fibres, whereas

random fibre orientation is less efficient at reinforcing a material but does allow a composite to behave isotropically.¹⁰²

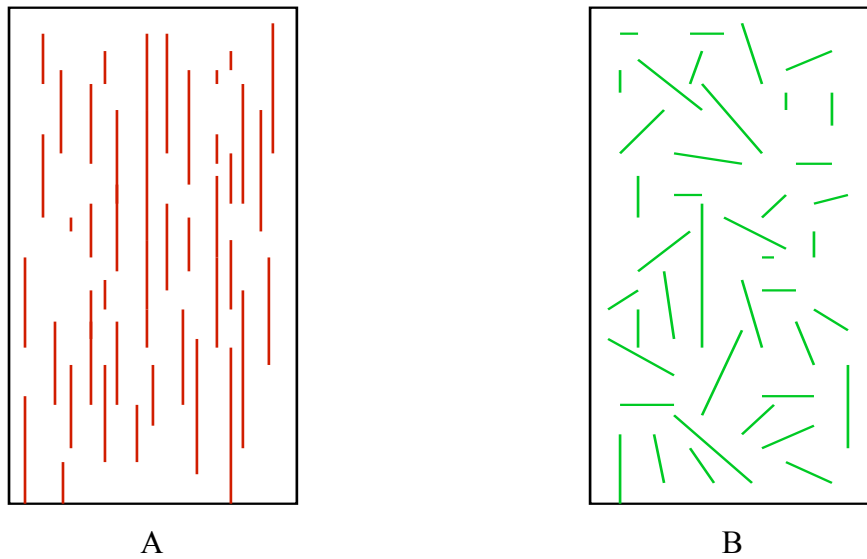


Figure 5.24 The extremes of fibre alignment: a parallel alignment along the load axis (A), and a totally random arrangement of fibres (B)

The UTS values of a series of fibreboards prepared using corn-starch plasticised with salt:glycerol mixtures were measured using a tensiometer, the results of which are shown in Figure 5.25. Even though there was little observable difference in UTS between the PSs shown in Figure 5.17, more significant differences were observed when the same PSs were formed in the presence of wood fibres. $\text{MgCl}_2 \cdot 6\text{H}_2\text{O}$ (0.70 ± 0.17 MPa), $\text{CaCl}_2 \cdot 2\text{H}_2\text{O}$ (0.56 ± 0.19 MPa) and NaCl (0.31 ± 0.21 MPa) all appeared to provide little benefit over fibreboards prepared with starch plasticised solely by glycerol (0.44 ± 0.26 MPa). Other research groups have used calcium chloride to cross-link starch, and Ca^{2+} ions are known to crosslink pectin-based composites.^{103, 104, 105} Considering the cross-linking characteristics of the Ca^{2+} ion, $\text{CaCl}_2 \cdot 2\text{H}_2\text{O}$, $\text{MgCl}_2 \cdot 6\text{H}_2\text{O}$ were expected to act as cross-linking agents between cellulose and starch polymer chains, although this is highly unlikely due to the minimal improvement in UTS provided by the addition of these salts to glycerol. Gough *et al.* found the chloride anion has a small effect on the gelation of starch at low concentrations, and at high concentrations provides almost no penetration of the starch granule.¹⁰⁶

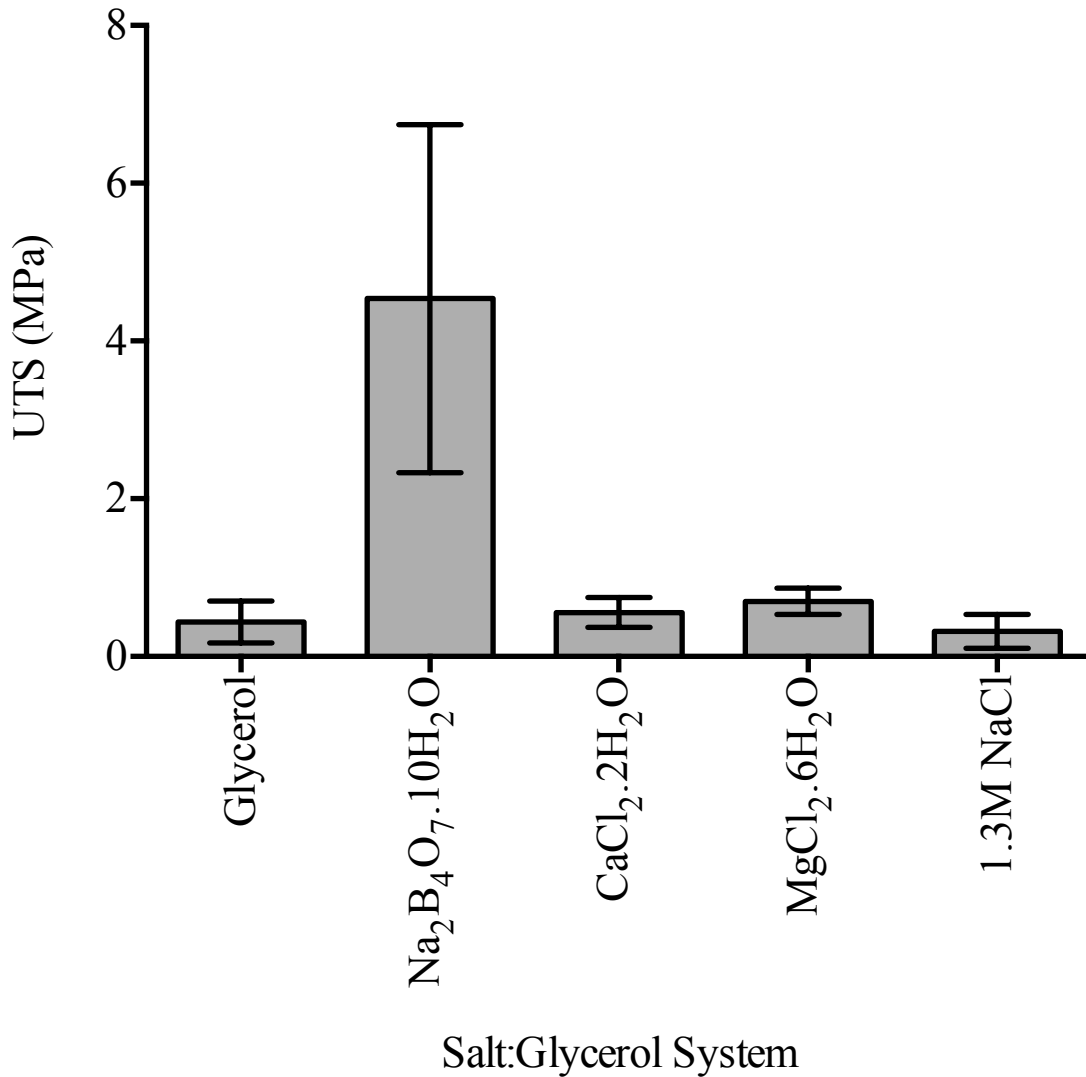


Figure 5.25 UTS values of corn starch plasticised with different salt:glycerol mixtures

The fibreboard prepared with the borax:glycerol mixture showed a significantly larger UTS of 4.54 ± 2.20 MPa. The starch cross-linking properties of borax are well known within the paper industry, and it is suspected that some degree of cross-linking is occurring within the plasticised starch.⁸⁴ There is evidence to suggest borax can cross-link between starch and PVA chains, even though borax was added to the system after the starch had been gelled.¹⁰⁷ This suggests it may be possible for borax to facilitate the cross-linking of cellulose and starch polymer chains, but further work would be required to confirm this hypothesis.

Photographs of corn starch plasticised by different plasticisers are represented in Figure 5.26, where corn starch plasticised by: glycerol, NaCl:glycerol, $\text{CaCl}_2 \cdot 2\text{H}_2\text{O}$:glycerol and Borax:glycerol are presented in part A, B, C and D

respectively. Starch that was plasticised by glycerol displayed poor physical properties and was easily destroyed. Addition of NaCl to the starch:glycerol system did not improve its qualitative physical properties, and the addition of $\text{CaCl}_2 \cdot 2\text{H}_2\text{O}$ resulted in a material that was still fluid after the gelling process had completed. Addition of borax to glycerol gave a PS that was tacky and had the consistency of a tough rubber, whereas the other PSs were non-tacky and easily separated. These qualitative observations support the idea of borax cross-linking starch polysaccharides, and suggest $\text{CaCl}_2 \cdot 2\text{H}_2\text{O}$ and $\text{MgCl}_2 \cdot 6\text{H}_2\text{O}$ are not cross-linking starch polysaccharides.



A) No salt



B) NaCl



C) $\text{CaCl}_2 \cdot 2\text{H}_2\text{O}$



D) $\text{Na}_2\text{B}_4\text{O}_7 \cdot 10\text{H}_2\text{O}$

Figure 5.26 Photographs of corn starch plasticised with glycerol and different salts

The ϵ values of corn starch plasticised by plasticisers are shown in Figure 5.27. Materials that display higher UTS values are generally more brittle, and considering corn starch plasticised with the borax system was typically ten times stronger than the other materials tested, it was expected to have approximately a tenth of the elongation at break. However, its ϵ was larger ($2.99 \pm 0.54 \%$) than the other materials tested. Fibre-

reinforced composites utilise the interface between the matrix phase and the fibre phase to transfer stress. If the interface is poor, the mechanical stress will be absorbed by the dominant phase, which generally is the fibre phase.¹⁰² Without a supportive matrix, the fibre phase relies on the formation of knots between individual wood fibres to provide structural integrity, which requires nominal stress to overcome. Considering that corn starch plasticised by a borax:glycerol mixture is stronger than the other plasticised starches studied, better transfer of stress can be achieved, which provides additional integrity whilst knots in the wood fibre unravel to facilitate further extension before break.

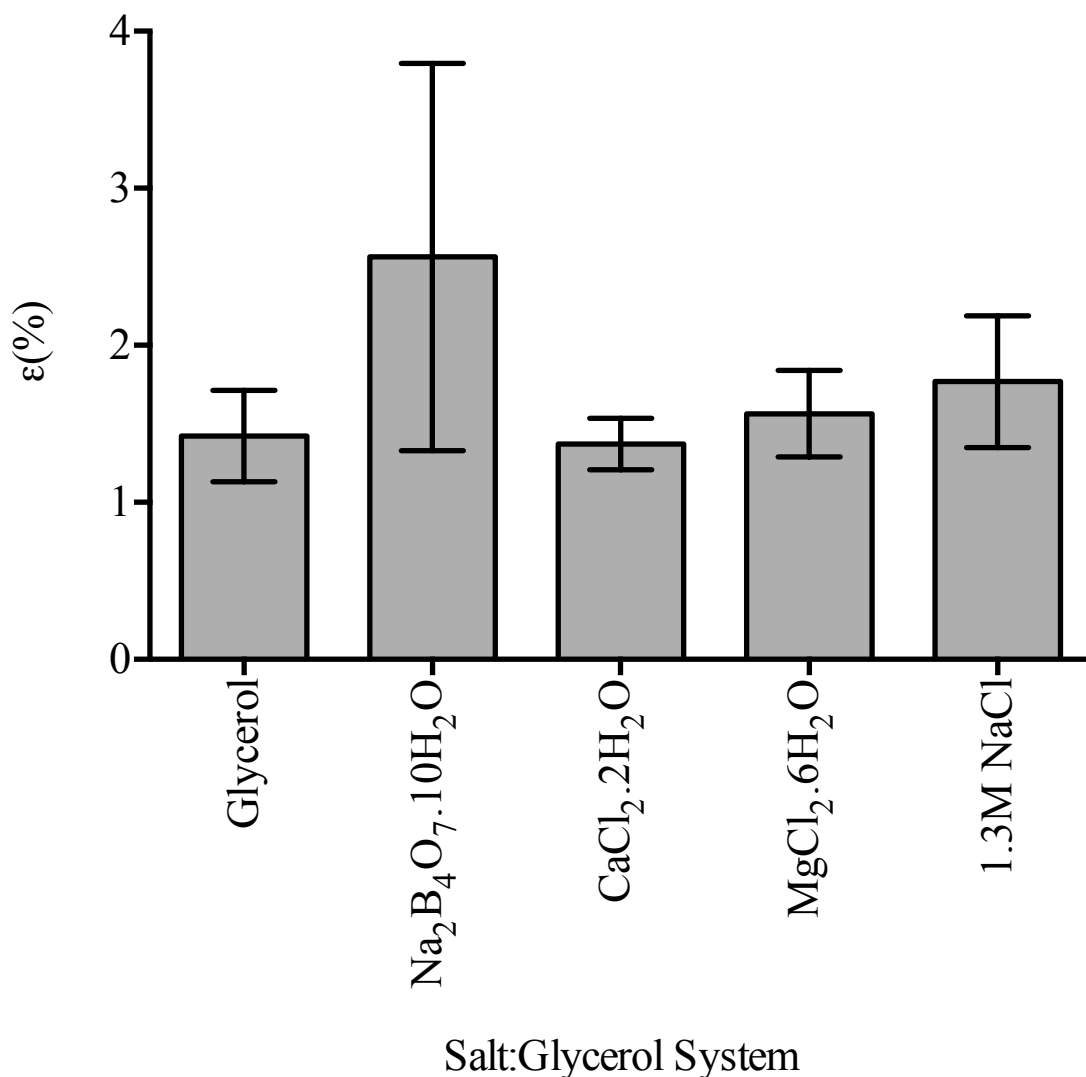


Figure 5.27 ϵ values of corn starch plasticised with different salt:glycerol mixtures

Corn starch plasticised by the borax system gave an E value of 326 ± 126 MPa, as shown in Figure 5.28, whereas MDF prepared using MUF resins typically have an E of 3600 MPa and generally have an ϵ of 0.5%.¹⁰⁸ Fibreboards bound with MUF are stiffer

than fibreboards bound with plasticised starch, but there is almost a 6-fold difference in the materials ductilities. At small elongation values, small differences in elongation values have a large effect of the subsequent E values, and when considered at equal elongations, the E value of the MDF bound with starch plasticised with borax and glycerol becomes 1960 ± 757 MPa.

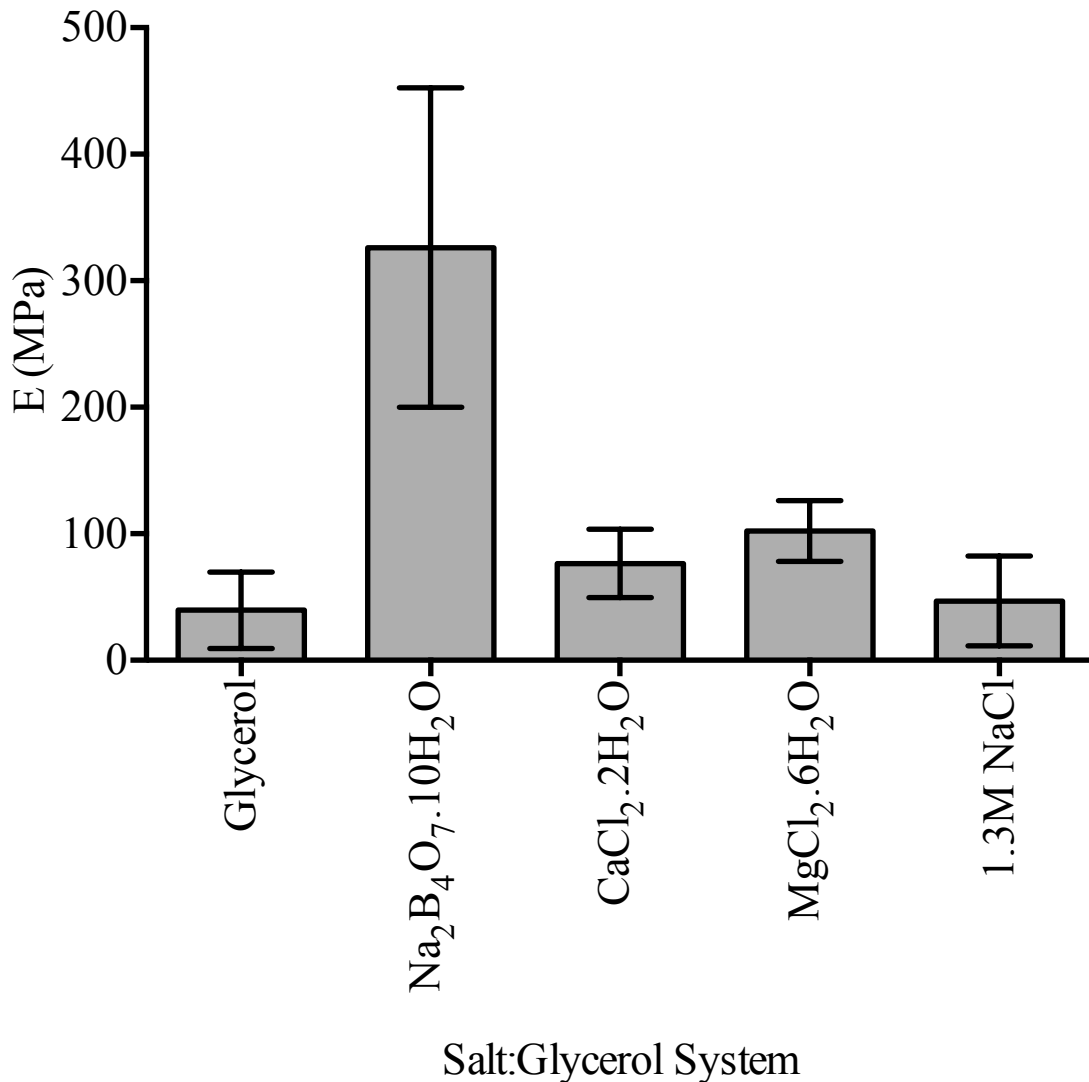


Figure 5.28 E values of corn starch plasticised with different salt:glycerol mixtures

All of the fibreboards prepared using the method outlined in section 2.9.2 showed significant error bars in all mechanical property data. The poor distribution of plasticiser, as shown in Figure 5.19, would account for the noticeable level of variance observed, as some of the samples tested would have had a plasticiser deficient test area and others would have a plasticiser rich test area. The presence of native starch deposits suggest the average values obtained for UTS and E are likely to be underestimates, as

the plasticised starch present would have been over plasticised as shown compromised mechanical properties.¹⁰⁹

After comparing the mechanical properties of fibreboards bound by plasticised starch, and MUF resin, the borax:glycerol plasticiser was considered for further experiments. The borax:glycerol plasticiser: showed superior tensile strength without a significant increase in ductility, has a unit cost of approximately \$1 per kg, which is comparable to MUF resins, and require no special synthesis techniques.⁸¹

The method of preparation outlined in section 2.9.2 does not represent the industrial process, as this method involves pouring a hot plasticiser mixture over a starch-wood fibre mixture, whereas the industrial method aspirates the adhesive mixture over a flow of wood fibres.⁹⁹ For plasticised starch binders to be commercially viable, they must be suitable for use in an aspirator-type resination system, which requires a suitable pre-gelled viscosity.

A 1:4 molar mixture of borax and glycerol respectively has a dynamic viscosity of 312 cP at 45 °C, which can be aspirated with an air pressure of 5 bar, was tested using the aspirator-type resination system at the BioComposites Centre (Bangor University, UK). The resination process at the BioComposites Centre uses a large rotating drum equipped with a pressurised spray system, as photographed in Figure 5.29 A & B respectively. A true industrial-type blow-line process could not be used for trials, and wood fibre was not made *in situ* as part of the resination process.



A



B

Figure 5.29 The rotating mixing drum (A) and internal spray system (B) used at the Biocomposites Centre

The process was used to test the spraying properties of the borax:glycerol plasticiser, and see if it could be adapted to work with the industry infrastructure. It was hypothesised that by aspirating wood fibre, that has previously been mixed with corn starch, it would be possible to achieve: a more even distribution of starch and plasticiser, enhanced and smaller variance in mechanical properties, and obtain a more uniform surface finish.

Figure 5.30 A shows the physical appearance of a typical fibreboard prepared using the Biocomposites Centre aspirator method, as outlined in section 2.9.3. All fibreboards prepared using this method displayed a homogeneous surface that was even in tone and showed no evidence of native starch. The homogeneous nature of the sample appearance suggests the plasticiser mixture is being efficiently dispersed throughout the sample. The small black spots that are visible all of the fibreboards prepared using this method are suspected to be small amounts of carbon, which were picked up when the resonated wood fibre was being transferred from the rotating drum to storage.

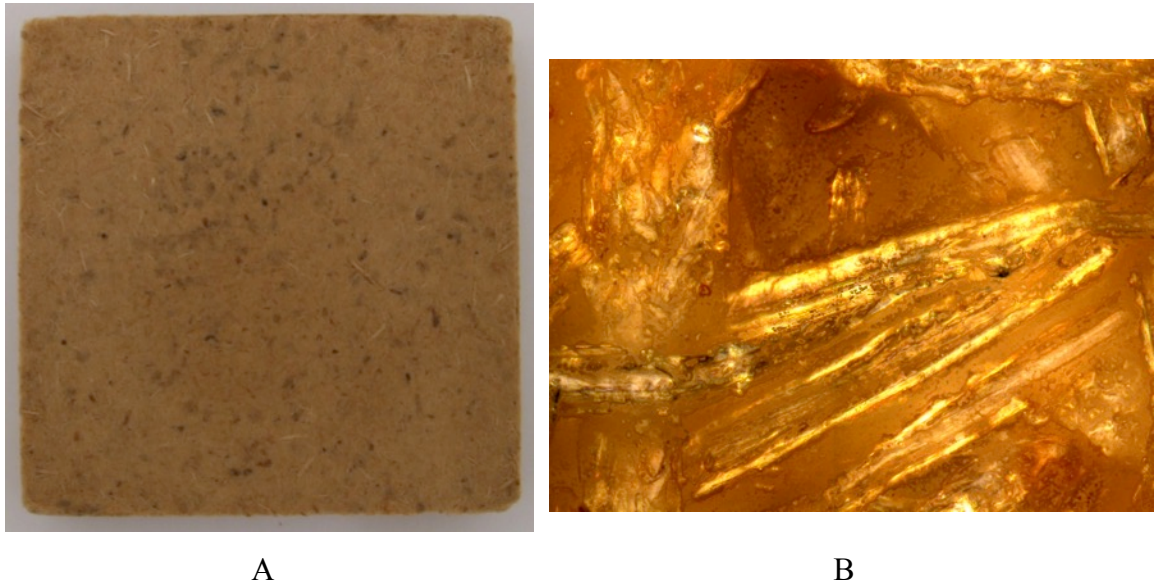


Figure 5.30 Photograph of a fibreboard prepared using the method outlined in section 2.9.3

The micrograph in Figure 5.30 B shows fibres that have a glass-like coating, suggesting a much more consistent gelation of starch throughout the board. Some native starch is present, but is at a far lower concentration compared to the deposits of native starch observed in Figure 5.20

The fibreboard shown in Figure 5.30 closely resembles the appearance of commercially prepared fibreboard, which is presented in Figure 5.31 A. The micrograph in Figure 5.31 B shows commercial MDF has an even distribution of its MUF resin throughout the fibre phase, but the crystalline regions of MUF can be seen.

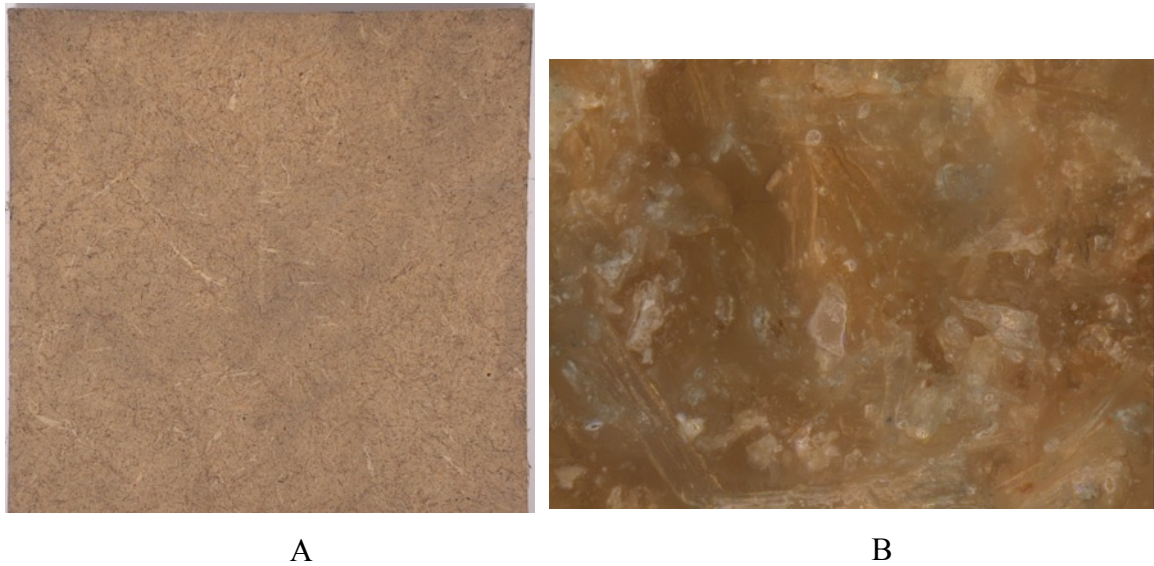


Figure 5.31 Photograph (A), and micrograph (B) of commercially manufactured MDF

The observations above show, that aspiration of the plasticiser over a mixture of corn starch and wood fibre can achieve improved adhesive-wood fibre mixing. Considering there is a more even distribution of plasticised starch, there should be a stronger interface between the matrix and fibre phase, and should lead to greater UTS and E properties and limit elongation at break.

Fibreboards were prepared using a 1:4 molar mixture of borax and glycerol, and consisted of: 35-50 % w/w plasticiser, 10 % w/w corn starch, and the remainder of the material was wood fibre. The wood fibre was resonated using the method outlined in section 2.9.3, and was pressed using the method summarised in section 2.10.1. As well as investigating the effect of plasticiser content, the effect of board pressing time was also studied, the UTS values of which, are shown in Figure 5.32.

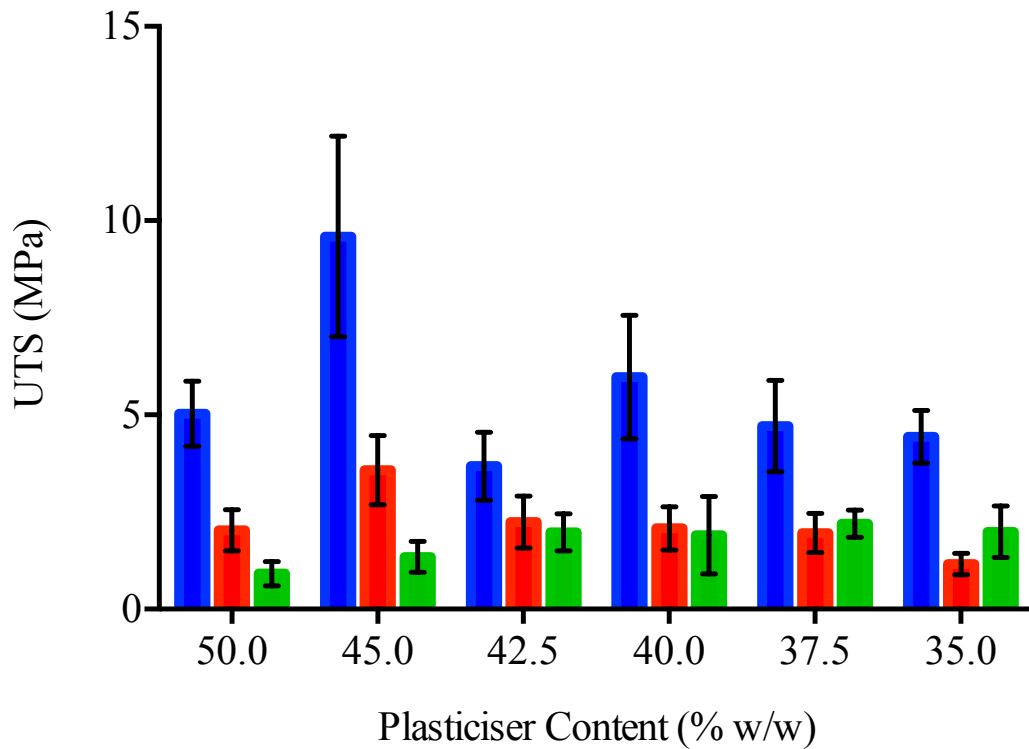


Figure 5.32 UTS values of fibreboards as a function of plasticiser content (1:4 borax:glycerol mixture), and pressing time: 30 mins (blue), 10 mins (red) and 5 mins (green)

A peak UTS of $(9.6 \pm 2.6 \text{ MPa})$ is achieved with a pressing time of 30 minutes, and a 45 % w/w plasticiser content. At lower plasticiser concentrations, UTS decreases as there is insufficient plasticiser and corn starch to form a strong enough matrix phase, whereas at higher concentrations, the wood fibre is too wet and the corn starch is over plasticised, thus compromising the material strength. Figure 5.33 shows that flash drying the material before pressing to reduce the water content, increased the UTS of a resonated wood fibre containing 50% w/w plasticiser from $5.5 \pm 1.04 \text{ MPa}$ to $8.6 \pm 2.9 \text{ MPa}$.

Fibreboards prepared using the aspiration-type method are significantly stronger, and less variable than the fibreboards previously tested, which is due to the better distribution of plasticised starch throughout the materials. The anomalous at 42.5 % can be attributed to a blockage in the spray system resulting in insufficient plasticiser mixing with the wood fibre- corn starch mixture.

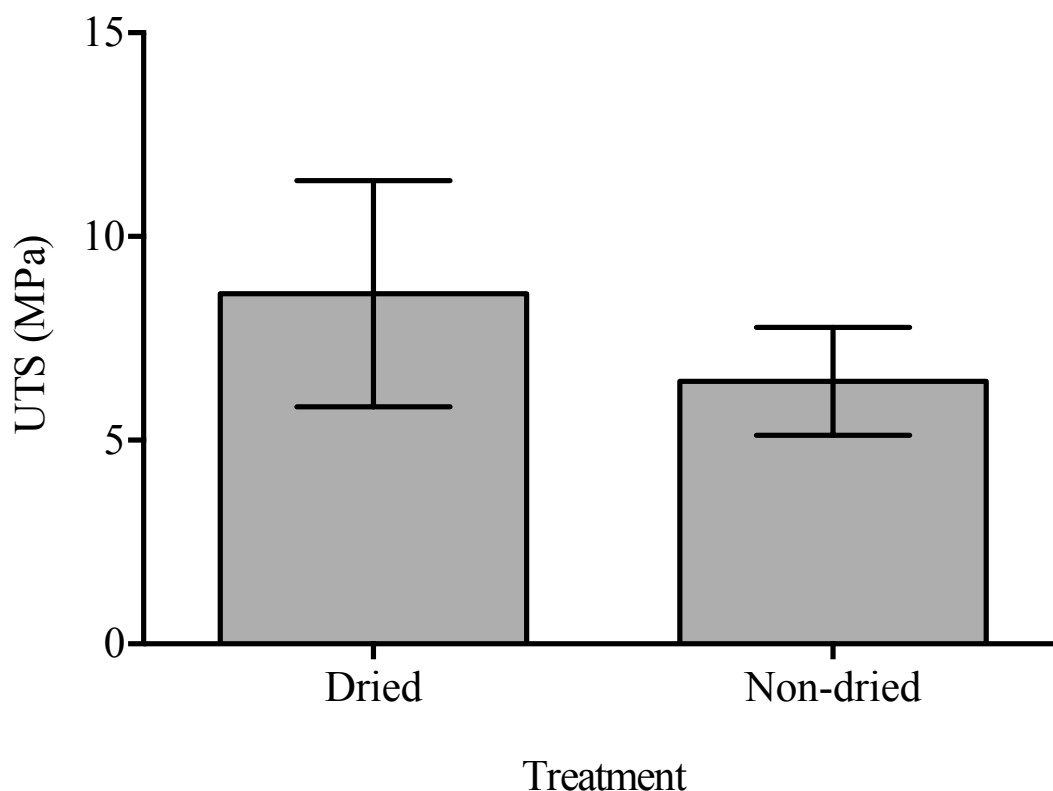


Figure 5.33 UTS of a fibreboard containing 50% w/w of 1:4 borax:glycerol, and a fibreboard of the same material that has been flash dried

Previous work by Abbott *et al.* shows that a thermoplastic wood composite material can be made using corn starch plasticised with a choline chloride:glycerol mixture, which had an UTS of 9.85 ± 0.69 MPa.⁷⁸ Basta *et al.* found that by blending corn starch with PVOH, a bonding strength of 9.8 MPa could be achieved.¹¹⁰ However, Wu *et al.* was capable of obtaining a Cellulose, starch and lignin composite with an UTS of 35.2 ± 2.1 MPa.¹¹¹

Pressing time had a much more pronounced effect on UTS compared to the effect of varying plasticiser content, with pressing times of less than 10 minutes resulting in boards with compromised physical strength. With a pressing time of 10 minutes, the fibreboard containing 45% plasticiser gave the highest UTS of 3.58 ± 0.89 MPa, and with a pressing time of 5 minutes, the same composition gave an UTS of 1.35 ± 0.40 MPa.

Analysis of fractured material can be used as an indicator of the fibre-matrix interface strength, as evidence of stretched fibre indicates a poor interface, Figure 5.34 A, whereas broken fibres suggest poor fibre strength with respect to the fibre-matrix

bond, Figure 5.34 B.⁵⁰ Inspecting the fibreboard test pieces after failure, as shown in Figure 5.34, demonstrates these two very different breaking mechanisms.

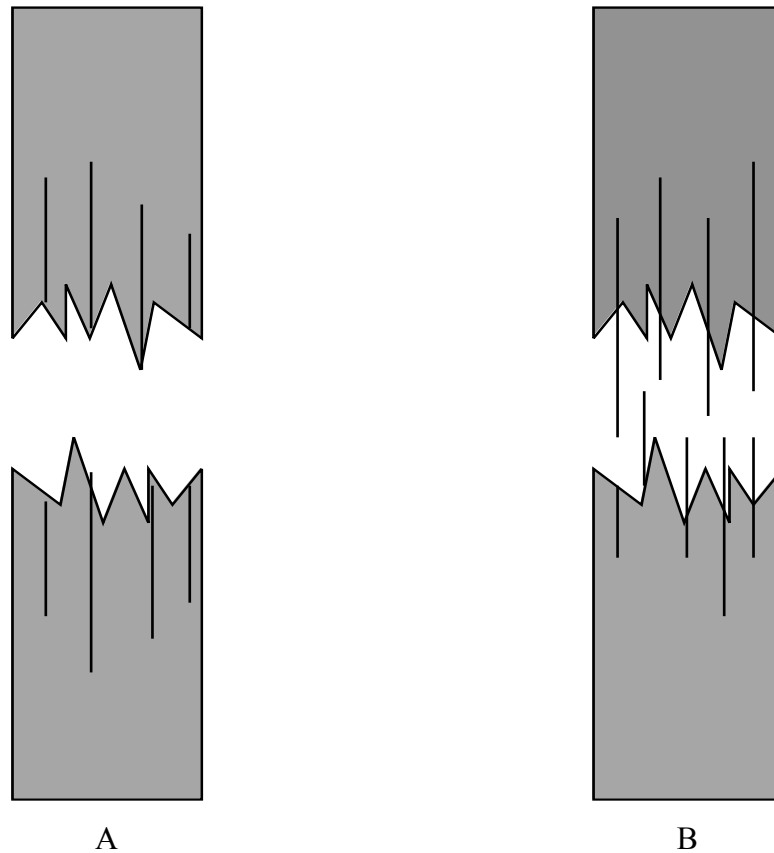


Figure 5.34 Types of fibre-reinforced composite fracture: Fibre limited (A), and fibre-matrix interaction weak (B)

Figure 5.35 A is a photograph of the fractured test piece of a material that was pressed for 30 minutes, and is an example of a material that has failed through a fibre-limited mechanism. The fibres at the fracture surface are short suggesting a good fibre-matrix interaction was present. Figure 5.35 B is a photograph of a fractured test piece that was pressed for 5 minutes, and is an example of a material that has failed through an interface-limited mechanism. The fibres at the fracture surface are long and drawn out suggesting the fibre-matrix interaction was poor. It is suspected that at lower pressing times, the plasticised starch matrix phase had not fully formed, and was not able to strongly interact with the fibre phase.



A

B

Figure 5.35 Photographs of fractured test pieces containing 45% w/w plasticiser pressed for: 30 min (A), and 5 min (B)

The stress-strain profiles of the samples, as shown in Figure 5.36, follow the material behaviour associated with their respective failure mechanisms. The blue trend presented in Figure 5.36, represents the material that was pressed for 30 minutes, which suggests the material is relatively stiff and little plastic deformation occurs before failure. The red trend presented in Figure 5.36, represents the material that was pressed for 5 minutes, which suggests the material is relatively ductile and most of the material deformation is plastic.

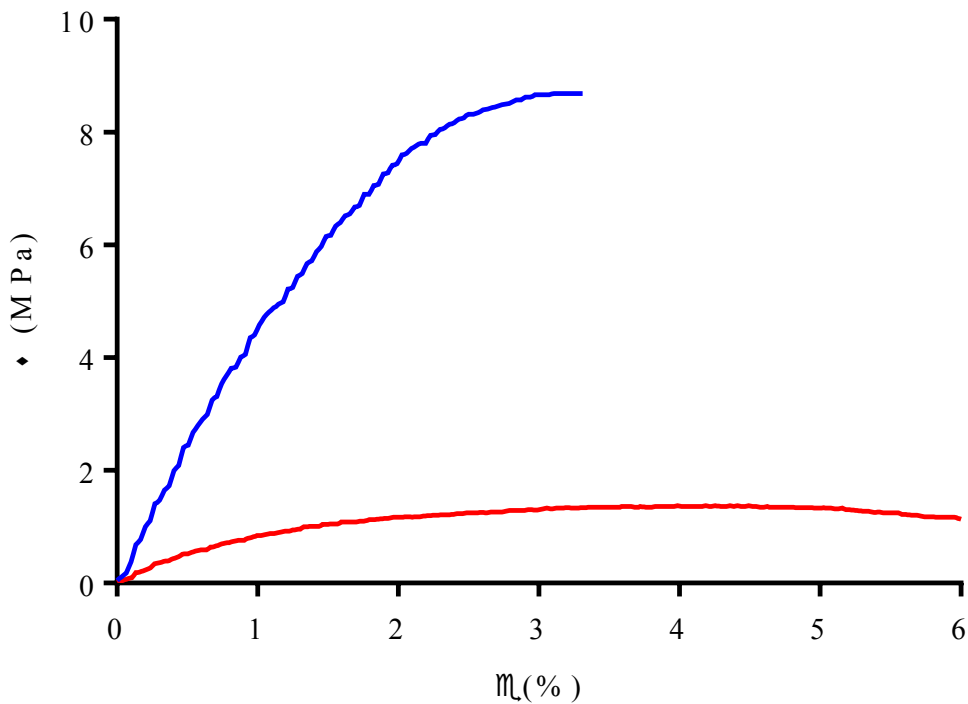


Figure 5.36 Stress-strain profiles of test pieces containing 45% w/w plasticiser pressed for: 30 min (blue), and 5 min (red)

The ductility of the tested fibreboards generally increased with plasticiser content, as shown in Figure 5.37. At the highest plasticiser content the wood fibres are too wet and the corn starch is over plasticised, which leads to a more ductile material. Figure 5.38 shows that flash drying the material before pressing to reduce the water content, decreased the ϵ of a resonated wood fibre containing 50% w/w plasticiser from 3.45 ± 0.9 % to 2.41 ± 1.13 %. At lower plasticiser concentrations, ϵ decreases as there is insufficient plasticiser and corn starch to form a strong enough matrix phase. Without a supportive matrix, the fibre phase relies on the formation of knots between individual wood fibres to provide structural integrity, which requires less stress to over power.

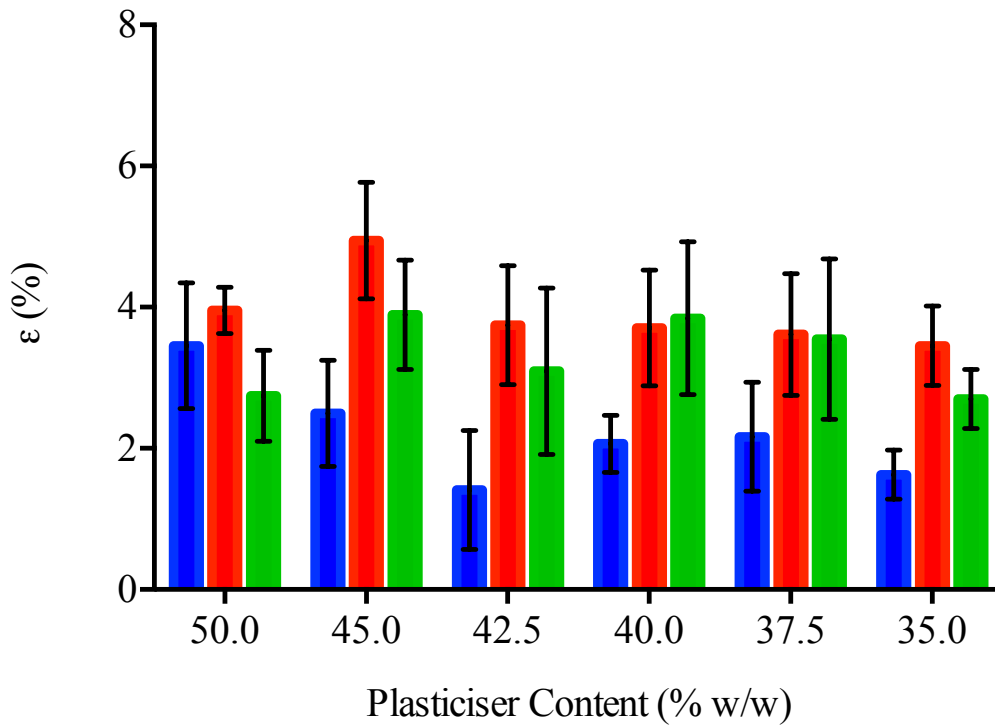


Figure 5.37 ϵ values of fibreboards as a function of plasticiser content (1:4 borax:glycerol), and pressing time: 30 min (blue), 10 min (red) and 5 min (green)

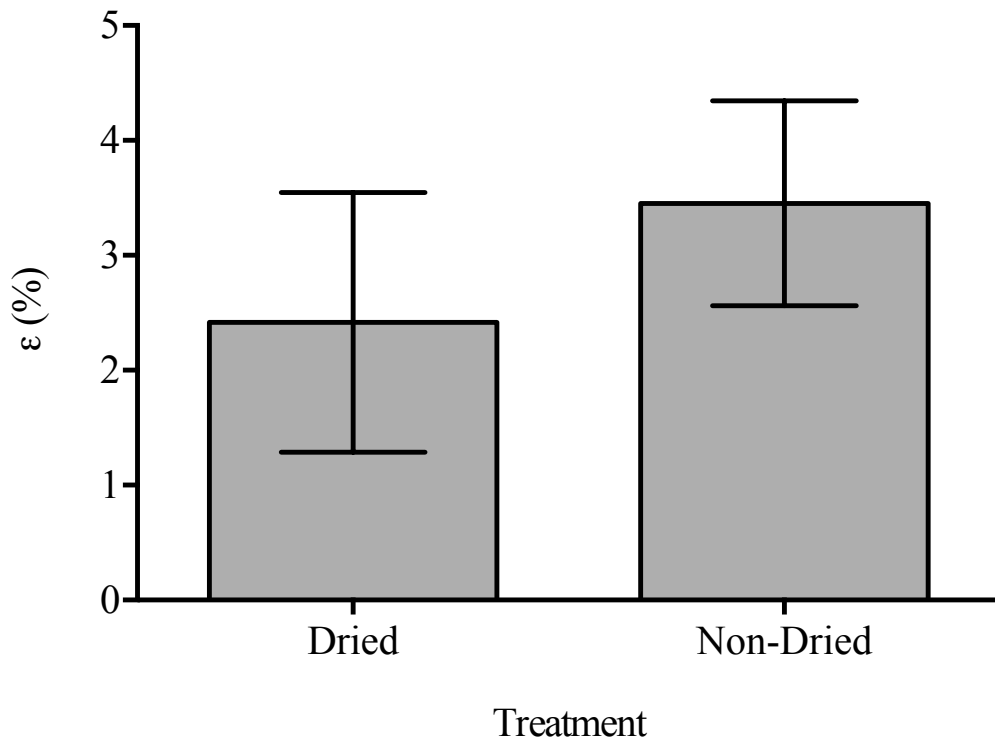


Figure 5.38 ϵ of a fibreboard containing 50% w/w of a 1:4 borax:glycerol, and a fibreboard of the same material that has been flash dried

After a pressing time of 30 minutes the starch has fully plasticised, and the differences in ductility can be attributed to how the fibre-matrix interactions change as a function of plasticiser content. After a press time of 5 or 10 minutes, the longer elongation values are due to knotting between fibres provides most of the structural integrity, which can stretch further before material failure. After taking into account the error bars associated with the data in Figure 5.37, there appears to be no quantifiable difference in ductility between the 5 and 10 minute trends.

The highest chordal modulus of 579 ± 84 MPa is achieved with a pressing time of 30 minutes, and a 45% w/w plasticiser content, which is shown in Figure 5.39. Materials that were pressed for 30 minutes were stronger and more brittle compared to materials that were pressed for 5 or 10 minutes, which all expressed E values of less than 200 MPa. There is little variance between materials that have been pressed for 30 minutes, which is not surprising considering that materials with lower UTS values generally also expressed lower elongations at break, resulting in a more consistent chordal modulus.

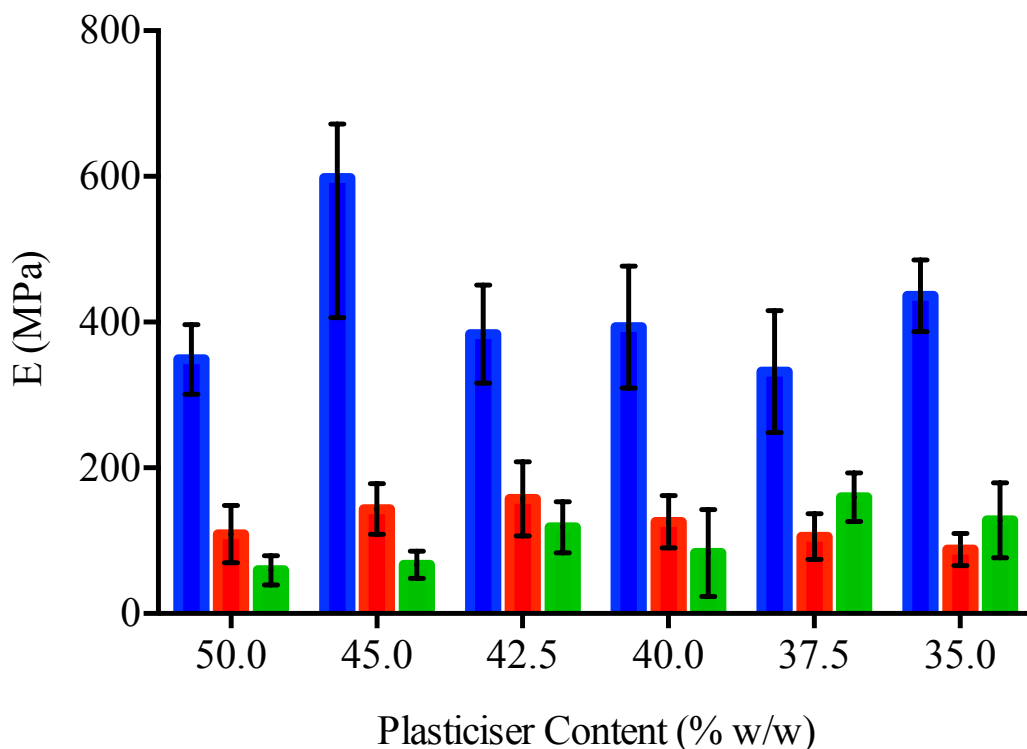


Figure 5.39 E values of fibreboards as a function of plasticiser content (1:4 borax:glycerol mixture), and as a function of pressing time: 30 min (blue), 10 min (red) and 5 min (green)

Plasticised starches are only one of a range of formaldehyde-free engineered wood binders that are investigated by other research groups: tannins, proteins and wood fibre cross-linking are the three most common alternatives to plasticised starch. Geng *et al.* found that by carefully selecting the wood fibre source it is possible to manufacture binderless fibreboard by utilising the naturally occurring tannins within tree bark.¹¹² Fibreboards manufactured without modifying the natural tannins within the bark gave a MOE value of 1643 MPa whereas, fibreboards manufactured with alkali treated spruce barks gave a MOE of 3255 MPa, which is similar to the 3590 MPa of commercially manufactured MDF.^{108,112} Although, this methodology requires a tree bark, which is only a small proportion of a trees mass, and requires a bark that is rich in natural phenolics, thus limiting its industrial viability.

Li *et al.* is capable of binding wood fibres with a soybean protein extracted from defatted soybean flour, and obtained a MOE of 2992 MPa, which required a pressing time of only 10 minutes.¹¹³ Widsten *et al.* manufactured high density fibreboard using mimosa tannins in the presence of glycidyltrimethylammonium chloride, which forms cationic tannin that interacts strongly with cellulose hydroxyl groups. High-density fibreboards manufactured in this way are claimed to have a MOE in excess of 5000 MPa.¹¹⁴

Although commercially manufactured MDF and many of the other forms of formaldehyde-free binder appear to have significantly larger MOE values than what can be achieved with a plasticised starch, MOE values are rarely quoted with ductility measurements. Without a ductility measurement to complement the MOE measurement, it is difficult to establish the difference between a weak, brittle material, and a strong, brittle material. MDF manufactured with a MUF resin typically has a MOE of 3590 MPa, and generally has a ductility of 0.5 %, whereas MDF manufactured with a plasticised starch containing borax has a MOE of 579 ± 84 MPa, and a ductility of 2.50 ± 0.75 %.¹⁰⁸ The difference in ductility between the two types of MDF is only 2 %, yet that equates to a five-fold difference, which has a serious impact on the subsequent MOE value. The ductility of plasticised starches can be reduced, and increase the MOE, by increasing the plasticiser-to-corn starch ratio however, further studies would be required to investigate the impact on material strength and industrial viability.¹⁰⁹

Tensile strength, ductility and MOE are important material properties that need to be known, but a fibreboard's: internal bond strength (IB), thickness swelling (TS) and total emitted formaldehyde (TEF) are the physical properties that need to be quantified

for a fibreboard to pass EN 622 European fibreboard guidelines. IB is the tensile stress required acting across the face of a material to cause a fracture, as shown in Figure 5.40, and to pass EN 622 standards a value of 0.55 MPa is required.

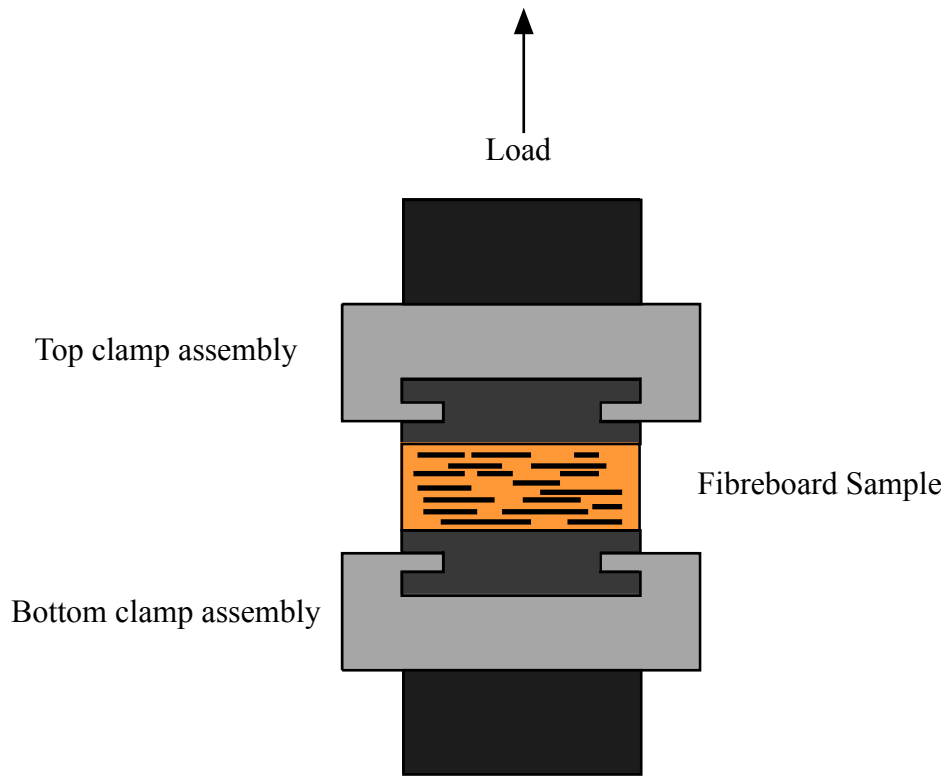


Figure 5.40 Representation of an IB test

Table 5.2 lists the IB, TS and TEF for MDF manufactured with MUF, and corn starch plasticised with a borax:glycerol mixture. As well as investigating the effect of the binder, the effects of pressing time, and the addition of water or wax, to aid flow of plasticiser, were studied. In cases where a wax was added, a slack wax emulsion with a solids content of 50% was used. All boards were pressed for either 5 or 9 minutes to allow a comparison with MDF that has been manufactured with MUF resins, which is typically prepared on this timescale.

Table 5.2 Comparison of IB, TS and TEF results compared to EN 622 standards^a

Binder	Additive	Additive quantity (% w/w)	Pressing time (min)	IB (MPa)	24 Hr Swell (%)	TEF (mg HCHO 100g ⁻¹)
MUF	-	-	5	0.57	21.19	5.0
MUF	Wax	0.7	5	0.76	6.67	3.1
G4	-	-	9	0.04	-	-
G4	Wax	1.4	9	0.58	-	2.4
G4	Water	16.0	9	0.33	46.00	2.8
G4			5	0.07	-	3.5
G4	Wax	1.4	5	0.16	-	2.1
G4	Water	16.0	5	0.35	-	3.0
EN622 Guidelines			-	>0.55	<12	<8

^aTests conducted by Hexion Specialty Chemicals

Fibreboards manufactured using plasticised starch were only able to obtain an IB sufficient to pass the EN 622 standards with a pressing time of 9 minutes and the addition of 1.4 % w/w slack wax emulsion, which aided plasticiser flow and reduced the rate of water absorption. The addition of water also improved IB suggesting the non-diluted plasticiser was too viscous to be aspirated efficiently at room temperature. However, the addition of water further plasticised the corn starch as the IB was lower than what was achieved when using wax, which does not act as a plasticiser. Regardless of the addition of either water or wax, when pressed for 5 minutes, fibreboards utilising the plasticised starch binder failed to meet EN 622 requirements. It has been previously explained that a 5 minutes pressing time lead to incomplete formation of a fibre-matrix bond, which lead to a material with poor mechanical strength.

All fibreboards tested passed the TEF test, which is not surprising considering the binder used is formaldehyde-free. However, the TEF value for MDF manufactured with MUF and wax is much lower than expected and comparable to what was achieved with a formaldehyde-free binder. Glycerol has been known to decompose in to aldehydes at high temperatures and pressures.¹¹⁵ Watanabe *et al.* found that at high temperatures and pressures, glycerol could be converted to acrolein at high temperatures and pressures, and as a consequence, traces of formaldehyde and acetaldehyde were detected.¹¹⁶

Unfortunately, all fibreboards tested failed the 24-hour TS test as the samples lost all structural integrity and could not be measured. This outcome is not surprising considering the hygroscopic nature of glycerol and borax. Failure of the 24-hour TS test suggests moisture readily penetrates deeply into the fibreboard, which is needed for

biological activity to degrade cellulose and starch polysaccharides via biochemical pathways.⁵⁰ Maiti *et al.* found that starch/ PVOH films that were cross-linked with borax were able to biodegrade more quickly compared to films that were cross-linked with formaldehyde.¹¹⁷ The plasticised starches tested are intended as binders for engineered woods that will only have a short service life and require a biologically active degradation pathway.

As well as biological degradation, broken fibreboards utilising plasticised starches can ground down and repressed into new fibreboards, as shown in Figure 5.41. Abbott *et al.* found that recycling fibreboards bound with a mixture of starch, choline chloride and glycerol resulted on average a 10% drop in tensile strength and a 1.5 % drop elongation at break.⁷⁸



Figure 5.41 Recyclability of used material

The ability to recycle broken fibreboards into new fibreboards of comparable tensile strength demonstrates that the plasticised starch systems used express thermoplastic nature. Considering borax is known to have a cross-linking effect on starch, thermoset behaviour was expected, however, borax-polyol mixtures known to show viscoelastic behaviour due to reversible borate ester cross-links.¹¹⁸ The formaldehyde-based resins currently used in MDF are thermosetting, and cannot be recycled in this way.

5.3.3. Effect of Ionic solvent on Thermal properties

Thermogravimetric analysis (TGA) was employed to investigate the volatiles content of fibreboards containing 45 % w/w borax:glycerol plasticiser that were pressed for 0-30 minutes, the results of which are shown in Figure 5.42, and the moisture contents are shown in Table 5.3. The moisture content was assumed to be the mass difference between 300 and 420 K.

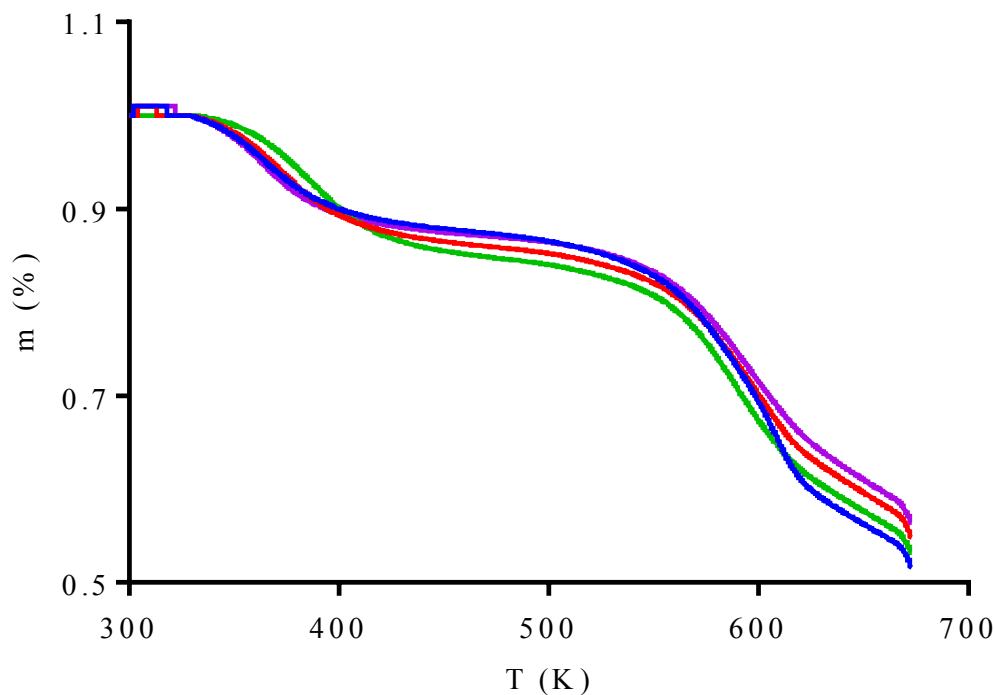


Figure 5.42 Mass loss profiles of fibreboards containing 45 % w/w borax:glycerol plasticiser that were pressed for: 0 min (blue), 5 min (red), 10 min (green) and 30 min (purple)

Table 5.3 Moisture contents of fibreboards containing 45 % w/w borax:glycerol plasticiser that were pressed for 0-30 min

Pressing time (min)	Volatile loss (%)
0	11.9
5	13.3
10	14.4
30	12.2

The average water content of the fibreboards tested here is 13.0%, which is similar to the 7-12 % water content of MDF that has been manufactured with formaldehyde-based resins has a moisture content.¹¹⁹ Water content appears to be independent of pressing time, which is surprising as fibreboards that were pressed for longer times were expected to have lower contents. Abbott *et al.* found that corn starch that had been heated in an oven at 50 °C did not change the water content irrespective of the heating time.⁵³ The mass loss with an average onset temperature of 565 ± 5.8 K can be attributed to the boiling of glycerol.¹²⁰ The mass loss profile for corn starch is shown

in Figure 5.43 and suggests the onset of starch degradation occurs at 553 K, which coincides with the exothermic peak at 600 K, shown in the thermogram in Figure 5.43

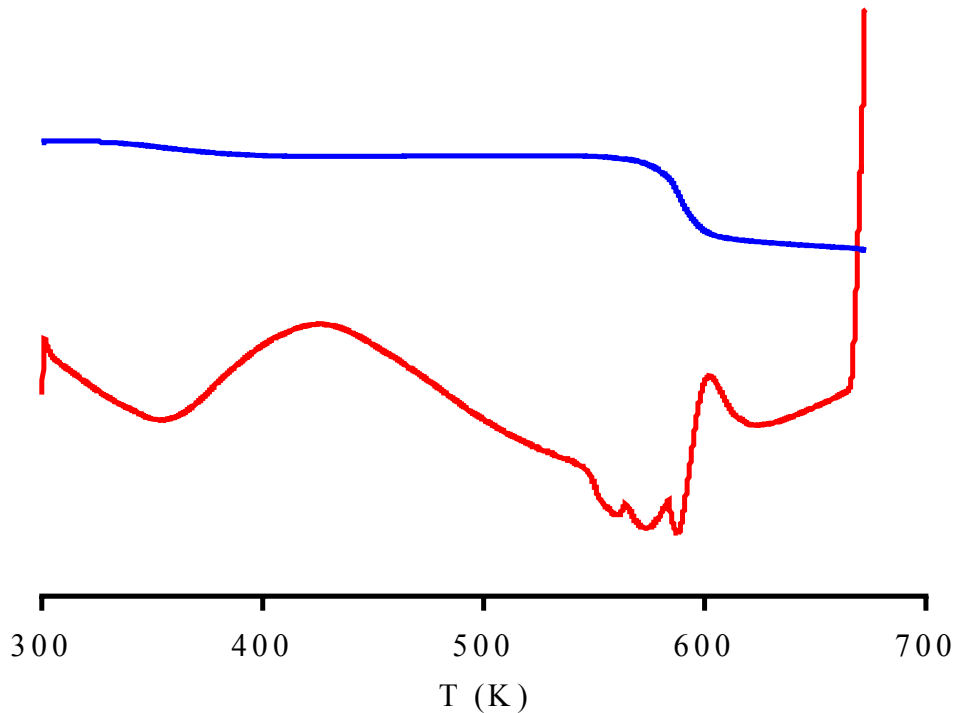


Figure 5.43 Mass loss profile (blue) and thermogram (red) of corn starch

The thermograms shown in Figure 5.44 exhibit a typical water evaporation endotherm up to 450 K, but the evaporation endotherm for glycerol is not clear. The exotherm present at 610 ± 1.0 K is suggestive of starch oxidation, which is not expected as the experiments were conducted with an N_2 atmosphere as stated in section 2.11.3. However, the samples were not prepared under a N_2 atmosphere and oxygen may be trapped within the sample. Sreedhar *et al.* found soluble starch decomposition started at 552 K through a one-step decomposition pattern, whereas commercially available MDF begins to decompose at approximately 523 K.^{121,122}

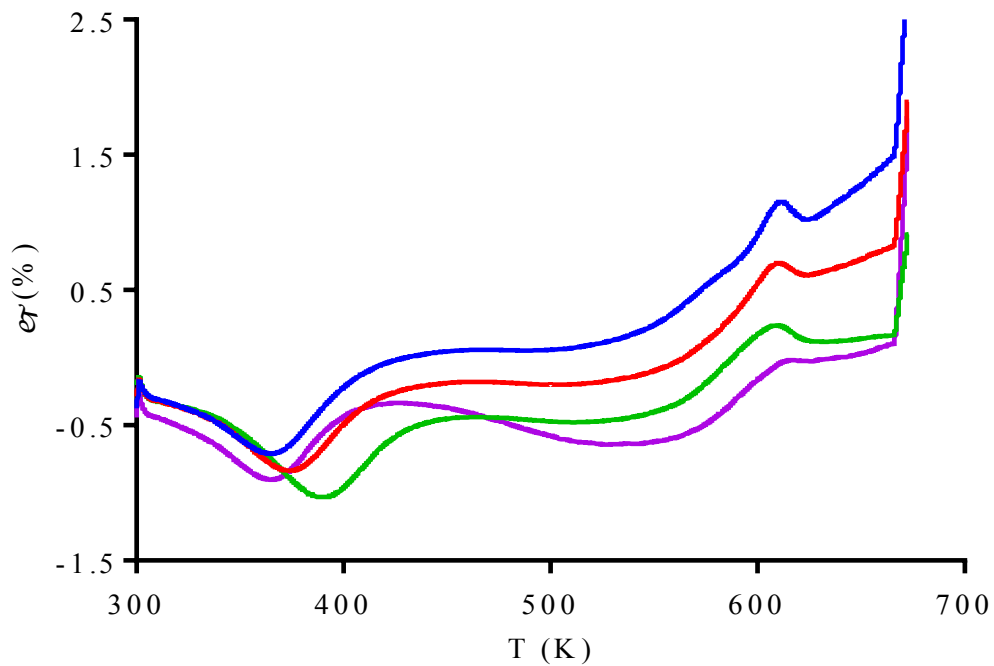


Figure 5.44 Thermograms of fibreboards containing 45 % w/w borax:glycerol that were pressed for: 0 min (blue), 5 min (red), 10 min (green) and 30 min (purple)

5.3.4. Pilot Scale production Medium Density Fibreboard

Utilising the resination process outlined in section 2.9.3, a 500 kg pilot scale trial was conducted. From the results shown in section 5.3.2, fibreboards prepared during the pilot scale trials consisted of 45 % wood fibre, 10 % starch and 45% 1:4 molar mixture of borax and glycerol, with a pressing time of 30 minutes. The exact details of the exact process are presented in section 2.10.2. Figure 5.45 shows 30 MDF boards prepared during the pilot scale trials, where all boards produced had the dimensions 1 x 1 x 0.015 m.



Figure 5.45 Photograph of large boards produced during pilot scale trials

The success of the pilot scale trials demonstrates that the current infrastructure can be utilised, without modification, for the large scale production of MDF utilising a plasticised starch as a binder. The pilot scale trials show: the plasticiser requires minimal synthesis, can be easily stored, and be aspirated at 40 °C as well as be easily handled and pre-formed before being pressed into a board.

5.4. Future Developments

The fibreboards manufactured from the pilot scale trials required a pressing time of 30 minutes, whereas fibreboards manufactured with formaldehyde-based resins typically require a pressing time of less than 5 minutes.¹²³ A pressing time of 30 minutes is not feasible on an industrial scale and further development is required to minimise the processing time. Figure 5.46 shows the temperature profiles of fibreboards prepared during the pilot scale trials, which suggests the fibreboards reach the set peak temperature of after 300 s. Figure 5.47 shows the pressure profiles of the same fibreboards and suggests full compression of the fibreboards can be achieved after 300 seconds. The transfer of heat and dissipation of pressure through the fibreboard suggests a theoretical minimum press time of 5 minutes. Tondi *et al.* found that fibreboards bound with a mixture of starch and sugar powder required a pressing time of 240 s suggesting a pressing of less than 300 s can be achieved.⁷⁵

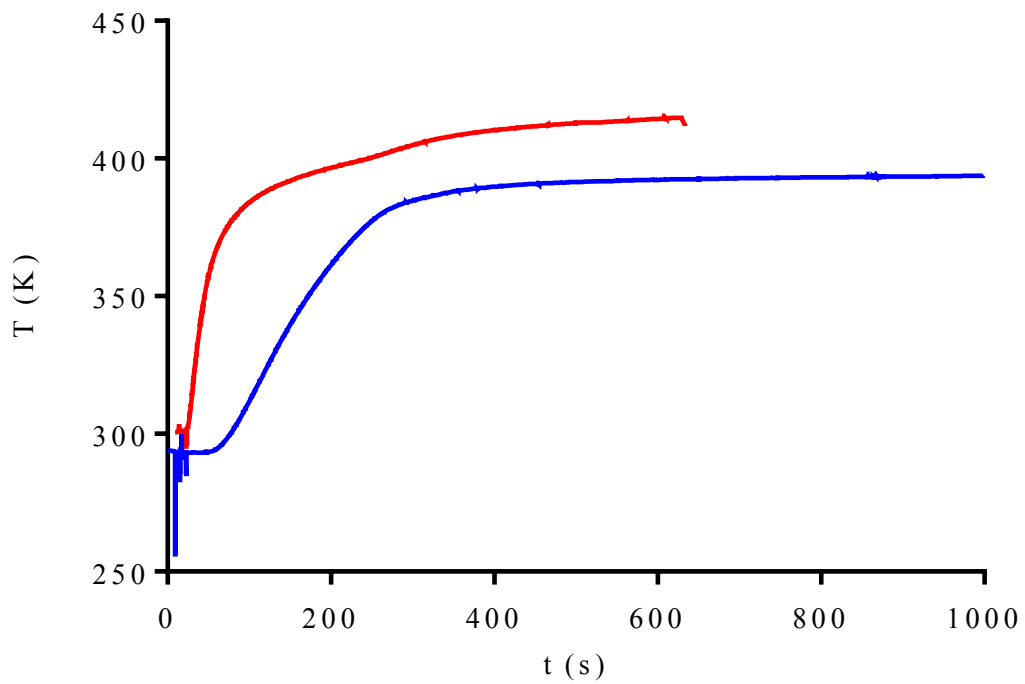


Figure 5.46 Temperature profile of pilot scale fibreboards: peak temperature 145 °C (blue), peak temperature 165 °C (red)

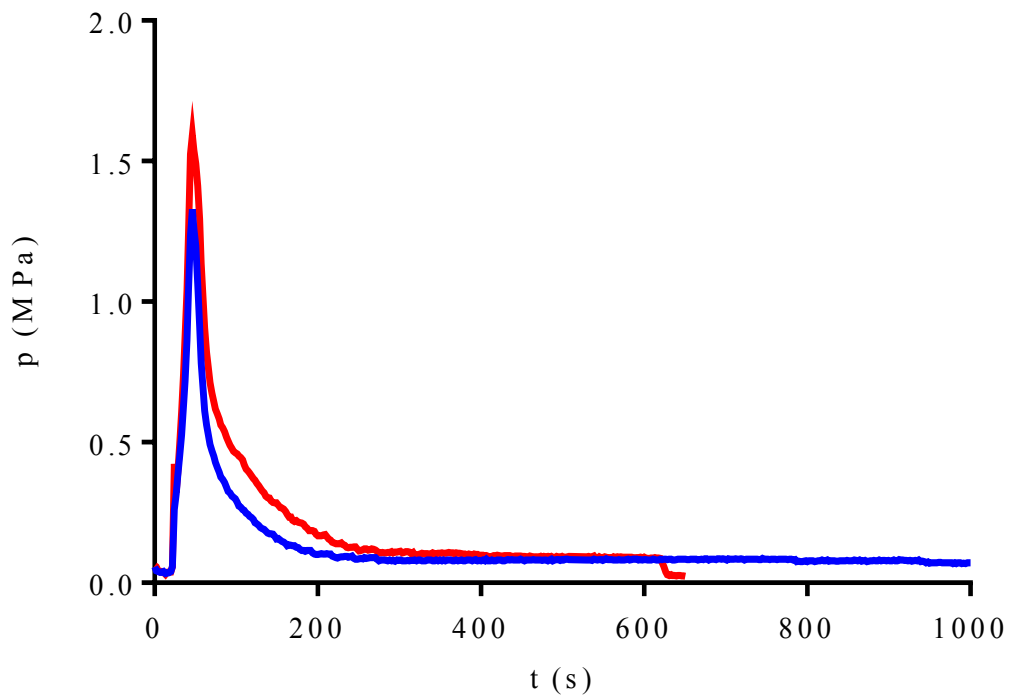


Figure 5.47 Pressure profile of pilot scale fibreboards: peak temperature 145 °C (blue), peak temperature 165 °C (red)

The corn starch and plasticiser contents make up for 55 % of the mass of the board, whereas MDF utilising formaldehyde-based resins are typically 15 % of the weight of the wood fibre used to furnish the board.¹²⁴ To be more suited to the aspiration systems equipped to commercial MDF production lines, the corn starch and plasticiser components need to be combined into a single component binder, which can be aspirated at similar quantities to the commercial process.

As well as a binder for MDF, starches plasticised with borax:glycerol mixtures could potentially be used as a general engineered wood binder, as formaldehyde-based adhesives are also used as binders for: PB, OSB and plywood. Figure 5.48 demonstrates that plasticised starches can be used to glue laminates and bind plywood, suggesting the potential application as a general-purpose wood adhesive.

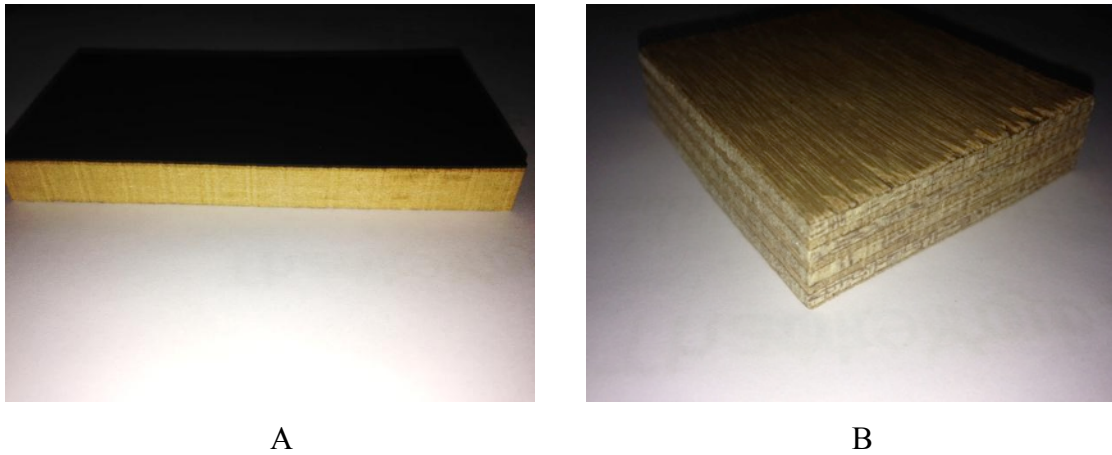


Figure 5.48 Plasticised corn starch used as a general purpose wood adhesive: For binding laminates (A) and for binding plywood (B)

5.5. Conclusions

It has been shown that glycerol-based, highly ionic solutions containing group I and II inorganic salts, are capable of plasticising corn starch into a thermoplastic material with gelation onset temperatures, which are similar to that of MUF resins. The starch gels formed have similar UTS to MUF resins thus making them desirable as binders for MDF.

Medium density fibreboards have been prepared using plasticised starch as a binder, although initial tests have shown that through poor mixing and distribution of plasticiser and starch, the physical properties of the boards were poor compared to commercially manufactured MDF. Adoption of a resination method involving the aspiration of plasticiser over a wood fibre- starch blend resulted in homogenous

fibreboards, that when pressed for 30 minutes gave UTS values comparable to commercially manufactured MDF. MDF bound by corn starch plasticised by a borax:glycerol mixture were able to pass EN 622 regulations with the exception of the 24 hour cyclic swell test. Failure of the cyclic swell test is not a surprise and suggests moisture can quickly penetrate into a fibreboard, which is crucial for biodegradation processes to take place.

Pilot scale production of starch plasticised MDF was successful, demonstrating the current industrial infrastructure can be utilised for large scale production at a similar cost to MDF bound with MUF resins. However, further developments are required to lower fibreboard pressing time from 30 min to the timescale is achieved commercially. Binder contents are significantly higher compared to MUF resins and further work is needed to reduce binder contents to 15-20 % of the wood fibre content.

5.6. References

-
- ¹T. G. Williamson, *APA Engineered-Wood Handbook*, McGraw-Hill, USA, 2002,
 - ² Whole Building Design Guide: Particleboard Green Report,
<https://www.wbdg.org/ccb/GREEN/REPORTS/cgrparticleboard.pdf> (Accessed August 2015)
 - ³ R. L. Youngs, *Forest and product plants Vol. II*, EOLSS, USA, 2001, Ch. 6, 131
 - ⁴ J. Wadsworth, *Wood Based Panels Int.*, 2007, **27**, 12
 - ⁵ R. C. Petterson, *The Chemistry of Solid Wood*, ACS, USA, 1984, Ch. 2, 57
 - ⁶ S. B. Leschine, *Annu Rev Microbiol.*, 1995, **49**, 399
 - ⁷ B. L. Browning, *The Chemistry of Wood*, Interscience, New York, 1963
 - ⁸ E. Sjöström, *Wood Chemistry: Fundamentals and Application*, Academic press, Orlando, 1993, 2nd ed
 - ⁹ E. J. Biblis, *Forest Products Journal*, 2000, **50**, 47
 - ¹⁰ S. H. Lee, W. C. Lum, A. Zaidon and M. Maminski, *Eur. J. Wood Prod.* 2015, **73**, 607
 - ¹¹ T. Kawasaki, M. Zhang and S. Kawai, *J Wood Sci*, 1998, **44**, 354
 - ¹² R. M. Rowell, *Handbook of Wood Chemistry And Wood Composites*, CRC Press, Florida, 2000, Ch. 10, 297
 - ¹³ E. J. Biblis, *Forest Products Journal*, 1989, **39**, 55

-
- ¹⁴ S. M. Nicole, C. Zhiyong and C. G. Charlie, *Wood handbook, Forest Products Laboratory*, USA, 2010, Ch. 11
- ¹⁵ J. A. Youngquist, *Wood-based Composites and Panel Products, Forest Products Laboratory*, USA, 1999, Ch 10
- ¹⁶ Wood Solutions <https://www.woodsolutions.com.au/Wood-Product-Categories/Plywood> (Accessed August 2015)
- ¹⁷ A. J. Kinloch, *Adhesion and Adhesives: Science and Technology*, Chapman & Hall, London, 1987, 1st ed.
- ¹⁸ W. Grigsby and A. Thumm, *Eur. J. Wood Wood Prod.*, 2012, **70**, 507
- ¹⁹ J. R. Fried, *Polymer Science and Technology*, Prentice Hall PTR, New Jersey, 1995
- ²⁰ R. B. Seymour and C. E. Carraher, *Seymour and Carraher's polymer chemistry*, M. Dekker, New York, 2003
- ²¹ I. Campbell, *Introduction to synthetic polymers*, Oxford University Press, Oxford, 2nd ed. 2000
- ²² L. Zhao, Y. Liu, Z. Xu, Y. Zhang, F. Zhao, And S. Zhang, *Forest Product*, 2011, **13**, 321
- ²³ A. Pizzi, and K. L. Mittal, *Handbook of Adhesives*, Mercel Dekker, New York, 2nd ed., 2003, Ch. 31, 635
- ²⁴ A. Pizzi, *Advanced Wood Adhesives Technology*, Mercel Dekker, New York, 1994
- ²⁵ Z. Cai and R. J. Ross, *Wood Handbook: wood as an Engineering Material*, Forest Products Laboratory, USA, Ch. 12, 2010, 280
- ²⁶ S. Tohmura, A. Inoue and S.H. Sahari, *J. Wood Sci.*, 2001, **47**, 451
- ²⁷ X. Lu and A. Pizzi, *Holz Roh Werkstoff*, 1998, **56**, 393
- ²⁸ P. Kavvouras, *Holz Als Roh-und Werkst.*, 1997, **55**, 323
- ²⁹ G. Myers, *For. Prod. J.*, 1984, **34**, 35
- ³⁰ C. Burton, L. Bradshaw, R. Agius, S. Burge, V. Huggins and D. Fishwick, *Occup. Med. Oxf.*, 2011, **61**, 357
- ³¹ A. Pizzi, and R. Marutzky, *Wood Adhesives: Chemistry and Technology*, Mercel Dekker, New York, Ch. 10, 1989, 307
- ³² IARC Monographs
<http://monographs.iarc.fr/ENG/Classification/ClassificationsCASOrder.pdf> (Accessed August 2015)
- ³³ G. D. Nielsen, S. T. Larsen and P. Wolkoff, *Arch. Toxicol.*, 2013, **87**, 73

-
- ³⁴ K. Umemura, A. Inoue and S. Kawai, *Journal of Wood Science*, 2003, **49**, 221
- ³⁵ Z. L. Que, T. Furuno, S. Katoh and Y. Nishino, *Build. Environ.*, 2007, **42**, 1257
- ³⁶ S. Boran, M. Usta and E. Gümüşkaya, *Int. J. Adhes. Adhes.*, 2011, **31**, 674
- ³⁷ S. Boran, M. Usta, S. Ondaral and E. Gümüşkaya, *Compos. Pt. B-Eng.*, 2012, **43**, 2487
- ³⁸ A. Pizzi and P. Tekely, *J. Appl. Polym. Sci.*, 1995, **56**, 1645
- ³⁹ S. H. Imam, L. Mao, L. Chen and R. V. Greene, *Starch*, 1999, **51**, 225
- ⁴⁰ A. Pizzi, *J. Adhes. Sci. Technol.*, 2006, **20**, 829
- ⁴¹ E. M. Ciannamea, P. M. Stefani and R. A. Ruseckaite, *Bioresource Technology*, 2010, **101**, 818
- ⁴² X. Mo, X.S. Sun, D. Wang, *J. Am. Oil Chem. Soc.*, 2004, **81**, 395
- ⁴³ J. Valenzuela, E. von Leyser, A. Pizzi, C. Westermeyer and B. Gorrini, *Eur. J. Wood Prod.*, 2012, **70**, 735
- ⁴⁴ S. Sowunmi, R. Ebewe, A. H. Conner And B. H. River, *Journal of Applied Polymer Science*, 1996, **62**, 577
- ⁴⁵ P. Widsten and A. Kandelbauer, *Biotechnology Advances*, 2008, **26**, 379
- ⁴⁶ S. Alavi, *Food Research International*, 2003, **36**, 307
- ⁴⁷ S. Janicki and A. Fiebica, *Pharmacy applications*, PZWL, Warsaw, 1996
- ⁴⁸ H. F. Zobel, *Starch*, 1988, **2**, 44
- ⁴⁹ M. Mitrus, PhD thesis, Lublin Agricultural University, Poland, 2004
- ⁵⁰ L. Janssen and L. Moscicki, *Thermoplastic Starch*, Wiley-VCH, Germany, 1st edition, 2009
- ⁵¹ T. Y. Bogracheva, Y. L. Wang, T. L. Wang and C. L. Hedley, *Biopolymers*, 2002, **64**, 268
- ⁵² R. L. Shogren, G. F. Fanta and W. M. Doane, *Starch*, 1993, **45**, 276
- ⁵³ T. Abolibda, PhD thesis, University of Leicester, 2015
- ⁵⁴ W. Aichholzer, H. G. Fritz, *Starch*, 1998, **50**, 77
- ⁵⁵ R. C. R. Souza and C. T. Andrade, *Advances in Polymer Technology*, 2002, **21**, 17
- ⁵⁶ J. J. G. Van Soest and J. F. G. Vliegthart, *Trends in Biotechnology*, 1997, **15**, 208
- ⁵⁷ J. J. G. Van Soest, S. H. D. Hulleman, D. De Wit and J. F. G. Vliegthart, *Carbohydrate Polymers*, 1996, **29**, 225
- ⁵⁸ J. M. Harper, *Food Technology*, 1986, **40**, 70
- ⁵⁹ L. Averous, L. Moro, P. Dole and C. Fringant, *Polymer*, 2000, **41**, 4157

-
- ⁶⁰ H. Li and M. A. Huneault, *J Appl Polym Sci*, 2011, **119**, 2439
- ⁶¹ M. Sjoqvist and P. Gatenholm, *Journal of Polymers and the Environment*, 2007, **15**, 43
- ⁶² X. Ma and J. Yu, *Carbohydr. Polym.*, 2004, **57**, 197
- ⁶³ Y. Zhang, C. Rempel and Q. Liu, *Crit. Rev. Food Sci. Nutr.*, 2014, **54**, 1353
- ⁶⁴ A. Mohammadi Nafchi, M. Moradpour, M. Saeidi and A. K. Alias, *Starch*, 2013, **65**, 61
- ⁶⁵ J. Yang, J. Yu and X. Ma, *Carbohydr. Polym.*, 2006, **66**, 110
- ⁶⁶ L. Chalmers, *Chemical Specialties: Domestic and Industrial Vol II*, Leonard Hill, London, 2nd ed., 1979
- ⁶⁷ ASI Adhesives Magazine <http://www.adhesivesmag.com/articles/84472-packaging-enduser-starch-and-dextrin-based-adhesives> (Accessed Aug 2015)
- ⁶⁸ B. H. William, *Corrugating and Adhesive Industries in Modified Starches: Properties and Uses*, CRC Press, Florida, 1986
- ⁶⁹ M. G. D. Baumann and A. H. Conner, *Handbook of Adhesive Technology, Revised and Expanded*, Marcel Dekker, New York, 2nd ed., 2003, Ch.22, 495
- ⁷⁰ Lazarus, D.M., *Adhesives and Adhesion Vol. 7*, Applied Science, London, 1983, Ch. 10, 197
- ⁷¹ M.H.M. Amini, R. Hashim, S. Hiziroglu, N. S. Sulaiman, O. Sulaiman, *Composites: Part B*, 2013, **50**, 259
- ⁷² A. H. Basta, H. El-Saied and V. F. Lotfy, *Pigment & Resin Technology*, 2013, **42**, 24
- ⁷³ P. Baishya, and T. K. Maji, *ACS Sustainable Chemistry & Engineering*, 2014, **2**, 1760
- ⁷⁴ E. Agnantopoulou, V. Tserki, S. Marras, J. Philippou and C. Panayiotou, *J Appl Polym Sci*, 2012, **126**, E272
- ⁷⁵ G. Tondi, S. Wieland, T. Wimmer, T. Schnabel and A. Petutschnigg, *Eur. J. Wood Wood Prod.*, 2012, **70**, 271
- ⁷⁶ A. P. Abbott, A. D. Ballantyne, J. P. Conde, K. S. Ryder and W. R. Wise, *Green Chem*, 2012, **14**, 1302
- ⁷⁷ E. Leroy, P. Jacquet, G. Coativy, A. L. Reguerre and D. Lourdin, *Carbohydr. Polym.*, 2012, **89**, 955
- ⁷⁸ A. P. Abbott, J. P. Conde, S. J. Davis and W. R. and Wise, *Green Chem*, 2012, **14**, 3067
- ⁷⁹ C. Barron, B. Bouchet, G. Della Valle, D. Gallant and V. Planchot, *J. Cereal Sci.*, 2001, **33**, 289

-
- ⁸⁰ N. Reddy and Y. Yang, *Carbohydrate Polymers*, 2013, **96**, 270
- ⁸¹ Alibaba, www.alibaba.com, (accessed August 2015)
- ⁸² Q. Li L. Zhang, Y. Ye and Q. Gao, *Food Hydrocolloids*, 2015, **51**, 468
- ⁸³ J. C. O'Brien, MChem Report, University of Leicester, 2013
- ⁸⁴ S. Kim, *J. Hazard. Mater.*, 2010, **182**, 919
- ⁸⁵ B. Sreedhar, M. Sairam, D. Chattopadhyay, P. Rathnam and D. Rao, *J Appl Polym Sci*, 2005, **96**, 1313
- ⁸⁶ Z. Qiao, J. Gu, Y. Zuo, H Tan and Y. Zhang, *Bioresources*, 2014, **9**, 6117
- ⁸⁷ Z. Qiao, J. Gu, S. Lv, J. Cao, H Tan and Y. Zhang, *Journal of Adhesion Science and Technology*, 2015, **29**, 1368
- ⁸⁸ J. Y. Han and R. T. Tyler, *Starch*, 2003, **55**, 457
- ⁸⁹ Y. Liu, C. Zhang, C. J. Zhang, Y. Guo, J. C. Zhao, L. Cui And P. Zhu, *Acta Polymerica Sinica*, 2015, **4**, 374
- ⁹⁰ X. Jiang, T. Jiang, L. Gan, X. Zhang, H. Dai and X. Zhang, *Carbohydrate Polymers*, 2012, **90**, 1677
- ⁹¹ M. Schirmer, M. Jekle And T. Becker, *Starch*, 2015, **67**, 30
- ⁹² S. Dumitriu, *Polysaccharides: structural diversity and functional versatility*, CRC Press, 2012
- ⁹³ F. B. Ahmad and P. A. Williams, *J. Agric. Food Chem.*, 1999, **47**, 3359
- ⁹⁴ W. D. Callister and D. G. Rethwisch, in *Materials Science and Engineering*, John Wiley & Sons, Asia, 8th Ed., 2011, Ch. 6, 156
- ⁹⁵ W. D. Callister and D. G. Rethwisch, in *Materials Science and Engineering*, John Wiley & Sons, Asia, 8th Ed., 2011, Ch. 15, 570
- ⁹⁶ S. H. D. Hulleman, F. H. P. Janssen and H. Fei, *Polymer*, 1998, **39**, 2043
- ⁹⁷ F. Chivrac, E. Pollet, P. Dole and L. Avérous, *Carbohydrate Polymers*, 2010, **79**, 941
- ⁹⁸ A. P. Abbott, T. Z. Abolibda, S. J. Davis, F. Emmerling, D. Lourdin, E. Leroy and W. R. Wise, *RSC Adv.*, 2014, **4**, 40421
- ⁹⁹ M. Sundin, Masters Thesis, Luleå University of Technology, 2007
- ¹⁰⁰ S. A. Osemeahon J. T. Barminas, *International Journal of Physical Sciences*, 2007, **2**, 169
- ¹⁰¹ C. Y. Hse, Z. H. Xia And B. Tomita, *Holzforschung*, 1994, **48**, 527
- ¹⁰² W. D. Callister and D. G. Rethwisch, in *Materials Science and Engineering*, John Wiley & Sons, Asia, 8th Ed., 2011, Ch. 16, 627

-
- ¹⁰³ K. P. R. Chowdary and D. K. Vijaya, *Asian Journal of Chemistry*, 2010, **22**, 5113
- ¹⁰⁴ A. Roy, J. Bajpai and A. K. Bajpai, *Carbohydrate Polymers*, 2009, **76**, 222
- ¹⁰⁵ M. A. Silva, A. C. K. Bierhalz and T. G. Kieckbusch, *Carbohydrate Polymers*, 2009, **77**, 736
- ¹⁰⁶ B. M. Gough and J. N. Pybus, *Starch*, 1973, **25**, 123
- ¹⁰⁷ K. Das, D. Ray, N. R. Bandyopadhyay, A. Gupta, S. Sengupta, S. Sahoo, A. Mohanty and M. Misra, *Ind. Eng. Chem. Res.* 2010, **49**, 2176
- ¹⁰⁸ Ashby, M.F. and Jones, D.R.H., in *Engineering Materials 2: an Introduction to Microstructures, Processing and Design*, Elsevier, oxford, 2nd ed., 1992, Ch. 3, 263.
- ¹⁰⁹ J. Yu, J. Gao and T. Lin, *Journal of Polymer Science*, 1996, **62**, 1491
- ¹¹⁰ A. H. Basta, H. El-Saied and V. F. Lotfy, *Pigment & Resin Technology*, 2013, **42**, 24
- ¹¹¹ R. L. Wu, X. L. Wang, F. Li, H. Z. Li and Y. Z. Wanga, *Bioresource Technology*, 2009, **100**, 2569
- ¹¹² X. Geng, S. Y. Zhang and James Deng, *Journal of Wood Chemistry and Technology*, 2006, **26**, 313
- ¹¹³ X. Li, Y. Li, Z. Zhong, D. Wang, J. A. Ratto, K. Sheng, X. S. Sun, *Bioresource Technology*, 2009, **100**, 3556
- ¹¹⁴ P. Widsten and A. Kandelbauer, *Journal of Adhesion Science and Technology*, 2014, **28**, 1256
- ¹¹⁵ Y. S. Stein And M. J. Antal Jr., *Journal of Analytical and Applied Pyrolysis*, 1983, **4**, 283
- ¹¹⁶ M. Watanabe, T. Iida, Y. Aizawa, T. M. Aida and H. Inomata, *Bioresource Technology*, 2007, **98**, 1285
- ¹¹⁷ S. Maiti, D. Ray, D. Mitra, A. Mukhopadhyay, *International Biodeterioration & Biodegradation*, 2013, **82**, 9
- ¹¹⁸ Y. Alesanco, J. Palenzuela, An. Viñuales, G. Cabañero, H. J. Grande and I. Odriozol, *ChemElectroChem* 2015, **2**, 218
- ¹¹⁹ Engineered Wood Products Association Of Australasia
http://www.ewp.asn.au/library/downloads/ewpaa_facts_about_pb_and_mdf.pdf
(Accessed August 2015)
- ¹²⁰ D. R. Lide, *CRC Handbook of Chemistry and Physics*, CRC press, Florida, 89th Ed., 2008, Ch. 3

-
- ¹²¹B. Sreedhar, M. Sairam, D. K. Chattopadhyay, P. A. Syamala Rathnam, D. V. Mohan Rao, *Journal of Applied Polymer Science*, 2005, **96**, 1313
- ¹²²K. Y, Li, C. M. Fleischmann and M. J. Spearpoint, *Chemical Engineering Science*, 2013, **95**, 211
- ¹²³ Y. No and M. G. Kim, *Journal of Applied Polymer Science*, 2005, **97**, 377
- ¹²⁴ W. J. Grigsby, J. P. Carpenter And R. Sargent, *Journal of Wood Chemistry and Technology*, 2014, **34**, 225

6. Conclusions and Future Work

6.1. Conclusions	207
6.2. Future Work	211

6.1. Conclusions

It has been shown that concentrated non-aqueous ionic mixtures can be prepared using alkali metal salts and glycerol, which have: densities, viscosities and ionic conductivities comparable to some DESs and ILs. All of the systems investigated showed Newtonian fluid behaviour over the shear rate range of the rotational viscometer used, except for the NaOAc:glycerol system where a shear thickening response was observed, which is also observed amongst protic ILs. The phase behaviour of all the sodium salt:glycerol mixtures do not show a eutectic composition, which may be linked to the super cooling ability of glycerol masking the true freezing temperatures, and a non-calorimetric technique may be able avoid problems caused by super cooling.

Investigations into Dole-Jones viscosity relationships, density and system free volume have been used to study the effect of salts on the structure of glycerol. In general, alkali metal salts have been shown to have a kosmotropic effect on the structure of glycerol, which is linked to salts increasing solvent-solvent interactions, and electrostriction. In contrast, QASs have a chaotropic effect on the structure of glycerol, which is linked to QASs disrupting the hydrogen bonding network in glycerol.

As a consequence of the kosmotropic properties of alkali metal salts, a characteristic decrease in conductivity is observed, which is supported by observed increases activation energy of fluid flow having a positive effect on the activation energy of conduction. At high salt concentrations, conductivity decreases upon salt addition suggesting a shift from an ion concentration limited, to a mobility limited ionic conductivity regime. Molar conductivity trends with respect to salt content follow the pattern of regimes outlined by Fuoss and Kraus with the exception of the $\text{Na}_2\text{B}_4\text{O}_7 \cdot 10\text{H}_2\text{O}$:glycerol system, where the waters of hydration are suspected to play an unknown role in the charge transport mechanism. The NaOAc:glycerol and NaBr:glycerol systems appear to only display the mobility-limited regime over the concentration range investigated, and lower concentrations would need to be studied to observe ion pairing effects.

Sodium salt:glycerol systems have Walden products slightly higher than what is typically seen for DESs and ILs, and appear above the *ideal* line on a logarithmic Walden plot. Systems that appear above the *ideal* line on a Walden plot are suggestive of an unknown charge transport mechanism, but further investigations are needed to understand this phenomenon.

PFG NMR has been utilised to probe the molecular dynamics and self-diffusion in sodium salt:glycerol systems, and has shown the systems investigated exhibit complex behaviour at the microscopic level. The self-diffusion coefficients of the systems investigated have been shown to be in the 10^{-11} - 10^{-13} m^2s^{-1} range, which is similar to many DES and IL systems. Within the NaBr:glycerol system, the glycerol aliphatic and hydroxyl protons appear to be diffusing together, whereas in the NaOAc:glycerol system the glycerol hydroxyl protons appear to be diffusing with the acetate anion.

There appears to be a clear link between system dynamic viscosity and the self-diffusivity of a species, however the role of water complicates the diffusion mechanism. Hydrate waters increase species self-diffusivity, and reduces the viscosity of the NaOAc.3H₂O:glycerol system however, water in this system appears to be more restricted compared to the Na₂B₄O₇.10H₂O:glycerol system. Hydrate waters appear to preferentially increase the diffusivity of the glycerol hydroxyl protons in the Na₂B₄O₇.10H₂O:glycerol system resulting in higher dynamic viscosity yet higher ionic conductivity. The relatively free water in the Na₂B₄O₇.10H₂O:glycerol system may be the cause of the increase in the system free volume.

Comparisons between PFG NMR diffusion studies and theoretical self-diffusion coefficients from the Stokes-Einstein relationship have been made. In all of the systems investigated, the Stokes-Einstein relationship underestimated the self-diffusion coefficients of all of the ¹H species probed. The most significant deviation from theory was observed for the glycerol hydroxyl/water exchange protons, suggesting a non-Stokesian transport mechanism for the Na₂B₄O₇.10H₂O:glycerol system.

The self-diffusion coefficients determined from PFG NMR were fitted to an Arrhenius model, and the activation energies of diffusivity were calculated, which were found to be similar to many DES and IL systems. The activation energies of diffusivity were cross-referenced with the activation energies of fluid flow and conduction, and were found to be slightly lower in magnitude but followed the same general trend.

The ¹H longitudinal T_1 relaxation times have been investigated using an inversion recovery pulse sequence, and all systems showed a transition from a diffusion limited, slow molecular tumbling regime to a fast molecular, high mobility, tumbling regime. A link between the tumbling regime transition temperature, viscosity and ion-ion interactions has been observed and agrees with observations made with other IL systems. The ²³Na T_1 relaxation times were found to be significantly faster than the ¹H containing species, and were found to be in the fast tumbling, high mobility regime over

the temperature range investigated. Water was found system to dramatically increase the ^{23}Na T_1 relaxation rate in the NaOAc.3H₂O:glycerol, whereas little effect was observed for the Na₂B₄O₇.10H₂O:glycerol system.

Sodium salt:glycerol mixtures have been shown to have electrochemical windows similar to type III DESs where a polyol has been utilised as a HBD. The positive limit of electrochemical windows of the systems investigated was restricted by the oxidation of glycerol at approximately 1.2 V, which is likely to be oxidised to glyceraldehyde. The negative limit of the electrochemical window is due to the reduction of hydroxyl groups to give hydrogen gas, which occurred at -0.7 V. Significant oxidation of the NaBr:glycerol system was observed at 0.85 V, which is due to the oxidation of the bromide anion to elemental bromine.

The redox behaviour of Copper has been investigated in sodium salt:glycerol systems and compared with a ChCl:glycerol DES. The NaBr:glycerol system was shown to stabilise the Cu^I species, which allowed the resolution of separate Cu^{II}/Cu^I and Cu^I/Cu⁰ redox couples. Stabilisation of the Cu^I species observed in chloride concentrated DESs and is a consequence of the [CuCl₄]²⁻ speciation, which suggests a [CuBr₄]²⁻ speciation for Cu^{II} in the NaBr:glycerol system. Both the Na₂B₄O₇.10H₂O and NaOAc:glycerol systems showed a single redox couple suggesting a Cu^{II}/Cu⁰ process, which implies the Cu^I species is not stabilised by these systems. The instability of the Cu^I species and lack of halide concentration suggests the [CuX₄]²⁻ speciation does not exist in these systems, and a more complex ion structure relating to the [Cu(OH₂)₆]²⁺ is expected.

Cu^{II} in a ChCl:glycerol DES shows a rapid, reversible electrochemical response and through application of the Randles-Sevcik relationship, the diffusion coefficient of the Cu^{II} species was deduced to be $1.55 \pm 0.07 \times 10^{-12} \text{ m}^2 \text{ s}^{-1}$. The Cu^{II} species in all of the sodium salt:glycerol mixtures of interest showed slow, irreversible electrochemistry, and as a consequence the Randles-Sevcik relationship is not valid, therefore deduction the diffusion coefficient was not possible. A microelectrode was employed in an attempt to generate a steady-state electrochemical response as an alternative method of determining the Cu^{II} diffusion coefficient, but absolute currents were smaller than the resolution of the potentiostat used, and diffusion coefficients were not determinable.

The low absolute peak currents during electrochemical experiments were a consequence of poor solubility of the Cu^{II} probe in the sodium salt:glycerol systems of interest, which has been attributed to the complex speciation resulting from the presence

of borate and acetate ligands. The speciation of Cu^{II} in the $\text{Na}_2\text{B}_4\text{O}_7 \cdot 10\text{H}_2\text{O}$:glycerol system is unknown, but a complex structure involving Cu-O-B bonds is likely due to the Cu^{2+} being Lewis acidic. The acetate anion probably acts as a bidentate ligand for Cu^{II} in the NaOAc:glycerol system and give a $[\text{Cu}(\text{OAc})_2]$ speciation, which is neutral and therefore poorly soluble. Poor solubility was experienced with a range of transition metal salts, which was also attributed to complex ion speciation in the $\text{Na}_2\text{B}_4\text{O}_7 \cdot 10\text{H}_2\text{O}$ and NaOAc:glycerol systems.

Poor solubility of a range of electrochemical probes suggests the sodium salt:glycerol systems studied are not ideal for electrochemical investigation, and adjustment of the system components is needed to provide media that are suitable for electrochemical processes.

It has been shown that glycerol-based, highly ionic solutions containing group I and II inorganic salts, are capable of plasticising corn starch into a thermoplastic material with gelation onset temperatures, which are similar to that of MUF resins. The starch gels formed have similar UTS to MUF resins thus making them desirable as binders for MDF.

Medium-density fibreboards have been prepared using plasticised starch as a binder, although initial tests have shown that through poor mixing and distribution of plasticiser and starch, the physical properties of the boards were poor compared to commercially manufactured MDF. Adoption of a resination method involving the aspiration of plasticiser over a wood fibre- starch blend resulted in homogenous fibreboards, that when pressed for 30 minutes gave UTS values comparable to commercially manufactured MDF. MDF bound by corn starch plasticised by a borax:glycerol mixture were able to pass EN 622 regulations with the exception of the 24 hour cyclic swell test. Failure of the cyclic swell test is not a surprise and suggests moisture can quickly penetrate into a fibreboard, which is crucial for biodegradation processes to take place.

Pilot scale production of starch plasticised MDF was successful, demonstrating the current industrial infrastructure can be utilised for large scale production at a similar cost to MDF bound with MUF resins. However, further developments are required to lower fibreboard pressing time from 30 minutes to the timescale is achieved commercially. Binder contents are significantly higher compared to MUF resins and further work is needed to reduce binder contents to 15-20 % of the wood fibre content.

6.2. Future Work

The investigations carried out in this section of the thesis require supplementary experimentation to give a deeper insight into the thermophysical properties of alkali metal salt:glycerol mixtures, as well as to gain a better understanding of the properties of DES and ILs. The research carried out thus far has left some questions unanswered, and adoption of other analytical techniques could be used to support current analyses.

Phase behaviour was investigated using DSC with the intention to deduce the eutectic composition of salt:glycerol systems however, a depression in glass transition temperatures was not observed for any sodium salt:glycerol system. Research into the phase behaviour of glycerol: water mixtures suggest the eutectic trends seen in the melting points of mixtures may not be observed in changes in glass transition temperatures. Unfortunately, due to the super-cooling ability of glycerol, measurements of the melting points of glycerol solutions are not viable by DSC and an alternative method is required to confirm observed phase behaviour. As liquid water freezes into ice, a change in the density-temperature profile is observed, which is common in many liquids therefore, changes in density could be used as a probe for the freezing temperature of system.

A limited number of sodium salts have been investigated, which have been chosen according to the justifications in section 3.2, and further investigations into other salt: HBD combinations may lead to useful replacements for aqueous electrolytes. IL and DES formation has utilised large, charge-diffuse species, and using sodium salts with large, charge diffuse anions may also provide interesting systems.

Complex metal speciation has restricted the application of electrochemical methods to probe the dynamics and diffusion behaviour of transition metals in sodium salt:glycerol mixtures. Copper, chromium, iron, zinc and silver all have spin active nuclei that could potentially be probed by PFG NMR, which could provide a non-electrochemical method of investigating ion dynamics and diffusion.

Ion speciation must be known to allow a deeper understanding of phenomena in physical properties, which can be investigated using EXAFS. To provide a preliminary insight into ion structure in solution, fast atom bombardment mass spectrometry (FAB-MS) can be used until synchrotron access can be granted. As well as providing detailed

speciation for novel systems, the knowledge gained can be used to predict the speciation of unknown systems.

Selection of the system components plays a critical role in determining physical properties, and alternatives are required. Utilisation of glycols with sodium salts may provide more electrochemically useful systems, with properties that may allow better speciation of transition metal salts, and may consequently be more suitable for electrochemical applications.

The fibreboards manufactured from the pilot scale trials required a pressing time of 30 minutes, whereas fibreboards manufactured with formaldehyde-based resins typically require a pressing time of less than 5 minutes. A pressing time of 30 minutes is not feasible on an industrial scale and further development is required to minimise the processing time. To be more suited to the aspiration systems equipped to commercial MDF production lines, the corn starch and plasticiser components need to be combined into a single component binder, which can be aspirated at similar quantities to the commercial process. As well as a binder for MDF, starches plasticised with borax:glycerol mixtures could potentially be used as a general engineered wood binder, as formaldehyde-based adhesives are also used as binders for: PB, OSB and plywood.

7. Appendices

7.1. Appendix A	214
7.2. Appendix B.....	230
7.3. Appendix C.....	235

7.1. Appendix A

Table 7.1 Quantities, densities and concentrations of salt-glycerol systems

Salt	Quantity (g)	Glycerol (g)	Density (g)	Concentration (mol dm ⁻³)
NaOAc	52.58	160.02	1.32	3.98
	42.13	161.06	1.32	3.34
	31.29	159.97	1.30	2.60
	20.83	160.25	1.28	1.80
	10.41	160.02	1.27	0.94
	11.81	226.85	1.26	0.76
	8.86	226.60	1.26	0.58
	5.91	226.83	1.26	0.39
	2.95	226.80	1.25	0.20
	1.12	226.80	1.25	0.08
	0.89	226.90	1.25	0.06
	0.59	226.80	1.25	0.04
	0.30	226.60	1.25	0.02
NaBr	52.30	161.04	1.46	3.48
	39.50	160.06	1.41	2.72
	26.15	159.18	1.35	1.85
	13.22	157.08	1.29	0.98
	14.82	226.75	1.31	0.78
	11.12	226.79	1.29	0.59
	7.42	226.75	1.28	0.39
	3.70	226.89	1.27	0.20
	1.48	226.57	1.26	0.08
	1.11	226.72	1.26	0.06
	0.72	226.86	1.26	0.04
	0.37	226.90	1.26	0.02
	Na ₂ B ₄ O ₇ ·10H ₂ O	152.35	126.33	1.41
114.38		126.28	1.38	1.72
152.61		252.35	1.35	1.34
76.20		251.76	1.30	0.79
61.52		252.38	1.31	0.67
45.82		252.42	1.29	0.52
31.17		251.67	1.28	0.37
15.25		252.27	1.28	0.19
6.14		250.71	1.27	0.08
4.54		252.13	1.27	0.06
3.08		250.39	1.25	0.04
1.51		252.07	1.25	0.02
NaOAc·3H ₂ O	80.95	151.60	1.27	2.83

	64.76	150.60	1.27	2.28
	64.76	200.86	1.27	1.65
	43.18	200.65	1.26	0.90
	24.29	225.20	1.26	0.74
	19.43	221.24	1.26	0.56
	14.57	225.87	1.26	0.38
	9.71	226.23	1.26	0.20
	5.40	250.22	1.26	0.08
	2.16	250.06	1.26	0.06
	1.62	250.99	1.26	0.04
	1.08	251.36	1.26	0.02
	0.54	250.18	1.27	2.83

Table 7.2 Quantities, densities and concentrations of DESs

Hydrogen bond donor	Quantity (g)	Choline chloride (g)	Density (g)	Concentration (mol dm ⁻³)
Glycerol	92.00	139.60	1.18	5.10
	184.00	139.60	1.20	3.70
	252.38	105.03	1.21	2.55
	252.46	83.65	1.22	2.17
	252.46	62.84	1.23	1.75
	252.67	41.60	1.24	1.25
	252.22	20.91	1.25	0.68
	252.54	16.64	1.25	0.55
	252.05	12.51	1.25	0.42
	252.02	8.30	1.26	0.29
	252.32	4.07	1.26	0.14
	252.26	1.65	1.26	0.06
	252.45	1.20	1.26	0.04
	252.16	0.81	1.26	0.03
	252.80	0.41	1.26	0.01
Ethylene glycol	124.12	139.60	1.13	4.27
	224.85	104.23	1.12	2.53
	224.41	83.80	1.12	2.17
	222.72	61.70	1.11	1.73
	223.14	41.86	1.11	1.26
	221.66	20.80	1.11	0.68
	221.69	16.82	1.11	0.56
	222.45	12.48	1.11	0.42
	220.46	8.38	1.11	0.29
	224.77	4.16	1.11	0.15
	223.69	1.66	1.11	0.06

	224.70	1.24	1.11	0.04
	224.25	0.82	1.11	0.03
	225.30	0.42	1.11	0.02

Table 7.3 Glass transition temperatures of DESs and salt:glycerol systems

NaOAc:glycerol			NaBr:glycerol			Na ₂ B ₄ O ₇ .10H ₂ O:glycerol		
c (mol dm ⁻³)	T _g (°C)	ΔT _g (°C)	c (mol dm ⁻³)	T _g (°C)	ΔT _g (°C)	c (mol dm ⁻³)	T _g (°C)	ΔT _g (°C)
3.97	-56.67	0.63	3.55	-67.28	0.28	2.02	-52.11	1.72
3.35	-60.81	0.29	2.75	-68.82	0.11	1.72	-59.31	0.65
2.60	-69.35	0.08	1.88	-75.32	0.32	1.34	-65.82	0.64
1.81	-70.64	0.03	0.99	-78.58	0.15	0.79	-75.90	0.44
0.95	-77.98	0.31	0.76	-80.39	0.10	0.67	-77.61	1.39
0.77	-78.29	0.19	0.58	-81.98	0.17	0.52	-80.40	0.11
0.58	-80.23	0.03	0.39	-83.09	0.09	0.37	-81.34	0.33
0.39	-80.38	0.08	0.20	-83.61	0.06	0.19	-84.06	0.16
0.20	-84.32	0.27	0.08	-82.82	0.24	0.08	-83.46	0.16
0.08	-83.62	0.48	0.06	-82.67	0.02	0.06	-83.15	0.37
0.06	-82.66	0.09	0.04	-82.92	0.02	0.04	-83.07	0.06
0.04	-82.83	0.04	0.02	-83.61	0.01	0.02	-84.98	0.25
0.02	-83.78	0.32						

Table 7.4 Glass transition temperatures of DESs and salt:glycerol systems

ChCl:glycerol			NaOAc.3H ₂ O:glycerol		
c (mol dm ⁻³)	T _g (°C)	ΔT _g (°C)	c (mol dm ⁻³)	T _g (°C)	ΔT _g (°C)
3.65	-96.60	0.45	2.83	-68.26	0.54
2.51	-94.50	0.43	2.28	-75.57	0.00
2.17	-93.27	0.08	1.65	-77.49	1.19
1.75	-91.88	0.18	0.90	-81.27	0.10
1.26	-90.72	0.25	0.74	-81.06	0.40
0.68	-87.77	0.15	0.56	-77.45	4.69
0.55	-87.48	0.35	0.38	-83.66	0.54
0.42	-86.45	0.47	0.20	-83.33	0.18
0.29	-85.62	0.35	0.08	-83.26	0.24
0.14	-86.59	0.08	0.06	-84.72	0.12
0.06	-87.94	0.48	0.04	-82.86	0.42
0.04	-84.32	0.40	0.02	-84.13	0.31
0.03	-86.48	0.45			
0.01	-84.80	0.25			

Table 7.5 Densities of DESs and salt:glycerol systems

NaOAc:glycerol			NaBr:glycerol			Na ₂ B ₄ O ₇ ·10H ₂ O:glycerol		
c (mol dm ⁻³)	ρ (g cm ⁻³)	Δρ (g cm ⁻³)	c (mol dm ⁻³)	ρ (g cm ⁻³)	Δρ (g cm ⁻³)	c (mol dm ⁻³)	ρ (g cm ⁻³)	Δρ (g cm ⁻³)
3.97	1.317	0.014	3.55	1.491	0.015	2.02	1.412	0.015
3.35	1.324	0.014	2.75	1.429	0.015	1.72	1.381	0.014
2.60	1.301	0.013	1.88	1.374	0.014	1.34	1.351	0.014
1.81	1.290	0.013	0.99	1.316	0.014	0.79	1.295	0.013
0.95	1.275	0.013	0.76	1.277	0.013	0.67	1.305	0.013
0.77	1.267	0.013	0.58	1.271	0.013	0.52	1.286	0.013
0.58	1.273	0.013	0.39	1.272	0.013	0.37	1.284	0.013
0.39	1.263	0.013	0.20	1.275	0.013	0.19	1.281	0.013
0.20	1.262	0.013	0.08	1.250	0.013	0.08	1.274	0.013
0.08	1.260	0.013	0.06	1.250	0.013	0.06	1.266	0.013
0.06	1.254	0.013	0.04	1.268	0.013	0.04	1.254	0.013
0.04	1.259	0.013	0.02	1.265	0.013	0.02	1.248	0.013
0.02	1.248	0.013						

Table 7.6 Densities of DESs and salt:glycerol systems

ChCl:glycerol			NaOAc.3H ₂ O:glycerol		
c (mol dm ⁻³)	ρ (g cm ⁻³)	Δρ (g cm ⁻³)	c (mol dm ⁻³)	ρ (g cm ⁻³)	Δρ (g cm ⁻³)
3.65	1.180	0.012	2.83	1.275	0.013
2.51	1.194	0.012	2.28	1.270	0.013
2.17	1.218	0.013	1.65	1.264	0.013
1.75	1.224	0.013	0.90	1.261	0.013
1.26	1.244	0.013	0.74	1.263	0.013
0.68	1.241	0.013	0.56	1.260	0.013
0.55	1.247	0.013	0.38	1.259	0.013
0.42	1.251	0.013	0.20	1.257	0.013
0.29	1.251	0.013	0.08	1.256	0.013
0.14	1.260	0.013	0.06	1.256	0.013
0.06	1.255	0.013	0.04	1.255	0.013
0.04	1.253	0.013	0.02	1.256	0.013
0.03	1.259	0.013			
0.01	1.260	0.013			

Table 7.7 Free volumes of DESs and salt:glycerol systems

NaOAc:glycerol			NaBr:glycerol			Na ₂ B ₄ O ₇ .10H ₂ O:glycerol		
c (M)	V _{free} (cm ³ mol ⁻¹)	ΔV _{free} (cm ³ mol ⁻¹)	c (M)	V _{free} (cm ³ mol ⁻¹)	ΔV _{free} (cm ³ mol ⁻¹)	c (M)	V _{free} (cm ³ mol ⁻¹)	ΔV _{free} (cm ³ mol ⁻¹)
3.97	15.86	0.20	3.55	14.15	0.22	2.02	27.29	0.37
3.35	16.14	0.20	2.75	15.73	0.23	1.72	25.44	0.33
2.60	16.52	0.19	1.88	16.25	0.21	1.34	23.26	0.29
1.81	16.91	0.19	0.99	16.81	0.20	0.79	20.81	0.24
0.95	17.36	0.19	0.76	17.00	0.20	0.67	20.23	0.23
0.77	17.46	0.19	0.58	17.11	0.19	0.52	19.67	0.22
0.58	17.56	0.19	0.39	17.21	0.19	0.37	19.11	0.21
0.39	17.66	0.18	0.20	17.33	0.18	0.19	18.48	0.19
0.20	17.77	0.18	0.08	17.42	0.18	0.08	18.12	0.19
0.08	17.84	0.18	0.06	17.43	0.18	0.06	18.06	0.19
0.06	17.84	0.18	0.04	17.44	0.18	0.04	18.00	0.19
0.04	17.85	0.18	0.02	17.45	0.18	0.02	17.94	0.18
0.02	17.87	0.18						

Table 7.8 Free volumes of DESs and salt:glycerol systems

ChCl:glycerol			NaOAc.3H ₂ O:glycerol		
c (M)	V _{free} (cm ³ mol ⁻¹)	ΔV _{free} (cm ³ mol ⁻¹)	c (M)	V _{free} (cm ³ mol ⁻¹)	ΔV _{free} (cm ³ mol ⁻¹)
3.65	20.50	0.28	2.83	10.68	0.02
2.51	20.11	0.25	2.28	12.18	0.02
2.17	19.62	0.24	1.65	13.89	0.02
1.75	19.10	0.23	0.90	15.85	0.02
1.26	18.51	0.21	0.74	16.27	0.01
0.68	18.39	0.20	0.56	16.71	0.01
0.55	18.27	0.20	0.38	17.16	0.01
0.42	18.14	0.19	0.20	17.63	0.01
0.29	18.01	0.19	0.08	17.91	0.01
0.14	17.93	0.19	0.06	17.96	0.01
0.06	17.91	0.18	0.04	18.01	0.01
0.04	17.90	0.18	0.02	18.06	0.01
0.03	17.89	0.18			
0.01	17.91	0.18			

Table 7.9 Viscosities of DESs and salt:glycerol systems

NaOAc:glycerol			NaBr:glycerol			Na ₂ B ₄ O ₇ .10H ₂ O:glycerol		
c (M)	η (cP)	Δ η cP)	c (M)	η (cP)	Δ η cP)	c (M)	η (cP)	Δ η cP)
3.98	16322	91	3.48	3393	42	2.02	1982	76
3.34	9816	56	2.71	2147	84	1.72	1500	25
2.60	4372	1018	1.85	1420	45	1.34	1103	18
1.80	3169	20	0.98	1063	23	0.79	817	6
0.94	2413	1049	0.78	1063	35	0.67	785	16
0.76	1719	68	0.59	1048	7	0.52	724	14
0.58	1322	7	0.39	919	58	0.37	694	27
0.39	1301	118	0.20	822	17	0.19	685	33
0.20	958	0	0.08	784	8	0.08	764	37
0.07	913	80	0.06	829	34	0.06	783	4
0.06	805	37	0.04	805	27	0.04	781	36
0.04	808	21	0.02	610	27	0.02	813	15
0.02	873	109						

Table 7.10 Viscosities of DESs and salt:glycerol systems

ChCl:glycerol			NaOAc.3H ₂ O:glycerol		
c (M)	η (cP)	$\Delta \eta$ (cP)	c (M)	η (cP)	$\Delta \eta$ (cP)
3.70	302	3	2.83	487	3
2.55	348	7	2.28	538	11
2.17	365	1	1.65	605	3
1.75	439	19	0.90	750	8
1.25	507	6	0.74	740	1
0.68	639	9	0.56	753	12
0.55	699	37	0.38	752	46
0.42	733	7	0.20	806	14
0.29	759	41	0.08	804	15
0.14	794	25	0.06	868	31
0.06	851	40	0.04	791	71
0.04	824	11	0.02	808	14
0.03	835	20			
0.01	818	18			

Table 7.11 Specific viscosities of DESs and salt:glycerol systems

NaOAc:glycerol			NaBr:glycerol			Na ₂ B ₄ O ₇ .10H ₂ O:glycerol		
\sqrt{c} (mol ^{1/2} dm ^{-3/2})	η_s/\sqrt{c} (dm ^{3/2} mol ^{-1/2})	$\Delta\eta_s/\sqrt{c}$ (dm ^{3/2} mol ^{-1/2})	\sqrt{c} (mol ^{1/2} dm ^{-3/2})	η_s/\sqrt{c} (dm ^{3/2} mol ^{-1/2})	$\Delta\eta_s/\sqrt{c}$ (dm ^{3/2} mol ^{-1/2})	\sqrt{c} (mol ^{1/2} dm ^{-3/2})	η_s/\sqrt{c} (dm ^{3/2} mol ^{-1/2})	$\Delta\eta_s/\sqrt{c}$ (dm ^{3/2} mol ^{-1/2})
0.97	1.918	0.844	0.97	0.271	0.007	0.89	-0.031	0.000
0.87	1.198	0.053	0.88	0.299	0.011	0.82	-0.081	0.002
0.77	0.745	0.008	0.76	0.322	0.004	0.72	-0.194	0.005
0.62	0.876	0.084	0.63	0.148	0.010	0.61	-0.288	0.013
0.45	0.312	0.002	0.44	-0.051	0.000	0.44	-0.422	0.023
0.28	0.306	0.028	0.28	-0.239	0.004	0.28	-0.325	0.017
0.24	-0.179	0.009	0.24	-0.056	0.003	0.24	-0.285	0.003
0.20	-0.197	0.006	0.20	-0.221	0.008	0.20	-0.356	0.018
0.14	0.271	0.035	0.14	-	-	0.14	-0.233	0.006

Table 7.12 Specific viscosities of DESs and salt:glycerol systems

ChCl:glycerol			NaOAc.3H ₂ O:glycerol		
\sqrt{c} (mol ^{1/2} dm ^{-3/2})	η_s/\sqrt{c} (dm ^{3/2} mol ^{-1/2})	$\Delta\eta_s/\sqrt{c}$ (dm ^{3/2} mol ^{-1/2})	\sqrt{c} (mol ^{1/2} dm ^{-3/2})	η_s/\sqrt{c} (dm ^{3/2} mol ^{-1/2})	$\Delta\eta_s/\sqrt{c}$ (dm ^{3/2} mol ^{-1/2})
0.83	-0.291		0.90	-0.120	0.002
0.74	-0.227	0.013	0.74	-0.162	0.001
0.65	-0.197	0.003	0.56	-0.186	0.001
0.54	-0.181	0.011	0.38	-0.275	0.018
0.38	-0.146	0.005	0.20	-0.212	0.005
0.24	-	-	0.08	-0.556	0.013
0.21	-0.098	0.002	0.06	-	-
0.17	-0.042	0.001	0.04	-	-
			0.02	-	-

Table 7.13 Dynamic viscosity as a function of viscometer spindle speed of DESs and salt:glycerol systems

ω (min ⁻¹)	NaOAc:glycerol		NaBr:glycerol		Na ₂ B ₄ O ₇ .10H ₂ O:glycerol		ChCl:glycerol	
	η (cP)	$\Delta\eta$ cP)	η (cP)	$\Delta\eta$ cP)	η (cP)	$\Delta\eta$ cP)	η (cP)	$\Delta\eta$ cP)
40	2166	24	1671	10	2130	0	394	3
50	2278	13	1656	1	2151	10	392	2
60	2416	6	1659	3	2181	10	391	2
70	2438	4	1656	4	2204	9	390	2
80	2462	4	1661	4	2244	8	385	1
90	2482	3	1666	0	2260	11	385	1
100	2511	3	1674	1	2250	11	385	1
110	2531	2	1680	1	2259	12	384	1
120	2564	0	1687	3	2252	16	384	0
130	2591	2	1712	0	2264	7	383	1
140	2628	2	1723	0	2267	8	381	1
150	2647	3	1724	1	2276	19	379	0
160	2747	6	1728	1	2276	13	378	0
170	2764	8	1729	0	2252	12	379	1
180	2777	10	1730	0	2240	9	381	0
190	-	-	1738	2	2226	7	380	0
200	-	-	1752	0	2233	7	377	0

Table 7.14 Dynamic viscosity as a function of viscometer spindle speed of DESs and salt:glycerol systems

NaOAc.3H ₂ O:glycerol			Glycerol		
ω (min ⁻¹)	η (cP)	$\Delta \eta$ cP)	ω (min ⁻¹)	η (cP)	$\Delta \eta$ (cP)
20	799	5	25	534	4
30	800	3	45	535	1
40	801	2	65	536	1
50	806	2	85	536	0
60	805	1	105	538	0
70	805	1	125	537	1
80	806	1	145	537	1
90	803	2	165	536	1
100	801	2	185	534	2
110	795	1	200	533	2
120	800	3			
130	801	4			
140	802	2			

Table 7.15 Activation energies of viscous flow of DESs and salt:glycerol systems

NaOAc:glycerol			NaBr:glycerol			Na ₂ B ₄ O ₇ .10H ₂ O:glycerol		
c (M)	E _a (kJ mol ⁻¹)	ΔE_a (kJ mol ⁻¹)	c (M)	E _a (kJ mol ⁻¹)	ΔE_a (kJ mol ⁻¹)	c (M)	E _a (kJ mol ⁻¹)	ΔE_a (kJ mol ⁻¹)
3.95	94.63	0.07	3.48	80.65	0.04	2.02	66.18	0.05
3.31	86.84	0.07	2.76	71.51	0.04	1.72	64.51	0.02
2.56	80.59	0.04	1.84	63.28	0.02	1.34	63.53	0.02
1.83	70.52	0.02	0.95	61.28	0.03	0.79	61.35	0.02
0.95	66.10	0.05	0.78	62.96	0.04	0.67	59.43	0.03
0.76	63.58	0.04	0.58	58.24	0.07	0.52	60.74	0.01
0.59	62.40	0.06	0.39	62.64	0.02	0.37	60.24	0.01
0.39	59.88	0.02	0.20	61.62	0.02	0.19	60.08	0.02
0.20	60.18	0.02	0.08	60.05	0.07	0.08	58.91	0.01
0.08	59.89	0.02	0.06	60.74	0.02	0.06	60.21	0.01
0.06	59.14	0.02	0.04	59.74	0.02	0.04	59.95	0.01
0.04	58.82	0.02	0.02	57.49	0.02	0.02	-	-
0.02	-	-						

Table 7.16 Activation energies of viscous flow of DESs and salt:glycerol systems

ChCl:glycerol			NaOAc.3H ₂ O:glycerol		
c (M)	E _a (kJ mol ⁻¹)	ΔE _a (kJ mol ⁻¹)	c (M)	E _a (kJ mol ⁻¹)	ΔE _a (kJ mol ⁻¹)
3.70	46.96	0.02	2.83	60.66	0.03
2.55	48.96	0.02	2.28	59.85	0.03
2.17	51.15	0.01	1.65	60.50	0.03
1.75	53.68	0.02	0.90	58.26	0.02
1.25	54.58	0.02	0.74	61.90	0.03
0.68	60.53	0.02	0.56	58.78	0.03
0.55	55.55	0.01	0.38	59.18	0.02
0.42	57.81	0.01	0.20	59.74	0.02
0.29	58.92	0.02	0.08	58.76	0.03
0.14	60.71	0.02	0.06	58.67	0.02
0.06	60.64	0.02	0.04	59.31	0.02
0.04	60.48	0.01	0.02	60.93	0.04
0.03	61.08	0.01			
0.01	70.18	0.03			

Table 7.17 Activation energies of ionic conduction of DESs and salt:glycerol systems

NaOAc:glycerol			NaBr:glycerol			Na ₂ B ₄ O ₇ .10H ₂ O:glycerol		
c (M)	E _a (kJ mol ⁻¹)	ΔE _a (kJ mol ⁻¹)	c (M)	E _a (kJ mol ⁻¹)	ΔE _a (kJ mol ⁻¹)	c (M)	E _a (kJ mol ⁻¹)	ΔE _a (kJ mol ⁻¹)
3.95	92.24	1.45	3.48	61.66	0.71	2.02	48.09	0.49
3.31	83.98	3.08	2.76	55.42	0.35	1.72	51.05	0.52
2.56	74.39	0.36	1.84	56.98	1.44	1.34	49.36	0.53
1.83	70.24	1.98	0.95	56.88	0.72	0.79	47.44	0.45
0.95	68.36	0.71	0.78	47.89	0.33	0.67	46.76	0.53
0.76	52.24	0.49	0.58	48.88	0.63	0.52	46.08	0.45
0.59	53.13	0.54	0.39	48.94	0.51	0.37	46.74	0.29
0.39	45.78	0.71	0.20	47.71	0.40	0.19	45.72	0.37
0.20	46.84	0.23	0.08	46.39	0.62	0.08	48.65	0.55
0.08	45.97	0.57	0.06	48.07	0.43	0.06	47.51	0.30
0.06	47.75	0.37	0.04	47.41	0.30	0.04	46.89	0.43
0.04	45.64	0.38	0.02	46.47	0.39	0.02	47.11	0.49
0.02	45.57	0.52						

Table 7.18 Activation energies of ionic conduction of DESs and salt:glycerol systems

ChCl:glycerol			NaOAc.3H ₂ O:glycerol		
c (M)	E _a (kJ mol ⁻¹)	ΔE _a (kJ mol ⁻¹)	c (M)	E _a (kJ mol ⁻¹)	ΔE _a (kJ mol ⁻¹)
3.70	36.82	0.29	2.83	52.90	0.31
2.55	40.12	0.39	2.28	51.01	0.41
2.17	39.42	0.39	1.65	52.42	0.33
1.75	41.50	0.33	0.90	49.59	0.26
1.25	44.52	0.56	0.74	46.80	0.22
0.68	47.02	0.61	0.56	48.39	0.26
0.55	49.69	0.73	0.38	50.40	0.45
0.42	53.42	0.85	0.20	48.71	0.34
0.29	51.82	0.84	0.08	46.30	0.53
0.14	52.06	0.60	0.06	46.25	0.97
0.06	53.65	0.90	0.04	-	-
0.04	52.85	0.93	0.02	-	-
0.03	54.90	1.22			
0.01	53.40	0.88			

Table 7.19 Ionic conductivities of DESs and salt:glycerol systems

NaOAc:glycerol			NaBr:glycerol			Na ₂ B ₄ O ₇ ·10H ₂ O:glycerol		
c (M)	κ (mS cm ⁻¹)	Δκ (mS cm ⁻¹)	c (M)	κ (mS cm ⁻¹)	Δκ (mS cm ⁻¹)	c (M)	κ (mS cm ⁻¹)	Δκ (mS cm ⁻¹)
3.95	6.55E-5	1.06E-6	3.48	3.47E-4	3.54E-7	2.02	6.53E-4	1.31E-5
3.31	8.00E-5	7.07E-7	2.76	4.11E-4	4.77E-5	1.72	5.59E-4	8.13E-6
2.56	8.40E-5	2.16E-6	1.84	3.25E-4	1.77E-5	1.33	4.39E-4	7.42E-6
1.83	1.35E-4	2.65E-5	0.95	2.44E-4	1.06E-5	0.79	2.71E-4	2.83E-6
0.95	9.56E-5	1.77E-7	0.78	1.57E-4	2.93E-6	0.67	2.26E-4	2.12E-6
0.76	9.42E-5	5.16E-6	0.58	1.31E-4	3.89E-6	0.52	1.73E-4	8.13E-7
0.59	7.95E-5	2.12E-6	0.39	9.18E-5	1.10E-6	0.37	1.14E-4	4.11E-6
0.39	5.86E-5	2.19E-6	0.20	5.11E-5	3.54E-8	0.19	5.05E-5	3.54E-8
0.20	3.76E-5	5.09E-6	0.08	2.21E-5	1.77E-7	0.08	2.29E-5	1.41E-7
0.08	1.55E-5	3.46E-7	0.06	1.59E-5	5.66E-8	0.06	1.84E-5	1.31E-7
0.06	1.19E-5	2.33E-7	0.04	1.05E-5	4.29E-8	0.04	1.10E-5	9.19E-8
0.04	8.33E-6	9.19E-8	0.02	6.75E-6	3.18E-8	0.02	5.75E-6	1.06E-7
0.02	4.21E-6	1.84E-7						

Table 7.20 Ionic conductivities of DESs and salt:glycerol systems

ChCl:glycerol			NaOAc.3H ₂ O:glycerol		
c (mol dm ⁻³)	κ (mS cm ⁻¹)	Δκ (mS cm ⁻¹)	c (mol dm ⁻³)	κ (mS cm ⁻¹)	Δκ (mS cm ⁻¹)
5.09	1.57E-3	6.36E-6	2.83	7.67E-4	5.66E-6
3.70	1.38E-3	1.32E-5	2.28	6.02E-4	2.12E-6
2.55	9.06E-4	7.07E-6	1.65	3.74E-4	4.95E-6
2.17	7.42E-4	4.24E-6	0.90	1.81E-4	1.06E-6
1.75	5.36E-4	4.95E-6	0.74	1.46E-4	9.19E-7
1.25	3.47E-4	3.89E-6	0.56	1.11E-4	1.27E-6
0.68	1.61E-4	7.07E-7	0.38	7.93E-5	7.78E-7
0.55	1.51E-4	7.42E-6	0.20	3.92E-5	3.54E-7
0.42	8.53E-5	1.77E-7	0.08	1.77E-5	3.54E-8
0.29	5.53E-5	4.95E-7	0.06	1.50E-5	4.08E-7
0.14	2.94E-5	6.01E-7	0.04	1.16E-5	9.19E-7
0.06	1.16E-5	1.06E-8	0.02	6.28E-6	4.24E-8
0.04	8.17E-6	2.12E-8			
0.03	5.54E-6	3.18E-8			
0.01	2.80E-6	7.07E-9			

Table 7.21 Molar conductivities of DESs and salt:glycerol systems

NaOAc:glycerol			NaBr:glycerol			Na ₂ B ₄ O ₇ .10H ₂ O:glycerol		
√c (mol ^{1/2} dm ^{-3/2})	Λ (S cm ² mol ⁻¹)	ΔΛ (S cm ² mol ⁻¹)	√c (mol ^{1/2} dm ^{-3/2})	Λ (S cm ² mol ⁻¹)	ΔΛ (S cm ² mol ⁻¹)	√c (mol ^{1/2} dm ^{-3/2})	Λ (S cm ² mol ⁻¹)	ΔΛ (S cm ² mol ⁻¹)
1.99	0.017	0.000	1.87	0.202	0.004	1.42	0.323	0.006
1.82	0.024	0.000	1.66	0.100	0.000	1.31	0.325	0.005
1.60	0.033	0.001	1.36	0.149	0.017	1.16	0.329	0.006
1.35	0.073	0.014	0.97	0.177	0.010	0.89	0.344	0.004
0.97	0.101	0.000	0.88	0.224	0.007	0.82	0.337	0.003
0.87	0.124	0.007	0.76	0.234	0.003	0.72	0.334	0.002
0.77	0.135	0.004	0.63	0.259	0.000	0.61	0.307	0.011
0.62	0.150	0.006	0.44	0.278	0.002	0.44	0.264	0.000
0.45	0.188	0.025	0.28	0.268	0.001	0.28	0.287	0.002
0.28	0.196	0.004	0.24	0.276	0.001	0.24	0.314	0.002
0.24	0.210	0.004	0.20	0.341	0.002	0.20	0.275	0.002
0.20	0.210	0.002				0.14	0.295	0.005
0.14	0.212	0.009						

Table 7.22 Molar conductivities of DESs and salt:glycerol systems

ChCl:glycerol			NaOAc.3H ₂ O:glycerol		
\sqrt{c} (mol ^{1/2} dm ^{-3/2})	Λ (S cm ² mol ⁻¹)	$\Delta\Lambda$ (S cm ² mol ⁻¹)	\sqrt{c} (mol ^{1/2} dm ^{-3/2})	Λ (S cm ² mol ⁻¹)	$\Delta\Lambda$ (S cm ² mol ⁻¹)
2.26	0.307	0.001	1.68	0.271	0.002
1.92	0.371	0.004	1.51	0.263	0.001
1.60	0.356	0.003	1.28	0.226	0.003
1.47	0.341	0.002	0.95	0.200	0.001
1.32	0.306	0.003	0.86	0.198	0.001
1.12	0.277	0.003	0.75	0.197	0.002
0.83	0.236	0.001	0.62	0.207	0.002
0.74	-	-	0.44	0.200	0.002
0.65	0.202	0.000	0.28	0.224	0.000
0.54	0.193	0.002	0.24	0.253	0.007
0.38	0.205	0.004	0.20	0.291	0.023
0.24	0.199	0.000	0.14	0.316	0.002
0.21	0.191	0.000			
0.17	0.192	0.001			
0.12	0.194	0.000			

Table 7.23 Walden plot data for DESs and salt:glycerol systems

NaOAc:glycerol			NaBr:glycerol			Na ₂ B ₄ O ₇ ·10H ₂ O:glycerol		
φ (P ⁻¹)	Λ (S g cm ⁻¹ mol ⁻¹)	$\Delta\Lambda$ (S g cm ⁻¹ mol ⁻¹)	φ (P ⁻¹)	Λ (S g cm ⁻¹ mol ⁻¹)	$\Delta\Lambda$ (S g cm ⁻¹ mol ⁻¹)	φ (P ⁻¹)	Λ (S g cm ⁻¹ mol ⁻¹)	$\Delta\Lambda$ (S g cm ⁻¹ mol ⁻¹)
0.190	0.474	0.040	0.349	0.860	0.016	0.256	0.718	0.025
0.175	0.457	0.045	0.323	0.826	0.036	0.237	0.678	0.015
0.161	0.438	0.048	0.300	0.810	0.046	0.219	0.630	0.019
0.148	0.418	0.051	0.278	0.767	0.050	0.202	0.608	0.017
0.135	0.396	0.051	0.257	0.737	0.043	0.186	0.570	0.013
0.124	0.370	0.050	0.238	0.691	0.065	0.172	0.543	0.014
0.114	0.351	0.051	0.220	0.656	0.065	0.158	0.512	0.008
0.104	0.326	0.048	0.203	0.602	0.051	0.146	0.490	0.014
0.096	0.302	0.044	0.188	0.570	0.050	0.134	0.461	0.007
0.087	0.279	0.040	0.174	0.548	0.060	0.124	0.436	0.009
0.080	0.251	0.044	0.160	0.495	0.044	0.114	0.403	0.003
0.073	0.225	0.046	0.148	0.457	0.037	0.105	0.387	0.011
0.067	0.203	0.045	0.136	0.433	0.039	0.096	0.362	0.007
0.061	0.182	0.042	0.126	0.395	0.031	0.088	0.340	0.006
0.056	0.164	0.038	0.116	0.359	0.024	0.081	0.315	0.007
0.051	0.149	0.034	0.107	0.336	0.024	0.074	0.296	0.001
0.046	0.132	0.031	0.098	0.306	0.022	0.068	0.282	0.005
0.042	0.120	0.027	0.090	0.279	0.017	0.062	0.263	0.006
0.038	0.105	0.024	0.083	0.254	0.014	0.057	0.240	0.006
0.035	0.095	0.019	0.076	0.230	0.011	0.052	0.223	0.003
0.032	0.085	0.017	0.070	0.204	0.011	0.048	0.206	0.004

Table 7.24 Walden plot data for DESs and salt:glycerol systems

ChCl:glycerol			NaOAc.3H ₂ O:glycerol		
ϕ (P ⁻¹)	Λ (S g cm ⁻¹ mol ⁻¹)	$\Delta\Lambda$ (S g cm ⁻¹ mol ⁻¹)	ϕ (P ⁻¹)	Λ (S g cm ⁻¹ mol ⁻¹)	$\Delta\Lambda$ (S g cm ⁻¹ mol ⁻¹)
0.946	0.865	0.002	0.828	0.911	0.053
0.890	0.830	0.006	0.771	0.853	0.046
0.837	0.793	0.008	0.718	0.800	0.040
0.787	0.732	0.015	0.668	0.749	0.034
0.739	0.711	0.005	0.621	0.702	0.030
0.694	0.676	0.002	0.577	0.658	0.025
0.652	0.645	0.005	0.536	0.633	0.045
0.612	0.623	0.001	0.498	0.573	0.011
0.574	0.593	0.002	0.462	0.535	0.006
0.538	0.564	0.007	0.428	0.499	0.008
0.505	0.545	0.004	0.397	0.469	0.003
0.473	0.512	0.006	0.368	0.444	0.001
0.443	0.496	0.004	0.341	0.418	0.004
0.415	0.468	0.003	0.316	0.393	0.007
0.388	0.431	0.003	0.292	0.368	0.003
0.363	0.421	0.002	0.270	0.350	0.002
0.339	0.392	0.003	0.250	0.322	0.001
0.317	0.373	0.001	0.231	0.302	0.002
0.296	0.350	0.001	0.213	0.283	0.005
0.277	0.334	0.002	0.197	0.262	0.001
0.258	0.313	0.002	0.181	0.253	0.001

7.2. Appendix B

Table 7.25 Stokes-Einstein relationship data for the NaOAc:glycerol system

$1/T$ (1000 K ⁻¹)	D_{OH} (m ² s ⁻¹)	ΔD_{OH} (m ² s ⁻¹)	$D_{Aliph.}$ (m ² s ⁻¹)	$\Delta D_{Aliph.}$ (m ² s ⁻¹)	$D_{Acetate}$ (m ² s ⁻¹)	$\Delta D_{Acetate}$ (m ² s ⁻¹)
2.98	1.18E-11	2.01E-13	6.99E-12	1.19E-13	7.96E-12	1.36E-13
2.99	1.09E-11	1.86E-13	6.46E-12	1.10E-13	7.36E-12	1.25E-13
2.99	1.01E-11	1.73E-13	5.97E-12	1.02E-13	6.80E-12	1.16E-13
3.00	9.33E-12	1.60E-13	5.52E-12	9.44E-14	6.28E-12	1.07E-13
3.01	8.62E-12	1.48E-13	5.09E-12	8.73E-14	5.80E-12	9.94E-14
3.02	7.95E-12	1.36E-13	4.70E-12	8.07E-14	5.35E-12	9.18E-14
3.03	7.34E-12	1.26E-13	4.34E-12	7.45E-14	4.94E-12	8.48E-14
3.04	6.77E-12	1.16E-13	4.00E-12	6.88E-14	4.55E-12	7.83E-14
3.05	6.23E-12	1.07E-13	3.69E-12	6.35E-14	4.20E-12	7.23E-14
3.06	5.74E-12	9.91E-14	3.40E-12	5.86E-14	3.87E-12	6.67E-14
3.07	5.29E-12	9.14E-14	3.13E-12	5.40E-14	3.56E-12	6.15E-14
3.08	4.87E-12	8.42E-14	2.88E-12	4.98E-14	3.27E-12	5.67E-14
3.09	4.48E-12	7.76E-14	2.65E-12	4.59E-14	3.01E-12	5.22E-14
3.10	4.11E-12	7.14E-14	2.43E-12	4.22E-14	2.77E-12	4.81E-14
3.11	3.78E-12	6.57E-14	2.23E-12	3.89E-14	2.54E-12	4.42E-14
3.12	3.47E-12	6.05E-14	2.05E-12	3.57E-14	2.34E-12	4.07E-14
3.13	3.19E-12	5.56E-14	1.88E-12	3.29E-14	2.14E-12	3.74E-14
3.13	2.92E-12	5.11E-14	1.73E-12	3.02E-14	1.97E-12	3.44E-14
3.14	2.68E-12	4.69E-14	1.58E-12	2.77E-14	1.80E-12	3.16E-14
3.15	2.46E-12	4.30E-14	1.45E-12	2.54E-14	1.65E-12	2.90E-14
3.16	2.25E-12	3.95E-14	1.33E-12	2.33E-14	1.51E-12	2.66E-14
3.17	2.06E-12	3.62E-14	1.22E-12	2.14E-14	1.39E-12	2.44E-14
3.18	1.88E-12	3.32E-14	1.11E-12	1.96E-14	1.27E-12	2.23E-14
3.19	1.72E-12	3.04E-14	1.02E-12	1.80E-14	1.16E-12	2.04E-14
3.21	1.57E-12	2.78E-14	9.31E-13	1.64E-14	1.06E-12	1.87E-14
3.22	1.44E-12	2.54E-14	8.50E-13	1.50E-14	9.68E-13	1.71E-14
3.23	1.31E-12	2.33E-14	7.76E-13	1.37E-14	8.84E-13	1.57E-14
3.24	1.20E-12	2.13E-14	7.08E-13	1.26E-14	8.06E-13	1.43E-14
3.25	1.09E-12	1.94E-14	6.46E-13	1.15E-14	7.35E-13	1.31E-14
3.26	9.95E-13	1.77E-14	5.88E-13	1.05E-14	6.70E-13	1.19E-14

Table 7.26 Stokes-Einstein relationship data for the NaBr:glycerol system

$1/T$ (1000 K ⁻¹)	D_{OH} (m ² s ⁻¹)	ΔD_{OH} (m ² s ⁻¹)	$D_{\text{Aliph.}}$ (m ² s ⁻¹)	$\Delta D_{\text{Aliph.}}$ (m ² s ⁻¹)
2.98	1.87E-11	3.37E-13	1.11E-11	1.99E-13
2.99	1.74E-11	3.14E-13	1.03E-11	1.86E-13
2.99	1.62E-11	2.93E-13	9.60E-12	1.73E-13
3.00	1.51E-11	2.73E-13	8.94E-12	1.62E-13
3.01	1.41E-11	2.55E-13	8.32E-12	1.51E-13
3.02	1.31E-11	2.37E-13	7.74E-12	1.40E-13
3.03	1.22E-11	2.21E-13	7.20E-12	1.31E-13
3.04	1.13E-11	2.06E-13	6.69E-12	1.22E-13
3.05	1.05E-11	1.91E-13	6.21E-12	1.13E-13
3.06	9.76E-12	1.78E-13	5.77E-12	1.05E-13
3.07	9.06E-12	1.65E-13	5.36E-12	9.78E-14
3.08	8.41E-12	1.54E-13	4.97E-12	9.09E-14
3.09	7.80E-12	1.43E-13	4.61E-12	8.44E-14
3.10	7.23E-12	1.33E-13	4.27E-12	7.84E-14
3.11	6.70E-12	1.23E-13	3.96E-12	7.27E-14
3.12	6.20E-12	1.14E-13	3.67E-12	6.74E-14
3.13	5.74E-12	1.06E-13	3.39E-12	6.25E-14
3.13	5.31E-12	9.80E-14	3.14E-12	5.79E-14
3.14	4.91E-12	9.08E-14	2.90E-12	5.37E-14
3.15	4.54E-12	8.41E-14	2.68E-12	4.97E-14
3.16	4.20E-12	7.78E-14	2.48E-12	4.60E-14
3.17	3.87E-12	7.19E-14	2.29E-12	4.25E-14
3.18	3.58E-12	6.65E-14	2.11E-12	3.93E-14
3.19	3.30E-12	6.14E-14	1.95E-12	3.63E-14
3.21	3.04E-12	5.67E-14	1.80E-12	3.35E-14
3.22	2.80E-12	5.24E-14	1.66E-12	3.10E-14
3.23	2.58E-12	4.83E-14	1.53E-12	2.86E-14
3.24	2.38E-12	4.46E-14	1.41E-12	2.63E-14
3.25	2.19E-12	4.11E-14	1.29E-12	2.43E-14
3.26	9.24E-13	1.76E-14	5.46E-13	1.04E-14

Table 7.27 Stokes-Einstein relationship data for the $\text{Na}_2\text{B}_4\text{O}_7 \cdot 10\text{H}_2\text{O}$:glycerol system

$1/T$ (1000 K^{-1})	D_{OH} ($\text{m}^2 \text{s}^{-1}$)	ΔD_{OH} ($\text{m}^2 \text{s}^{-1}$)	$D_{\text{Aliph.}}$ ($\text{m}^2 \text{s}^{-1}$)	$\Delta D_{\text{Aliph.}}$ ($\text{m}^2 \text{s}^{-1}$)
2.98	1.46E-11	5.44E-13	8.63E-12	3.22E-13
2.99	1.36E-11	5.06E-13	8.01E-12	2.99E-13
2.99	1.26E-11	4.71E-13	7.44E-12	2.78E-13
3.00	1.17E-11	4.38E-13	6.91E-12	2.59E-13
3.01	1.08E-11	4.07E-13	6.41E-12	2.40E-13
3.02	1.01E-11	3.78E-13	5.94E-12	2.23E-13
3.03	9.32E-12	3.50E-13	5.51E-12	2.07E-13
3.04	8.63E-12	3.25E-13	5.10E-12	1.92E-13
3.05	7.99E-12	3.02E-13	4.72E-12	1.78E-13
3.06	7.40E-12	2.80E-13	4.37E-12	1.65E-13
3.07	6.85E-12	2.59E-13	4.05E-12	1.53E-13
3.08	6.33E-12	2.40E-13	3.74E-12	1.42E-13
3.09	5.85E-12	2.22E-13	3.46E-12	1.31E-13
3.10	5.41E-12	2.06E-13	3.20E-12	1.21E-13
3.11	4.99E-12	1.90E-13	2.95E-12	1.12E-13
3.12	4.61E-12	1.76E-13	2.72E-12	1.04E-13
3.13	4.25E-12	1.62E-13	2.51E-12	9.60E-14
3.13	3.92E-12	1.50E-13	2.32E-12	8.86E-14
3.14	3.61E-12	1.38E-13	2.14E-12	8.18E-14
3.15	3.33E-12	1.28E-13	1.97E-12	7.55E-14
3.16	3.06E-12	1.18E-13	1.81E-12	6.96E-14
3.17	2.82E-12	1.09E-13	1.67E-12	6.41E-14
3.18	2.59E-12	1.00E-13	1.53E-12	5.91E-14
3.19	2.38E-12	9.20E-14	1.41E-12	5.44E-14
3.21	2.19E-12	8.47E-14	1.29E-12	5.01E-14
3.22	2.01E-12	7.79E-14	1.19E-12	4.60E-14
3.23	1.85E-12	7.16E-14	1.09E-12	4.23E-14
3.24	1.69E-12	6.58E-14	1.00E-12	3.89E-14
3.25	1.55E-12	6.04E-14	9.18E-13	3.57E-14
3.26	1.42E-12	5.54E-14	8.41E-13	3.28E-14

Table 7.28 Stokes-Einstein relationship data for the NaOAc.3H₂O:glycerol system

$1/T$ (10^3 K^{-1})	D_{OH} ($\text{m}^2 \text{ s}^{-1}$)	ΔD_{OH} ($\text{m}^2 \text{ s}^{-1}$)	$D_{\text{Aliph.}}$ ($\text{m}^2 \text{ s}^{-1}$)	$\Delta D_{\text{Aliph.}}$ ($\text{m}^2 \text{ s}^{-1}$)	D_{Acetate} ($\text{m}^2 \text{ s}^{-1}$)	$\Delta D_{\text{Acetate}}$ ($\text{m}^2 \text{ s}^{-1}$)
2.98	4.15E-11	9.63E-13	2.45E-11	5.69E-13	2.79E-11	6.48E-13
2.99	3.88E-11	9.02E-13	2.29E-11	5.33E-13	2.61E-11	6.07E-13
2.99	3.63E-11	8.44E-13	2.14E-11	4.99E-13	2.44E-11	5.68E-13
3.00	3.39E-11	7.90E-13	2.00E-11	4.67E-13	2.28E-11	5.32E-13
3.01	3.17E-11	7.39E-13	1.87E-11	4.37E-13	2.13E-11	4.97E-13
3.02	2.96E-11	6.91E-13	1.75E-11	4.08E-13	1.99E-11	4.65E-13
3.03	2.76E-11	6.46E-13	1.63E-11	3.82E-13	1.86E-11	4.35E-13
3.04	2.58E-11	6.04E-13	1.52E-11	3.57E-13	1.73E-11	4.06E-13
3.05	2.40E-11	5.64E-13	1.42E-11	3.33E-13	1.62E-11	3.79E-13
3.06	2.24E-11	5.26E-13	1.32E-11	3.11E-13	1.51E-11	3.54E-13
3.07	2.09E-11	4.91E-13	1.23E-11	2.90E-13	1.40E-11	3.31E-13
3.08	1.94E-11	4.58E-13	1.15E-11	2.71E-13	1.31E-11	3.08E-13
3.09	1.81E-11	4.27E-13	1.07E-11	2.52E-13	1.22E-11	2.87E-13
3.10	1.68E-11	3.98E-13	9.95E-12	2.35E-13	1.13E-11	2.68E-13
3.11	1.57E-11	3.71E-13	9.26E-12	2.19E-13	1.05E-11	2.50E-13
3.12	1.46E-11	3.45E-13	8.61E-12	2.04E-13	9.80E-12	2.32E-13
3.13	1.35E-11	3.21E-13	8.00E-12	1.90E-13	9.11E-12	2.16E-13
3.13	1.26E-11	2.99E-13	7.43E-12	1.77E-13	8.46E-12	2.01E-13
3.14	1.17E-11	2.78E-13	6.90E-12	1.64E-13	7.86E-12	1.87E-13
3.15	1.08E-11	2.59E-13	6.41E-12	1.53E-13	7.29E-12	1.74E-13
3.16	1.01E-11	2.40E-13	5.94E-12	1.42E-13	6.77E-12	1.62E-13
3.17	9.32E-12	2.23E-13	5.51E-12	1.32E-13	6.27E-12	1.50E-13
3.18	8.64E-12	2.07E-13	5.11E-12	1.22E-13	5.82E-12	1.39E-13
3.19	8.00E-12	1.92E-13	4.73E-12	1.14E-13	5.39E-12	1.29E-13
3.21	7.41E-12	1.78E-13	4.38E-12	1.05E-13	4.99E-12	1.20E-13
3.22	6.86E-12	1.65E-13	4.06E-12	9.77E-14	4.62E-12	1.11E-13
3.23	6.35E-12	1.53E-13	3.75E-12	9.05E-14	4.27E-12	1.03E-13
3.24	5.87E-12	1.42E-13	3.47E-12	8.38E-14	3.95E-12	9.54E-14
3.25	5.42E-12	1.31E-13	3.21E-12	7.76E-14	3.65E-12	8.83E-14
3.26	5.01E-12	1.21E-13	2.96E-12	7.18E-14	3.37E-12	8.17E-14
2.98	4.62E-12	1.12E-13	2.73E-12	6.64E-14	3.11E-12	7.56E-14

Table 7.29 ^{23}Na T_1 relaxation times for salt:glycerol systems

T (K)	T_1 (μs)			
	1.80 M NaOAc:glycerol	1.88 M NaBr: glycerol	2.02M $\text{Na}_2\text{B}_4\text{O}_7 \cdot 10\text{H}_2\text{O}$:glycerol	2.28M NaOAc. $3\text{H}_2\text{O}$:glycerol
298	194	198	283	230
308	186	213	300	286
318	200	256	327	380
328	242	352	366	534
338	308	477	414	753

Table 7.30 Quantities and concentrations of copper solutions in ionic solvents

Ionic solvent	Copper salt	Salt mass (mg)	Solvent mass (g)	Concentration (mM)
2.17 M CuCl_2 in glycerol	CuCl_2	11.0	21.95	5.43
	CuCl_2	110.4	20.30	49.98
	CuCl_2	2752	51.20	498.4
	CuBr_2	17.8	20.63	4.85
	CuBr_2	4310	51.96	469.9
	$\text{Cu}(\text{OAc})_2$	15.5	21.45	5.20
	$\text{Cu}(\text{OAc})_2$	3506	50.65	470.1
1.88 M NaBr in glycerol	CuCl_2	9.3	21.61	4.75
	CuCl_2	84.8	20.58	43.33
	CuCl_2	2335	51.66	477.2
	CuBr_2	18.4	20.99	5.54
	CuBr_2	3961	50.06	487.3
	$\text{Cu}(\text{OAc})_2$	14.8	21.21	5.60
	$\text{Cu}(\text{OAc})_2$	3195	51.15	483.3
2.02 M $\text{Na}_2\text{B}_4\text{O}_7 \cdot 10\text{H}_2\text{O}$ in glycerol	CuCl_2	9.7	20.23	5.09
	CuCl_2	84.5	21.09	44.37
	CuCl_2	2350	50.25	493.5
	CuBr_2	15.3	21.08	4.84
	CuBr_2	3587	50.36	453.5
	$\text{Cu}(\text{OAc})_2$	13.8	1.030	5.36
	$\text{Cu}(\text{OAc})_2$	2898	51.90	450.6
1.80 M NaOAc in glycerol	CuCl_2	10.2	20.44	4.89
	CuCl_2	94.8	21.36	45.47
	CuCl_2	2387	51.79	458.1
	CuBr_2	18.3	21.47	5.28
	CuBr_2	4137	50.58	477.9
	$\text{Cu}(\text{OAc})_2$	13.2	20.41	4.69

		Cu(OAc) ₂	3470	51.82	492.8
2.28 M NaOAc.3H ₂ O in glycerol		CuCl ₂	10.2	21.45	4.81
		CuCl ₂	105.8	20.97	37.0
		CuCl ₂	2578	50.27	487.0
		CuBr ₂	18.1	20.47	5.14
		CuBr ₂	4530	51.97	494.7
		Cu(OAc) ₂	14.3	20.23	5.00
		Cu(OAc) ₂	3581	50.84	500.8

7.3. Appendix C

Table 7.31 Mechanical properties of corn starch plasticised with salt:glycerol mixtures

Salt:glycerol system	UTS (MPa)	ΔUTS (MPa)	ε (%)	Δε (%)
Glycerol	0.86	0.21	54.95	2.81
Na ₂ B ₄ O ₇ .10H ₂ O	1.13	0.11	234.74	36.42
CaCl ₂ .2H ₂ O	0.74	0.18	232.32	34.95
MgCl ₂ .6H ₂ O	0.45	0.11	125.23	14.84
NaCl	0.82	0.20	68.68	12.91

Table 7.32 Mechanical properties of fibreboards as a function of salt:glycerol plasticiser prepared using method outlined in

Salt:glycerol system	UTS (MPa)	ΔUTS (MPa)	ε (%)	Δε (%)	E (MPa)	ΔE (MPa)
Glycerol	0.439	0.265	1.422	0.291	39.578	30.055
Na ₂ B ₄ O ₇ .10H ₂ O	4.537	2.205	2.562	1.233	326.226	126.207
CaCl ₂ .2H ₂ O	0.558	0.188	1.372	0.163	76.522	26.991
MgCl ₂ .6H ₂ O	0.699	0.168	1.565	0.276	102.284	24.055
1.3M NaCl	0.319	0.213	1.769	0.420	46.856	35.453

Table 7.33 Mechanical properties of fibreboards as a function of Na₂B₄O₇.10H₂O:glycerol plasticiser prepared using method outlined in , pressed for 30 min

Modifier Content (%)	UTS (MPa)	ΔUTS (MPa)	ε (%)	Δε (%)	E (MPa)	ΔE (MPa)
50	5.03	0.84	3.45	0.89	349.02	47.78
45	9.59	2.58	2.50	0.75	597.92	73.85
42.5	3.68	0.88	1.41	0.84	383.79	67.19
40	5.97	1.59	2.06	0.40	393.34	83.60
37.5	4.71	1.18	2.16	0.77	332.15	83.93

35	4.44	0.68	1.63	0.35	436.19	48.96
----	------	------	------	------	--------	-------

Table 7.34 Mechanical properties of fibreboards as a function of $\text{Na}_2\text{B}_4\text{O}_7 \cdot 10\text{H}_2\text{O}$:glycerol plasticiser prepared using method outlined in , pressed for 10 min

Modifier Content (%)	UTS (MPa)	Δ UTS (MPa)	ϵ (%)	$\Delta\epsilon$ (%)	E (MPa)	Δ E (MPa)
50	2.03	0.53	3.95	0.33	109.02	39.11
45	3.58	0.89	4.95	0.83	143.60	34.88
42.5	2.24	0.67	3.75	0.84	157.64	50.79
40	2.08	0.56	3.70	0.82	125.90	35.97
37.5	1.96	0.50	3.61	0.86	105.68	31.49
35	1.16	0.28	3.45	0.56	87.92	22.01

Table 7.35 Mechanical properties of fibreboards as a function of $\text{Na}_2\text{B}_4\text{O}_7 \cdot 10\text{H}_2\text{O}$:glycerol plasticiser prepared using method outlined in , pressed for 5 min

Modifier Content (%)	UTS (MPa)	Δ UTS (MPa)	ϵ (%)	$\Delta\epsilon$ (%)	E (MPa)	Δ E (MPa)
50	0.91	0.31	2.74	0.64	59.53	20.08
45	1.35	0.40	3.89	0.77	66.93	18.56
42.5	1.98	0.48	3.09	1.18	118.37	35.01
40	1.90	1.00	3.84	1.08	83.28	59.67
37.5	2.20	0.35	3.55	1.14	159.71	33.29
35	1.99	0.66	2.70	0.42	128.27	51.50

Table 7.36 Comparison of mechanical properties of dried and non-dried fibreboards, containing 50% w/w of a 1:4 molar mixture of $\text{Na}_2\text{B}_4\text{O}_7 \cdot 10\text{H}_2\text{O}$ and glycerol

Material	UTS (MPa)	Δ UTS (MPa)	ϵ (%)	$\Delta\epsilon$ (%)
Dried	8.59	2.78	2.42	1.13
Non-dried	6.44	1.32	3.45	0.89

Table 7.37 Densities of fibreboards

Modifier	Modifier content (% w/w)	Density (kg m ⁻³)	Resination method
Glycerol	40	709±3	In-house
Na ₂ B ₄ O ₇ .10H ₂ O :glycerol	40	509±131	In-house
CaCl ₂ .2H ₂ O:glycerol	40	675±42	In-house
MgCl ₂ .6H ₂ O:glycerol	40	648±4	In-house
NaCl:glycerol	40	668±21	In-house
Na ₂ B ₄ O ₇ .10H ₂ O :glycerol	50	615±12	Aspiration
	50	678±13	Aspiration (flash dried)
	45	623±8	Aspiration
	42.5	529±4	Aspiration
	40	559±17	Aspiration
	37.5	514±20	Aspiration
	35	514±8	Aspiration